Amazon River and floodplain hydrodynamics

Mark Adam Trigg

A dissertation submitted to the University of Bristol in accordance with the requirements for award of degree of Doctor of Philosophy in the Faculty of Science.

School of Geographical Sciences, March 2010

Word count: ~58,400

Abstract

The annual monomodal flood pulse of the Amazon River is a key driver for this globally important hydrological system. Understanding the behaviour and characteristics of this flood wave and its influence on the dynamics of river and floodplain interaction is important to many studies attempting to quantify processes dependent upon it, including estimates of carbon fluxes from the wetlands and sediment movement to the ocean.

The main aim of the research presented in this thesis was to investigate the hydrodynamic behaviour of the Amazon River and its floodplain, in order to better understand its components and processes. The key scientific question underpinning this aim is: How do the floodplain storage and fluxes affect the passage of the Amazon flood wave and in turn how does the passage of the flood wave control the dynamics on the floodplain? Research was carried out using a synthesis of hydraulic characterisation, numerical modelling, spatial analysis of remote sensing data and field surveys. In combination with information from published floodplain studies, these results were then used to inform the development of a conceptual hydrodynamics framework for the Amazon floodplain.

Hydraulic characterisation of the Amazon flood wave was undertaken showing that it is subcritical and diffusive in nature with dominating backwater effects. Experiments with the main channel using hydraulic models showed that main channel water levels were relatively insensitive (0.5 m error on a 12 m flood wave amplitude) to the geometric representation of the channel and that simplified bathymetry is adequate for calibrated predictions, provided the mean cross sectional area can be reasonably well approximated. Hydraulic model results compare well with observed data despite

explicit exclusion of the floodplain, indicating that the storage volume of the floodplain has a minimal affect on the passage of the Amazon flood wave for this reach.

The spatial analysis of Landsat TM images shows a total of 1,762 floodplain channels in the study area with a mean width of 47 m. Shuttle radar topography mission data has difficulty in resolving many of these floodplain channels due to 96% of the channels having a width less than the SRTM spatial resolution of 90 m. Comparing floodplain channel widths with their frequency reveals a power law relationship, showing patterns of structure that are self-similar over many orders of magnitude. Analysis of the floodplain channel network connectivity showed that the complex floodplain can be divided into floodplain hydrologic units (FHU) and that each unit type has different geomorphic characteristics resulting from a different mixture of water inputs, with each unit isolated from other units for much of the flood cycle by sediment barriers.

A field survey of the floodplain channels was conducted in order to measure and characterise their morphology. The findings of this survey together with numerical connectivity experiments, demonstrate that floodplain channels could be playing a much more significant role in the floodplain hydrodynamics then previously acknowledged. Floodplain channels were grouped into three types by depth: (i) for channels carrying only river flood water, depth was strongly correlated with the flood wave's mean annual range of 11.4 m; (ii) for channels which carried river flood water and local runoff, the mean depth was substantially deeper at 15.9 m; and, (iii) main river island channels were deeper again, with a mean depth of 17.7 m.

Finally, a coherent, evidence based, conceptual floodplain hydrodynamics framework was developed to inform a broad range of future Amazon wetland research. The framework represents an extension to the macro level understanding available in the scientific literature and provides an important link between the macro and detailed level study scale.

Dedication and acknowledgements

When I embarked on this adventure, some three and a half years ago, I had no idea how it would turn out or what I would find. Even though the PhD process can be somewhat solitary at times, looking back, I am amazed at how many people have had input to my work, either directly or indirectly. I would like to name some of those people here, as I know I would not have learnt as much or achieved as much without their help.

Most of all I want to thank my wife, Stephanie, for embarking on this adventure together with me, and encouraging me at every step, even when we did not know where it might lead. She has been a sane sounding board for my crazy rambling ideas and provided the final polish by proof reading of this entire document at the last minute. I also want to thank both my children for being welcome distractions from what could be a bit intense and heavy at times. Thank you to Logan for being understanding when daddy had to work and you wanted to play, and thank you to Amber, who arrived after I started, for adding even more excitement to this adventure.

Having worked in “the real world” previously to my PhD, I am acutely aware of what an enormous privilege this time has been and I am grateful to the Natural Environment Research Council, and therefore implicitly the British tax payer, for the studentship funding which has given me the freedom to pursue something of great interest to me.

My supervisors Paul Bates and Matthew Wilson deserve special mention, as they have both allowed me to be me, with my unusual background, while still providing clear direction. I have learnt so much from both of them and their continued input throughout the PhD has been invaluable in making this thesis what it is. Others with specific inputs that should be mentioned are: Matthew Horritt for his help getting the

diffusive channel solver working; Tim Fewtrell & Jeff Neal for their many, many improvements to the LISFLOOD-FP hydraulic model that I have used. My thanks also go to the School of Geography computer and administration staff for their behind the scenes, but important, input to my work: Duncan Baldwin, Ed Thomas, Gethin Williams and Theresa Andrews.

Clive Maguire, my Irish guide to the Amazon cannot go without mention as he kept me safe during our long forays into the remote Amazon floodplain and also helped me plan and carryout what was very memorable field work, thanks for being up for an adventure.

Special thanks to Paul Valdes and Kat Michaelides for their input and guidance during my upgrades and ensuring that I stayed focused on the science and not the tools. There are also many other scientists that I have met during my PhD that have had an important input into my research. Many of these scientists also have a specific interest in the Amazon and I relied much on their accumulated knowledge and experience: Doug Alsdorf, John Melack, Bruce Forsberg, Laura Hess, Ed Beighley, Ernesto Rodriguez, Mike Durand.

As well as those scientists who have had a personal input to my work, there are the multitude of scientists who's work I have built upon here. One of these in particular requires special mention: Leal Mertes, who's own work has been the inspiration behind the combination of methods that I have used to develop my floodplain hydrodynamics framework. It would have been a privilege to meet her before her brilliant career was cut short, and I dedicate this thesis to her for showing me, through her work, that the complexity of the Amazon River and floodplain need not be daunting and for inspiring me to use all available methods to explore the hard science questions.

Authors' declaration

I declare that the work in this dissertation was carried out in accordance with the requirements of the University's Regulations and Code of Practice for Research Degree Programmes and that it has not been submitted for any other academic award. Except where indicated by specific reference in the text, the work is the candidate's own work. Work done in collaboration with, or with the assistance of, others, is indicated as such. Any views expressed in the dissertation are those of the author.

SIGNED: …….. DATE: …….....

Contents

List of figures

List of tables

List of abbreviations

1D	one Dimensional
2D	two Dimensional
ADCP	Acoustic Doppler Current Profiler
ArcMap	GIS software
ATTZ	Aquatic/Terrestrial Transition Zone
CO_2	Carbon Dioxide
Cr	Courant number
DEM	Digital Elevation Model
ENSO	El Niño-Southern Oscillation
FHU	Floodplain Hydrologic Unit
ET	Evapotranspiration
fpc	floodplain channels
GIS	Geographical Information System
GPS	Geographical Positioning System
HEC-RAS	1D hydraulic model software developed by the US Army Corps of Engineers at the Hydrologic Engineering Center.
HyBAm	Hydrology and Geochemistry of the Amazonian Basin research programme
HYDRA	flow storage model (Coe *et al.*, 2002)
IBIS	partially coupled surface process model (Coe *et al.*, 2002)
ITCZ	Intertropical Convergence Zone
JERS-1	Japanese Earth Resource Satellite 1
Landsat TM	Landsat Thematic Mapper
Landsat ETM+	Enhanced Thematic Mapper

LISFLOOD-FP	coupled 1D/2D storage cell hydraulic model
Matlab	mathematical analysis software
msl	mean sea level
RMS	Root Mean Squared
RMSE	Root Mean Squared Error
SACZ	South Atlantic Convergence Zone
SST	Sea Surface Temperature
SAR	Synthetic Aperture Radar
SRTM	Shuttle Radar Topography Mission
SWOT	Surface Water and Ocean Topography satellite mission (proposed)
TOPEX-POSEIDON	ocean surface topography mapping satellite
TRIP	simplified runoff and routing model (Chapelon *et al.*, 2002; Falloon and Betts, 2006)

List of units

%	percent
°C	degrees Celsius
cm	centimetres
cm/d	centimetres per day
cm/km	centimetres per kilometre
d/yr	days per year
hp	horsepower
KHz	Kilohertz
km	kilometres
km/hr	kilometres per hour
km^2	square kilometres
km^2/yr	square kilometres per year
km^3	cubic kilometres
m	metres
m/s^2	metres per second squared
m^3/s	cubic metres per second
mm/yr	millimetres per year
s	seconds
W	Watts

CHAPTER 1
Introduction

1.1 Introduction

The sheer scale of the Amazon River basin means that it holds the undisputed title of the most important river system on Earth. This introductory chapter begins by looking at the importance of the Amazon basin in a global context, noting current global research issues such as atmospheric feedbacks, carbon emissions and climate change induced vegetation dieback scenarios. This is then followed by a more detailed look at the specific importance of the central Amazon River and its extensive floodplain and the processes and issues that are of most significance there. The way in which the Amazon flood wave dominates these floodplain processes will then be explored and this will show why a better understanding of this fascinating natural phenomenon is important in its own right, as well as in order to facilitate further research in these dependent areas. The role of the science of hydraulics and the tools commonly employed in its practice, such as hydraulic modelling, are then demonstrated as the key to gaining this required understanding and quantification of the flow dynamics.

While the use of hydraulic science in studying the Amazon flood wave is not new, it has tended to play a secondary role in much of the research work to date. With the availability of new data, mainly from the discipline of remote sensing, but also from in-situ field measurements, and improved hydraulic modelling tools and computer resources, it is an opportune time to apply the science of hydraulics to the study of the Amazon. This leads finally to the presentation of the central aim of this thesis.

1.2 The global importance of the Amazon basin

Most people are aware that the Amazon River is the largest in the world; however, what is often not appreciated is by how much of a margin it is the largest. Its flow is estimated to account for some 20% of total continental runoff (Richey *et al.*, 1989b) and its flow is five times greater then the next biggest river, the Congo, in central western Africa. Even the flow in some of the Amazon's tributaries would rank them amongst the top ten rivers in the world (Costa *et al.*, 2002a). Its flow is a product of a huge catchment area of some 6.7 million km^2, which accounts for around 40% of the South American continent (Coe *et al.*, 2008). Its location in the Earth's warm equatorial zone results in a high mean tropical rainfall, which ranges from 2,000 mm/yr in the extreme northeast and southern parts of the basin to more than 3,500 mm/yr in the northwest lowlands, and increases to 7,000 mm/yr on the east side of the Andes (Richey *et al.*, 1989a). Evapotranspiration from the large tropical forests is significant enough to sustain regional climate and influence the global climate and ocean circulation (Richey *et al.*, 1989b). The local evaporation and precipitation from the forests account for a sizable portion of the regional water budget (Nobre *et al.*, 1991). The large forest biomass covering a significant portion of the basin's area may also contribute to higher rainfall through local climatic feedback effects which draw in moisture from the ocean, the so called "biotic pump" effect postulated recently by Makarieva and Gorshkov (2007).

The Amazon forest is one of the most biodiverse regions on Earth and with an area of 5.4 million km^2 (Malhi *et al.*, 2008), similar to the land area of Western Europe, it plays an important role in the Earth's biosphere. Recent compilations of Amazonian species indicate at least 40,000 plant species, 427 mammals, 1294 birds, 378 reptiles, 427 amphibians, and around 3,000 fishes (Da Silva *et al.*, 2005) and the estimated proportion of species in Brazil alone is around 9.5% of the world total (Lewinsohn and Prado, 2005). The tropical forests of Amazonia account for 45% of the world's tropical

forest and store 40% of the carbon residing in terrestrial vegetation (Malhi and Grace, 2000). This dynamic carbon store is characterised by high productivity and plays an important role in the global carbon cycle and although estimates of fluxes such as methane emissions are still being refined, its importance is undisputed (Houghton *et al.*, 2009).

While the Amazon is known to influence global climate and is undoubtedly important in global biodiversity, the potential impact of climate change on the Amazon is less well understood. There is now a scientific consensus that there is, with 90% certainty, measurable global warming resulting from human activities (Solomon *et al.*, 2007), and the potential impacts of this are only just starting to be identified. Recent research published by the Hadley Centre has caused considerable alarm because it raises the serious possibility that the Amazon forest could respond to global warming with a feedback induced dieback of primary forest (Cox *et al.*, 2000; Cox *et al.*, 2004). The consequential release of significant carbon reserves would further exacerbate global warming. While this result is not duplicated in all global climate models (Li *et al.*, 2006), it indicates a sensitivity that warrants close attention. At the end of the last glacial period, the Amazon warmed at only 0.1 °C per century, in recent decades the rate has been 0.25 °C, and under mid-range greenhouse emission scenarios, temperatures are projected to rise by 3.3 °C this century, or up to 8 °C if substantial forest dieback affects regional biophysical properties (Malhi *et al.*, 2008). In addition to the spectre of climate induced deforestation, there is already the measureable impact of human induced deforestation, estimated for the 1990s at around 25,000 km^2/yr (Achard *et al.*, 2002), which is another challenge facing the Amazonian biosphere. Evidence of dramatic changes to the central Amazon landscape brought about by historical changes in sea level (Irion *et al.*, 1995) add another source of concern regarding potential future climate change, because as well as potential reductions in precipitation, rising sea levels may also result in significant changes to the riverine environment.

The Amazon has been identified as one of the key pressure points in the Earth's system which are particularly sensitive to climate change (Steffen *et al.*, 2004). If these critical regions were subjected to stress, they could trigger large-scale, rapid changes across the entire planet. Not enough is known about these pressure points to be able to predict when these tolerance limits will be reached. The Amazon is consequently a focus for international research and the International Geosphere-Biosphere Programme has identified it as one of the primary focuses for their research agenda (Steffen *et al.*, 2005). Interestingly, there is now some evidence from recent research that the Amazonian forests may be more resilient to climatic drying than is currently represented in vegetation-climate models (Malhi *et al.*, 2008). Even if this is the case, a modest change to the dynamics of this system, induced by future climate change, may have serious consequences for the river basin and the planet, highlighting the importance of studying this region and the science of the underlying biogeochemical processes.

1.3 The central role of the Amazon River and its floodplain

At the core of the Amazon biosphere is the river and its floodplain. The Amazon River's headwaters lie on the eastern slopes of the Peruvian Andes, in places only 160 km from the Pacific Ocean, and it flows across almost the entire width of South America to join the Atlantic on the eastern side, a distance of some 6,400 km (Rossetti and Valeriano, 2007). On its way to the sea, the Amazon collects water from more than 1000 tributaries which drain over half of Brazil, and include contributions from the five other countries in the basin; Bolivia, Colombia, Ecuador, Peru and Venezuela, see Figure 1-1.

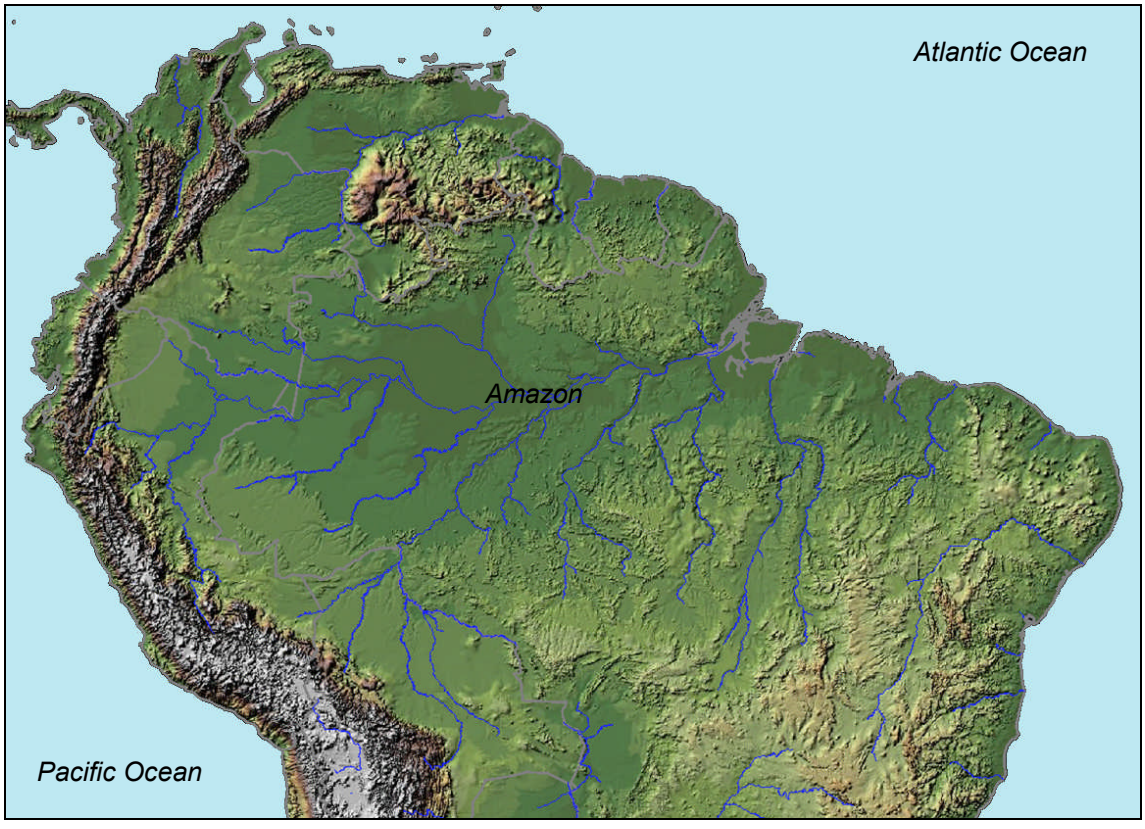

Figure 1-1 — Location of the Amazon basin. The northern part of South America is shown with terrain relief highlighting the Andes in the west and the central Amazon lowlands in the centre of the continent. Blue lines indicate major rivers and light grey lines are country borders. Based on the Hydrosheds dataset (http://hydrosheds.cr.usgs.gov/).

The modern Amazon River was born between 11.8 and 11.3 million years ago (middle to late Miocene) with the formation of the Andes, and reached its present shape and size during the late Pliocene, some 2.4 million years ago (Figueiredo *et al.*, 2009). Prior to this, there is strong geological and biological evidence that the flow on this part of the continent was originally in the opposite direction, east to west, before the formation of the Andes. After leaving the Andes, the headwater tributaries cross the foreland basin, depositing large volumes of sediment in the process (Horton and DeCelles, 1997). The tributaries then converge to cross an ancient craton (a stable piece of the Earth's crust), flowing along one of the world's largest subsidence troughs, filled with as much as 8000 m of sedimentary rocks aged from the Paleozoic to the Tertiary (Nunn and Aires, 1988). The main river mouth is fixed by a graben (depressed block of land flanked by faults) at its eastern end, where it enters the Atlantic Ocean. The trough is flanked by two shields of Precambrian rock with low relief and gradient, exhibiting very low rates of erosion (Dunne *et al.*, 1998).

Close to Iquitos in eastern Peru, the Ucayali and the Marañón, the two main headwaters of the Amazon join, forming the Amazon proper, although it is known locally as the Solimões from this point to Manaus in the east, and then as the Amazon until it reaches the sea. The Amazon waters vary in colour on their way to the mouth, with contributions from so called white water and black water tributaries (Barroux *et al.*, 2006). The white water tributaries are more of an opaque brown colour and carry huge quantities of suspended sediment, mostly eroded from the steep and relatively young Andes Mountains. The black waters in contrast carry very little sediment from their predominantly ancient basement rock catchments with low weathering rates and their clear dark colour is due to dissolved organic matter. The most well known example of a union of these different river types is near Manaus, where the Rio Negro, a black water river, joins the Solimões, a white water river, to create what is known as the meeting of the waters. For many kilometres, due to their different physical and chemical

properties, the black and white waters flow side by side but mostly separate before they finally merge. Low water channel widths for the main channel vary from 2 km at São Paulo de Olivença to more than 4 km near Obidos (Dunne *et al.* 1998), with floodplain widths typically 10 times the river width.

The accumulation and removal of sediment within the Amazon basin is strongly affected by the rivers geological setting, with at least three large structural arches imposing hydraulic controls on the flow (Tricart, 1977; Dunne *et al.*, 1998) as well as numerous other more localised lineaments (Latrubesse and Franzinelli, 2002). In addition, due to the very low channel gradient within the trough, sea level changes also impose a strong control on the sediment history of the central Amazon. At Iquitos, some 3600 km from the sea, the river level is 110 m above mean sea level (msl) and at the confluence with the Negro, 720 km from the ocean, it is only 23 m (Irion *et al.*, 1995). Tectonic activity and sea level changes have resulted in two distinct groups of floodplain deposits within the trough; the *terra firme*, dating from the Pliocene and Pleistocene (10,000 to 5,300,000 years old) and the modern Holocene (<10,000 years) floodplain known as *várzea* where it is nutrient rich and *igapó* where it is nutrient poor. The older deposits flank the modern floodplain as a series of terraces of different ages and can be up to 80 m above the current floodplain.

It has been estimated that 20 % of the Amazon lowland basin (usually defined as the area below 500 m in elevation) described above is covered by permanently or seasonally flooded wetlands. Interfluvial swamps and flooded savannas do cover extensive areas in some regions, but the river floodplains are the dominant wetland habitat in the Amazon (Forsberg *et al.*, 2000). A wetland mapping study by Hess *et al.* (2003) of the central third of the Amazonia lowland, an area of some 1.7 million km^2, showed that the wetland area accounted for 17% of the area, around ~300,000 km^2. Nearly 70% of this wetland area was covered in seasonally flooded forest and 51% comprise the floodplains of the main river stem and its tributaries. This Amazon floodplain is a complex mosaic of lakes, floodplain channels, scroll bars and overbank

deposits (Mertes *et al.*, 1996). As the Amazon crosses three structural highs and the downstream end of a fault block that tilts the valley floor toward the south-southeast (Tricart, 1977), its flood-plain width decreases, constraining the sinuosity of the channel and increasing its gradient (Dunne *et al.*, 1998). The consequences of these geological controls can be observed in the varied channel-floodplain geomorphology along the Amazon. Mertes *et al.* (1996) noted that the main stem could be divided up into three distinct zones of differing channel-floodplain geomorphology, controlled by river slope and sediment transport. The upper reach (São Paulo de Olivença to Itapeuá) is dominated by floodplain deposition through channels, producing intricate scroll-bar topography with hundreds of long narrow lakes. The central section (Itapeuá to São José do Amatari) is relatively narrow with few lakes and little evidence of channel migration. The lower reach (downstream of São José do Amatari) was characterised by channels restricted by levee building and overbank deposition, resulting in a flat floodplain with a patchwork of large, irregular, shallow lakes.

1.4 Dominance of the Amazon flood wave

The flow in large river systems generally shows a stronger response to seasonal rainfall patterns than to individual rain storm events. This results in an annual cycle closely correlated to the main rainfall season and can be seen in the Mekong, the Congo and most significantly the Amazon. This is in contrast to medium and small rivers where the flow can be seen to rise and recede on a timescale of weeks, days and even hours in response to individual storms and weather systems passing over the catchment. The Amazon's many tributaries do respond in a similar fashion, but when all these inputs are integrated together down the main stem of the river, this results in a single monomodal flood wave that occurs with regularity on an annual basis. The monomodal nature of the flood wave is illustrated in Figure 1-2, which shows the annual water level variation at Manaus on the Amazon mainstem. The flood wave elevation range at this location is around 9.5 m, with high water in June-July and the low water in October-November. The water elevation records for two of the more extreme years are also shown.

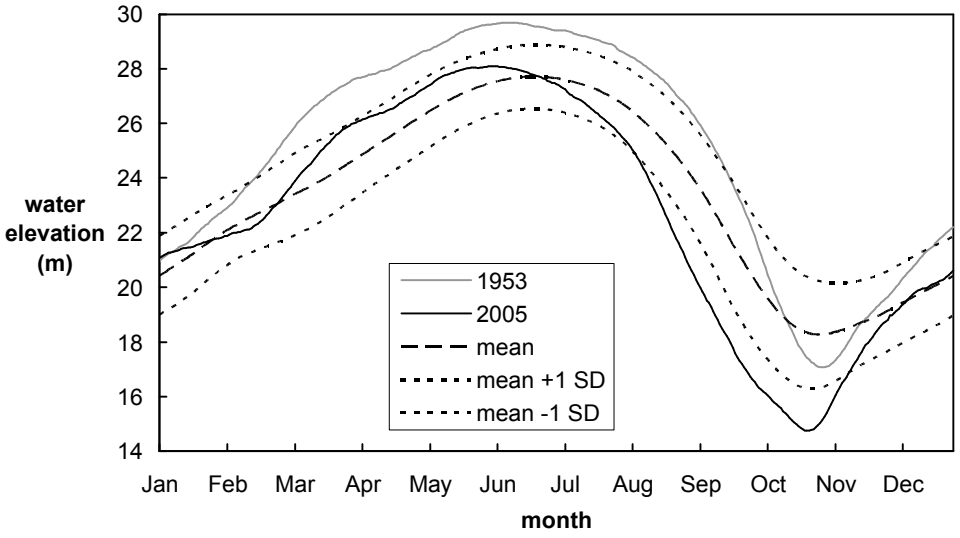

Figure 1-2 – Mean annual water level variation at Manaus gauging station. The plus and minus one standard deviation envelope is also shown together with a notable high year (1953) and low year (2005).

Seasonal precipitation has a pronounced pattern across the Amazon basin, closely tied to global climate processes. The Intertropical Convergence Zone (ITCZ), where winds converge from the southern and northern hemispheres, induces wet and dry periods alternately in the northern and southern sides of the basin. South of the equator there is a wet period from December to February and north of the equator the dry period is from June to August (Richey *et al.*, 1989a). The South Atlantic Convergence Zone (SACZ), another axis of convergent winds oriented northwest-southeast across southeast Brazil and into the southwest Atlantic Ocean also increases rainfall in these areas (Villar *et al.*, 2009). These alternating seasonal patterns of rainfall maintain a high base flow in the Amazon River which, together with storage of water on the floodplain, means that minimum and maximum flows differ only by a factor of three (Richey *et al.*, 1989b; Meade *et al.*, 1991).

Extremes in inter-annual flow variability are also strongly linked with global climate processes. For example, the El Niño-Southern Oscillation (ENSO), a periodic change in the atmosphere and ocean in the tropical Pacific region, causes large scale precipitation anomalies in the basin which result in high flood levels in the river during La Niña events (cold ENSO phases) and low flood levels during El Niño events (warm ENSO phases) (Schongart and Junk, 2007). Another example is the drought experienced in the western sub-basins during low water in 2005, which has been attributed to high sea surface temperature (SST) in the tropical North Atlantic (Villar *et al.*, 2009). This strong link between the river flow variability and global climate means that the Amazon basin will be sensitive to any changes in those processes.

The size and regularity of the monomodal flood wave has profound implications for the Amazon River and its floodplain. The dynamic exchange of water between the channel and floodplain plays a central role in biological and biogeochemical processes in the Amazon basin (Junk and Piedade, 1993; Melack and Forsberg, 2001; Wittmann *et al.*, 2004). This cyclic interaction process was defined as the flood-pulse concept by Junk *et al.* (1989) who put forward the view that rivers and their floodplains are

integrated components of a single dynamic system, linked by strong interactions between hydrological and ecological processes (Tockner *et al.*, 2000). The river and floodplain include permanent *lotic* (flowing water), and *lentic* (standing water) habitats as well as areas periodically exposed to advancing and receding floods. The areas oscillating between terrestrial and aquatic status are designated as the Aquatic/Terrestrial Transition Zone (ATTZ) (Junk *et al.*, 1989). This mix of permanently and periodically flooded environments provides an important habitat for aquatic flora and fauna (Junk and Piedade, 1993; Putz, 1997) and play a key role in sustaining regional fish production (Forsberg *et al.*, 2000; Petry *et al.*, 2003; Da Silva *et al.*, 2007). The nutrient-rich floodplains (*várzea*) have the highest human population density in Amazonia and economic activities such as fishing, agriculture, pasture and timber extraction are directly associated with water-level fluctuations (Schongart and Junk, 2007). The flooded forests, lakes and floating macrophytes of Amazonian wetlands are also believed to be globally significant sources of tropospheric methane (Bartlett *et al.*, 1988). Evasion of CO_2 from these wetlands to the atmosphere, extrapolated over the whole basin, is at least ten times the fluvial export of organic carbon from the basin to the ocean (Richey *et al.*, 2002).

1.5 Hydrology and hydraulics

Given the magnitude of the Amazon flood wave it is perhaps not surprising that many of the important biogeochemical processes outlined above are both controlled by or dependent upon the dynamic movement of water between the river and floodplain.

This movement of water provides the driving force for the changing geomorphology of the river and floodplain, with accretion through deposition of sediment as well as erosion of deposited sediments. The highest sedimentation rates, close to the river banks can be as high as 3 cm/d (Mertes, 1994) and erosion can wash out several hectares of forest at single bank locations during a single high-water period (Wittmann *et al.*, 2004). Sedimentation and content of the sediment are linked to the distance from the main-river channels and the period of inundation to which the sites are subjected (Mertes *et al.*, 1995; Wittmann *et al.*, 2004). Coarse fractions, such as sand, are deposited at fluvial islands and on the river banks where water velocities, and therefore sediment transport capacity, is still high. With reducing water velocities away from the river, fine grains, such as silt and clay, are deposited, especially when the floodwaters are nonturbulent and persist for several weeks or months in lakes and backwater depressions (Peixoto *et al.*, 2009).

The sediment movement and floodplain environment also play an important geochemical role. It has been estimated that dynamic sediment movement could recycle the Amazon floodplain in 1000 – 4000 years (Mertes *et al.*, 1996). In addition, such is the quantity of sediment exchanged between the river and floodplain that it takes most of the sediment load of the Amazon thousands of years to make its way from the Andes to the ocean (Mertes *et al.*, 1996). This long residency time for sediment minerals provides time for complex weathering processes to take place and also provides important nutrient inputs to the ecosystem. The importance of these inputs is illustrated by the stark contrast in biomass production between the two main floodplain types, *várzea* and *igapó*. The *várzea* has periodic flooding inputs from the

sediment laden white waters and has a high productivity, whereas water sources for the *igapó* are predominantly low sediment black water river inputs, direct rainfall and local runoff, resulting in low production (Junk and Piedade, 1993; Melack and Forsberg, 2001). This floodplain productivity has important implications for the calculation of global carbon fluxes (Grace and Malhi, 2002).

The distribution of the different *várzea* forest types is determined by adaptations of tree species to different levels and periods of flooding, and most habitats and species are strongly zoned along the flooding gradient (Junk *et al.*, 1989; Wittmann *et al.*, 2006a; Peixoto *et al.*, 2009). Geomorphological changes provide new habitat opportunities and result in a rapid colonisation and succession process by vegetation. Sites with coarse-grained substrates normally undergo high sedimentation rates, which impede tree regeneration and cover superficial root layers of mature individuals. Only a few pioneer plants can tolerate these conditions; grasses such as *Echinochloa polystachya* and *Paspalum spp.*, and a few tree species such as *Alchornea castaneifolia* and *Salix martiana* (Wittmann *et al.*, 2004). Once vegetation has become established, sedimentation rates increase due to the resistance to flow presented by the vegetation itself and conditions become more favourable for other tree species that can tolerate shallower waters. The movement of water into and out of the floodplain is also important to many fish species and there is a general migration of fish into the floodplain as water levels rise, providing access to rich feeding and spawning habitats (Petry *et al.*, 2003; Castello, 2008). There is also evidence that larval fish avoid predation as water levels drop by returning to the main channels (Araujo-Lima and Oliveira, 1998). In fact, the environmental gradients brought about by the flood pulse are vitally important for most of the ecology that is found in and adapted for life in the floodplain (Petry *et al.*, 2003).

Understanding and being able to quantify key water parameters such as the source of water, velocities, depths, and flood duration is fundamentally important to studying and predicting changes for the biogeochemical processes in the Amazon

floodplain. Thus the science of hydrology underpins the workings of this very large and globally important system and its application is key to understanding that system as well as the dependent processes. The science community has long recognised the importance of these hydrologically controlled processes and research efforts to unravel the complexity of the workings of this system have been underway for many years. A number of generalised hydrological models have been developed for the Amazon, beginning with a Muskingham routing model of a 2000 km reach of the Amazon main stem (Richey *et al.*, 1989a). Around the same time, work was also published exploring the use of water balance and transport models (rainfall runoff models) in demonstrating the feasibility of large scale simulation (Vorosmarty *et al.*, 1989). The level of detail in these models has steadily improved over the years (Coe *et al.*, 2002; Coe *et al.*, 2008; Beighley *et al.*, 2009). These models have helped develop an understanding of the whole basin hydrology, but are still hampered by limited data and resolution, and do not address the observed complexity of the floodplain dynamics. Recent work using spaceborne interferometric synthetic aperture radar (SAR) measurements has shown how complex the floodplain water level response is to the passing flood wave in the main river channel (Alsdorf *et al.*, 2000; Alsdorf *et al.*, 2007a). This work shows major spatial and temporal variation in the water level changes in the floodplain, indicating significantly more complex hydraulic processes at work than simple increasing and decreasing water levels.

Hydrology research that has been more focused on the floodplain has tended to be limited to specific well studied sites such as at Curuaí (Bonnet *et al.*, 2005; Barroux *et al.*, 2006; Bonnet *et al.*, 2008) and Lake Calado (Lesack, 1995; Williams *et al.*, 1997; Engle and Melack, 2000), making it difficult to apply the results to the broader floodplain. Another difficulty with many of the floodplain studies conducted to date is that while hydrology has been incorporated, it is most often of secondary importance to the main research topic, such as sediment movement (Mertes, 1994) or the carbon cycle (Moreira-Turcq *et al.*, 2000). Even those studies which incorporate hydrological

measurements and mass balance models commonly do not look in detail at the hydrodynamics of the water movement across the floodplain. In part, this is due to the difficulties of applying local site specific measurements across the macro scale floodplain. Newly available data, such as elevation data from the Shuttle Radar Topography mission (SRTM) and other remote sensing datasets, are transforming the study of the Amazon and providing new opportunities to study the dynamics of the flood wave, either directly (Alsdorf *et al.*, 2005; Martinez and Le Toan, 2007) or through incorporation into hydraulic models to simulate the dynamics (Wilson *et al.*, 2007). This work is providing a level of detail not previously available in single consistent datasets covering most of the floodplain environment, presenting the possibility of integrating the findings from the site scale studies across a large spatial scale. Melack and Forsberg (2001) state that further advances in understanding of how riverine and upland stream flows interact and influence the biogeochemistry of floodplain lakes will require the merging of remote sensing data and hydraulic and hydrological modelling with information on biogeochemical processes.

1.6 Thesis aim

The monomodal flood pulse that passes annually down the Amazon River is a key driver for this globally important hydrological system. Understanding the behaviour and characteristics of this flood wave and the influence it has on the dynamics of river and floodplain interaction is therefore important to any study attempting to quantify processes dependent upon it. The limited application of hydraulics in previous floodplain research together with newly available remote sensing data is providing new opportunities to study these hydrodynamics and integrate site specific findings.

Thus the overall aim of the research presented in this thesis is to investigate for the first time, the detailed hydrodynamic behaviour of the Amazon River and its floodplain in order to better understand its functioning, ultimately providing the beginnings of a coherent, evidence based, conceptual model to inform future research. The key scientific question underpinning this aim is: How do the floodplain storage and fluxes affect the passage of the Amazon flood wave and in turn how does the passage of the flood wave control the dynamics on the floodplain? More specifically, the aim is to use a synthesis of field survey, gauging station data, remote sensing data analysis and numerical modelling in order to investigate various hydraulic aspects of the flood wave. The findings from this work will be integrated with a collation of hydraulic specific details gleaned from the many previous floodplain studies in order to present the first detailed conceptual framework of the Amazon River and floodplain hydrodynamics. As well as providing important details on the underlying system processes in a single framework, it will also provide quantification of key hydraulic parameters. As well as a valid aim in its own right, this framework will be essential in ensuring that future hydraulic and hydrological modelling of the river and floodplain capture the dynamics of this important river system.

CHAPTER 2
Amazon research context

2.1 Introduction

In the first chapter, the important central role that the Amazon River and floodplain play in the functioning of the Amazon basin biosphere was identified, together with how an understanding of the hydraulic processes governing the dynamics of the river and floodplain interaction as the monomodal flood wave passes down the Amazon is crucial to quantification of many of the biogeochemical processes dependent upon that flood pulse. The application of hydraulic science to the study of the Amazon flood wave to date has been relegated to a largely secondary role, with emphasis so far on other research fields such as sedimentology, ecology, geology, hydrology and the carbon cycle. One of the difficulties of studying the complex hydraulics of the Amazon until recently has been the lack of sufficiently detailed elevation and bathymetric data with which to apply commonly used tools such as hydraulic modelling. The last chapter concluded that with the availability of new remote sensing data as well as improved hydraulic modelling tools and computer resources, it is an opportune time to apply the science of hydraulics to the study of the Amazon flood wave in order to develop a better understanding of this globally important system.

This chapter takes a more detailed look at what research has been conducted in terms of hydrology and hydraulics thus far and what the findings show regarding the flood wave and its effects as it passes down the river and through the floodplain, as well as what research questions this body of work leaves unanswered and how it might be possible to address them. Some key hydrological studies are examined, including several large scale hydrological modelling studies which look at the whole basin

response to climatic conditions and routing of the resulting runoff to the ocean. The increasingly important role that remote sensing data is now taking in Amazonian scientific studies is then explained, followed by a summary of studies where direct measurement of hydrological parameters have been undertaken. This review of previous work also encompasses many floodplain studies where the hydraulics are secondary to the main subject of the study, but the quantification of water parameters such as depth, source or duration, is central to explaining the primary subject's dependence, either directly or indirectly, upon the effects of the flood pulse. By combining field measurements, water balance modelling and remote sensing, a number of interdisciplinary studies are providing a more holistic understanding of Amazonian floodplain processes, and there is a need to expand this approach to cover a broader expanse of floodplain with a more varied character.

For the final element of the research context, the few Amazon floodplain studies specifically focused on hydraulic modelling are explored in detail and this shows how these make use of a combination of new model formulations, remote sensing data and direct measurement to simulate the passage of the flood wave through the floodplain. This combined approach promises to be a useful tool in quantifying and predicting changes to many of the important flood wave parameters on which many biogeochemical processes depend. Despite this promise, this approach is still in its infancy and difficulties in modelling the hydrodynamics of the floodplain demonstrate that there is room for improvement. By studying the hydrodynamics at a more fundamental level it should be possible to gain a more sound, evidence based understanding of the processes being simulated. A better understanding of the hydrodynamics should ensure numerical models are producing the right results for the right reasons and this will be particularly important if hydraulic model output is to be used to study dependent biogeochemical processes. Ultimately, this approach should also provide the beginnings of a rational framework of the hydrodynamics of the Amazon River and floodplain.

2.2 Generalised hydrological models

Generalised hydrological models are a common method of studying the hydrology of river basins and how runoff may respond to given changes in that system. In their simplest form, they allow a hydrologist to study a catchment, given relatively little information and are often based on general assumptions, for example regarding runoff percentages and simple routing methods. Whilst these provide a crude idea of overall runoff quantities and timings, there is an inevitable drive to improve these models by incorporating more detailed data and more accurate representations of the physical processes in order to allow them to be used to address more complex hydrological questions.

A number of generalised models have been developed for the Amazon, beginning with a Muskingham routing model of a 2,000 km reach of the Amazon main stem (Richey *et al.*, 1989a). While this was a useful first step at quantifying the main channel flow behaviour, it provided little information regarding the flow on the floodplain, other than a much cited estimate that up to 30% of the peak flow in the channel is derived from water that has passed through the floodplain. In addition, a key disadvantage of the Muskingham method, in this case, is that it does not include effects such as friction and diffusion which are known to be important for both in-channel and out of bank flows. Around the same time, work was also published exploring the use of water balance and transport models (rainfall-runoff models) in demonstrating the feasibility of large scale simulation (Vorosmarty *et al.*, 1989). This work used a ½ degree (~54 km) resolution and demonstrated the importance of floodplain inundation in defining the flow regime on the main stem Amazon through storage effects on the flood wave.

This work was improved upon with a partially coupled surface process model (IBIS) and flow storage model (HYDRA) which represents the floodplain with coarse two dimensional (2D), 9 km cells (Coe *et al.*, 2002) which was useful in confirming

general routing aspects of the Amazon flood wave from the previous work. However the IBIS/HYDRA model was still hampered by limited data and resolution, and suggested the need for more detailed modelling, particularly with regard to the topography, in order to improve water elevation and flood extent inundation accuracy. In due course, availability of new data, such as that from the Shuttle Radar Topography mission (SRTM), has allowed topography representation improvements to the above model (now known as THMB) to be made by the authors (Coe *et al.*, 2008). Whilst the model still uses 9 km cells to represent the floodplain, they are now fractionally flooded using a cumulative distribution function extracted from resampled 1 km SRTM data, with a crude vegetation correction to allow for the SRTM's partial canopy penetration. Several other improvements to the process representation were also made and the combined effect was an improvement in the match between the model's predicted flooded area and that derived from Japanese Earth Resource Satellite 1 (JERS-1) measurements.

Another recent macroscale hydrological model of the Amazon is that by Beighley *et al.* (2009). This uses a framework for the subdivision of the land surface and hydrographic network into nested basins which lends itself to the parallelisation of the computational code, which is of significant benefit as the models become more detailed and complex. As with the Coe *et al.* (2008) model, this also uses SRTM data to derive the topographic characteristics of the land surface units of which the smallest have a median area of 240 km^2.

These basin wide models are now being used to look at important topical issues such as the impact of current and future deforestation on basin hydrology (Costa and Foley, 1997; Coe *et al.*, 2009). They are also used to study the spatial and temporal variation of flows and their relation to climate across the basin (Coe *et al.*, 2002; Foley *et al.*, 2002). Coupling global climate models with these hydrological models will be one of the main ways of trying to provide detail as to the hydrological impacts that might be expect with climate change. This is already underway with simplified runoff

and routing models such as TRIP (Chapelon *et al.*, 2002; Falloon and Betts, 2006), which are embedded within Global Climate Models. However, as yet these simplified models do not provide for the Amazon basin, the level of detail and validation of the Coe *et al.* (2008) and Beighley *et al.* (2009) models.

Despite the progress made in recent years with the detail and complexity of the process representation with the basin wide hydrological models (Coe *et al.*, 2008; Beighley *et al.*, 2009), they still do not provide an adequate tool to investigate the detailed hydrodynamic behaviour of the Amazon River and its floodplain. This is because many of the detailed floodplain processes are occurring at scales which are below the smallest model unit dimensions and therefore not explicitly represented in the models. For example, most of the channels and lakes within the floodplain are smaller than the main river channel, which has a mean width of 4.5 km along the main stem (Mertes *et al.*, 1996) and yet even one of the more advanced hydrological models (Coe *et al.*, 2008) has a minimum 9 km cell size that is twice the mean width of the main channel. An additional problem is that these hydrological models are built on assumptions regarding hillslope runoff processes in order to provide a basin wide, computationally efficient, representation of the whole catchment. This hillslope process representation may not be fully applicable in the shallow sloping topographically complex floodplain.

What these basin wide hydrological models can provide at this stage, is an understanding of the drivers of the flood wave itself, such as climate influences and timings. Given that the floodplain hydrodynamics will be directly related to the amplitude and timing of the flood wave, then this is important information towards the understanding of the system as a whole. For example, these hydrological models show that the volume of water stored in the floodplain has a significant effect on the flood wave as it passes down the mainstem, attenuating the flow and altering the effect of timings of inflows, thus contributing towards the formation of the monomodal flood wave (Vorosmarty *et al.*, 1989). In addition, hydrological models show strong links

between climatic variability and discharge in cycles of ~3-4 years and ~28 years (Coe *et al.*, 2002) which has important implications for any hydrodynamic floodplain processes where thresholds may be important. These more extreme flow conditions may be particularly important in modifying the spatial pattern of floodplain processes in the longer term through modification of existing flow paths across the floodplain.

2.3 Remote sensing

As well as better physical process representation, improving data resolution and quality has provided many of the advancements in the hydrological modelling studies discussed in the previous section. Improved data has primarily come through the rapidly expanding field of remote sensing. With a remote and large scale river basin like that of the Amazon, remote sensing comes into its own in terms of quantification. Along with more and better data, remote sensing has also provided a new set of tools and methods in its own right with which to study the Amazon River and floodplain. Whilst the range of application of remote sensing in the Amazon is broad and especially prolific, the focus here is on those studies that are directly relevant to the study of the main stem flood wave and its interaction with the floodplain.

Various instruments have been applied to the study of the water surface of the Amazon floodplain with varying degrees of success. Principally, these have been satellite radar altimetry, synthetic aperture radar and satellite imagery. Many of the instruments and missions were not specifically designed for observing flooding and have through happenstance and ingenuity been successfully applied to the study of flooding in the Amazon. Satellite radar altimetry, which was originally developed and optimised for the measurement of open ocean elevations, has the ability to monitor variations in surface water height (stage) for large wetlands, rivers, and associated floodplains and can provide data where traditional gauges are absent (Birkett *et al.*, 2002). Coverage can be limited by the wide spacing between tracks, which is typically hundreds of kilometres. For smaller rivers this is a severe limitation, but for the Amazon, which typically has river widths in the order of 4.5 km and floodplain widths of 60 km (Mertes *et al.*, 1996), these datasets have been useful (Campos *et al.*, 2001; Leon *et al.*, 2006; Zakharova *et al.*, 2006). Passive microwave systems have also been used for large areas of South America to study inundation patterns of major rivers (Hamilton *et al.*, 2002), but suffer from a relatively coarse resolution of 1/4 degree (~27

km). SAR from the JERS-1 which has a relatively fine spatial resolution of ~25 m, has also been used to map flood extents for many Amazon floodplain studies (Forsberg *et al.*, 2000; Rosenqvist *et al.*, 2002; Hess *et al.*, 2003; Melack *et al.*, 2004; Martinez and Le Toan, 2007). Another success of synthetic aperture radar is the Shuttle Radar Topography Mission (SRTM) flown in 2000. The SRTM mission used interferometric SAR to collect a globally consistent dataset of digital elevations covering 80% of the Earth's land surface at 30 m resolution (available for areas outside the US at 90 m). These data have been through extensive calibration and validation and are already revolutionising research in many locations, including the Amazon, where alternative sources of topographic data are limited (LeFavour and Alsdorf, 2005; Kiel *et al.*, 2006; Rossetti and Valeriano, 2007). Landsat Thematic Mapper (TM) imagery has also been used to map spatial patterns of hydrology, geomorphology and vegetation within the Amazon (Mertes *et al.*, 1993; Mertes *et al.*, 1995; Peixoto *et al.*, 2009).

2.3.1 Water elevation, slopes and volumes

Both satellite radar altimetry (profiling) and interferometric SAR imagery have been used to measure water elevations and elevation changes of wetlands in the central Amazon floodplain. The first general application of profiling altimetry methods employed for this purpose, date back to work by Morris *et al.* (1994a, 1994b) and Birkett (1995), and the first test of their potential in the Amazon was undertaken by Koblinsky *et al.* (1993) and Birkett (1998) followed by more detailed work by Campos *et al.* (2001). Interferometric SAR imagery methods were applied to the Amazon by Alsdorf *et al.* (2000, 2001a, 2001b). Many of these early studies focused on assessing the new methods and their applicability to the Amazon, rather than analysis of the flood wave itself. These pioneering studies found that the methods were generally suitable for the Amazon wetlands due to its spatial scale and the fact that the changes in the flood wave can be monitored usefully over weekly and monthly timescales. However,

the significant vegetation coverage and flat topography did cause some signal return problems with the methods resulting in data gaps, particularly at low water (Campos *et al.*, 2001). Virtual altimetry stations, defined where altimetry tracks crossed sufficiently large water bodies, provided data at ungauged locations with a common datum that was complementary to the *in situ* gauging stations. Errors were in the order of 0.5 to 1 m RMS, relative to the flood wave amplitude of 10-12 m. Interferometric radar provided measurements of relative water level changes in the floodplain with errors in the order of 1 cm (Alsdorf *et al.*, 2001b). These images showed that, in general, and over a period of 24 hrs, water level changes during falling water were greatest close to the Amazon mainstem and decreased with increased distance from the effects of the flood wave. Alsdorf *et al.* (2001a) point out that combining the high temporal resolution of altimetry (10 days for TOPEX-POSEIDON) and the blanket spatial coverage provided by SAR, should provide progress towards a complete mapping of water surface heights and variations during the flood wave throughout the Amazon Basin.

Birkett *et al.* (2002) was the first in-depth study of note to use altimetry to examine the overall dynamics of the Amazon flood wave. They used 7.5 years of radar altimetry from the TOPEX-POSEIDON mission, concentrating on 230 targets across the whole basin. They found that 1 km was the minimum river width that could be reliably measured and elevation accuracies ranged from 10 cm to 1.1 m. They also demonstrated that it was possible to use a number of these virtual gauges to measure the slope of the surface waters, which ranged from 1.5 cm/km at 700 km from the mouth of the Amazon to 4.0 cm/km at 4000 km upstream. Significant hysteresis behaviour was noted for the flood wave, and that this hysteresis varies along the main stem, and the derived altimetric velocity for the flood wave was estimated at 0.35 m/s for the full reach. The development of these methods and their application to the Amazon has continued with the demonstration of river discharge estimation using the virtual stations (Leon *et al.*, 2006; Zakharova *et al.*, 2006) and derivation of daily water stage data using interpolation with *in situ* gauges (Roux *et al.*, 2008). Interestingly, the

use of SRTM elevation data in a similar manner has identified similar water slopes and reasonable estimates of river discharge (LeFavour and Alsdorf, 2005). Getirana *et al.* (2009) show the utility of altimetry measurements when combined with hydrological monitoring of a sub-basin of the Negro River. Radar altimetry has also been used together with SAR flood mapping to derive flood volumes (Frappart *et al.*, 2005), which will be covered in the next section.

These recent altimetry studies add useful information regarding the macro-scale properties of the Amazon flood wave and provide essential measured corroboration for the findings from the hydrological models outlined earlier. They will also prove to be indispensable for the calibration and validation of future hydraulic models of the river and floodplain. However, due to limited spatial and temporal resolutions they still leave many questions to be answered, regarding the detail of the river and floodplain dynamics. In this regard, interferometric SAR data has recently been demonstrated to present new possibilities in terms of measuring the complexity of the dynamic floodplain water level changes (Alsdorf *et al.*, 2005; Alsdorf *et al.*, 2007a).

Alsdorf *et al.* (2005) used SAR and simple linear diffusion modelling of the flow paths across the Amazon, Purus and Negro floodplains to represent the collective behaviour of the water moving through and across multiple channels and lakes with flooded forests. This demonstrated the importance of capturing the temporal changes of water height across the floodplain and was aimed at improving the floodplain representation in coarse, continental scale water cycle models. Alsdorf *et al.* (2007a) used repeat pass JERS-1 SAR data to construct multi-temporal interferograms, showing water level change over a 44 day period at 200 m resolution for a floodplain area of around 4000 km^2. This was done for a mid rising stage and high water stage of the Amazon flood wave and also compared to data based on gauged river water levels interpolated along the river and assumed the same for the floodplain. A figure from the paper is reproduced in Figure 2-1 to illustrate the complex patterns of water level change across the floodplain and therefore the inferred complexity of the water

dynamics. The hydraulic interpretation of these patterns yielded the following important points: (i) timing and source of flooding is important to the pattern of inundation; (ii) the scroll bar topography and floodplain channels present a strong control during rising water; and (iii) at high water, patterns are simpler, implying less micro-topographic control of water flow at higher water levels. Despite these findings, there is still a need to explain how the topographic features control the flood dynamics and what scale of feature is important at different points through the hydrograph.

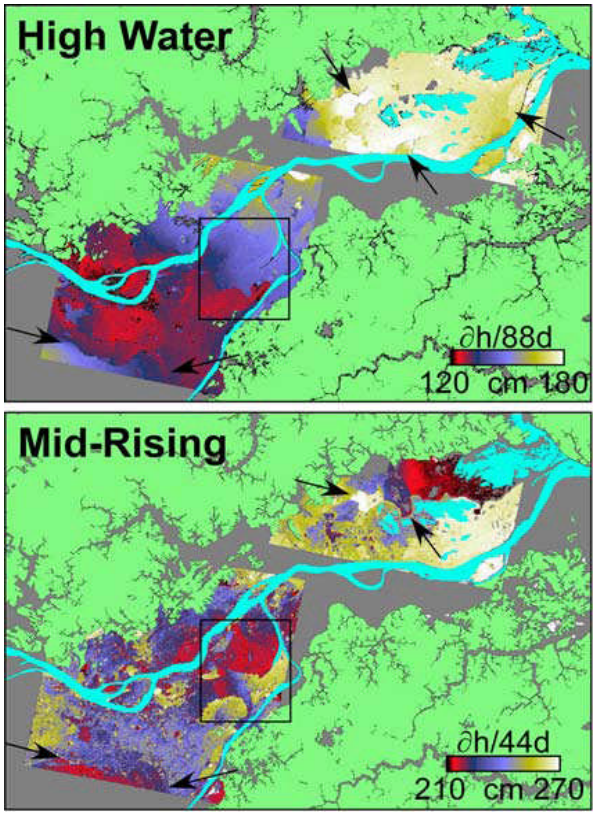

Figure 2-1 – Measurements of water level changes over a high water 88 day period and mid-rising 44 day period, reproduced from Alsdorf *et al.* (2007a). Light green colours are non-flooded upland, grey marks no data and light blue main rivers and permanent lakes.

2.3.2 Mapping flood extent, volumes, related geomorphology and vegetation

The possibilities of using remote sensing data for the purpose of mapping wetlands and their associated features were recognised in the early 1990s (Hess *et al.*, 1990) and its application specifically to the Amazon began soon after. These early

studies included airborne radar (Sippel *et al.*, 1992), and satellite microwave sensors (Sippel *et al.*, 1994; Sippel *et al.*, 1998) and SAR (Hess *et al.*, 1995). Results showed the value of these techniques for the purpose of determining the seasonally changing flood area of the Amazon floodplain and mapping of wetland vegetation types and features such as lakes. Sippel *et al.* (1998) showed how 9 years of data could be used to determine a simple relationship between flood extent and river stage with r^2 of 0.87, which was then used together with the 94 year stage record at Manaus to look at flood extent over the last century. Mertes *et al.* (1995) also mapped wetland vegetation types using Landsat TM images, and importantly also pulled together important research from published literature regarding Amazon floodplain dynamics which highlighted the importance of the hydraulic connectivity on the floodplain.

These mapping studies have continued as new instruments and extended data sets have become available (Hamilton *et al.*, 2002), and particularly from JERS-1 (Rosenqvist *et al.*, 2000; Costa *et al.*, 2002b; Hess *et al.*, 2003; Costa, 2004; Martinez and Le Toan, 2007; Toivonen *et al.*, 2007). Hamilton *et al.* (2002) demonstrated the complexity of the relationship between flood extent and river stage, highlighting the importance of rate of rise and recession of the flood wave. Hess *et al.* (2003) provided a comprehensive mapping of floodplain vegetation across the central Amazon and this showed that: (i) 17% of the 1.77 million km^2 studied was occupied by wetlands; (ii) 96% of the wetland was inundated at high water and 26% inundated at low water; (iii) half of the wetland was accounted for by floodplains and river channels; and (iv) 70% of the wetland was flooded forest. Costa (2004) determined flood durations of 300, 150 and 60 d/yr for primary colonisers (semi-aquatic vegetation), secondary colonisers (floodplain forest) and floodplain climax forest, respectively.

Extending these mapping techniques by combining them with altimetry and ground-based data is providing researchers with the tools to investigate the more dynamic aspects of flooding such as changing flood volumes and durations. Frappart *et al.* (2005) combined altimetric water level observations and inundation patterns to

determine water volume variations which showed that the water volume stored in floodplains cannot be inferred from the flood extent, and that the elevation of the flood cannot be inferred by its extent. Frappart *et al.* (2005) also showed that there appears to be significant geographical discrepancies in the way the flood extends with increasing water level, again highlighting the complexity of the dynamics. This hydrodynamic complexity may explain some of the variability in the simple relationship between flood extent and river stage used by Sippel *et al.* (1998). One of the drawbacks of combining extent mapping with altimetry, noted by Frappart *et al.* (2005), is the problem of a mismatch between the data acquisition date and event minima and maxima resulting in an incomplete picture of the processes. Martinez and Le Toan (2007) use the same method to look in more detail at the well studied Curuaí floodplain near Óbidos and extended the method to produce flood duration maps. The information regarding flood extent and duration derived from these methods is now being used to derive estimates for processes dependent upon the flood wave's influence, and especially of methane fluxes (Rosenqvist *et al.*, 2002; Melack *et al.*, 2004). Both of these studies emphasise the need for more detail and understanding regarding the floodplain dynamics in order to improve future estimates and they point to combining field measurements with modelling and remote sensing data as a potential solution.

The fields of geology and sedimentology have also benefited from remote sensing techniques in the Amazon, and sedimentology in particular, due to its close ties with hydrodynamics, has provided some key insights to current knowledge of floodplain dynamics. Geological studies provide important information regarding the history of the river and floodplain and therefore evidence of the long term changes in dynamics and processes that shape the basin. For example, Forsberg *et al.* (2000) use JERS mapping to demonstrate that tectonic faults exert a strong control on the wetlands distribution in the central Amazon floodplain. SRTM data have also been shown to be useful in reconstructing the evolution of the lower Amazon (Rossetti and Valeriano, 2007). As well as tectonic faults, geological troughs and changing sea levels

have also played their part in the history of the river, which is recorded in the sediment deposits across the basin (Mertes *et al.*, 1996). Mertes *et al.* (1996) draw on this geological history and use mapping of wetland features from radar images and radar altimetry to present a framework from which to understand the channel floodplain geomorphology of the river and floodplain. This important study divided the central floodplain into three reaches, each with a distinct geomorphology and linked the active processes to geological controls. Although the work by Mertes *et al.* (1996) provides some useful information on macro controls of the floodplain dynamics, ultimately the focus was on the sedimentology rather than the hydraulics. Landsat TM images have also been used in studying sediment movement in the Amazon, primarily because of the contrast between the optical properties of the sediment rich “white” water and sediment poor “black” water rivers. As well as providing quantification of sedimentation and erosion rates (Peixoto *et al.*, 2009), these sediment studies also show very clearly the importance of local rainfall and runoff to the flooding dynamics (Mertes *et al.*, 1993). Mertes (1997) goes on to define the area of mixing between the river and local water as the perirheic zone and demonstrates that for the Amazon, only part of the floodplain is flooded by the river, with significant areas of floodplain inundation being dominated by local water.

2.4 Direct measurement and field studies

In addition to modelling and remote sensing, direct measurement of processes is another tool that is aiding the understanding and quantification of the Amazon River and its floodplain dynamics. This is despite the difficulties of access and scale that present substantial sampling difficulties. These issues inevitably result in two categories of field study: the detailed study of one small area of floodplain; and the sparse sampling along large reaches of the Amazon. Both types of study have provided valuable advances in the knowledge of the systems at work in the central Amazon. In addition, field studies provide important validation data for the large modelling and remote sensing studies already outlined in Sections 2.2 and 2.3. Although there are many studies that touch on aspects of river/floodplain dynamics indirectly, the focus in the following subsections is on those studies that are most directly related to water movement.

2.4.1 River gauging stations

Gauging stations are the mainstay of the current understanding of surface water systems. They provide a good single point quantification of the flow in river channels, but comparatively little information regarding the flow of water once it is out of the channel. Indeed, the accuracy of the actual channel flow measurement at the gauging station also tends to suffer once flow is out of bank, as the flow is no longer confined to a channel with known hydraulic characteristics.

Observations of river stage (height) have been collected over much of the developed world's river basins for over half a century, however stream gauge network densities in the non-industrialised nations are generally much sparser. For example, the area surrounding Washington D.C. includes about 700 stream gauges, some on the Potomac River which has an annual average discharge of approximately 400 m^3/s.

The same sized area centred on Manaus in the central Amazon Basin includes about 10 gauges, and the Negro River with its approximately 40,000 m^3/s annual average flow, is almost completely ungauged. Essentially, the gauge density (expressed as number of gauges per unit discharge) in the Amazon is roughly four orders of magnitude less than for a typical area in the eastern United States (Alsdorf *et al.*, 2007b). This is one of the reasons why virtual stations derived from altimetry, discussed in Section 2.3, are so important in the Amazon.

Despite their sparsity, the gauges that are present have provided an important data resource for many Amazon studies. Richey *et al.* (1989b) used the long record at Manaus, dating back to 1903, to show how the discharge is linked to the El Niño-Southern Oscillation (ENSO) with oscillations on a 2 to 3 year timescale and Schongart and Junk (2007) extend this to look at predictability and the impact of climate cycles on the duration of flooding. A more recent study was carried out by Villar *et al.* (2009) at a more detailed regional level using 18 gauges across the Amazon basin. This study showed that despite both positive and negative runoff changes in different regions, downstream flows at Óbidos have remained relatively stable due to the integrating effect of the main stem. The significant impact of backwater effects on the dynamics of the mainstem was demonstrated by Meade *et al.* (1991) using gauged data and this in particular has important implications for the hydraulics of water movement in the channel and on the floodplain.

2.4.2 Floodplain lakes

Floodplain lakes cover a large proportion of the Amazon floodplain and are important ecosystems that have received significant attention in the field of limnology. Two particular lake complexes have received most of this attention: Lake Calado near Manaus and the Curuaí lake complex near Óbidos. Both sites' close proximity to population centres allows for easy access and also a more regular sampling regime.

Lake Calado is a ria lake, a drowned river valley, which are common along the periphery of the Amazon floodplain. Lake Calado is connected to the Amazon by a narrow channel cutting through a sediment bar deposited by the main stem across its mouth. Engle and Melack (1993) looked at the consequences of flooding on the floating vegetation in the lake. Findings showed the importance of abnormal flood years on the flood dynamic processes and that there were distinct phases to the flood cycle in terms of processes and water characteristics. The authors also underlined the need for detailed knowledge of both spatial and temporal hydrological conditions in order to understand the ecology of the floodplain. Lesack and Melack (1995) looked in more detail at the water balance of the lake and identified a net export to the river of three times the amount of water that entered the lake from the river during flood. They also showed that storage in the lake can allow water to be retained between annual flood cycles and that this can cause significant interannual variation in the dynamics. Lesack (1995) showed through measurement and water balance modelling that the interaction with ground water also plays an important role in the water balance of the lake.

The complex of interconnected lakes at Curuaí has been studied under the HyBAm (Hydrology and Geochemistry of the Amazonian Basin) research programme. Studies have used a combination of direct measurement, water balance modelling and remote sensing techniques to investigate and quantify the floodplain processes at work (Bonnet *et al.*, 2005; Bourgoin *et al.*, 2007; Bonnet *et al.*, 2008) and their effects on the geochemistry (Moreira-Turcq *et al.*, 2004; Barroux *et al.*, 2006; Maia *et al.*, 2009). This programme has added an important subset of knowledge regarding river-floodplain interactions and has corroborated many of the findings and hypotheses of earlier work in the Amazon. The Curuaí lakes are quite different from Lake Calado, and although these studies also found a net contribution from the lakes to the river, Bonnet *et al.* (2008) found that: (i) the flood water from the Amazon dominated (77%) the inputs to the lakes year round; (ii) rainfall, runoff and seepage accounted for 9%, 10% and 4% respectively of the total annual inputs; and (iii) the average residence time of water in

the lake was around three months. These studies demonstrate the importance and relative stability of floodplain channels connecting the river to the lakes and between the lakes themselves, and provide some of the few published measurements of a limited number of floodplain channels (Bourgoin *et al.*, 2007). Sediment rates across the lakes were found to be variable, highlighting again the heterogeneity of the dynamics (Moreira-Turcq *et al.*, 2004).

Also worth mentioning is a seepage study of a lake on a large river island by Cullman *et al.* (2006). This work used direct measurements of cation concentrations and balance modelling to quantify seepage influx. The authors then postulated a three phase model of seepage dynamics in the lake linked to the flooding phases: (i) an isolation phase at low water; (ii) a through flow phase at high water; and (iii) a drainage phase during falling water. Given the fact that the Amazon river islands are composed of coarser sediments than the wider floodplain, it remains to be seen if the same behaviour applies more widely.

2.4.3 Sediment studies

Sediment studies using direct measurements have contributed much to the current knowledge of the floodplain. Early work provides a general understanding of the controlling geology and history of the basin (eg Johnsson and Meade, 1990; Rasanen *et al.*, 1991; Quay *et al.*, 1992; Irion *et al.*, 1995). Dunne *et al.* (1998) drew on much of this earlier work and used a sediment budget model to calculate river/floodplain sediment fluxes for ten reaches of the Amazon mainstem. This study provides macro level detail of the sediment budget of the Amazon and characterised the reaches into net erosion, net deposition, or balanced reaches. More recent sediment studies have continued to provide detail on the geological history of the Amazon basin, for example: the effect of sea-level fluctuations on the lowermost Amazon hydrodynamics (Vital and Stattegger, 2000a; Vital and Stattegger, 2000b); and the effect of sediment movement

and backwater conditions on the long term evolution of the floodplain in the Negro river basin (Latrubesse and Franzinelli, 2002).

2.4.4 Ecology studies

While principally not directly measuring hydraulic parameters, ecological field studies can provide important clues as to the hydrological processes occurring on the floodplain and their importance to the ecology. If any floodplain hydrology research is to be of use in future ecology, and indeed geochemistry studies, it is important to understand how these processes relate to the dynamics and which parameters and what level of detail is important.

The migration of many fish species has been shown to be closely tied to the annual flood pulse (Tejerina-Garro *et al.*, 1998; Araujo-Lima and Oliveira, 1998; Petry *et al.*, 2003; Da Silva *et al.*, 2007; Castello, 2008). These studies show fish behaviour responds closely to depth of flooding and flow velocity. This work also highlights the importance of the floodplain channels in providing important access routes into the spawning and feeding grounds on the floodplain, as well as to the floodplain lakes for relative safety during low water.

Studies of macrophytes and phytoplankton in the floodplain show that biomass production closely follows seasonal changes in water nutrients and light availability (Junk and Piedade, 1993; Putz, 1997; Melack and Forsberg, 2001; Phlips *et al.*, 2008). Biomass production was shown to relate to water source and flood duration as well as depths and velocities. Durations and depths of flooding have also been shown to be important for the successional development of the floodplain forest (Worbes *et al.*, 1992; Wittmann *et al.*, 2004; Wittmann and Parolin, 2005; Wittmann *et al.*, 2006a; Wittmann *et al.*, 2006b). These different forest types provide a way of mapping hydrological conditions and recent sediment movement on the floodplain. Dense

vegetation will also have a significant effect on the hydraulics by increasing friction relative to the open channels (Gran and Paola, 2001).

2.5 Hydraulic modelling

The macro level hydrological and water balance models used in many of the studies outlined in Section 2.2 incorporate elements of hydraulics, often in a simplified form for the purposes of routing flow or estimating channel capacity or discharge. Hydraulic models provide a more direct simulation of the hydraulics of flows in channels and across floodplains by way of partial or full solution of the Saint Venant equations for open channel flow. These models are commonly used in a 1 Dimensional (1D) form, composed of a series of river channel cross sections, or a 2 Dimensional (2D) form comprising a regular or irregular grid representing a topographic surface, eg floodplain and channel. Coupled 1D/2D models are also used, with the river represented in 1D and the floodplain in 2D. Hydraulic models of this latter type have been in common use for some time now, particularly in assessing flood risk, but are now also becoming more widely used for environmental studies of rivers and floodplains (Bates *et al.*, 2005). Typically, the flow dynamics found on floodplains is very complex (Lewin and Hughes, 1980) and 2D models are particularly suited to representing these dynamics (Hervouet and Van Haren, 1996). They also have the potential to provide the parameters for studies of associated biogeochemical processes, including water depths, dynamics and flood duration.

The use of hydraulic modelling in the Amazon has, until recently, been limited due to a lack of topographic data with which to construct the models. A pioneering study by Mertes (1994) modelled a small area of approximately 1000 km^2 of the south bank floodplain near Manaus using a 500 m 2D grid to investigate sediment movement from the main channel into the floodplain. Due to the limited topographic data, which were taken from Brazilian Navy charts and field measurements, the floodplain topography was divided into only four categories: deep lakes, drainage channels, and shallow flows on forested and grass covered surfaces. Whilst the modelled

sedimentation rates showed reasonable agreement with field measurements they were still described as order of magnitude estimates only.

Most recently, Wilson *et al.* (2007) demonstrated the feasibility of applying 2D hydraulic modelling techniques to a large 30,000 km^2 area of the Amazon River and floodplain, at a ~270 m resolution. This work was made possible by newly available remote sensing data sets and computationally efficient hydraulic models capable of tackling the large spatial areas involved. The integration of remote sensing data with hydraulic modelling has been demonstrated as a useful technique for improving understanding of floodplain processes (Bates *et al.*, 1997). Wilson *et al.* (2007) used digital elevation data for the Amazon basin from the SRTM in February 2001 (Rodriguez *et al.*, 2006) and other remote sensing calibration datasets for water levels from radar altimetry and flood extent from SAR. The work utilised the LISFLOOD-FP hydraulic model, which was introduced to address the need to model larger domains with computational efficiency, as well as to allow the use of now more commonly available, and highly detailed, digital elevation data. LISFLOOD-FP is a coupled 1D/2D hydraulic model based on a raster grid and flooding is treated using an intelligent volume-filling process based on hydraulic principles that satisfy key physical notions of mass conservation and hydraulic connectivity (Bates and De Roo, 2000).

The Wilson *et al.* (2007) model was constructed for a 240 by 125 km area using a 1D kinematic channel of a ~260 km reach of the Solimões River with one major tributary, the Purus. Bathymetric data for the channels was collected by field survey using a boat mounted sonar. The 2D floodplain used SRTM data which had been processed with a first-order correction to remove vegetation artefacts, based on a habitat classification (Hess *et al.*, 2003) and field measurements of vegetation heights. Calibration and validation used a mixture of the gauged main channel water level record, satellite altimetry for floodplain elevations and JERS-1 SAR images processed to yield flood extent at approximately high and low water periods. Results at high water showed a good fit (72%) to the SAR derived flood extent but a poor fit at low water

(23%). The poor low water results were thought to relate to incomplete drainage of the floodplain resulting from errors in the topographic data as well as omission of floodplain hydrodynamic processes. The use of a kinematic channel solver limited the full use of the collected bathymetric data and also raises questions of applicability in an area dominated by backwater. Additionally, the use of a fixed timestep of 20 s for the 2D solver, for computational efficiency reasons, affects the modelled dynamics on the floodplain, as demonstrated by Hunter *et al.* (2005). Nonetheless, despite these issues, the work represents a step forward in attempts to simulate the complex dynamics of the river and floodplain at this scale and resolution, and is the first application of a hydraulic model at this scale, an order of magnitude bigger that anything previously attempted. Importantly, the Wilson *et al.* (2007) study simulated a full 12 month low to high water cycle of the Amazon flood wave rather than just the peak of the flood event which is the more common practice in general hydraulic modelling of rivers. Simulating the full cycle is an important step to understanding the full dynamics of the Amazon flood wave as it potentially allows the complete floodplain filling and draining processes to be accounted for.

2.6 Summary

This review of the existing body of knowledge shows that there are many important processes at work controlling and influencing the hydrodynamics of the Amazon River and floodplain, leading to a complex topography across very large areas. These include, but are not limited to: interannual variability of water levels; decadal climate cycles; long-term geological history; sediment erosion and deposition; vegetation coverage and succession; influence of local rainfall and runoff inputs; and a multitude of floodplain channels interacting with more diffusive overbank flows.

Several tools have been used to study these complex dynamics, with knowledge contributions related to each method's strengths. Hydrological models have provided a method for studying the macro level response of the basin and sub basins to climate cycles. They are of limited use for studying floodplain dynamics as they do not explicitly model floodplain processes, but may provide a means of quantifying important local rainfall and runoff inputs. In the future, large scale hydrological modelling may also provide a link between global climate models and floodplain processes models for the purposes of studying the impacts of climate change. Remote sensing has contributed much to recent advances in measuring and quantifying processes on the floodplain as well as providing build, calibration and validation datasets for modelling purposes. Temporal and spatial characteristics of the instruments still limit identification of the full detail of floodplain processes, but this may change as new missions are launched. Detailed field work at several sites in the Amazon floodplain is providing important details of the floodplain fluvial processes and their links with dependent biogeochemical processes. Being confined to specific study locations can make it difficult to apply the results basin wide, but integrating findings with wider scale modelling and remote sensing mapping can overcome this to some extent, especially as a wider variety of sites are studied. Hydraulic modelling shows great potential for simulating the hydrodynamics of the floodplain and therefore

providing wide scale water depth, velocity and flood duration quantification. Hydraulic modelling can also be used as a predictive tool to study possible future changes. However, its application in the Amazon is very recent and crucially its success will depend on how well it represents those hydrodynamic processes.

As well as a basic need to elucidate the science underpinning hydrodynamic processes, as was identified in Chapter 1, it is also very important to be able to quantify these processes in order to make advances in related biogeochemistry studies. The findings outlined in this chapter provide some details regarding these floodplain processes, but also raise many questions, particularly related to the hydraulics of the flows, that as yet remain unanswered. For example, how do main river channel properties affect the passage of the flood wave, particularly given the very significant movements of sediment in the main channel? What is the relative importance of the flow carried by floodplain channels to diffusive overbank flow and does it change significantly with interannual and climatic variability? What level of detail is required for hydraulic modelling to represent these processes well? In addition, no one has yet attempted to integrate the many details discovered so far in order to present a detailed conceptual framework of the process dynamics for the majority of floodplain types found within the central Amazon main stem floodplain.

2.7 Thesis objectives and outline

2.7.1 Thesis objectives

The overall aim of the research presented in this thesis was to investigate the detailed hydrodynamic behaviour of the Amazon River and its floodplain, in order to better understand its functioning, ultimately providing the beginnings of a coherent, evidence based, conceptual framework to inform future research. In order to draw on the strengths of the different investigation methods available, a synthesis of field survey, gauging station data, remote sensing data analysis and numerical modelling was used. The detailed objectives required in order to achieve this aim were:

1. Identify the basic hydraulic characteristics of the Amazon flood wave and the importance of the main channel morphology using flood wave characterisation techniques and detailed 1D hydraulic models.
2. Investigate floodplain hydraulic connectivity and how important the floodplain channels may be to the overall hydrodynamics of the floodplain, using Landsat Thematic Mapper images to identify and characterise the floodplain channels and experiments with samples of the floodplain topography to explore the representation of the floodplain channels within a digital elevation model (DEM).
3. Use field measurements of morphological properties of a range of representative floodplain channels at high water to identify what the depth and width of channels is related to and if there is a representative relationship between width and depth that can be used more widely.
4. Set out a conceptual framework of the main hydraulic processes governing the hydrodynamics in the main channel and on the floodplain using the results from the first three objectives together with key information already identified by previous studies.

2.7.2 Thesis study area

Given that the aim of this thesis was to investigate the detailed hydrodynamics of the river and floodplain, it was necessary to limit the spatial scope to maintain practicality, especially given the scale of the floodplain. Yet, for the findings to be applicable across the whole floodplain, it is important that the study area is representative of the variations found along most of the Amazon mainstem. Mertes *et al.* (1996) noted that the main stem could be divided up into three distinct zones of differing channel-floodplain geomorphology, controlled by river slope and sediment transport. While the upper reach is dominated by scroll bar topography and differs significantly from the lower reach with its large shallow lakes, the middle reach combines both of these sets of features making it an ideal area in which to base this study. Many of the previous studies outlined above have also chosen this area for these reasons, as well as for the practicality of the close proximity of Manaus, the capital city of the Brazilian state of Amazonia. The study area selected was the same as for the Wilson *et al.* (2007) hydraulic modelling work. This was to allow a direct comparison of the results of hydraulic model improvements here with the Wilson *et al.* (2007) model and to allow use of the large amount of data collected for the Wilson *et al.* (2007) model, in particular the bathymetric data for the main channel which were not available anywhere else on the Amazon. This location also has the benefit of including the Purus tributary which allowed confluence dynamics to be considered.

The study area is shown in Figure 2-2 and centres on the Solimões and Purus confluence upstream of Manaus. The total area of 30,000 km^2 covers a significant portion of the central mainstem floodplain and includes many of the general features found in the wider floodplain. A 285 km reach of the Solimões (Amazon River) passes from west to east through the study area and a 107 km reach of the Purus tributary flows from the south to join it in the centre.

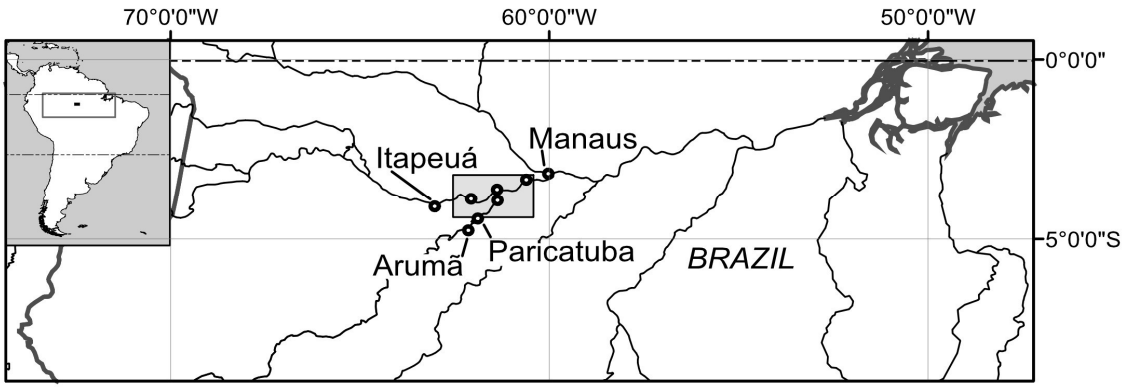

Figure 2-2 – Location overview, showing the study area centred on the Solimões River and Purus River confluence. The study area is located between the city of Manaus and the town of Itapeuá on the Solimões, and the town of Arumã on the Purus. Circles indicate population centres.

2.7.3 Thesis outline

Figure 2-3 shows a diagrammatic outline of the thesis structure. There are three main research chapters, relating to objectives 1 to 3 above, each using a different approach to investigate the river and floodplain hydrodynamics. The following chapter, relating to objective 4, draws together the findings from these preceding chapters together with the relevant published work identified in this chapter in order to present a conceptual framework of the river and floodplain hydrodynamic processes.

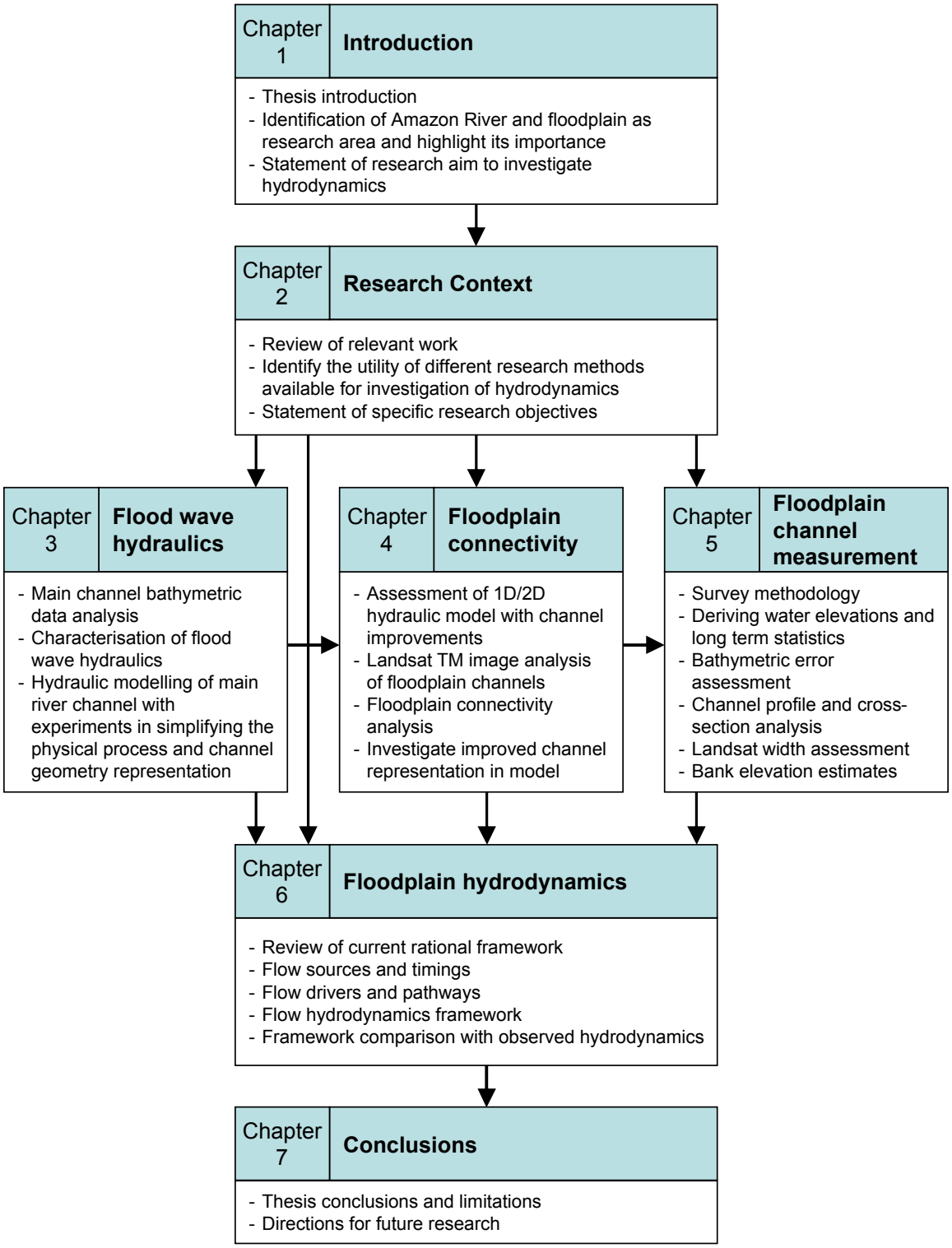

Figure 2-3 – Thesis structure

CHAPTER 3
Flood wave hydraulics

3.1 Introduction

From Chapters 1 and 2 it can be seen that the monomodal flood wave is the main driver for the hydrological system that is the Amazon River and floodplain. Therefore, a fundamental understanding of the hydraulic properties of the flood wave and its propagation down the Amazon are essential to the study of the river system's hydraulics. Hydraulic modelling has the potential to provide a level of detailed information regarding flood duration and depth for the Amazon River and floodplain that will enable a host of other research on processes that depend upon these important variables. The accuracy of results from hydraulic modelling depends heavily on the application of appropriate hydraulic methods to the study of a river system's hydraulics, as well as an appropriate level of topographic and bathymetric detail to enable the model to represent the processes being modelled.

Unfortunately, there are very few studies that provide information related specifically to the hydraulic characteristics of the Amazon flood wave. Of the studies to date, some of the most significant are those of Meade *et al.* (1991) and Alsdorf *et al.* (2005). Meade *et al.* (1991) used analysis of the stage-discharge behaviour of river gauging stations to demonstrate the extensive backwater effects along the main stem. Alsdorf *et al.* (2005) used linear diffusion modelling to characterise floodplain flow, showing that the water elevation from the main channel propagates across the floodplain as a diffusion wave.

Remote sensing data have provided insights into the variations of surface water height and flood extents of the rivers and wetlands in the basin and so provide a wealth of calibration and validation datasets for hydraulic modelling. In particular, satellite

radar altimetry (Birkett *et al.*, 2002), passive microwave systems (Hamilton *et al.*, 2002) and synthetic aperture radar (SAR) data (Alsdorf *et al.*, 2000; Rosenqvist *et al.*, 2002; Hess *et al.*, 2003; Melack *et al.*, 2004) have all been used to quantify variations in the Amazon River and floodplain surface water extent and elevation. However, a limitation of the use of many remote sensing methods in hydraulic modelling is the inability of the optical or radar signal to penetrate the water surface, thus providing little or no bathymetric detail for the main river channels and floodplain channels. Bonnet *et al.* (2008) demonstrated that it is possible to use a time series of SAR images (Martinez and Le Toan, 2007) to map periodically flooded areas of floodplain, but this study still required bathymetric data collected by acoustic doppler current profiler (ADCP) for the permanently flooded areas such as the channels.

While some bathymetric data are available for isolated gauging stations and localised study areas, partly due to the Amazon's scale and the fact that sediment dynamics play an active role in shaping and reshaping the channel (Mertes, 1994, Mertes *et al.*, 1996, Dunne *et al.*, 1998), there is no consistent up-to-date bathymetry dataset for the Amazon channel. This lack of data is commonly tackled by applying simplifications such as using channels with mean widths and slopes (Wilson *et al.*, 2007) or by using old shipping charts and assumptions about bed slope (LeFavour and Alsdorf, 2005; Leon *et al.*, 2006). Satellite missions which seek to derive discharge from space, such as the proposed Surface Water and Ocean Topography (SWOT) instrument, must also rely on assumptions regarding the bathymetry data and this has been identified as a potentially significant source of uncertainty for such undertakings (Durand *et al.*, 2008).

In this chapter, the relative importance of these bathymetric issues for hydraulic modelling and other studies on the central Amazon River channel is identified. This was achieved in two stages. First, using channel bathymetry data collected by Wilson *et al.* (2007) for a 430 km reach of the Amazon (Solimões) and a 145 km reach of its tributary, the Purus (Figure 3-1), a study of the Amazon channel flow was undertaken

in order to understand the basic hydraulic characteristics of the Amazon flood wave. As well as providing key hydraulic properties, this ensured a sound theoretical basis for the correct application of hydraulic models to the main channel. The bathymetric data provided a level of information of a consistent standard for analysis that has not been previously available for the main channel. Second, the hydraulic properties and understanding derived from the bathymetric data were used to construct detailed 1-dimensional (1D) hydraulic models of the Amazon and the Purus main channel. These 1D main channel models explicitly exclude the floodplain based on the hypothesis that for this reach, with its relatively narrow floodplain (Section 1.3), the effect of the floodplain system on the flood wave is only minor. Experiments were then undertaken with these models to see the effect of simplifying the physical process and channel geometry representation on flood wave routing by comparing model results to independent water surface elevation data derived from ground gauging stations and satellite radar altimetry.

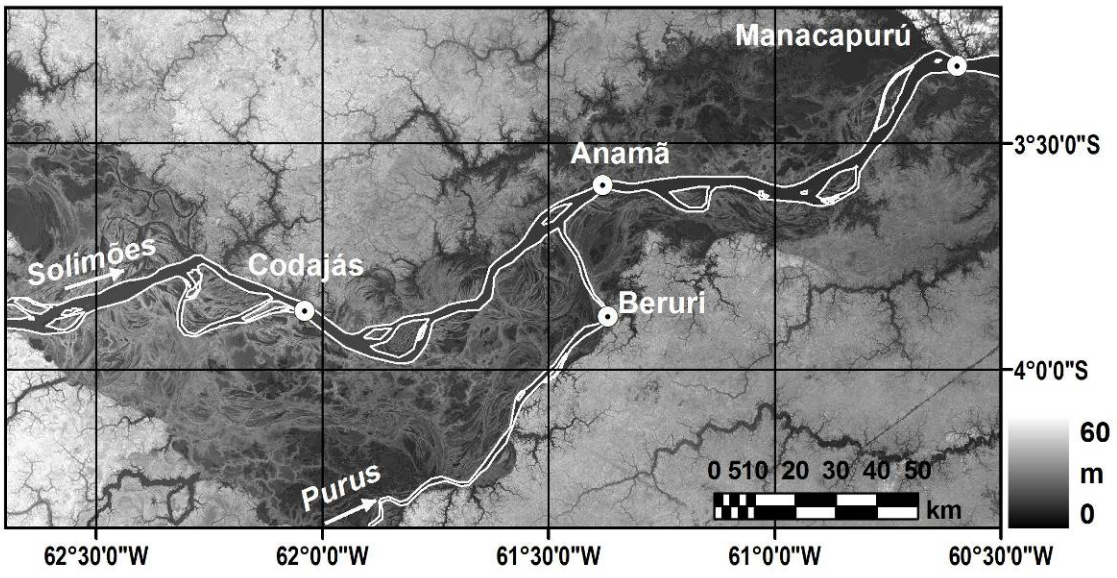

Figure 3-1 – Study site centred on Solimões and Purus confluence, showing the river channels with background SRTM DEM, and the locations of available river stage data (Manacapurú, Anamã, Codajás and Beruri gauging stations). See Figure 2-1 for location overview.

The work presented here addresses four key questions. Firstly, what are the basic hydraulic characteristics of the Amazon flood wave? Secondly, how important is the floodplain to the passage of the flood wave in the main channel? Thirdly, what is the simplest physical and geometrical representation of the channel flow that can be used in hydraulic models and still have predictions of water levels match available observed data? Fourthly, how important are the changing bed conditions to the overall hydraulics of the channel flow? Understanding the answers to these questions will enable appropriate assumptions to be made regarding flow modelling where limited data are available for the central Amazon channel and floodplain.

The work detailed in this chapter has been published recently in the Journal of Hydrology (Trigg *et al.*, 2009). The LISFLOOD-FP diffusive channel solver developed in this chapter for modelling the Amazon flood wave has also been applied to the Ohio River (Durand *et al.*, in press).

3.2 Channel bathymetry

3.2.1 Bathymetric data collection and interpolation

Bathymetric data provides essential first order parameters for the study of a river's hydraulics or the application of hydraulic modelling to a river. In this section bathymetric data collection undertaken by Wilson *et al.* (2007) along the Solimões River channel and one of its tributaries, the Purus, is described. This data collection was necessary as there were no up-to-date data available at the level of detail required for hydraulic analysis. Sonar data were collected between the 8th and 21st June 2005, just after the high water peak, using a Lowrance sonar connected to a GPS unit fitted to a small boat. The total distance surveyed was around 1900 km over 14 days, along a 430 km reach of the Solimões between Manaus and Coari and a 145 km reach of the Purus beginning at the confluence with the Solimões and ending just downstream of Arumã. A total of 234,863 sonar data points were collected for the Solimões and Purus reaches.

The survey route was chosen such that diagonal rather than perpendicular cross sections were obtained, which allowed the coverage of extensive reaches relatively quickly so that as much detail of the whole channel as possible was collected, rather than just the representative cross sections normally required for hydraulic modelling. The aim was to create as complete a three dimensional channel as possible in order to select later the required cross sections as well as increase potential utility of the resulting data. The final collection path is shown in Figure 3-2. All branches of the main channel were surveyed as well as a section of one of the main floodplain channels.

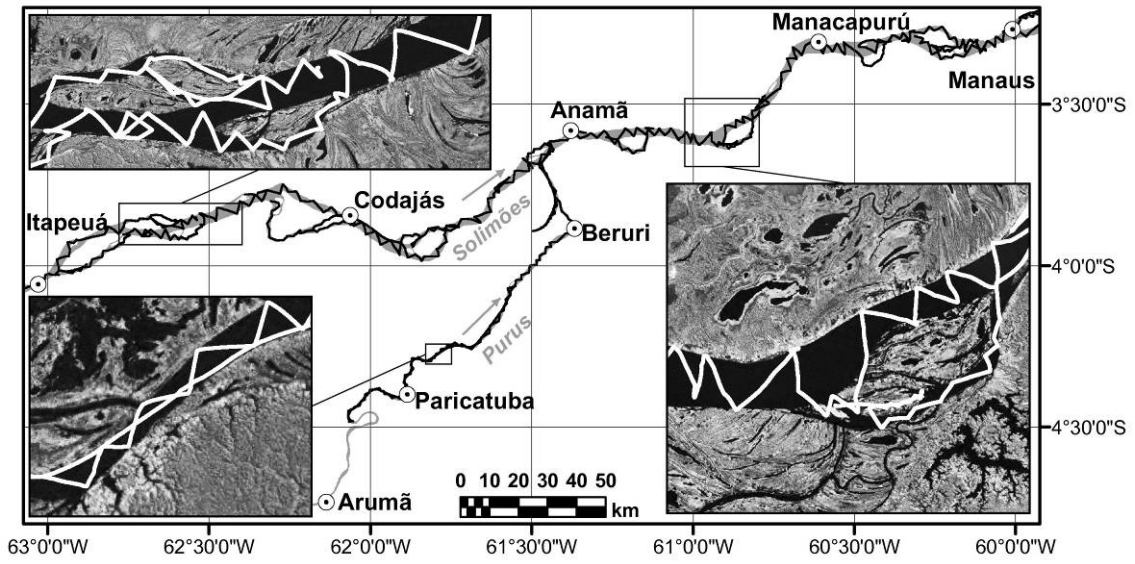

Figure 3-2 – Sonar collection route showing three larger scale insets.

Sonar depths were converted to bed elevations using a planar water surface as a reference, fitted to the mean stage records from Itapeuá and Manacapurú for the survey period. During the 14 day period of the survey, stage elevations changed by 10 cm at Itapeuá and 23 cm at Manacapurú, and given that the measured channel depths were between 16 and 52 m, this error was considered minor and not corrected for. All gauged data were tied to a common elevation datum which uses a geiod model (Kosuth *et al.*, 2006). The resulting bed elevations were then sampled onto a triangular irregular mesh representing the channel, and then interpolated along the river channel to maintain an approximately prismatic channel form. Interpolation along the channel reduces the bias that would be introduced by standard 2D interpolation which would result in shallower channel centre elevations due to the bias of the river banks in the interpolation. The irregular mesh topography was then sampled back to a 90 m grid.

Errors in the bathymetric grid are difficult to quantify, but are likely to be acceptable for hydraulic modelling. For this sonar-GPS method they are likely to be of the order of 1 m or less (Kvernevik *et al.*, 2002), an order of magnitude less than low flow depths (~10 m). The sonar unit was factory calibrated and signal returns provided a clearly defined bed throughout the main channel and so provided accurate depth

measurements. The principal source of error is the uncertainty in the water surface elevation used to convert depth measurements to bathymetric elevation. The spatial sampling of the survey was found to capture the large scale bed structures which were thought most likely to affect the hydraulics. Bed forms too small to be captured by the sampling, are likely to be short lived in a mobile bed channel, and therefore dependent on when the data are acquired. Moreover, such features will also have smaller height variability than the large scale structures and are therefore likely to have only a minor impact on the flow.

3.2.2 Bathymetric data analysis

The 90 m bathymetry grid interpolated from the sonar data is shown for the model domain in Figure 3-3. The resulting channel structure shows deep pools from 5 to 10 km in length where the river is narrow and extensive areas of relatively shallow topography where the river is wide. During high water, the pools can be up to 50 m deep in places. The mean amplitude of the bed undulations is around 20 m. The river bed is known to be mobile with significant channel migration and the scale and impact of these factors on the development of the floodplain geomorphology has been studied in detail by Mertes (1994), Mertes *et al.* (1996) and Dunne *et al.* (1998).

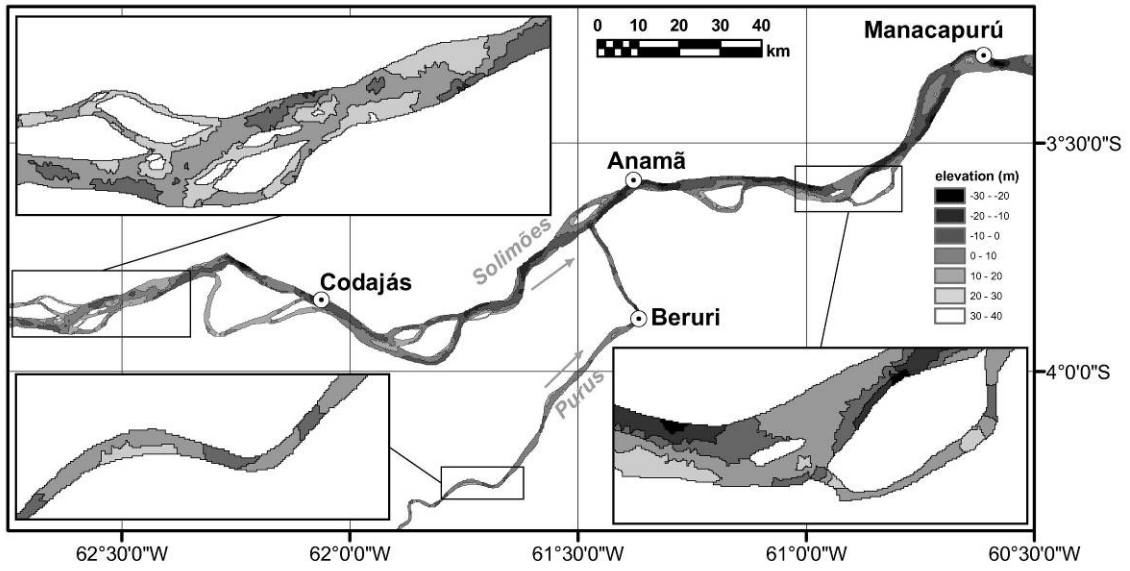

Figure 3-3 – 90m bathymetry elevation grid, with three insets. Elevations shown as 10m interval contours for clarity.

For the Solimões reach, the channel width varies from 1620 m to 5624 m with a mean of 3711 m and the minimum bed elevation varies from -26.45 m to 8.03 m with a mean of -8.44 m, based on the Kosuth *et al.* (2006) datum. This means that significant portions of the channel are well below sea level even though the centre of the study location is approximately 1500 km inland (a third of the Amazon River's total length), which further illustrates the extraordinary nature of the Amazon River and also explains the very shallow water slopes. At high water, channel depths range from 20 m to 52 m. For the Purus reach, the channel width varies from 600 m to 1678 m with a mean of 1114 m and the minimum bed elevation varies from -9.78 m to 9.48 m with a mean of 2.08 m. At high water, channel depths range from 16 m to 35 m.

3.3 Flood wave characterisation

3.3.1 Characterisation methods

Understanding the hydraulic characteristics of the flood wave and properties of a river are important for the application of appropriate modelling methods and boundary conditions in any hydraulic study. Using the bathymetric data collected by Wilson *et al.* (2007), described in the preceding section, it was possible to quantify key parameters for the Amazon flood wave and to apply standard techniques to characterise the flood wave hydraulics.

The propagation of river waves within river channels is described by the full 1D Saint Venant equations. These describe unsteady flow in an open channel using equations for mass and momentum conservation. Solving these equations is non-trivial and a number of simplifications have been shown to be appropriate under certain flow conditions. It may also be advantageous to use such approximations where speed of execution is a requirement or where limited data are available, both being applicable to modelling of the Amazon River.

The unsteady spatially varying momentum equation arranged in a form normally used to illustrate the three common approaches used in simplifications of the Saint Venant equations for flood routing, is:

$$S_f = S_0 - \frac{\partial y}{\partial x} - \frac{u}{g}\frac{\partial u}{\partial x} - \frac{1}{g}\frac{\partial u}{\partial t} \qquad (3\text{-}1)$$

where, S_f is the friction slope, S_0 the bed slope, y is the depth, x the distance along the river, u the velocity averaged over a cross section, t time and g the acceleration due to gravity (9.81 m/s^2). The two most common approximations are the kinematic wave

approximation which is represented by the first right hand side term, and the diffusive wave represented by both the first and second right hand side terms.

Two methods for characterising the hydraulics of the Amazon were identified and applied to the Amazon flood wave. The first of these was developed by Vieira (1983). This method derives from an extensive numerical analysis comparing different approximations of the Saint Venant equations applied to a range of hydraulic conditions. The non-dimensionalised parameter space defined by F_0, the Froude number and k, the kinematic wave number is divided up into zones where the various approximations were found to be valid. Application of this method is straightforward and involves estimating the two parameters, F_0 and k, and identifying the valid approximation that applies. The formulations of the two parameters used by Vieira that were applied in this analysis are:

$$F_0 = \frac{V}{(gy)^{1/2}} \quad \text{and} \quad k = \frac{S_0 L}{y F_0^{\,2}} \qquad \text{(3-2) (3-3)}$$

where, V is the mean flow velocity, L channel length.

The second method used was developed by Moussa and Bocquillon (1996) who based their analysis on the concept that river wave behaviour is determined by the balance between friction and inertia. Small perturbation analysis of wave propagation on steady uniform flow was then used to determine parameter ranges representing each wave type. Again two parameters are used; F_0^2, the square of the Froude number of the unperturbed condition and T+, the non-dimensionalised period. Equations 3-4 and 3-5 show the formulations for these parameters:

$$F_0^{\,2} = \frac{V_0^{\,2}}{g y_0} \quad \text{and} \quad T+ = \frac{T V_0 S_{f0}}{y_0} \qquad \text{(3-4) (3-5)}$$

where, V_0 is the velocity of the unperturbed condition, y_0 depth of flow of the unperturbed condition, T is the period of perturbation and S_{f0} the friction slope of unperturbed condition.

3.3.2 Hydraulic characteristics

Henderson (1966) classified a shallow wave as one where the ratio of water depth to wave length is usually less than 0.05. For the Amazon flood wave, the depth of flow is between 20 and 30 m, with an annual wave length resulting in a ratio of approximately $3x10^{-5}$. The shallow wave description assumption is therefore appropriate.

For application of the characterisation method of Vieira (1983) and that of Moussa and Bocquillon (1996), estimates of the parameter values for the Amazon channel were made using the bathymetric data described in Section 3.2 and mean annual low and high water data from Itapeuá and Manacapurú gauging stations, obtained from the Hidroweb website of the Brazilian National Water Agency (ANA). A summary of the key parameter values for the Solimões and Purus reaches are presented in Table 3-1 and results of the characterisation methods for the Amazon flood wave, using high water conditions, on the Solimões are presented in Table 3-2.

Table 3-1 – Summary of key parameter values for the Solimões and Purus reaches

Parameter	Description	units	Solimões Low Water	Solimões High Water	Purus Low Water	Purus High Water
V	mean velocity	*m/s*	0.77	1.30	0.26	0.86
y	mean depth	*m*	21.91	33.50	10.93	23.13
S_0	mean bed slope	*cm/km*	4.96	4.96	6.50	6.50
S_f	mean water slope	*cm/km*	2.92	2.90	1.00	1.66

Table 3-2 – Characterisation analysis results

Parameter	Description	Value
F_0	Froude number	0.0524
k	kinematic wave number	82.7
F_0^2	Froude number squared	0.0027
T+	non-dimensionalised period	32.3

Both characterisation methods use plots of the parameter space divided into zones where different approximations are appropriate. The results in Table 3-1 are plotted on these characteristic plots in Figure 3-4 and Figure 3-5. It should be emphasised that these results were derived from estimates and assumptions relevant to the central section of the Amazon considered in this study, but none-the-less provide an important insight into the overall hydraulic characteristics of the Amazon flood wave.

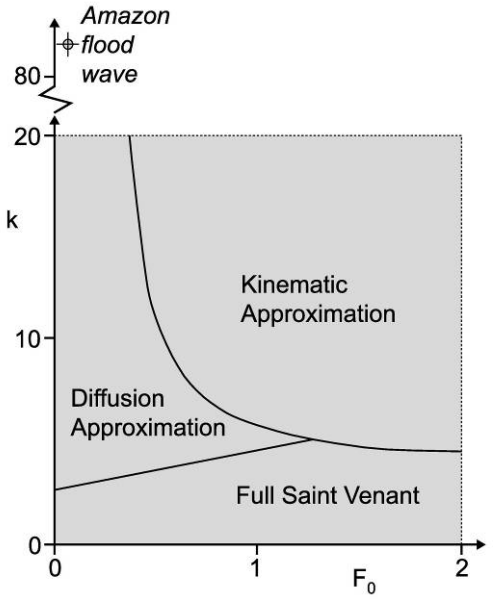

Figure 3-4 – Extended plot after Vieira (1983) showing the parameter values for the Amazon flood wave.

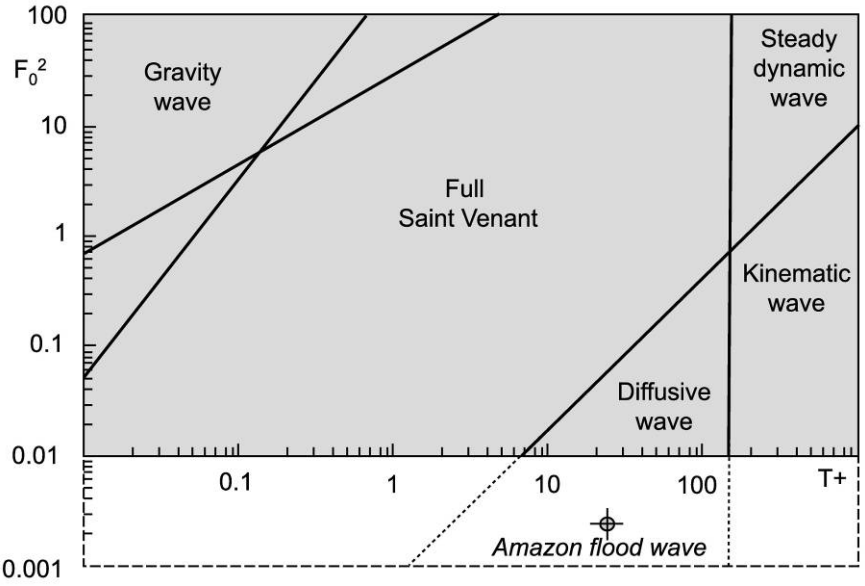

Figure 3-5 – Extended plot after Moussa and Bocquillon (1996) showing the parameter values for the Amazon flood wave.

The results of both characterisation methods place the Amazon flood wave in the zone where a diffusive approximation is valid. Flow in the channel is entirely in the subcritical range. Of particular interest in these results is the relatively extreme nature of the values derived for the Amazon compared to those more commonly encountered in typical rivers. This is illustrated by the fact that both characteristic plots have had to be extended well beyond the range originally envisaged by their creators as being sufficient for most flood waves. This limitation of existing methods applied to the Amazon has also been noted by Latrubesse (2008), who classifies the Solimões at this location as an “anabranching mega river”.

In general terms, the flow is relatively slow moving and deep, resulting in a very low Froude number. The Froude number is the ratio of inertia and gravitational forces and is the hydrodynamic equivalent of the Mach number. It is the ratio of the characteristic velocity of the flow (V) to the characteristic flood wave propagation velocity (c). In other words, when F_0 is equal to one, the velocity of the surface wave and that of the flow is the same, a condition known as critical flow. When F_0 is less than one, the flow velocity is smaller than the velocity of the flood wave travelling on the

surface and flow is considered to be subcritical, with gravitational forces dominant. When F_0 is greater than one, the flow is supercritical and inertial forces are dominant. Low slopes on the Amazon mainstem result in very low inertia forces and hence low flow velocity compared to the gravitational forces represented by the relatively deep flow conditions in this central reach.

The kinematic wave number (k) can be defined as the product of the ratio of elevation differences between low and high points in a reach to the flow depth times the inverse Froude number. Although low slopes on the Amazon main stem mean the ratio of elevation differences to flow depth is not particularly high, because F_0 is so low, this results in a relatively high kinematic wave number.

The friction slope S_f, also known as the energy surface slope, is the rate of energy head loss due to friction. Under uniform flow conditions with no temporal variation, the friction slope is parallel to the water surface and to the river bed. For the Amazon mainstem, friction slopes are extremely mild and interestingly both the Solimões and Purus friction slopes are shallower than their mean bed slopes, particularly for the Purus, indicating the potential importance of backwater effects on both reaches.

3.4 Hydraulic modelling

3.4.1 Model choice and development

LISFLOOD-FP was chosen for the initial modelling work carried out on the Amazon by Wilson *et al.* (2007), since it was developed to provide rapid calculation for large 2D domains (Bates and De Roo, 2000). For the research presented in this chapter, LISFLOOD-FP was further developed as part of an overall aim to understand better the complex river and floodplain hydraulics of the Amazon and to provide information on water surface dynamics required for ecological and biogeochemical studies.

LISFLOOD-FP consists of a 1D river channel, composed of a chain of cross sections perpendicular to the river, coupled to a 2D floodplain represented by a bare earth digital elevation model (DEM). Hydrodynamic channel flow is represented using the kinematic approximation to the full 1D Saint Venant equations solved using a fully implicit Newton-Raphson scheme and 2D floodplain flows are treated using a storage cell approach implemented for a raster grid to give an approximation to a 2D diffusive wave (for a complete description see Bates and De Roo, 2000, and Hunter *et al.*, 2005).

Detailed 1D hydrodynamic models were constructed using the bathymetric data and the results of the flood wave characterisations and these models were used to undertake an analysis of the main river channels, without floodplains, to ascertain the relative importance of the floodplain, bathymetric data and the process representation. The floodplain was explicitly excluded from the model in order to identify how important the effect of the floodplain volumes are to the passage of the flood wave.

In order to incorporate more fully the complexity of the channel found in the bathymetry data, and to incorporate expected backwater effects identified by Meade *et al.* (1991), as well as allowing for the diffusive character of the flood wave identified in

the preceding section, a hydrodynamic diffusive wave 1D channel solver for LISFLOOD-FP was developed. This enabled a more complete representation of the channel hydraulics and boundary conditions, while minimising any significant increase in computation time and potential decrease in stability for a full 1D/2D coupled Amazon model. In this chapter, only the 1D component of LISFLOOD-FP was used (the main channel), while the 2D component (floodplain) is explored in Chapter 4.

In developing a diffusive solver for LISFLOOD-FP, it was important to obtain a stable and fast implementation that adapts easily to LISFLOOD-FP's 1D/2D coupled structure. An early version of LISFLOOD-FP had a limited diffusive solver implementation, but this had only been validated for two flood events on a single reach of the river Severn, UK (Horritt and Bates, 2002). However, it had proved stable and straightforward to use and thus was adopted and further developed and tested for this research. The solver was rewritten to allow a wider variety of user-definable boundary conditions, expanded to allow full multi-branching river networks and a decoupled 1D/2D timestep was implemented, in which separate time steps can be specified for the 1D and 2D model components. Specifically, for this chapter, these developments allowed the construction of a 1D LISFLOOD-FP hydrodynamic model of the Amazon main-stem (without floodplains) and the Purus tributary with a downstream stage hydrograph boundary condition.

The one-dimensional diffusive approach to channel flow is capable of capturing the downstream propagation of a flood wave and the response of flow to free surface slope, and can be described in terms of continuity and momentum equations, presented below in the form used in the LISFLOOD-FP solver:

$$\frac{\partial Q}{\partial x} + \frac{\partial A}{\partial t} = q \tag{3-6}$$

$$S_0 - \frac{n^2 P^{4/3} Q^2}{A^{10/3}} - \left[\frac{\partial y}{\partial x}\right] = 0 \tag{3-7}$$

where, Q is the volumetric flow rate in the channel, A the cross sectional area of the flow, q the flow into the channel from other sources, n the Manning's coefficient of friction, and P the wetted perimeter of the flow. For the implementation of this solver for the Amazon study reach, there is only one tributary (Purus) providing a q flow into the main channel and much smaller local inputs along the reach are excluded so for these $q = 0$.

In this case, the channel is assumed to be wide and shallow, so the wetted perimeter is approximated by the channel width, which is reasonable for the Amazon reach studied here. In Equation 3-7, the term in brackets represents diffusion and forces the flow to respond to both the bed slope and the free surface slope. The resulting band diagonal system of linear equations are solved using LU Decomposition (Crout's method) within an implicit Newton Raphson scheme. L and U are the lower and upper triangular matrices respectively. The new LISFLOOD-FP (v3.6.0) diffusive channel solver was tested against analytical test cases (MacDonald *et al.*, 1997) and a range of simplified channel test models specifically developed to ensure correct implementation. More complicated test cases specifically created to test new features such as the full range of boundary conditions, branching networks and decoupled timesteps, were implemented and also compared to identical models built and run using HEC-RAS (v4.0.0), software developed by the US Army Corps of Engineers at the Hydrologic Engineering Center. HEC-RAS provides a full hydrodynamic 1D Saint Venant solution using irregular cross sections. For diffusive flow conditions, the maximum difference between the predicted water elevations for LISFLOOD-FP and HEC-RAS models was in the order of 0.7%. Even under subcritical flow conditions that should require a full Saint Venant solution, the maximum difference in water elevation between the diffusion wave approximation in LISFLOOD-FP and the full Saint Venant solution in HEC-RAS was 4%. Tests were not undertaken for supercritical conditions

(Froude number > 1) as these are not present in the reaches under consideration and are also not appropriate for the application of a diffusive solver, see Figure 3-4.

3.4.2 Model construction

The newly developed LISFLOOD-FP 1D diffusive channel solver was applied to the Amazon River as the primary investigative tool. In order to understand the overall implications of using a diffusive approximation and a rectangular channel, a model with identical geometry was constructed using HEC-RAS for direct comparison purposes. These river channel models were applied to a 285 km reach of the main-stem of the Amazon (Solimões) and a 107 km reach of the Purus tributary. All key model elements described here are illustrated in Figure 3-6.

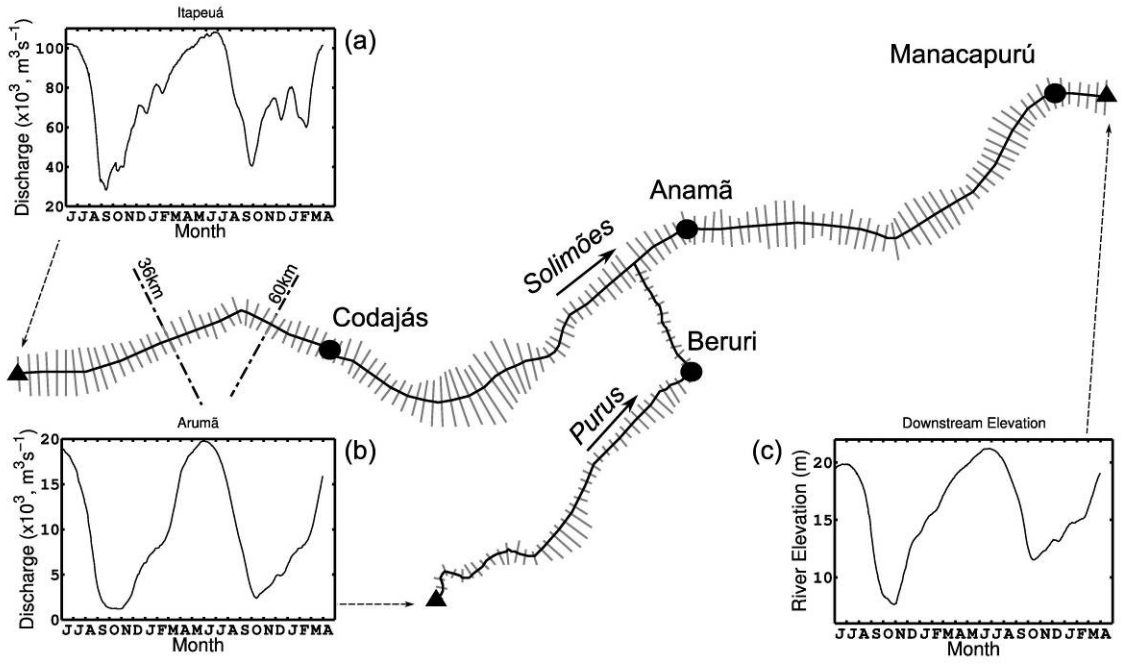

Figure 3-6 – Amazon channel model schematic. Main figure shows Solimões and Purus reaches with channel cross sections and gauging station locations. Gauged flow data from 1 June 1995 to 31 March 1997 used for (a) Solimões river boundary (Itapeuá) and (b) Purus river boundary (Arumã). (c) Downstream river elevation boundary derived from Manacapurú gauged stage and river slope. Locations of example cross sections illustrated in Figure 3-7 are also shown at 36 and 60 km from upstream boundary.

Full irregular cross sections perpendicular to the river centrelines were extracted from the interpolated bathymetry grid at a spacing of 2 km for the two reaches, giving 136 for the Solimões reach and 54 for the Purus. These included all parts of the major channel where it branched around islands but did not include the floodplain on either side above the low water level. Rectangular cross sections with an equivalent flow area were also derived from the irregular cross sections for use in LISFLOOD-FP and HEC-RAS. Two Manning's friction parameters were used, one for the Solimões channel and one for the Purus channel. Figure 3-7 shows two example cross sections from Figure 3-6 in more detail. Figure 3-7 also shows the derived equivalent flow area rectangular channel for the area below the low water level and a background SRTM DEM to illustrate the floodplain topography on either side of the channel.

Three boundary conditions were applied to the models. The inflows for the two channels were extracted from gauged flow data from Itapeuá, 38 km upstream of the model boundary on the Solimões, and Arumã, 85 km upstream of the model boundary on the Purus. For the downstream boundary, a stage hydrograph was derived from Manacapurú gauging station stage data. Manacapurú is 12 km upstream of the model lower boundary, so the data were adjusted using the water slope calculated on a daily basis from the water level difference between the Anamã and Manacapurú gauging stations. Model runs were carried out for the same period used in Wilson *et al.* (2007): 1st June 1995 to 31st March 1997. This allowed for direct comparison as well as use of the same calibration and validation data. All models were run with a 12 hour time step. Tests showed results were insensitive to a time step below 24 hours, the implicit solvers allowing a large Courant number (Cr ~20).

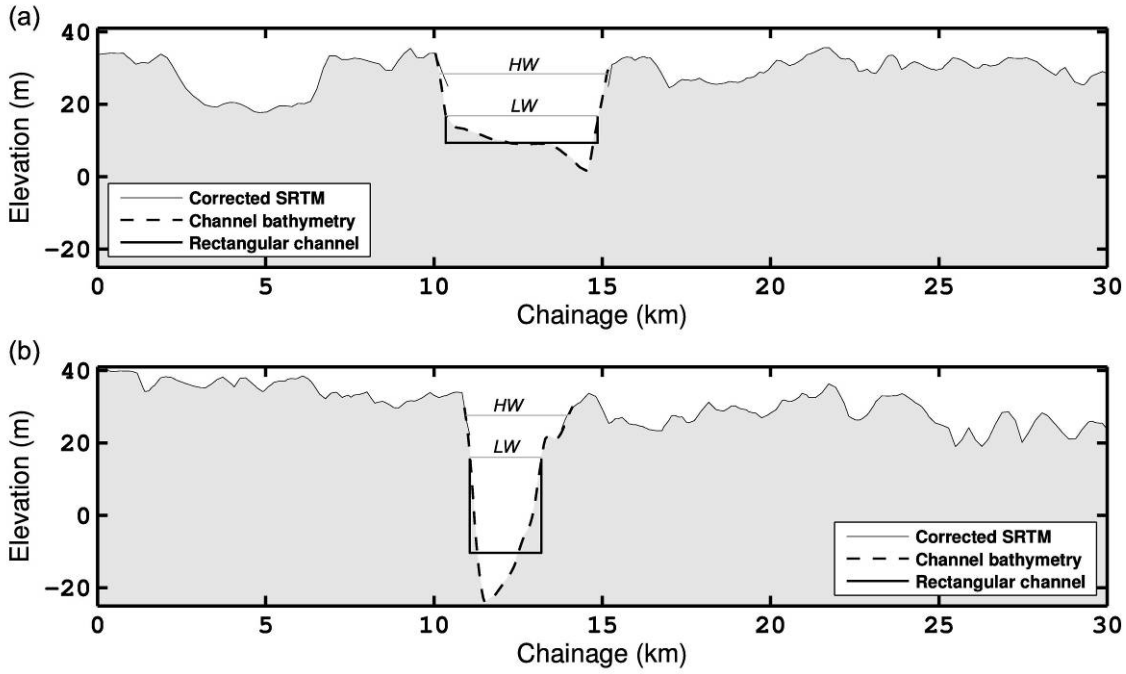

Figure 3-7 – Example cross sections perpendicular to the channel, shown facing downstream, extracted from bathymetry data: (a) a wide relatively shallow cross section (36km from upstream boundary) and (b) a narrow deep cross section (60km from upstream boundary). Both the irregular cross section and equivalent area rectangular cross section for the area below the low water level are shown. The background SRTM DEM (with vegetation artefacts removed using the method described in Wilson *et al.* (2007) was not used in the channel model and is shown only to illustrate the floodplain either side of the channel. The grey shaded area is a composite of the SRTM and bathymetry. High and low water elevations are also shown, and denoted HW and LW respectively.

3.4.3 Model testing

Friction parameters were calibrated for the two channels by varying Manning's *n* from 0.02 to 0.04 using 0.001 increments for each channel independently (a total of 441 simulations). Goodness of fit was assessed by comparing model results to water surface elevation data from four gauges internal to the model domain. These were the Manacapurú, Anamã and Codajás gauging stations on the Solimões and the Beruri

station on the Purus. It should be reiterated here that the Manacapurú gauge data was used to derive the model's downstream boundary condition and so this does not represent a fully independent test. The root mean squared error (RMSE) was calculated for each model run at all four gauging station locations for the complete model time series using a daily time step. Selecting the Manning's *n* values that minimise the RMSE values, with each gauging station weighted equally, provides the parameter values for the calibrated model.

Model validation was carried out by comparison of the calibrated model results with an independent set of water surface elevations derived from satellite altimetry for both the Solimões and Purus, see location in Figure 3-1. The RMSE was calculated for the model results for both locations for the complete model time series using a daily time step. A comparison was also made between the modelled and gauged water surface slopes for the two reaches. For the Solimões, the slope between the Codajás and Manacapurú gauging stations was used. For the Purus, the slope between Paricatuba gauging station, just upstream of the model boundary, and the confluence with the Solimões, interpolated from the slope between Anamã and Codajás gauging stations was used. In addition, sensitivity tests were carried out to explore the implications of backwater effects. To achieve this, 16 extra model runs were undertaken with a modified downstream boundary condition. The elevation of the stage data used for the boundary was increased and decreased in 0.5 m intervals to cover a range of -4 m to +4 m, ± a third of the annual flood wave amplitude of ~12 m.

Once the LISFLOOD-FP hydrodynamic channel model was fully calibrated and validated, experiments were performed to determine the effect of using kinematic and diffusive approximations as well as simpler channel geometries. For direct comparison, all these experiments used the same Manning's *n* parameter values determined in the calibration exercise as well as identical boundary conditions. All test runs were compared with the HEC-RAS, full Saint Venant, fully irregular channel, which gives as complete a process and geometric representation as possible. A relative comparison

was made with the full HEC-RAS model rather than just the four gauging stations as this allowed use of all 190 model cross sections and isolate the effects of each element of the study. The predicted water elevations for each simplified model, for each cross section, were compared for the full time series on a daily timestep against the predicted water elevations from the irregular HEC-RAS model water elevations and an overall RMSE calculated.

In the first test, a rectangular channel with varying width and depth was compared with the an irregular channel with fully varying geometry. Both model runs were undertaken with HEC-RAS using a full Saint Venant representation of the flood wave. The second test used the LISFLOOD-FP diffusive solver with a rectangular channel with varying width and depth, allowing an assessment of the impact of simplifying the flow representation to a diffusive flood wave approximation. The third, fourth and fifth tests were carried out with LISFLOOD-FP and test even simpler channel geometries: one with mean channel width but variable depth, one with mean channel depth but variable width and the last and simplest representation with mean channel width and depth. The sixth and final test uses the mean channel width and depth geometry and the kinematic solver to test the impact of the channel flow and geometry assumptions made by Wilson *et al.* (2007). The rectangular channel with varying width and depth, the mean width channel and the mean depth channel are all equivalent in flow area to the fully irregular channel. The mean depth channel and mean width channel do not have the same flow area and are primarily used to test the effects of estimating only one of these two parameters.

3.5 Results and discussion

3.5.1 LISFLOOD-FP model calibration

Calibration of the hydraulic model was straightforward, with the selection of one model which best fits the observed data from the matrix of runs obtained by varying the Solimões and Purus Manning's *n* values. In this case the best fit is determined by the minimum sum of the RMSEs for the four gauging stations internal to the model domain. The LISFLOOD-FP, rectangular cross section, diffusive solver model with the best fit had a Manning's *n* of 0.032 for the Solimões and 0.034 for the Purus. These values are what would be expected for a large, sand bed river of low sinuosity such as the Solimões, from standard tables, e.g. (Chow, 1959). The Purus is much more sinuous than the Solimões, so higher Manning's *n* might be expected, but interestingly, the water levels in the Purus were more sensitive to the Solimões friction parameter than that for the Purus itself, as the reach modelled is heavily controlled by the backwater effect from the confluence.

The summed RMSE results over the range of friction values tested resulted in a single clear optimum Manning's *n* for the Solimões, with results being insensitive to the Manning's *n* for the Purus. Individually, the station RMSEs for Manacapurú, Anamã and Beruri showed an optimum Solimões *n* of around 0.032-0.033, with a slightly lower optimum Solimões *n* of 0.029 at Codajás. The variation of RMSE with the Manning's *n* for the Solimões for each station is illustrated in Figure 3-8. As results were insensitive to the variation of Purus Manning's *n*, this is not shown.

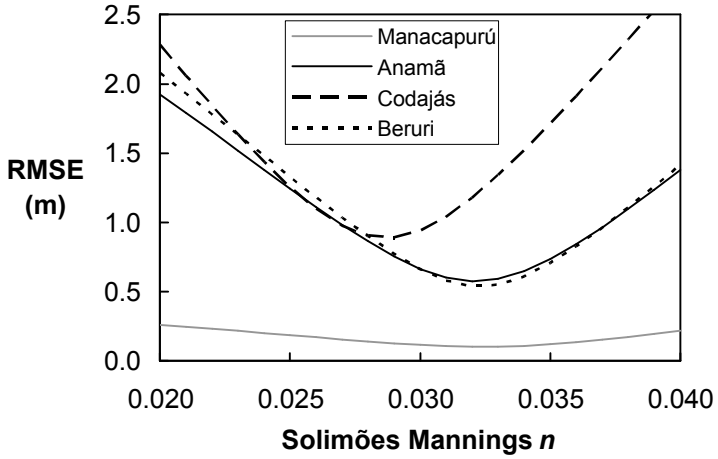

Figure 3-8 – Variation of station RMSE with Solimões *n*.

Friction values are model dependent and it would be expected for these values to be somewhat different for a coupled channel and floodplain model. The Amazon model of Wilson *et al.* (2007) was calibrated by minimising the difference between the predicted floodplain extent and JERS images for the same period. This resulted in a Manning's *n* of 0.028 for the Solimões and 0.031 for the Purus. The calibration of the Wilson *et al.* (2007) model was complicated by the fact that the average kinematic channel slopes that were used also acted as model parameters.

With the large water level changes observed in the channel, Manning's *n* is likely to vary vertically within the channel cross section as well as seasonally, although it would be hard to quantify and apply this in a meaningful manner for this reach at this stage. Where it has been possible to look at such effects, significant variations have been found, for example, an independent study of the Negro river, a main tributary of the Amazon, deriving virtual stage-discharge relationships using altimetry, gave a Manning's *n* value of 0.039 for the in-channel, dry season flow in the main river (Leon *et al.*, 2006).

For the calibrated LISFLOOD-FP, rectangular cross section, diffusive solver model, the RMSE for each of the four gauging stations for the full run of 670 days was less than 1 m and therefore within the likely error in the surveyed bathymetric data.

The RMSE values were: Manacapurú 0.10 m, Anamã 0.69 m, Codajás 0.90 m and Beruri 0.74 m. Full hydrograph plots for the four stations are presented in Figure 3-9. The closest fit, as expected, was at the downstream end of the model at Manacapurú. This was due to the fact that the model has a constrained downstream boundary derived from the Manacapurú data. For Codajás, the station with the worst fit, the error range is -2.59 m to 1.05 m with a standard deviation of 0.87 m. Even for Codajás, 528 days of the run (79%) result in an error of less than 1 m. This is a good fit to the observed data, given likely errors are in the order of metres. These results are an improvement on the model of Wilson *et al.* (2007), which had overall RMSE values in the channel of 3.56 m and 2.09 m for Beruri and Manacapurú respectively, although the models are not directly comparable since the LISFLOOD-FP model used here represented the channel only.

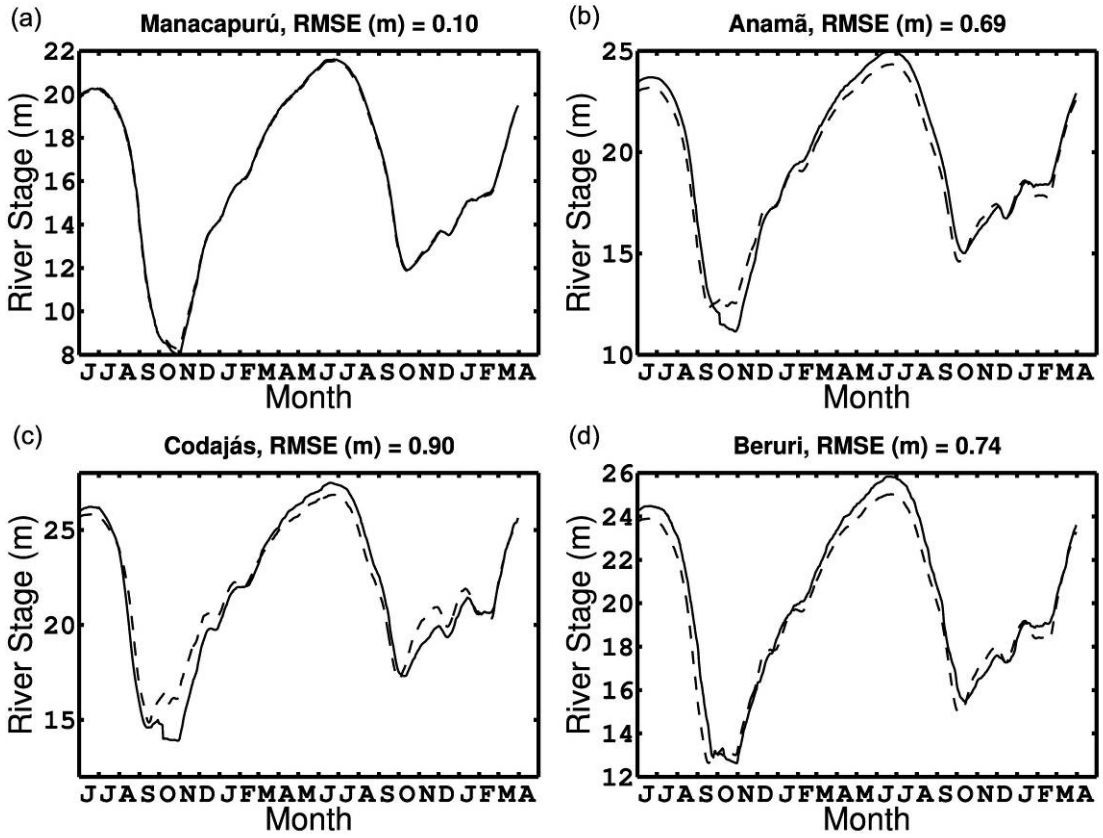

Figure 3-9 – Calibrated model results (dashed line) compared to the four gauging stations (solid line) internal to the model. Solid line is observed data and dotted is model output.

3.5.2 LISFLOOD-FP model validation

Comparison of model results to the independent set of satellite altimetry data for the Solimões and Purus rivers (location in Figure 3-1b) is shown in Figure 3-10, with Figure 3-10c showing a scatter plot comparison for all data.

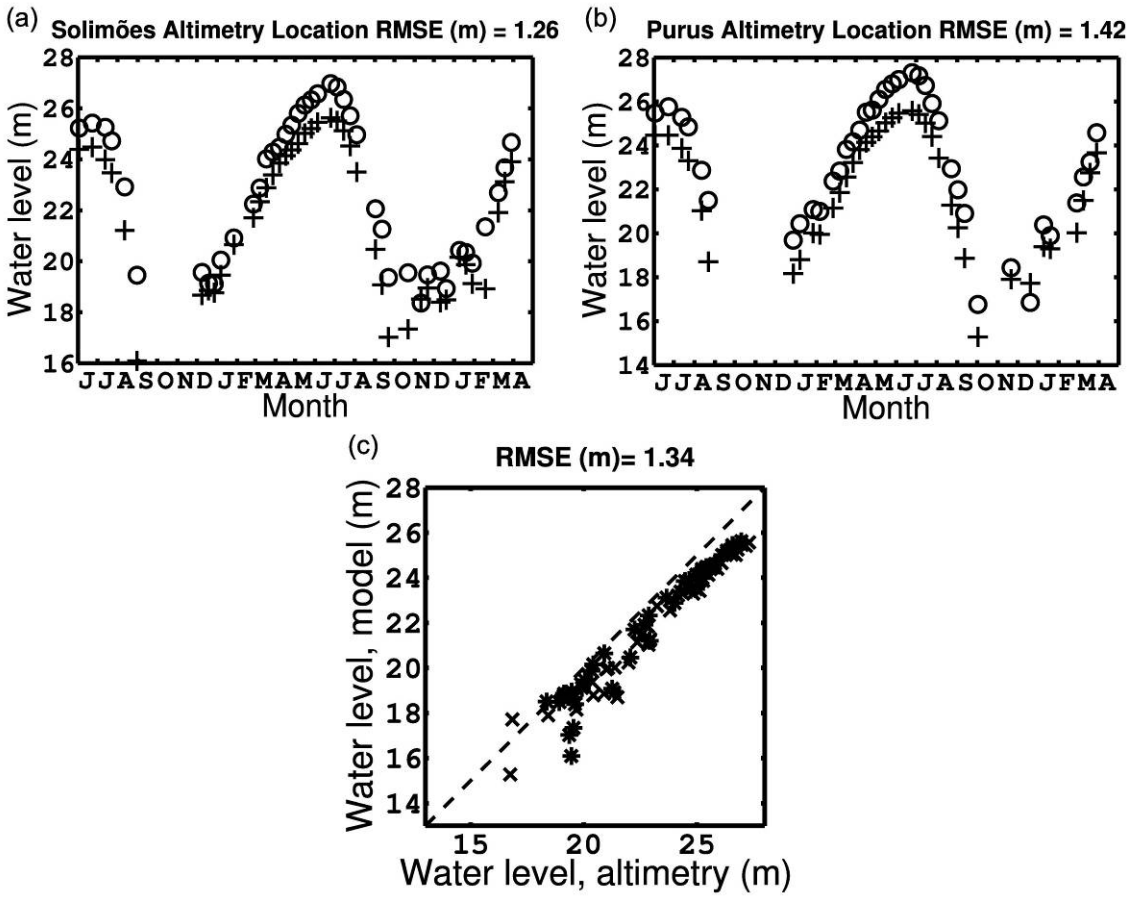

Figure 3-10 – Altimetry water level (circles) compared to predicted water level (crosses) for (a) Solimões and (b) Purus altimetry data locations, with corresponding RMSE for the full simulation. (c) Altimetry water level versus model water level for all available data and the overall RMSE (symbols: * for Solimões and x for Purus).

The overall RMSE for the Solimões was 1.26 m and for the Purus 1.42 m. Similar results were reported for the model of Wilson *et al.* (2007) at high water (Solimões 1.83 m, Purus 1.26 m), but at low water, Wilson *et al.* (2007) results were

worse resulting in an overall RMSE of 2.70 m for the Solimões and 2.64 m for the Purus. Low water elevation estimates derived from altimetry are associated with the greatest uncertainty (Birkett *et al.*, 2002) and it is likely that the remotely sensed altimetry data used for this validation is subject to higher errors than the directly measured gauge data used for the calibration. However, Figure 3-10 shows that there is a systematic underestimation by the model compared to the altimetry data at both high and low flows which could be the result of a mismatch in datums.

Although slope derived from the gauging stations is not strictly an independent validation data set, the model was calibrated to water elevations and comparison of slopes can yield important information about the hydraulics. The modelled and observed slopes for the Solimões and Purus reaches are shown in Figure 3-11. The mean RMSE, calculated for the full model run period, for the Solimões slope was 0.43 cm/km and for the Purus 0.62 cm/km.

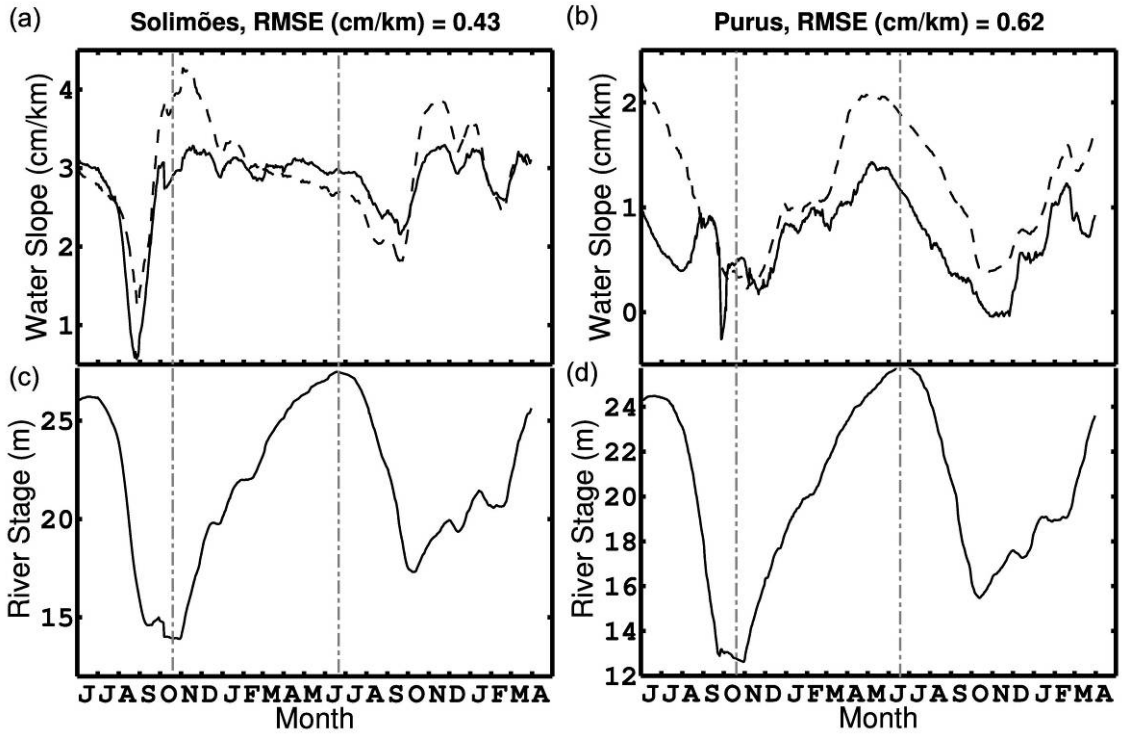

Figure 3-11 – Modelled slopes (dashed line) compared to the gauged slopes (solid line), for (a) the Solimões, (b) the Purus reaches. Plots of gauged stage at (c) Codajás and (d) Beruri are shown below the slope plots for discussion purposes.

The gauged water surface slope for the Solimões varies from a low of 0.57 cm/km to a high of 3.29 cm/km, and with a mean of 2.81 cm/km for the modelled period. There is a noticeable sharp drop in slope that coincides with the recession limbs of the hydrographs. It is hypothesised that this occurs because, once the flood wave peak has passed there is no longer the hydraulic gradient, from the channel to the floodplain, driving the flow onto the floodplain and instead drainage of the floodplain begins to dominate the system. The remainder of the time, the water surface slope remains relatively steady at around 3 cm/km, which suggests a river system whose response is well dampened by the storage present on the floodplain. This is corroborated by the fact that the model, which contains no floodplain storage, shows the largest mismatch to the gauged slope on the rising limb of the hydrograph, where storage will have the biggest effect on water slope.

The gauged water surface slope for the Purus is shallower and more variable than the Solimões, despite a steeper mean bed slope of around 6.5 cm/km. The water surface slope varies from a minimum of -0.26 to a maximum of 1.43, with mean of 0.69 cm/km. The shallow water surface slopes are primarily due to the backwater effects from the confluence with the Solimões and also a significant cross-floodplain flow from the Solimões into the Purus across the confluence floodplain which exists between the two rivers, as noted by Alsdorf *et al.* (2007a).This acts to reduce the hydraulic slopes in the Purus. As with the Solimões, the lack of floodplain in the model means that the simulation fails to reproduce the water surface slope well at the times when floodplain storage is important. These fairly large and rapid seasonal changes in the observed water surface slope have been highlighted before by Birkett *et al.* (2002) and may be particularly important for studies that use remote sensing to determine flow from water elevations and slopes, such as the proposed SWOT mission (Alsdorf *et al.*, 2007b).

The 16 model runs carried out using the LISLFOOD-FP, rectangular cross section, diffusive solver model to test the sensitivity of results to the downstream

boundary condition show that the whole of both reaches are affected by the downstream boundary, at both high and low water. For example, decreasing the boundary by 1 m results in a decrease in water elevation at the upstream end of the Solimões reach of 0.27 m for high water and 0.05 m for low water. For the Purus, upstream water levels decrease by 0.40 m and 0.20 m respectively. Increasing the boundary by 1 m results in an increase in water elevation at the upstream end of the Solimões reach of 0.31 m for high water and 0.08 m for low water. For the Purus, upstream water levels increase by 0.45 m and 0.31 m respectively. These results highlight that the backwater effect applies for the whole of the channel in this region under both low and high water conditions. Further work will be necessary to distinguish the extent to which these effects are due to simple hydraulic backwater effects from the filled downstream floodplain and low valley slopes and that due to the geometry of the passing flood wave resulting in hysteresis effects.

Figure 3-12 shows the variation of RMSE for the gauging stations locations, altimetry locations and river slopes. The RMSEs at the gauging stations worsen as the downstream stage is decreased, but show a slight improvement with an increase in downstream boundary up to about 1 m, except for Manacapurú, from which the downstream boundary is derived. An increase in boundary above 1 m shows rapidly worsening RMSEs for all stations. The RMSE at the altimetry locations show a minimum of 0.57 m for the Solimões and 0.47 m for the Purus with a stage increase of 2 m and 2.5 m respectively. Slope RMSE show an optimum, Solimões 0.22 cm/km and Purus 0.41 cm/km, with a downstream stage increased by 2 m. This could be explained by the lack of storage in the model resulting in overly steep slopes, thus raising the downstream stage reduces the slope, giving a better fit. It does imply that compound parameter sensitivity tests would be worth exploring in the extended model that incorporates the 2D floodplain.

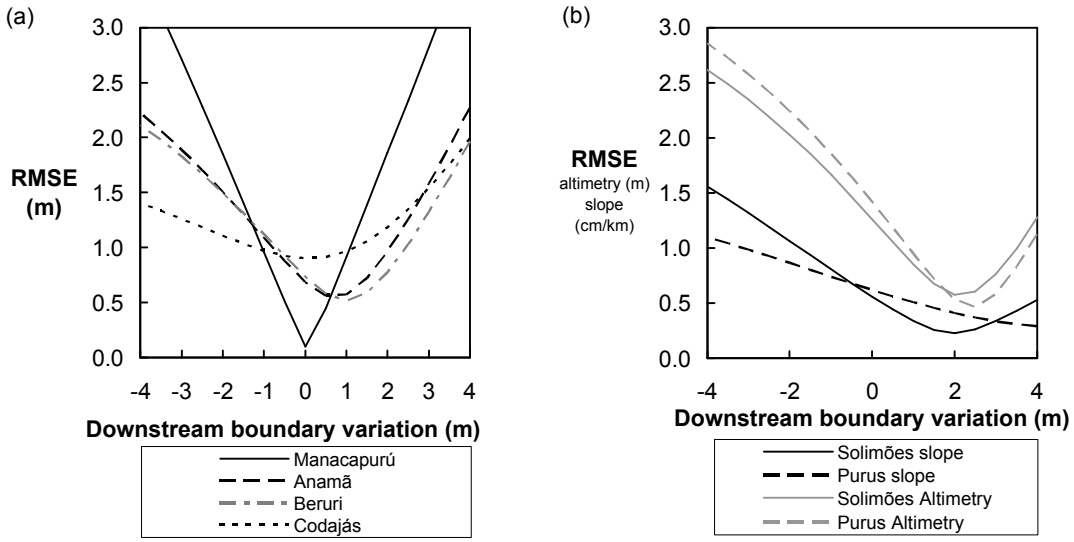

Figure 3-12 – RMSE variation with model downstream boundary for (a) gauging station locations and (b) altimetry locations and river slopes.

For applications of the model in conditions where downstream water elevations are not known, for example, in climate change simulations, it may be possible to use a stage-discharge relationship as the downstream boundary. This method has not been tested explicitly in this study, but if used would need to take into account the hysteresis in the stage discharge relationships for the Amazon River due to backwater effects noted by Meade *et al.* (1991).

3.5.3 Diffusive approximation and channel detail tests

A total of 7 different models were run to examine the impact of using the diffusive wave approximation, a rectangular channel and other channel simplifications. The same Manning's *n* parameter values, derived in the earlier LISFLOOD-FP calibration, were used for all models The water elevation results at all 190 cross sections for these runs were compared to the results of the full Saint Venant, fully irregular HEC-RAS channel model. This control model allowed a relative comparison,

isolating the effect of each test. A summary of the models and water elevation RMSE results are presented in Table 3-3.

Table 3-3 – Test models summary and RMSE results

Test No.	Model code	Process Representation	Channel Geometry	Solimões RMSE (m)	Purus RMSE (m)
Control	HEC-RAS	Saint Venant	fully irregular cross sections	-	-
1	HEC-RAS	Saint Venant	varying width and bed rectangular cross sections	0.126	0.241
2	LISFLOOD-FP	Diffusion wave	varying width and bed rectangular cross sections	0.151	0.235
3	LISFLOOD-FP	Diffusion wave	mean width, varying bed	0.414	0.565
4	LISFLOOD-FP	Diffusion wave	mean bed, varying width	0.431	0.504
5	LISFLOOD-FP	Diffusion wave	mean bed, mean width	0.530	0.381
6	LISFLOOD-FP	Kinematic wave	mean bed, mean width	1.319	2.941

The first test explores the effect of simplifying the channel cross sections from fully irregular sections to rectangular sections of the same flow area. The RMSE results show that the impact on the results of this simplification is small and demonstrates that a wide rectangular channel representation is a reasonable approximation in this case. Longitudinal plots of the high and low water results for the fully irregular channel model and rectangular channel model are shown in Figure 3-13 together with the bed inverts (thalweg) for the irregular and rectangular channels.

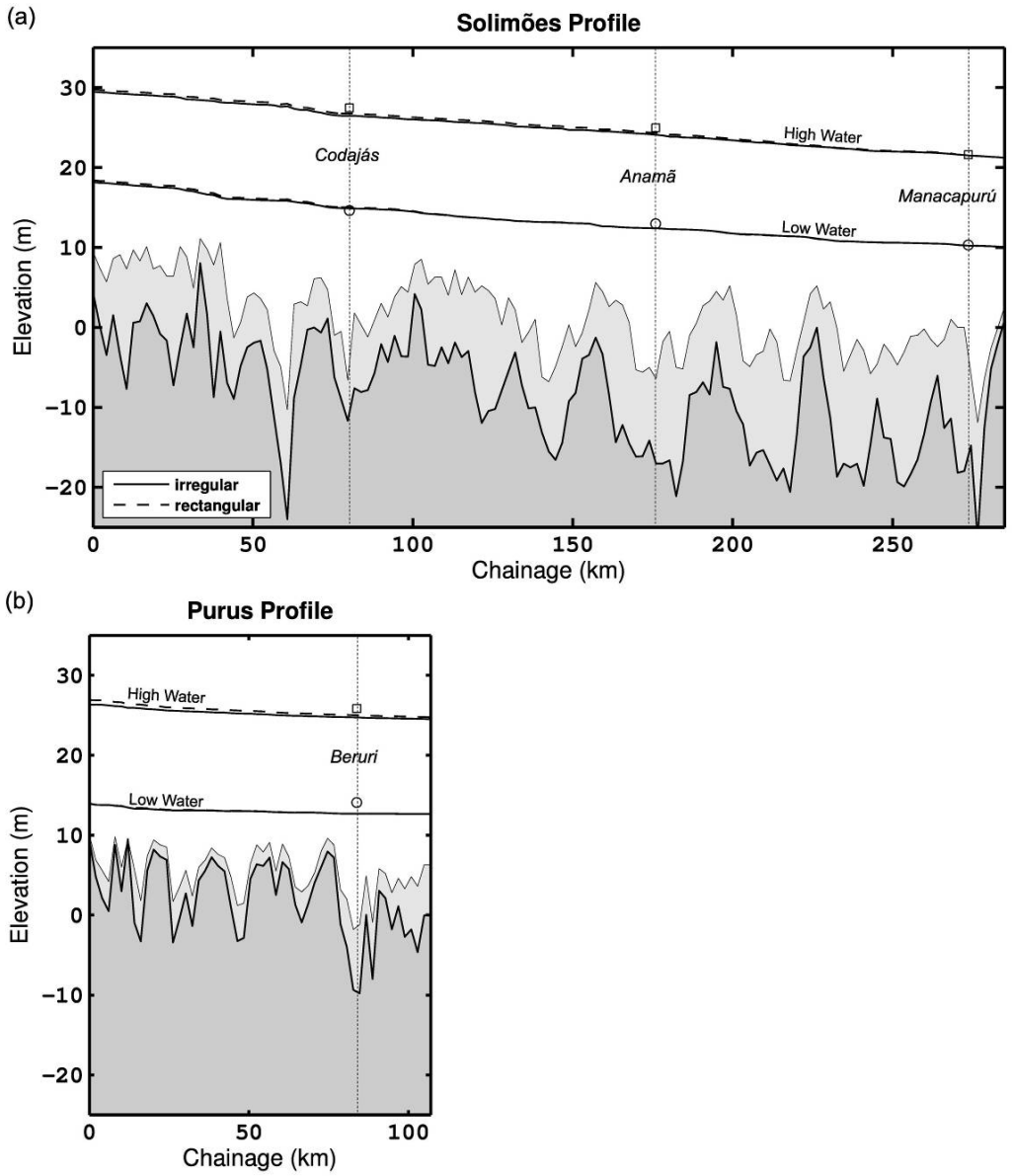

Figure 3-13 – (a) Solimões longitudinal profile plot of high and low water results from fully irregular channel model and rectangular channel model, together with both channel inverts (thalweg) (filled lighter grey is rectangular bed and filled darker grey is fully irregular) and gauged elevations; squares for high water and circles for low water. (b) Purus profile.

The second test exploring the effect of using the diffusive wave approximation instead of the full Saint Venant solution also shows that the impact is minimal. Given that the results of the flood wave characterisation show that a diffusive wave

approximation should be valid, this is expected, but does provide further support for this approach.

The three bathymetry tests use simplifications to the geometry of the channel to explore how important this information content is to the results. Profile results for the three models at high and low water are presented in Figure 3-14. All three model results give RMSE values in the order of 0.5m. This is true even for the simplest representation, which is essentially a uniform rectangular cross section per channel with an average reach slope. This demonstrates that compared to the amplitude of the Amazon flood wave, results are relatively insensitive to the bathymetry information content of the channel model and the use of a mean slope. This means that for studies of the central Amazon channel, such as the virtual missions for designing the SWOT satellite mission (Alsdorf *et al.*, 2007b), even relatively crude assumptions regarding the bathymetry will be valid if they can approximate well the mean width, depth and slope for a reach. Remote measurements of water elevations and hence derived slope and discharge will implicitly take into account backwater effects through the slope. This insensitivity to channel geometry is likely due to the very low Froude numbers. Low Froude numbers show that inertia forces, which are sensitive to channel geometry, are low compared to gravitation forces, which are only sensitive to the mean depth of flow. This findings suggest that this approach should be applicable to other large slow flowing deep rivers with low Froude numbers.

The final test uses the simplest channel geometry as well as the kinematic solver and shows the significant additional error, of the order of 1 to 3 m, introduced by ignoring the diffusive term in the Saint Venant equations. Overall these results show that a diffusive wave channel flow representation is needed to match observed data and include backwater effects, but that it is not necessary to represent the floodplain for short reaches of around 100-200 km in order to obtain a good fit to observed channel elevation data. They also show that a rectangular channel approximation is valid and it is possible to get a reasonable fit with depth errors in the region of 0.5 m on a 11-12 m

flood wave amplitude using simple cross section and slope models. Finally, in terms of modelling overall hydraulics at this scale, the result that using a mean depth and implicitly uniform slopes does not lead to large errors, suggests that the model is relatively insensitive to the bar and bed forms. This means that it is likely that the changing bed conditions can be ignored for model runs of less than decadal timescales. For longer timescales it may be necessary to assess the importance of channel migration, although an assumption that the channel retains a similar flow capacity may still be valid in this case.

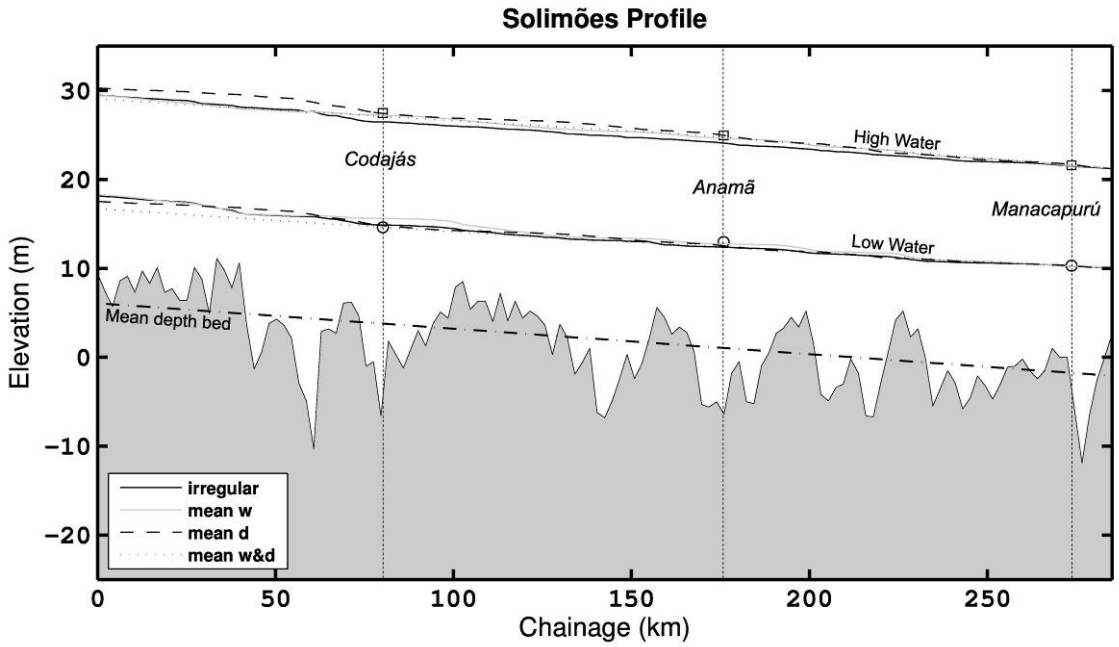

Figure 3-14 – Solimões longitudinal profile plot of high and low water results of the irregular channel model, mean width, mean depth and mean width & depth channel models. The rectangular channel bed (grey filled) is shown as well as the mean depth bed (dot dash line) and gauged elevations; squares for high water and circles for low water.

3.6 Conclusions

Research presented in this chapter shows that the Amazon flood wave is subcritical and diffusive in character. For the whole of the Solimões reach during the period of 1996/97, the mean model flow depth varied between 21.9 m at low water and 33.5 m at high water, giving a flood wave amplitude of 11.6 m. Mean bathymetric bed slopes are 5.0 cm/km with a mean gauged water surface slope of 2.8 cm/km. The flow is deep and relatively slow moving, resulting in very low Froude numbers of the order of 0.05.

Due to very shallow slopes, backwater conditions control significant reach lengths in the central Amazon and these backwater conditions are present for low as well as high water states. The modelled lower reaches of the Purus tributary also show backwater effects from the confluence with the Solimões main-stem. To accurately predict water elevations using hydraulic models requires that these backwater effects are represented.

A diffusive channel solver for the LISFLOOD-FP model was implemented and applied to a channel only model of the central Amazon. Calibration of the hydrodynamic hydraulic model gave a Manning's n of 0.032 for the Solimões and 0.034 for the Purus. Calibrated RMSE for the water elevations at the four gauging stations internal to the model were all less than 1 m for low and high water results. Validation using water elevation altimetry data at one location on each river resulted in RMSEs under 1.5 m, and comparing the model to gauged slopes, gives a maximum RMSE of 0.62 cm/km.

Despite excluding the floodplain from the models, comparison of results to the observed data shows a reasonably good fit. It can be deduced therefore that the floodplain volume is relatively small compared to the volumes of the passing flows in the main channel and thus has relatively little effect on the geometry of the flood wave itself.

Experimentation with the physical process representation of the channel flow as well as bathymetric information content of the channel showed that when compared to the amplitude of the Amazon flood wave, water levels are relatively insensitive to the bathymetry information content of the channel model. This means that for studies of the central Amazon channel such as virtual missions for the proposed SWOT satellite mission, even relatively crude assumptions regarding the bathymetry will be valid as long as the mean cross sectional area can be reasonably well approximated. Remote measurement of water elevations and hence a derived slope and discharge will also implicitly take into account backwater effects through the water surface slope. These conclusions may well be applicable to other large rivers, where similar hydraulic conditions prevail, specifically the shallow sloped lower reaches of continental scale river systems. In addition, SWOT satellite mission measurements will also provide valuable calibration and validation data for future hydraulic modelling.

For the application of hydraulic modelling methods to these reaches of the central Amazon, it is has been demonstrated that it is necessary to include at least the diffusion term in the channel model. The error on predicted water elevation introduced by using a wide rectangular channel is in the order of 0.10 to 0.15 m and by ignoring the acceleration and advection terms from the full 1D Saint Venant equations a further error in water elevation of the order of 0.02 to 0.03 m was introduced. Both these errors are small in comparison to the mean annual flood wave amplitude of 11 to 12 m. The application of appropriate boundary conditions has also been demonstrated as essential, in order to incorporate the backwater effects present along these reaches. These backwater effects are so important that even when reducing the complex bathymetry, which under free flow conditions would be hydraulically significant, to a simple bed slope with a mean cross section in the model, only a relatively small error in the order of 0.5 m in the water elevation resulted.

It should be emphasised here that while the work presented in this chapter demonstrates that it is sufficient to use 1D hydraulic modelling and basic bathymetric

data to simulate the key characteristics of the Amazon flood wave within the main channel, it provides no direct information regarding the complex dynamics between the channel and floodplain. Indeed, the analysis of interferometric SAR data by Alsdorf *et al.* (2007a) clearly demonstrates that the floodplain water levels cannot be assumed to be the same as channel water levels, highlighting the need for the addition of a detailed 2D floodplain element to the model in order to simulate these floodplain dynamics. However, as has been demonstrated in this chapter, it is important to get the hydraulics of the main channel correct before tackling the more complex interactions with the floodplain. Flow on the floodplain and its interaction with the channel will be the subject of the following chapters of this thesis.

CHAPTER 4
Floodplain connectivity

4.1 Introduction

In Chapter 2, it was identified that there is a need to address the lack of knowledge regarding the hydraulic science of the Amazon main channel and floodplain. Chapter 3 addressed the hydraulics of the main river channel and the Amazon flood wave itself. This chapter looks more closely at the floodplain and, specifically, the floodplain channels to try and gain an understanding of their importance in the dynamics between the main channel and floodplain. The following research questions were addressed: what are the important components of the floodplain system, and what are the characteristics of those components?

Wilson *et al.* (2007) identified filling and draining problems with the 2D representation of the floodplain in the 1D/2D Amazon model. Given that the primary driver of the river and floodplain interaction is the flood wave, it would be expected that providing an improved representation of this flood wave in the 1D/2D model would also lead to improved flood dynamics on the floodplain. This hypothesis is tested by implementing the LISFLOOD-FP diffusive channel solver developed in Chapter 3 with a full 2D floodplain similar to that of Wilson *et al.* (2007).

As shown in Chapter 2, there has been very little direct study of the floodplain channels and how they might affect the hydrodynamics on the floodplain. In order to better understand these channels, Landsat enhanced thematic mapper (ETM+) images were analysed to quantify image measureable parameters, such as length, width and connectivity, of all visible channels within the study area.

With the relative importance of the floodplain channels in terms of their role in the hydrodynamics of the floodplain established, research then considered how well these channels are represented in the current topographic data that are available for the Amazon floodplain, specifically SRTM data. Initially this involved study, by way of example, of a medium sized (100 m width) floodplain channel to see what information regarding the channel is available in the SRTM data. This was followed by connectivity analysis of a subset of the floodplain. These analyses allowed a better understanding of the importance of these channels as connections, as well as of the general cell-to-cell connectivity of a 2D model grid representation of the floodplain. This work included some experiments into the effects of “burning” the channels explicitly into the SRTM, effectively fusing the Landsat information with the SRTM topography, allowing a more detailed representation of the floodplain channels within the digital elevation model (DEM).

4.2 LISFLOOD 1D/2D hydraulic model

4.2.1 Model development

The first large scale hydraulic model of the Amazon river and floodplain (Wilson *et al.*, 2007) was described in Chapter 2. This model was constructed using a simple 1D kinematic channel of the main river and one tributary, and had a 270 m spatial resolution 2D floodplain which used resampled 90 m SRTM data, which had been corrected for vegetation errors using a habitat classification (Hess *et al.*, 2003) and limited field measurements of vegetation heights. The Amazon flood wave analysis carried out in Chapter 3, showed that the flow in the main channel must be represented as at least a diffusive approximation and therefore a new diffusive channel solver was developed for LISFLOOD-FP. With the ability to use an improved flood wave representation, the next step was to run a full model including the 2D floodplain. Before this was done, a number of developments and improvements were made to both the model build and model code.

Model build improvements;

1. The simple 1D channel geometry was replaced with a fully detailed rectangular channel constructed from bathymetric data collected by Wilson *et al.* (2007), as described in Chapter 3.
2. Replacement of the previous DEM, which used publicly available SRTM v1, with one based on publicly available SRTM v2, which uses improved void filling (Slater *et al.*, 2006, Farr *et al.*, 2007). The same vegetation correction method used by Wilson *et al.* (2007) was applied to the SRTM DEM. This provided a first-order correction of vegetation artefacts using the habitat classification from Hess *et al.* (2003) and field measurements of vegetation heights collected by Wilson *et al.* (2007).

Model code improvements between LSFLOOD-FP version 3.4.0 and version 3.6.3;

1. The kinematic 1D channel solver was replaced with a diffusive solver as used in Chapter 3.
2. Decoupling of the 1D channel solver timestep from the 2D floodplain timestep was undertaken to improve computation speed, which suffered from the introduction of the more complex diffusive solver. Tests with the Amazon model showed a channel timestep ten times longer than that for the floodplain compensated for the extra computation time required by the more complex solver without increasing mass error.
3. The 2D solver computation time was also reduced significantly by extensive parallelisation of the code (Neal *et al.*, 2009). For a 20 second timestep, the model run times are now in the order of 3 days compared to 3 weeks previously.
4. Channel chainage (distance) was made independent of the 2D grid resolution to allow better comparison of the model at different scales.
5. Output options were extended for river profiles to show additional parameters such as in-channel flow.

The combined 1D/2D diffusive model was run for the same time period as the Wilson *et al.* (2007) model. In order to allow direct comparison with the Wilson *et al.* (2007) model, the new model also ignores local runoff inputs, terrace catchments and rainfall. While these could be important, the purpose here is to assess the improvements of the new diffusive solver and channel to the results. Further study of the relative importance of the local hydrology is explored in Chapter 6. Two separate calibrations of the new model were undertaken; one using calibration of channel roughness to gauged water levels in the channels as was carried out for the channel only model in Chapter 3, and one using calibration of channel roughness to JERS flood extent as was carried out in Wilson *et al.* (2007).

Accuracy for all simulations was calculated using the measure of fit, *F* as used in Wilson *et al.* (2007):

$$F = \frac{A_{obs} \bigcap A_{\mathrm{mod}}}{A_{obs} \bigcup A_{\mathrm{mod}}} \times 100 \qquad (1)$$

where A_{obs} and A_{mod} represent the sets of pixels observed to be inundated and predicted as inundated, respectively. *F* ranges between 0 (where observed and predicted areas are completely different) to 100 (where observed and predicted areas are identical).

4.2.2 Model calibration and results

The calibration of the original Wilson *et al.* (2007) model was carried out by running a matrix of 28 simulations with values of channel friction varying from 0.022 to 0.028 (Solimões) and 0.025 to 0.031 (Purus) in 0.001 increments and floodplain friction varying from 0.06 to 0.12 in 0.02 increments. Accuracy for all simulations was then calculated using the measure of fit, F described above. Using this equation, the fit at high water ranged from 57% with the lowest channel friction values (Solimões: 0.022; Purus: 0.025) to 73% with the highest (Solimões: 0.028; Purus: 0.031).

The calibration of the 1D/2D diffusive channel model to JERS extents was carried out in exactly the same manner as the Wilson *et al.* (2007) model described above. The calibration of the 1D/2D diffusive channel model to gauged water levels was carried out as described in detail in Chapter 3. For all model runs, values of floodplain friction were found to make very little difference to the results, due to running the models with a fixed timestep (see model discussion in Section 4.2.3).

The calibrated friction values for the three calibrated model runs, described above, are summarised in Table 4-1. The new 1D/2D diffusive model, calibrated to gauged water levels, shows a much improved fit for channel levels for the whole hydrograph over those obtained from the Wilson *et al.* (2007) model, particularly at low water (detailed in Chapter 3). Friction values are similar, although, as noted in Chapter 3, the calibration of the Wilson *et al.* (2007) model was complicated by the fact that the average kinematic channel slopes that were used also acted implicitly as additional model parameters, making direct comparison of friction values difficult. Calibration of the new 1D/2D diffusive model to the JERS flood extent shows significantly higher river friction parameters than the Wilson *et al.* (2007) model.

Table 4-1 – 1D/2D Model calibration values

Model	LISFLOOD-FP version	Calibrated to	Solimões Manning's *n*	Purus Manning's *n*	Floodplain Manning's *n*
Wilson *et al.* (2007)	3.4.0	JERS extent	0.028	0.031	0.100
1D/2D diffusive model	3.6.3	Channel water levels	0.032	0.034	0.100
1D/2D diffusive model	3.6.3	JERS extent	0.070	0.070	0.100

Table 4-2 shows the associated fit statistic (*F*) results for the three model runs. These are for approximately the low water period (19-Oct-95) and approximately the high water period (26-May-96).

Table 4-2 – 1D/2D Models, low and high water JERS *F* results

Model	Calibrated to	*F* Oct 95 (~low water)	*F* May 96 (~high water)
Wilson *et al.* (2007)	JERS extent	22.73%	71.70%
1D/2D diffusive model	Channel water levels	27.70%	46.90%
1D/2D diffusive model	JERS extent	23.47%	74.00%

Figure 4-1 shows the flood extent comparison between the model results and JERS images for the three model runs. Figure 4-1(a-c) shows a binary comparison between the flooded cells in the model and the flooded cells derived from the JERS images (Figure 4-1(d)). Low water comparison is shown in the first image (i) and high water shown in the second image (ii). Three primary colours illustrate the results of the binary comparison: blue shows cells that are wet in the model and in the JERS image; red cells show where the model predicts the DEM is wet, but the JERS image shows it is dry (overprediction) and green shows where the JERS image is wet but the model predicts it is dry (underprediction). Grey shows areas excluded from the fit statistic (*F*) results.

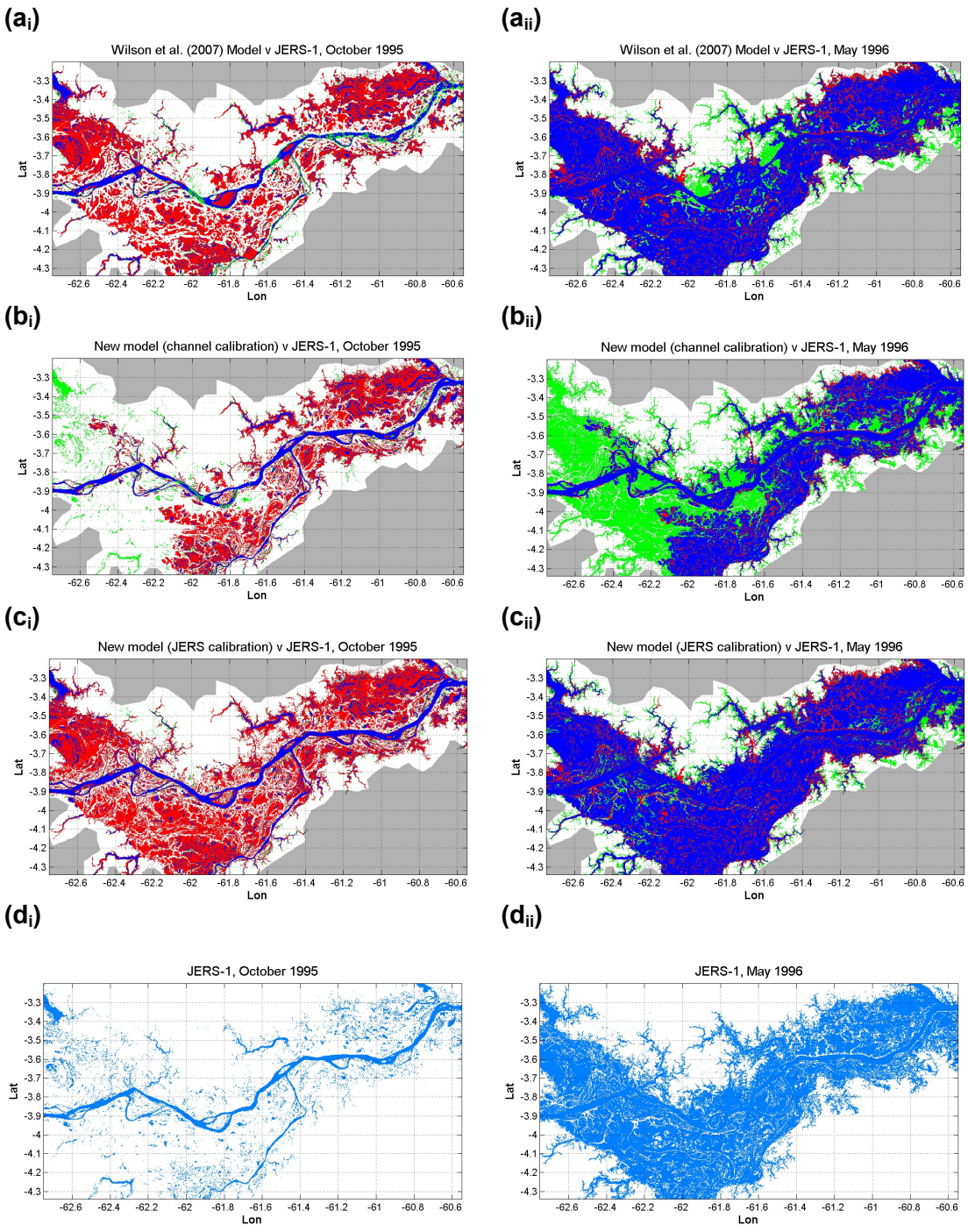

Figure 4-1 – 2D low ($_i$) and high ($_{ii}$) water results, (a) Original Wilson *et al.* (2007) model, (b) 1D/2D diffusive model calibrated to channel water levels, (c) 1D/2D diffusive model calibrated to JERS flood extent. Blue is flooded in both model and JERS, red is overprediction by the model, green is underprediction, white is non-flooded. Grey shows masked out non-floodplain areas. (d) JERS flood extents for both low and high water for direct comparison.

4.2.3 Model discussion

Despite the promising results from the Wilson *et al.* (2007) model, improvements in the geometric detail of the modelled channel and use of a diffusive solver introduced in Chapter 3, there are still notable discrepancies in the coupled 1D/2D model highlighted by the results presented here. With the new model, it is not possible to provide even a reasonable match to the flood extents, as illustrated by Figure 4-1 (b), while maintaining the very good fit to observed gauging station data (gauged data calibration). If the new model is calibrated to flood extent only (JERS calibration) as was done with the Wilson *et al.* (2007) model, a similar good fit at high water but poor fit at low water is achieved. However to obtain this fit unrealistically high friction values are used for the channels and the predicted water levels in the model channel are 7 m higher than those measured at the gauging stations. This suggests that, at realistic water levels, the model has difficulty in propagating the water from the channel into the floodplain. This is more noticeable at the upstream end of the model, as the downstream end is constrained by boundary conditions. This difficulty in moving water onto the floodplain may be related to the same lack of topographic detail in the 2D floodplain DEM that was noted by Wilson *et al.* (2007) as preventing correct drainage of the floodplain at low water. It may also indicate other possible underlying issues such as errors in the vegetation correction, leaving an artificially high DEM, or even datum mismatches.

An initial visual comparison of the 270 m model DEM with the 90 m DEM it was derived from, as well as with Landsat TM images and Google Earth imagery (Geoeye, Aug 2001), shows that the most likely omission from modelled topography is that of the floodplain channels. There are many of these floodplain channels and they are known to be important for conveying flow into the floodplain before the main river banks overtop. While some of these channels are very large, up to 1 km across, even the many smaller channels <100 m have been shown to be important in connecting the

channel with the floodplain (Bonnet *et al.*, 2005; Bourgoin *et al.*, 2007), and their omission will certainly limit the models ability to represent the dynamics of the floodplain.

A simple experiment using a Geographical Information System (GIS) to intersect a planar water surface to the model topography gives very similar, unrealistically high water levels compared to gauged data, and an even better high water fit statistic of 76.13%, than either JERS calibrated model. This could be partly due to the lack of topographic connectivity already postulated, limiting the ability of the models to propagate water to the furthest extents of the floodplain. However, the poorer fit of the more complex hydraulic models is most likely due to the lack of representation of floodplain hydrological processes in the model; direct rainfall, Evapotranspiration (ET), seepage and local runoff. This omission from the model was also noted in Wilson *et al.* (2007). Direct rainfall and local runoff are known to be a very important component of the floodplain system from a number of studies, providing pre-filling of the floodplain prior to the arrival of the out of bank flood water from the main river (Mertes *et al.*, 1993, Mertes, 1997).

All the models were run with computational timestep limited to 20 s for computational efficiency reasons. Hunter *et al.* (2005) showed that a fixed timestep in storage cell codes limits the representation of the system dynamics and so introduced an adaptive timestep approach which showed considerable improvements. Hunter *et al.* (2005) highlighted that LISFLOOD-FP results are insensitive to the floodplain friction when the model is not running with an adaptive timestep (as is the case here) because of the artificial flow limiter used to maintain stability. Unfortunately, despite speed improvements resulting from extensive parallelisation of the code (Neal *et al.*, 2009), the 270 m Amazon model would take around 3-4 months to run with an adaptive timestep, given current computers, compared with 3 days for the 20 s fixed timestep.

4.3 Floodplain channel spatial analysis

4.3.1 Current knowledge of Amazon floodplain channels

Attempts to use the 1D/2D diffusive hydraulic model in Section 4.2 as a tool to simulate and better understand the channel and floodplain hydrodynamics show very clearly that a lack of representation of essential components of those processes hinders this approach. The most obvious omission from the models is the lack of floodplain channel representation. A review in Chapter 2 of previous work on floodplain processes reveals that although the floodplain channels are acknowledged as important pathways connecting the channel and floodplain, there have been no dedicated studies of these important floodplain features.

Mapping and sedimentation studies show the floodplain channels are an important part of the Amazon riverine landscape. The floodplain channels provide important routes for conveying sediment from the main river into the floodplain (Mertes *et al.*, 1993) and the quantity and characteristics of the channels vary along the length of the Amazon mainstem (Mertes *et al.*, 1996; Toivonen *et al.*, 2007). Lake studies show that the channels provide important inputs to and outputs from the floodplain lake systems even during low to mid water conditions, and can reverse flow direction depending upon hydraulic conditions (Lesack and Melack, 1995; Bonnet *et al.*, 2005; Bonnet *et al.*, 2008; Cullmann *et al.*, 2006). A study of the Amazon main channel and floodplain geomorphology by Mertes *et al.* (1996) used navigation chart data to carryout a study of the width and depth of 105 of the wider floodplain channels (>100 m). They identified that the width of the largest channels in each reach increased in the downstream direction towards Óbidos, and that smaller channels (<100 m) were also present in all reaches. Navigation chart depths, where available, showed no correlation with downstream river distance.

Alsdorf (2003) used automated stream network extraction algorithms to identify flow path distance from the main river for locations in the Amazon floodplain and showed that water level changes measured with space shuttle based SAR data are inversely correlated to this distance. This work highlights the convoluted nature of the flow paths on the floodplain and the effect on floodplain water levels caused by the balance between water supply and drainage, as well as water storage. Alsdorf *et al.* (2005) attempt to model this complex floodplain flow through a simple diffusion model of the floodplain with the aim of moving away from the commonly used assumption that floodplain water levels equate to channel water levels. While the Alsdorf *et al.* (2005) model shows some broad correlation with interferometrically measured water level changes, more recent work (Alsdorf *et al.*, 2007a) shows the water level changes across the floodplain are even more complicated than thought previously and that some of these changes can be spatially correlated with the bigger floodplain channels.

Given the observed scale and quantity of these floodplain channels, it is certain that they play an important role in the hydrodynamics of the floodplain processes. The difficulties encountered in modelling these hydrodynamics by Wilson *et al.* (2007) and in Section 4.2 indicate further study of these floodplain channels and their representation in the hydraulic model is required. Lewin and Hughes (1980) show that floodplain dynamics are composed of many complex processes which introduce hysteresis in the inundation behaviour of the floodplain that varies by event, even on small rivers in the UK. Nicholas and Mitchell (2003) use detailed surveyed topography and 2D hydraulic modelling to show the importance of topography as a control on overbank flows over a range of spatial scales. Nicholas and Mitchell (2003) also show that abandoned river channels and floodplain ditches dominate the water routing on the floodplain, particularly at the start and end of the flood.

Some of the specific research questions regarding the Amazon floodplain hydrodynamics that remain to be answered are: (i) what are the basic hydrologic processes and components of the floodplain system; (ii) how important are the

floodplain channels in this system; (iii) what role do the floodplain channels play in defining the location and extent of the perirheic zone, where local runoff meets main river floodwater (Mertes, 1997), for the Amazon floodplain; and (iv) what is the balance between diffusive overbank flow and channelised flow? Related to these questions, in terms of hydraulic modelling are: (v) how well are these channels represented in the current SRTM topographic data used for the model; (vi) how well and at what scale do these channels need to be represented in order to simulate floodplain hydrodynamics correctly?

4.3.2 Analysis methodology

In order to address the current lack of knowledge regarding the floodplain channels, a spatial study of the channels was carried out utilising Landsat TM images (15 m resolution), SRTM data (90 m resolution), and Geoeye imagery, Aug 2001, obtained via Google Earth (1-2 m resolution). In a general review of the use of remote sensing of riverine landscapes, Mertes (2001) highlights the importance of river and floodplain connectivity to the study of river ecology. Mertes (2001) also references the use of Landsat TM images and image thresholding techniques to map this connectivity for the Mackenzie River delta (Mouchot *et al.*, 1991). Landsat TM images have already demonstrated their utility in the study of the Amazon wetlands (Mertes *et al.*, 1993; Mertes *et al.*, 1995; Peixoto *et al.*, 2009). Their free availability, well documented characteristics, long running programme (since 1972) and spatial coverage and resolution make them highly suitable for studying the floodplain channels.

Landsat 7 data was used for the majority of the analysis, specifically the Enhanced Thematic Mapper (ETM+) pansharpened mosaic from the period 1999 to 2003, ETM+Pan(99-03). This has an approximately 15 m spatial resolution, which is sufficient to resolve most of the floodplain channels of interest, with smaller channels likely to be obscured from overhead by overhanging vegetation. The Landsat 4-5 TM

1987-1997 mosaic was also used as a comparison in order to determine the relative changes in the channels over a decade timescale. Where available, detailed images from Google Earth were used for comparison, and to aid with the interpretation of features in the Landsat images. The Google Earth images were detailed enough to resolve individual tree canopies of 1-2 m across.

The primary methodology involved manual digitisation of all visible floodplain channels in the 30,000 km^2 study area using GIS software (ArcMap v9.2). Although there has been some success in applying automated and semi-automated methods of stream network extraction to remote sensing images (eg. Dillabaugh *et al.*, 2002; Pavelsky and Smith, 2008), many of these methods use assumptions related to the terrain slopes and flow behaviour of typical rivers that may not be applicable to the complexity of the Amazon floodplain channel network. Alsdorf (2003) notes this complexity problem when applying similar automated network extraction methods to SAR analogue topographic data in the Amazon floodplain. Once a better understanding of these floodplain channels is achieved, it may be appropriate to apply automated methods, but in the meantime in order to maintain more control over the finished vector product for future use in the hydraulic model, a manual method was adopted for this study.

Channels digitised included all visible channels except for the main Solimões channel and Purus tributary channel, but did include small tributaries feeding the floodplain from small local runoff catchments. Channels draining water out of the study area and therefore not directly contributing to the river and floodplain at this location were excluded from the analysis. Figure 4-2 shows the Landsat ETM+Pan(99-03) image for the study area, together with a number of detail views showing individual digitised channels and a detailed Google Earth image for comparison. Water bodies were very clear on the images as black or dark blue objects with pink indicating exposed beds at low water. This contrasted sharply with the green vegetation covering

much of the images. Channels were digitised in reaches of roughly equal width, and a separate reach was defined where there is an obvious branch or connection.

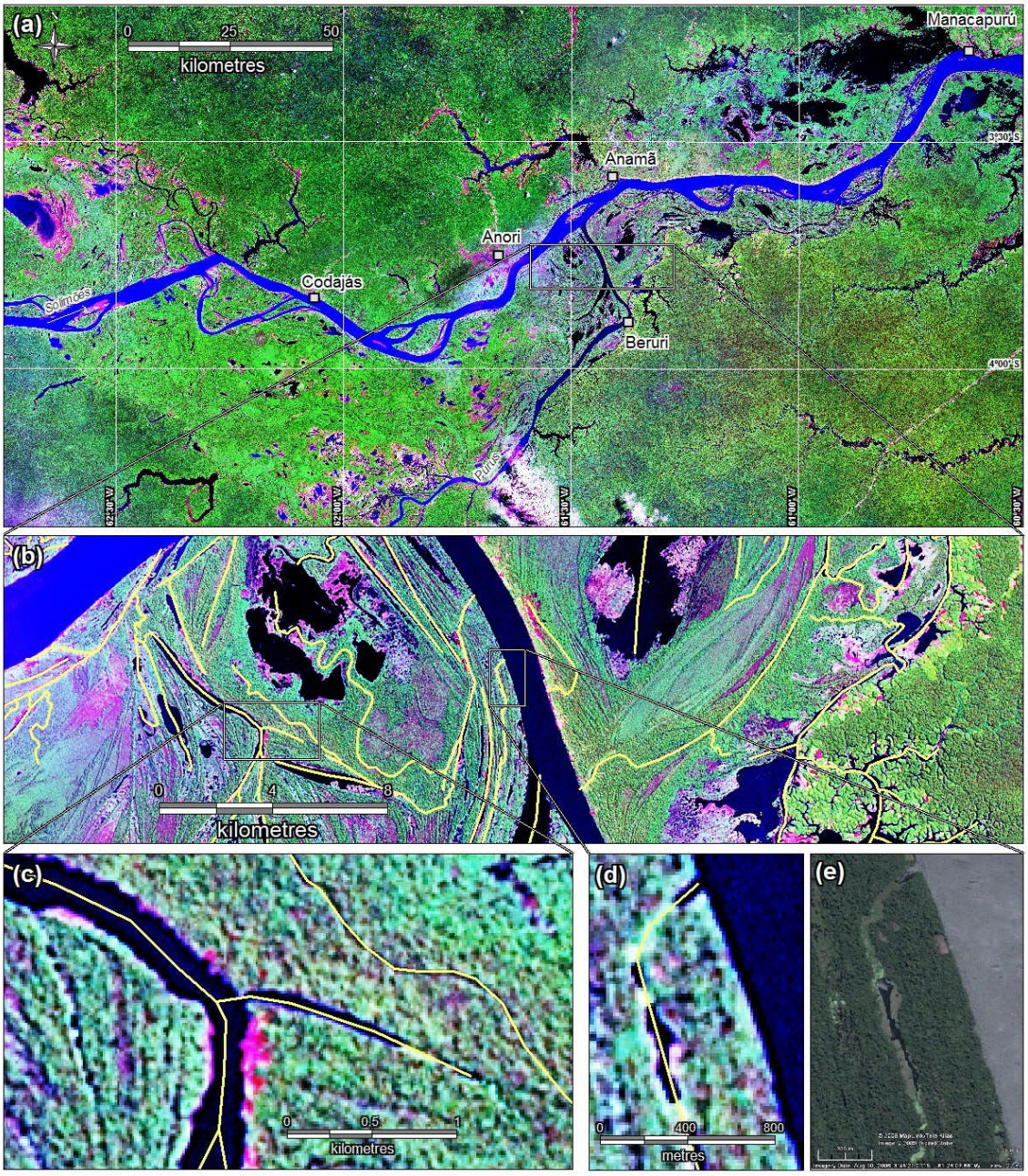

Figure 4-2 – (a) Landsat ETM+Pan(99-03) image for the study area, (b) detail showing a large area of digitised channels, (c) detail showing a smaller area of channels (d) detail a single 70 m wide channel (e) the same 70 m wide channel in a Google Earth image.

Figure 4-2 illustrates some of the practical difficulties in digitising the channels. The Landsat ETM+ mosaics are composed of cloud free images over several years, so

cannot be taken as a fixed point in the flood wave cycle. Most of the images used appear to come from the low water period when there is generally less cloud cover. This means that in the mosaic image, the floodplain is well drained, revealing large areas of lake bed or sediment deposits which can be seen as the pink areas in the images. In addition, the remaining visible channels that were digitised were the bigger and deeper channels that still contain water during the low water period. The smaller channels of 20-30 m, were the most difficult to digitise, as this was close to the image spatial resolution of 15 m, making them less clear. In addition, overhanging tree canopies obscure a greater proportion of the width of the smaller channels making it hard to determine the continuity of the channel on occasions. Floating macrophytes blocking channels also made it hard in some locations to determine channel continuity. Where available, the Goggle Earth images were invaluable in determining continuity with more confidence. Figure 4-2 (c) shows some very small channels on the left side of the image, in a north-south orientation, where only small areas of water are visible. Figure 4-2 (d) and (e) show floating macrophytes blocking a 70m wide channel, clearly visible in the Google Earth image and showing as brighter green in the Landsat image.

For each of these vectorised channels, a number of different physical characteristics were quantified and assigned to an attribute table. Details of each attribute and their quantification methodology are summarised in the metadata in Table 4-3. The digitisation and characterisation of the floodplain channels described above has resulted in a large computerised dataset of 1,762 vectorised floodplain channels, suitable for a wide range of spatial and numerical analyses as well as other future uses, such as incorporation into hydraulic models of the floodplain.

Table 4-3 – Floodplain channels dataset metadata

Attribute	Description
id	Unique object ID
type	Grouping based on channel size and connectivity: “main” - very wide (>~150 m) well connected channels that drain large areas; “medium” - medium width channels (~50-150 m) with good connections; “minor” - other small channels (<~50 m) or poorly connected channels.
network	Channels that are obviously connected in the same network are classified as belonging to the same network group.
width	The width of each channel was measured manually with the distance tool in ArcMap. This was done three times, once at each end and once in the centre of the reach, then the mean width is recorded. Where a channel passes through a lake, the width of channelised section was used rather than the lake width. Measurements were rounded to the nearest 10 m due to the image resolution and the smallest channels detectable clearly are around 20 m wide.
length	Length was extracted automatically from the GIS object and rounded to nearest metre.
buffer	This was half the channel width or 90 m, whichever was larger. This value was used in extracting the minimum vegetation-corrected SRTM elevation along the channel reach. It is sized so the buffer area will cover the lowest elevation along the channel reach, allowing for data translation error, and diagonally gridded channels.
minimum SRTM DEM elevation	Minimum vegetation-corrected elevation along the channel reach, automatically extracted using the region inspection tool and channel buffer width from the 90m SRTM DEM. This is the lowest elevation from the DEM that was present within the buffered area.
estimated depth	A tentative estimate of channel depth assuming a 1 m depth per 10 m channel width. There are very little data to base this on so it was only used to give an indication of how deep the channel might be and, therefore, what the bed elevation might be. A small amount of data collected in the floodplain by Wilson *et al.* (2007) during the 2005 bathymetric survey indicates that depths might not exceed 10 m and therefore values were capped at 10m if the channel was wider than 100 m.
minimum bed elevation	Calculated by subtracting the tentative estimate of channel depth from the minimum SRTM elevation along the reach. Provides an indication of bed elevation.

4.3.3 Analysis results

Overview

A total of 1,762 channels were digitised within the study area. The channels ranged in width from 900 m down to the minimum resolvable width of around 20 m, with a mean width of 47 m and length from 160 m to 67 km, with a mean of 5.3 km and total length of 9,293 km. Figure 4-3 shows all the digitised floodplain channels with line thickness relative to width. Overall statistics of the channels are detailed in Table 4-4 and mean values grouped by channel type are given in Table 4-5.

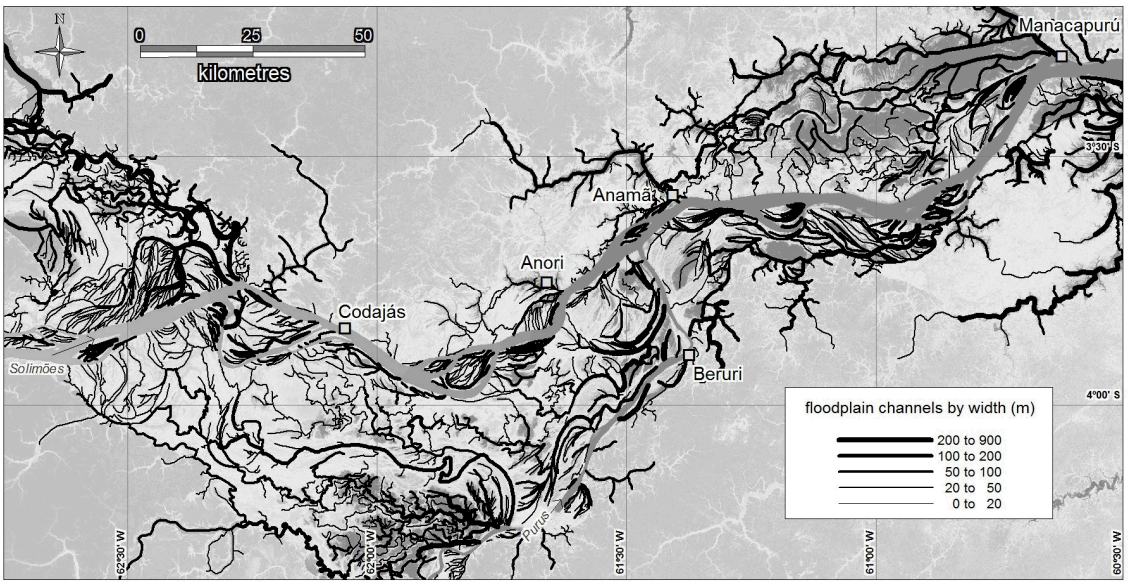

Figure 4-3 – Digitised floodplain channels

Table 4-4 – Overall floodplain channel statistics

statistic	width (m)	length (m)	minimum SRTM DEM elevation (m)	estimated depth (m)	estimated bed elevation (m)
minimum	20	160	-7.0	2.0	-17.0
mean	47	5,274	7.9	4.2	3.7
maximum	900	67,384	32.0	10.0	29.2
Standard Deviation	48	5,517	6.3	2.4	7.5

Table 4-5 – Mean values by floodplain channel type

type	count	mean width (m)	mean length (m)	mean minimum SRTM DEM elevation (m)	mean estimated depth (m)	mean estimated bed elevation (m)
main	13	309	24,001	2.3	10.0	-7.7
medium	147	104	12,994	4.2	8.0	-3.8
minor	1,602	40	4,414	8.3	3.8	4.5
Total	**1,762**	**47**	**5,274**	**7.9**	**4.2**	**3.7**

These statistics show that the smaller channels are much more common than the medium channels and these in turn are more common than the large channels. Figure 4-4 shows log-log plots of the derived floodplain channel characteristics. Plotting frequency against channel width with logarithmic axes and fitting a power law to the data, as shown in Figure 4-4 (a), reveals that each channel width bin has approximately twice the number of channels as the next largest width. This is an example of the classic scaling relationships that have been described for river networks, showing patterns of structure that are self-similar or fractal-like over many orders of magnitude (Brown *et al.*, 2002; Rinaldo *et al.*, 2006).

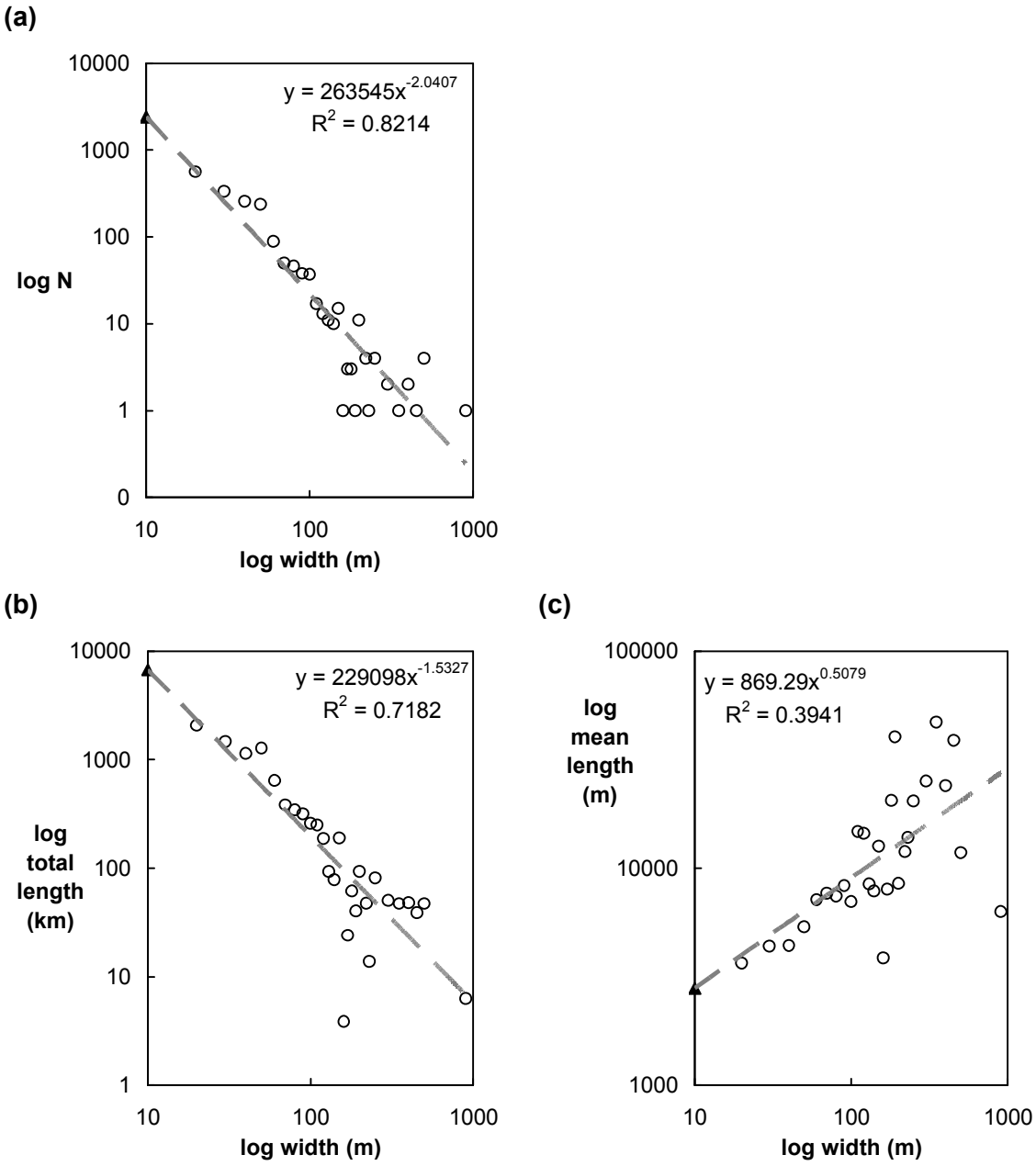

Figure 4-4 – log-log plots of channel characteristics (a) frequency versus channel width, with power fit (b) total channel length versus width, with power fit, (c) mean channel length versus width, with power fit. Data are shown as hollow circles, extrapolated value for 10 m channels is a filled triangle, and power law fit is a dotted grey line.

Figure 4-4 (b) & (c) also show power law behaviour for total channel length and mean channel length, respectively. More scatter for the longer channels is to be expected as they are represented by a smaller sample size. These power law

relationships provide a method of predicting the parameters for the channels below the measurement threshold of 20 m, and as the channels are grouped by 10 m intervals, this means there is no information for the 10 m channel group. The extrapolated values for the 10 m channels are plotted in Figure 4-4. The extrapolated values for frequency show that the 10 m channels account for an extra 2,400 channels, more than the sum of all the other channels. While the mean length (2.8 km) of these smaller channels is shorter than the other channels, they still add another 6,719 km (+72%) to the total length of floodplain channels. Including the 10 m channels allows a revised estimate of 4,162 channels, with total length of 16,013 km, for the study area.

Extraction of the channel elevation from the vegetation-corrected SRTM DEM was found to be problematical, given that the mean width of floodplain channels was 47 m and the DEM spatial resolution was 90 m. While the overall pattern of elevation levels extracted followed a down-slope trend with drainage, it was not clear if this trend was due to a better representation of the larger channels in the DEM or a real trend. Nonetheless, this method does at least provide an estimate of what the channel elevations might be. Although channel depths were calculated from the channel width, there are very few data to support this and analysis of the resulting depths did not provide any additional understanding at this stage. As a consequence, estimated depths were not considered any further. At this stage, floodplain channel depths remain an unknown channel characteristic requiring further research.

Floodplain channel networks

In addition to an overall assessment of the floodplain channel characteristics, a detailed inspection of the channel network groups identified during channel digitisation was undertaken. This showed that most of the network groups had very little in the way of obvious channel connections to other networks. Some networks obviously drained into others, but were otherwise separate. Signs of possible connections between

networks were observed at the upstream end of some networks but were obviously dry in the Landsat ETM+ mosaic, implying connection only at high water. Figure 4-5 shows the resulting 66 separate networks.

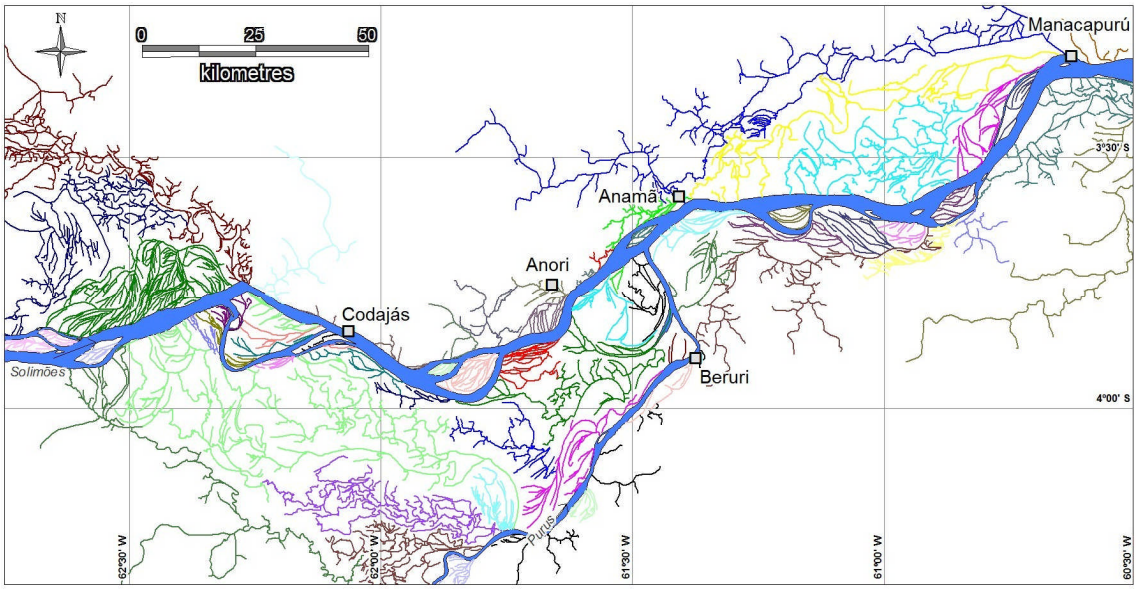

Figure 4-5 – digitised floodplain channels coloured by networks isolated from each other except at high water

Differences between the channel and network characteristics, as well as the separation of these networks, implies that there are different processes at work in these areas. Delineation of the "catchment" areas represented by each network allow these areas to be grouped into six types based on differing hydrological inputs as well as quantification of their differing area and network characteristics. These areas are here termed "*floodplain hydrologic units*" (FHU) as they represent distinct separate areas of floodplain thought to function as single units from a hydrological perspective. While it is not suggested that these units are totally isolated from each other, it is thought that the hydrological inputs, hydraulic gradients and sediment availability in each area ensures relative isolation of surface flows for considerable portions of the flood cycle. The units are expected to become connected at high water through diffuse flow across the boundaries between them, and are likely to be connected all the time

through groundwater flow. Table 4-6 shows a detailed breakdown of the characteristics of these FHUs that have been used to group them by class and type. These characteristics are also shown graphically in Figure 4-6.

Six types of FHU were indentified, which can be grouped into three classes, each with two types. The first class are those units found closest to the river and which are completely dominated by river floodwater and sediment deposition and have very little in the way of local hydrology runoff input other than direct rainfall. The second class covers central areas of floodplain with low topography that are generally isolated to some extent from river flow by the first class of unit, but also receive little input from terrace runoff bordering the floodplain. The final class of unit encompasses direct and indirect runoff inputs from the hillslopes.

Table 4-6 – Characteristics of floodplain hydrologic units

Class	FHU type	count	area (km^2)	% of total area	mean area (km^2)	mean SRTM DEM elevation (m)	total channel length (km) *	drainage density (km/km^2)
1a	**island**	11	501	2.0%	46	22.0	998	1.99
1b	**bypass**	17	1,918	7.7%	113	20.3	3,616	1.88
2a	**connect**	7	4,492	17.9%	642	18.1	4,308	0.96
2b	**basin**	4	2,019	8.1%	505	19.3	2,289	1.13
3a	**indirect**	6	12,082	48.2%	2,010	31.4	3,914	0.32
3b	**direct**	5	4,037	16.1%	807	31.8	987	0.24
	Total	**50**	**25,050**	**-**	**501**	**22.8**	**16,012**	**0.64**

**** includes estimated length of 10m channels***

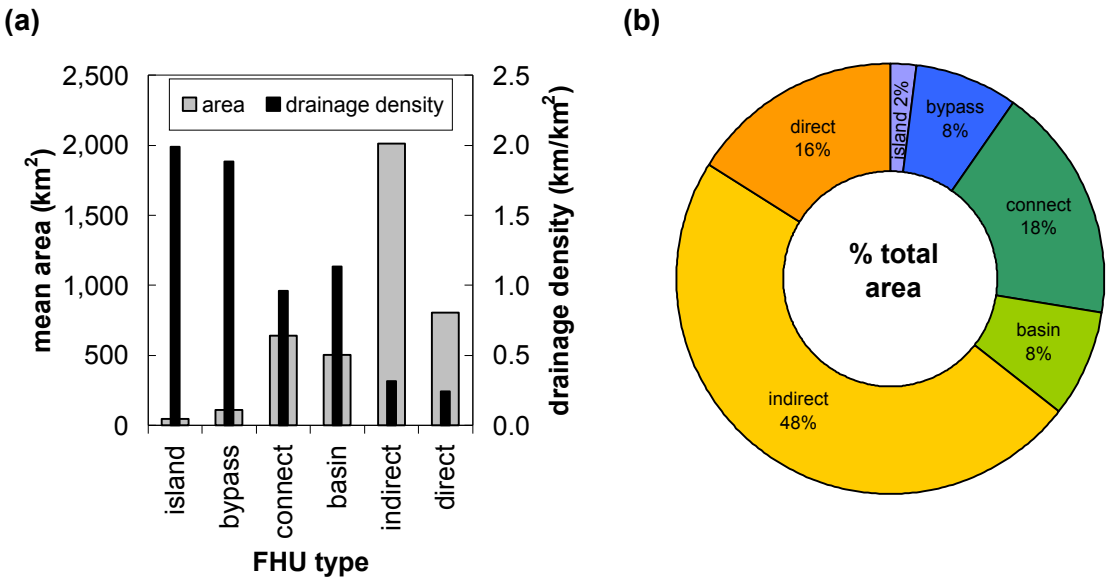

Figure 4-6 – (a) mean area and drainage density by FHU type (b) Percentage of total contributing area for FHU types

The data in Table 4-6 shows that FHU types belonging to class 1, *island* and *bypass* units, are more numerous and smaller than the other types due to the more active sediment deposition and erosion processes active in these units. The mean area of *indirect* FHUs is by far the largest, mainly due to the fact that each collecting channel, of which there is only one in each unit, runs along the edge of large areas of floodplain picking up runoff from numerous small terrace catchments. The mean elevation characteristic shows *direct* and *indirect* types of class 3 are the highest, due to the inclusion of terrace catchments. The next highest is class 1 with its high sediment deposition, and the lowest mean elevation is the central basin areas of class 2 which receive considerably less sediment (Latrubesse and Franzinelli, 2002). This pattern is also reflected in the difference in drainage density of the classes. The *island* and *bypass* units have double the drainage density of the central floodplain types, *connect* and *basin,* which in turn have 3.5 times the drainage density of the terrace slope types *direct* and *indirect*. A number of factors are known to collectively influence stream density; climate, topography, soil infiltration capacity, vegetation, and geology, as well as map scale and delineation method (Gregory and Walling, 1968). More study

will be required to identify the exact controls for the drainage density differences observed on the Amazon floodplain. However, these variations reflect fundamental differences in the processes that dominate in each floodplain hydrologic unit type.

A detailed description of each type of floodplain hydrologic unit and its class are given in Table 4-7. The floodplain hydrologic units defined for the study area are shown in Figure 4-7. Some separate floodplain channel networks draining directly into the main river have been grouped together into single floodplain hydrologic units to improve clarity. This results in a total of 50 floodplain hydrologic units for the 66 networks.

This is the first time that a method of breaking down the complex heterogeneity of the Amazon floodplain into functional units has been demonstrated. Whilst it is not claimed that this method is definitive, it does show broad patterns that appear to be correct overall and further study should be able to confirm this and hopefully extend it, whilst providing more objective classification of the units. The fact that these floodplain areas have different hydrological characteristics (e.g. drainage density and water sources) has important implications for many biogeochemical studies in the Amazon which rely on an understanding of these characteristics in order to quantify and estimate dependent processes.

Table 4-7 – Floodplain hydrologic unit descriptions

Class	FHU type	Description
1a	island	Dominated by river flow, with a series of channels cutting across the island parallel to the main river. Channels can join up on the larger islands to form one or more larger exit channels draining back to the main river. Typically covered in scroll-bar topography with occasional long, narrow lakes.
1b	bypass	A floodplain area directly adjacent to the main river channel dominated by flood flow from the main river, bypassing the main channel through the floodplain. Characterised by a series of parallel channels curving away from and back to the river in arcs. In larger areas, channels can join up to form one or more larger exit channels draining back to the main river. Typically covered in scroll-bar topography with occasional long, narrow lakes. Some units may only have the channels carrying water away from the river which are then intercepted by a large drainage channel from an indirect unit type. Conversely, some units have only the return channels, to provide a return connection to the main river for diffuse floodplain flow.
2a	connect	Central area of floodplain that provides a connection across the floodplain from upstream to downstream along the river or even from river to river. Very different channel pattern to bypass units, consisting of an irregular dendritic drainage network. Low elevation topography and large lakes. Commonly separated from the main river along its side by bypass units. Probably dominated by drainage and local runoff except at high water when drainage network provides a connection for flood flows across the unit.
2b	basin	Central area of floodplain that is commonly only connected to the main river channel at one end, usually at the downstream end. Characterised by low elevation flood basin topography and a dendritic channel network with large lakes. Due to isolation from main river, very little sediment reaches these areas, so they have remained unfilled since the last post-glacial sea level rise and may also be undergoing subsidence (Dunne and Mertes, 2007). Connects with adjoining basins at high levels and may experience reverse flow backing up the main drainage channel when downstream river levels are high due to lack of channel connections to the main river channel at the upstream end.
3a	indirect	Small river terrace runoff catchments not directly connected to main river, usually due to floodplain sedimentation blocking direct flow from these catchments to the main river. Flows from a number of these catchments can join together in one long main collector/drainage channel that runs generally parallel to the terraces which border the floodplain until it reaches the main river. The channel is also commonly connected to the main river at the upstream end providing a flow path for flood flows across the floodplain. Hydrology dominated by local runoff until flood flows flush through main channel. The main floodplain collector/drainage channel of these units is often highly sinuous.
3b	direct	Small river terrace runoff catchments directly adjacent to main river channel. Dendritic drainage pattern with single main drainage channel. Outlet channel valley is commonly flooded forming a ria lake connected to the main channel through a channel in a spit formed by sediment from the main river. Dominated by local runoff.

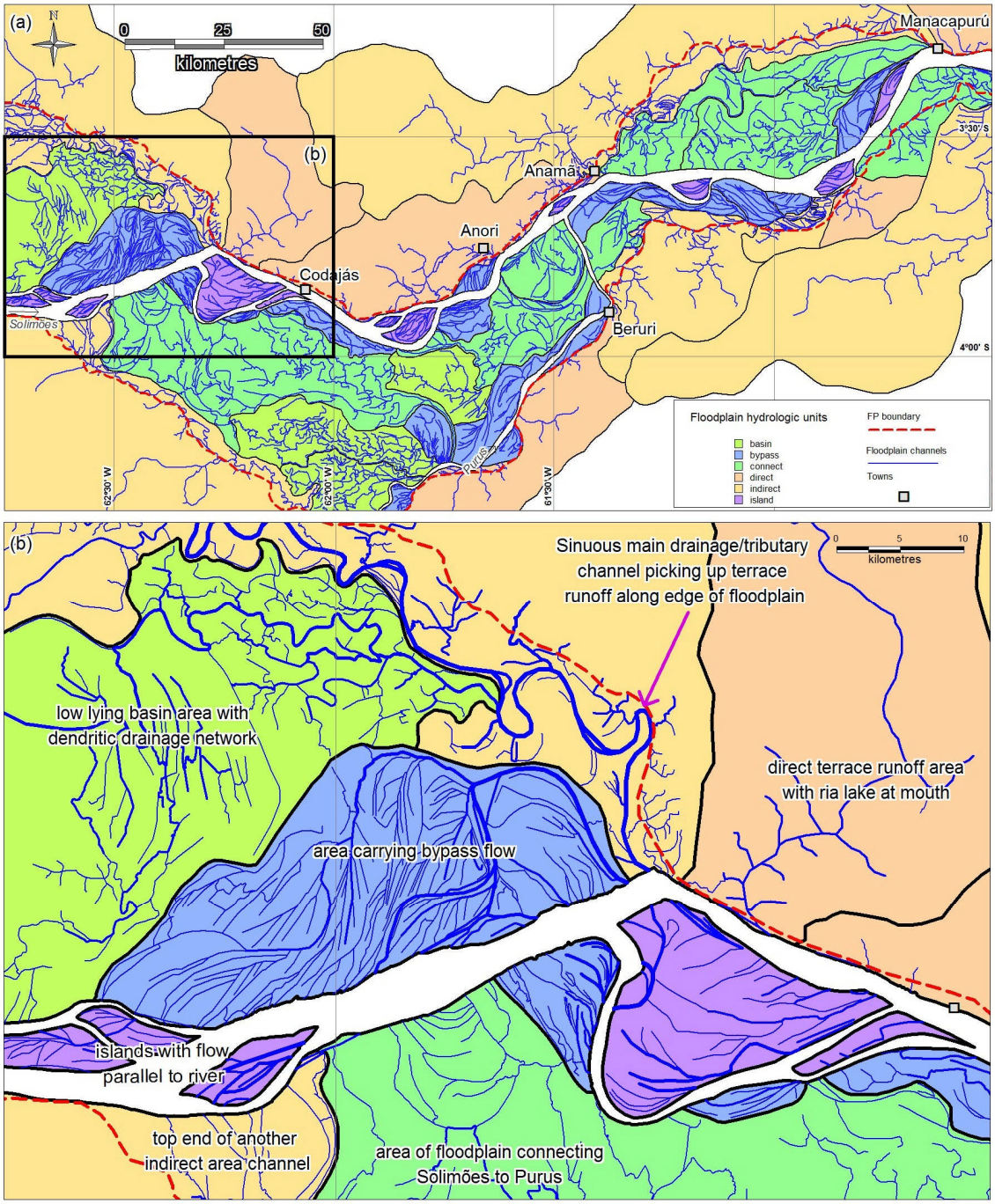

Figure 4-7 – (a) floodplain hydrologic units (b) detail showing examples of types of unit more clearly with annotations

Table 4-8 provides an area breakdown summary for the study area based on the floodplain hydrologic units. This shows that most of the study area (78%) directly contributes to the river flow by the time the Solimões exits at the eastern boundary of the study area. Of this contributing area, approximately 41% is mainstem floodplain confined by the river terrace along the edge of the floodplain. The remaining 59% of the contributing area is local runoff catchment area from the terrace slopes.

Table 4-8 – Area breakdown summary

	area (km^2)	% of total study area	% of contributing area
area draining out of study area	6,950	21.7%	-
area contributing to river (total FHU area)	25,050	78.3%	100%
mainstem floodplain area	10,390	32.5%	41.5%
internal catchment area that is non-floodplain	14,660	45.8%	58.5%
total study area	**32,000**	**100%**	**-**

Landsat imagery has been used previously to study the Amazon floodplain (Mertes *et al.*, 1995; Toivonen *et al.*, 2007; Puhakka *et al.*, 1992), but none of these studies have looked specifically at mapping the floodplain channels in detail and identifying networks by connectivity. Hamilton and Lewis (1990) used Landsat images to study the physical characteristics of the fringed floodplain of the Orinoco River in Venezuela and divided the floodplain into seven reaches for interpretation and also noted that the floodplain could be grouped into spatially discrete units, the location of which was dictated by hydraulic controlled points on the main river. However, these units were used to refer to large areas of floodplain on both sides of the river and not to divisions within the floodplain, and are therefore different to the FHUs described here.

The FHUs defined here are a subclass of more general hydrogeomorphic units, a term used to refer to a land form characterised by a specific origin, geomorphic setting, water source, and hydrodynamic (eg. Cole *et al.*, 2002; Nardi *et al.*, 2006).

Stability of networks

Visual comparison of the digitised floodplain channels with images from the preceding decade, i.e. the Landsat TM (87-97) mosaic, showed very little obvious change to location or width. This implies that these networks are relatively stable over the decadal timescales of interest to this study. A more comprehensive and quantitative assessment of channel movement may show that the channels in some floodplain hydrologic unit types are more active then others.

4.4 Hydraulic connectivity analysis

The spatial analysis of the floodplain channels in Section 4.3 shows that the floodplain can be divided into areas with varying degrees of connection to the main channel and the local runoff hydrology. The floodplain channel networks play an important role in this differing connectivity and their size and density imply that they carry significant flow and thus play an important role in the dynamics of floodplain wetting and drying in addition to any diffusive overbank flows. This general concept of hydraulic connectivity on the floodplain is important because, in addition to the local and regional hydraulic gradients, it controls the balance between channelised flows and diffusive flows on the floodplain, as well as fluxes between the main channel and different areas of the floodplain. In order to investigate this floodplain connectivity, SRTM data was used which, at the time of this analysis, was the current best topographic detail of the floodplain available for the study area.

The SRTM data are the same topography data used to represent the floodplain in the 2D element of the hydraulic model. Thus, this study of the hydraulic connectivity in the SRTM data also served to identify how the floodplain channels are represented in the hydraulic 2D model, in order to understand how well the model simulates the dynamic processes on the floodplain. In addition to how well the model explicitly represents the channels within the 2D DEM, there are related connectivity issues to do with how the hydraulic model represents hydraulic connectivity between the regular grid cells which also affects the modelling of the diffusive floodplain flow, particularly as the model code formulation does not allow diagonal flow between cells (Bates and De Roo, 2000).

4.4.1 Floodplain channel representation in SRTM DEM

The SRTM DEM in the study area has a spatial resolution of 90 m, absolute height error of 6.2 m and relative vertical error of around 5.5 m in South America (Rodriguez *et al.*, 2006). The relative vertical error is defined as the sum of the individual random errors, or noise error. For the hydraulic model, the DEM was resampled to 270 m to reduce the vertical noise to around 1.8 m (using a reduction factor of $1/\sqrt{n}$, where n is the number of pixels being aggregated, as suggested by Rodriquez *et al.* (2006)), as well as to improve computation speed. From the Landsat ETM+ analysis of floodplain channels, 95.7% of the channels are less than 90 m in width and 99.7% are less than 270 m in width. Clearly only the very widest channels will be represented well in either the 90 m or 270 m DEMs. Figure 4-8 shows a typical 100 m wide floodplain channel on both the Landsat image and SRTM DEM. Elevation values extracted along its digitised length from the vegetation-corrected SRTM DEM are also plotted.

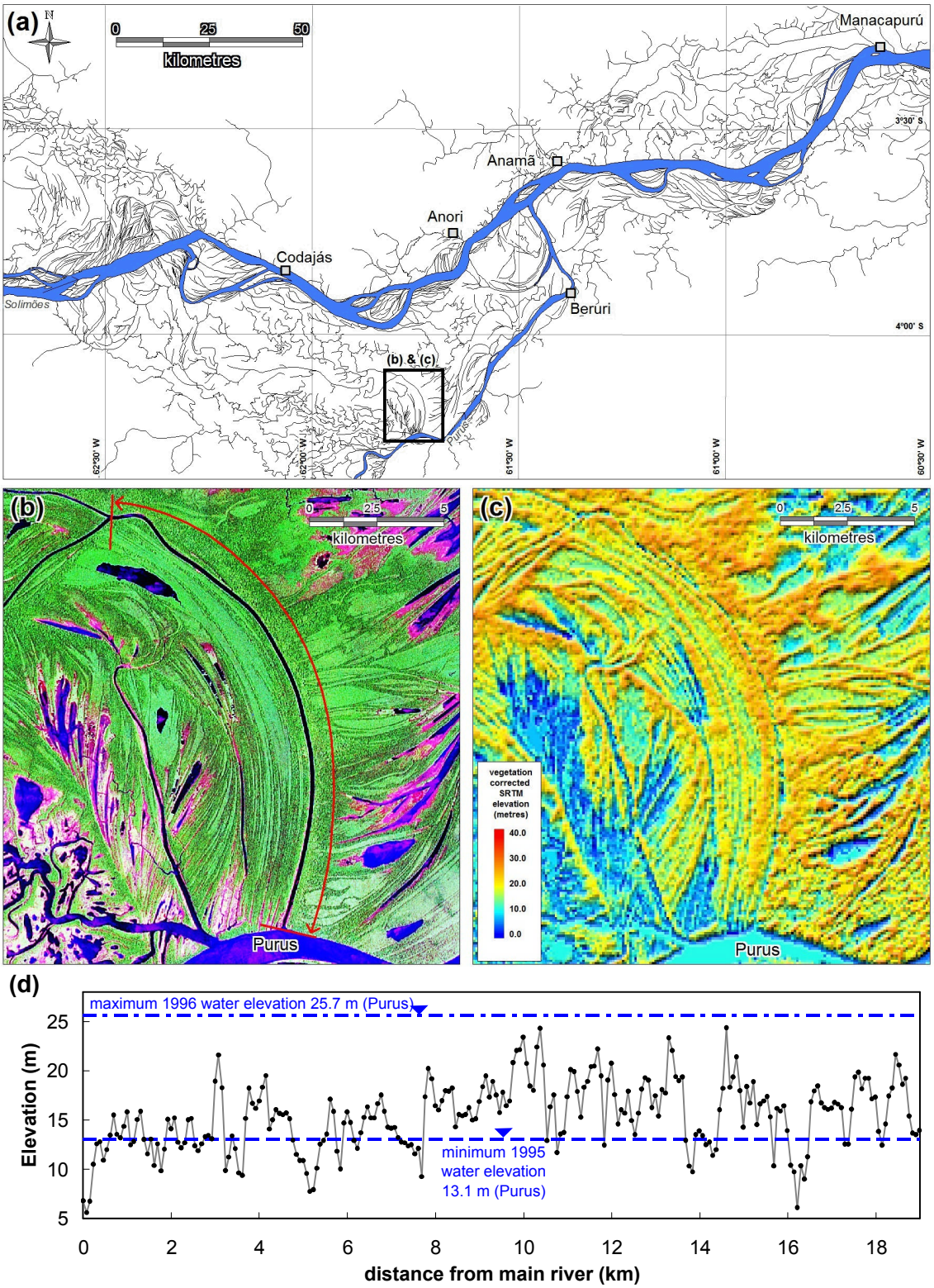

Figure 4-8 – (a) Digitised floodplain channels, (b) Landsat image showing a typical 100 m floodplain channel, (c) SRTM 90 m DEM of same area, (d) elevation extracted along digitised channel reach from vegetation-corrected SRTM data and 1995 low water (below mean annual low water) and 1996 high water (above mean annual high water).

The profile in Figure 4-8 (d) illustrates how poorly even a medium sized channel is represented in the SRTM data. The 19 km profile shows a rapidly varying elevation along the length of the channel, ranging from a minimum of around 5 m to a maximum of 24 m. In reality, a channel profile is likely to have a shallow slope of low elevation. The SRTM instrument does not always map the true ground surface. Where there are smooth surfaces such as water, very little signal is returned, resulting in voids in the data. Vegetation causes further complications with the return signal being influenced by vegetation height, structure and density (Farr *et al.*, 2007).

The SRTM data was collected in February 2001, during the low water season in the study area. This means that the low points in the channel profile probably represent low water elevations or even the exposed bed or banks of the channels. Although normally no radar signal is received from open water, the presence of floating vegetation or a disturbed water surface is likely to provide some return along these channels. The high points in the channel profile will obstruct flow at this scale within any hydraulic model constructed using the SRTM data. The high points in the profile result from the coarseness of the SRTM data as well as factors such as overhanging vegetation along the banks.

Whilst this channel represents only one example, carrying out the same procedure on other floodplain channels reveals the same lack of representation. It is reasonable to assume that the lack of representation will be worse for smaller channels and with 95.7% of the channels being less than 90 m SRTM resolution in width, there is every reason to believe that this is common for all floodplain channels.

4.4.2 DEM connectivity assessment methodology

In order to investigate the implications of the lack of floodplain channel representation in the SRTM DEM, as well as issues related to general cell to cell connectivity, a DEM connectivity assessment tool was written in Matlab v7.1. This tool

carries out a four stage assessment of top to bottom connectivity for a given DEM. The code cycles through a range of test elevations, with a given increment of elevation, and carries out the following functions:

(1) Identify as wet, all cells that are below the test elevation, irrespective of whether they are connected or not. This is for comparison to the outputs of the following stages.
(2) Assuming that orthogonally adjacent wet cells will allow flow to occur, identify all cells that would be wet by iteratively propagating water across a "dry" DEM from the top edge. This is the DEM's 'four-side rule' connectivity (Poulter and Halpin, 2008).
(3) Explicitly remove cell groups that do not connect all the way across the DEM, as these do not contribute to the flow connectivity.
(4) For each row of the connected DEM, sum the number of connected cells and identify the minimum. A minimum flow area at a given elevation across the DEM is then calculated as the minimum number of connected cells multiplied by the cell width and elevation interval.

The aim of the tool was to assess connectivity in one direction across a 2D DEM, so it was not appropriate to apply it to the full study area with its complex channel interaction and multi directional flow. Therefore, a subset area of floodplain was chosen for testing for which there were known problems representing the flooding in the model, and which has an expected top to bottom flow direction (north to south). The test area also needed to be close to the main channel so that a range of expected water levels were known with which to test the DEM. The chosen test area is shown in Figure 4-9, together with the digitised floodplain channels for the area.

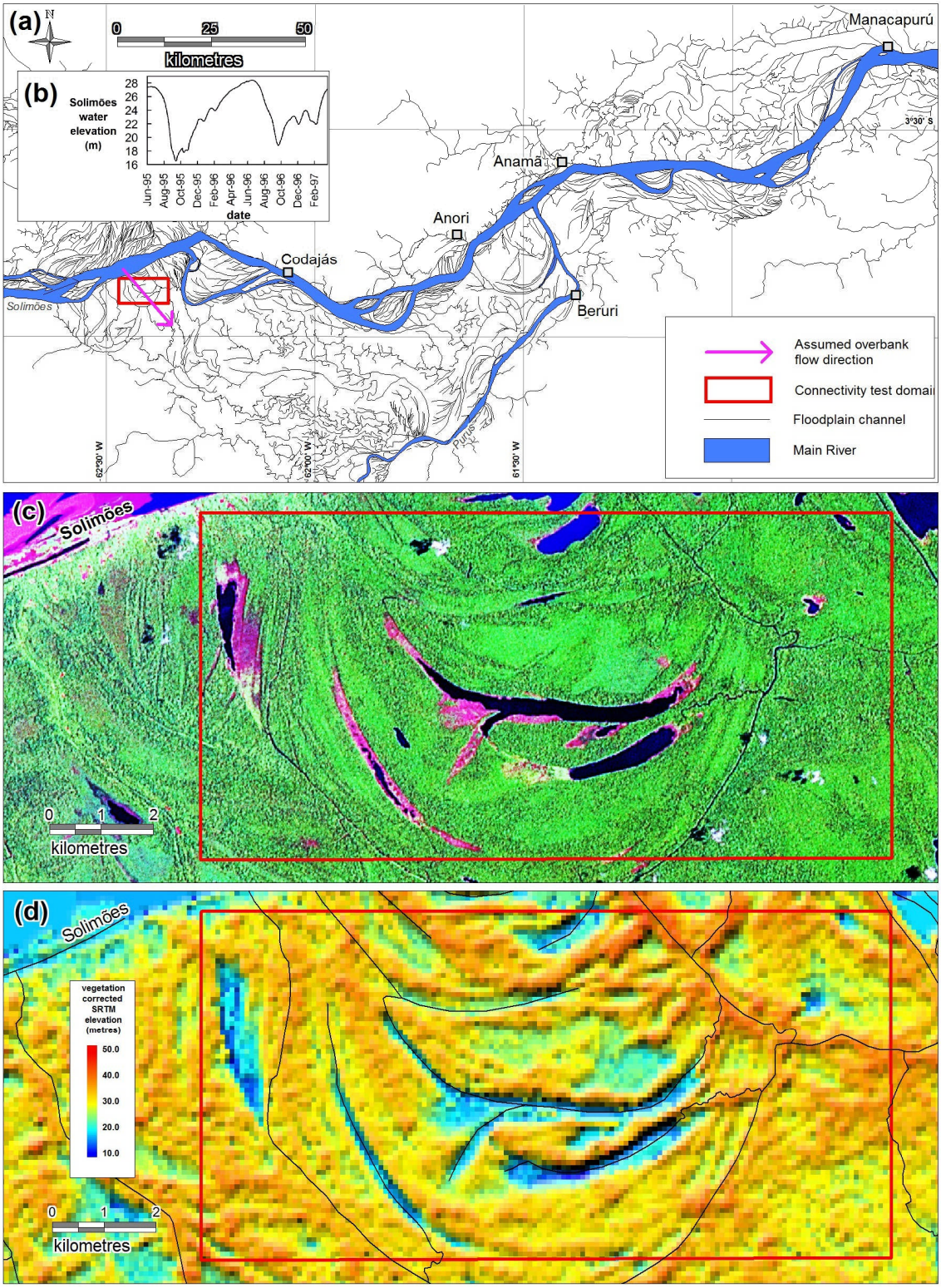

Figure 4-9 – (a) Test site location and floodplain channels, (b) water elevations in main channel adjacent to test area for 1995 – 1996, (c) Landsat detail of test area, (d) vegetation-corrected SRTM of test area.

The test subset of floodplain covers an area of 83.98 km^2 on the south bank of the Solimões towards the upstream end of the main study area. Analysis of the vegetation-corrected SRTM data shows a range of elevations from 10.0 to 46.6 m, and a mean of 31.6 m. Overbank flows are assumed to flow in a northeast to southwest direction across the area. Landsat TM images show five interconnected crescent shaped floodplain lakes with floodplain channels connecting north to south across the test area. There are 15 visible floodplain channels totalling 66 km in length. The floodplain channels vary between 20 and 40 m in width.

Although recent satellite measurements show clearly that water levels in the Amazon floodplain cannot be assumed to equal those in the main channel (Alsdorf *et al.*, 2007a), main channel water elevations still define a realistic range of elevations with which to test the connectivity of the floodplain subset. Water elevations in the main Solimões channel immediately adjacent to the test area, extracted from the channel calibrated model (Chapter 3), show an approximate minimum for the low water period (19-Oct-95) of 16.5 m and approximate high water period (26-May-96) of 28.4 m. The highest recorded water level in the 106 year Manaus gauging station record is the 2009 level which was 1.23 m higher than the peak in 1996. If a similar level of difference for the test location is assumed, then a maximum water elevation would be expected to be around 29.6 m. The JERS calibrated models from Section 4.2 show an approximate minimum for the low water period (19-Oct-95) of 19.9 m and approximate high water period (26-May-96) of 35.7 m, considerably higher than the measured elevations at the gauging stations, as noted in Section 4.2.3. The key elevations are summarised in Table 4-9. The chosen elevation range for the testing covered all of these elevations, 15 to 40 m with a 0.2 m interval.

Table 4-9 – Key water elevations for main river channel

Model	19-Oct-95 approximate low water (m)	26-May-96 approximate high water (m)	Estimated 2009 maximum (106 yr record) (m)
Channel calibrated model	16.5	28.4	29.6
JERS calibrated model	19.9	37.0	

Three different DEMs representing the chosen test area were assessed with the connectivity tool:

(1) a 90 m vegetation-corrected SRTM DEM (144 x 72 cells), representing the resolution and detail of the original SRTM data;

(2) a 270 m DEM (48 x 24 cells), as used in the hydraulic model, mean resampled from the 90 m vegetation-corrected DEM; and

(3) a 15 m DEM (864 x 432 cells), bilinear resampled from the 90 m vegetation-corrected DEM. This DEM was modified to include the floodplain channels by "burning in" the channels with an average width of 30 m using the minimum SRTM value extracted along their lengths. The channels had a mean minimum SRTM elevation of 18.5 m.

4.4.3 DEM connectivity assessment results

Figure 4-10 shows the connectivity test results for the 90 m DEM. Results are shown in pairs, the first plot ($_{i}$) showing cells that are below the test elevation and the second ($_{ii}$) showing connected cell flow paths below the test elevation. The first pair of plots shows the results for the near maximum 1996 main channel water elevation, 28.4 m. The second pair shows the results for the minimum water elevation for which there is a connection across the DEM, in this case 32.6 m and the final pair show the results

for the maximum 1996 JERS calibrated model water elevation, 37.0 m. Figure 4-11 shows the results for the 270 m DEM. For the 270 m DEM, the DEM does not connect across until 34.0 m. Finally, Figure 4-12 shows the results for the 15 m DEM tests. For the 15 m DEM, connection across the area first occurs at 20 m, and is shown first. The 15 m DEM results for the first connection elevation of 32.6 m from the 90 m DEM are also shown for comparison with the 90 m DEM.

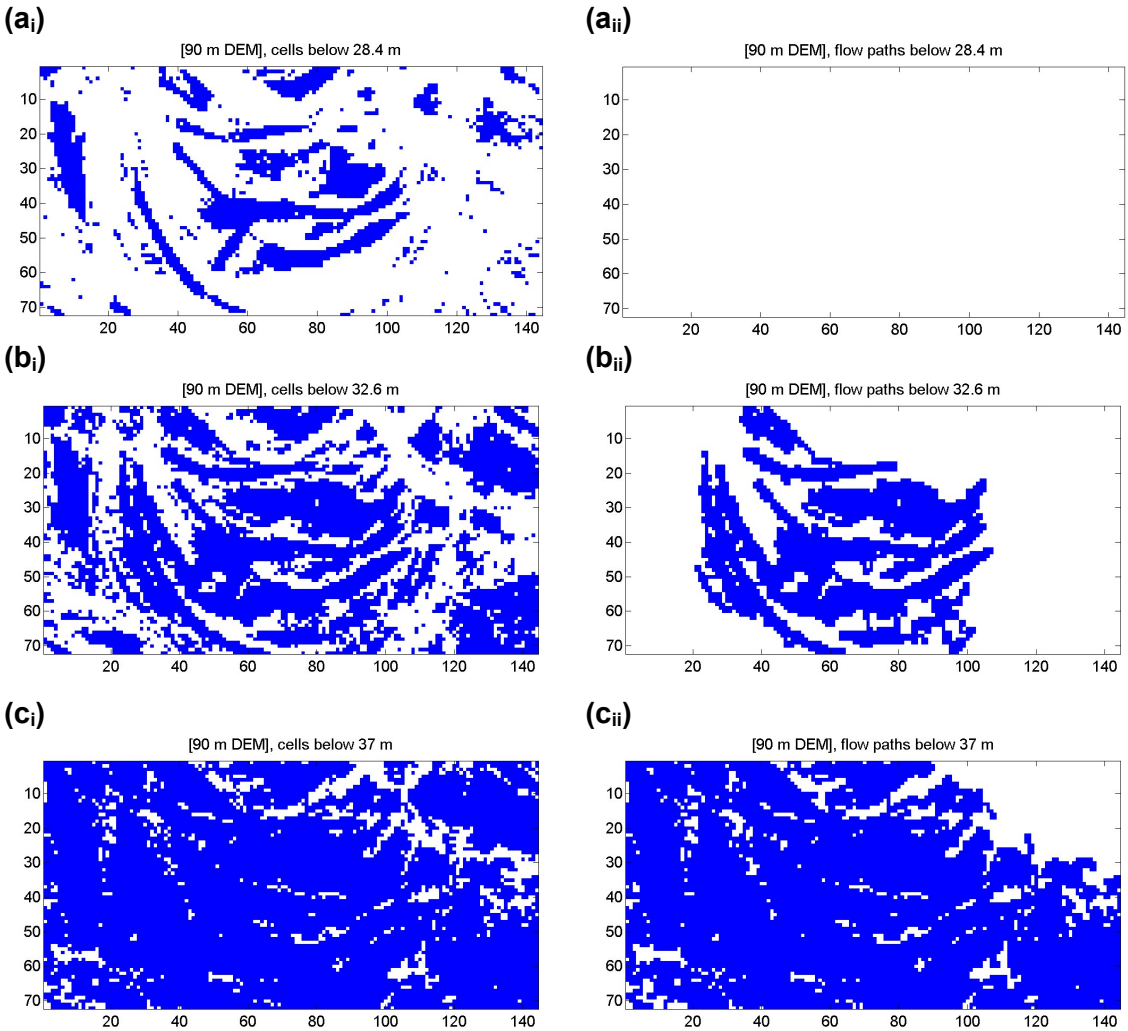

Figure 4-10 – 90 m DEM connectivity test results: (a) approximate maximum 1996 main channel water elevation [28.4 m]; (b) minimum water elevation for which there is a connection across the DEM [32.6 m]; and (c) approximate maximum 1996 JERS calibrated model water elevation [37.0 m]; with plots on the left ($_i$) showing cells below test elevation, and plots on the right ($_{ii}$) showing connected flow paths below test elevation. Axis numbers represent DEM cell count.

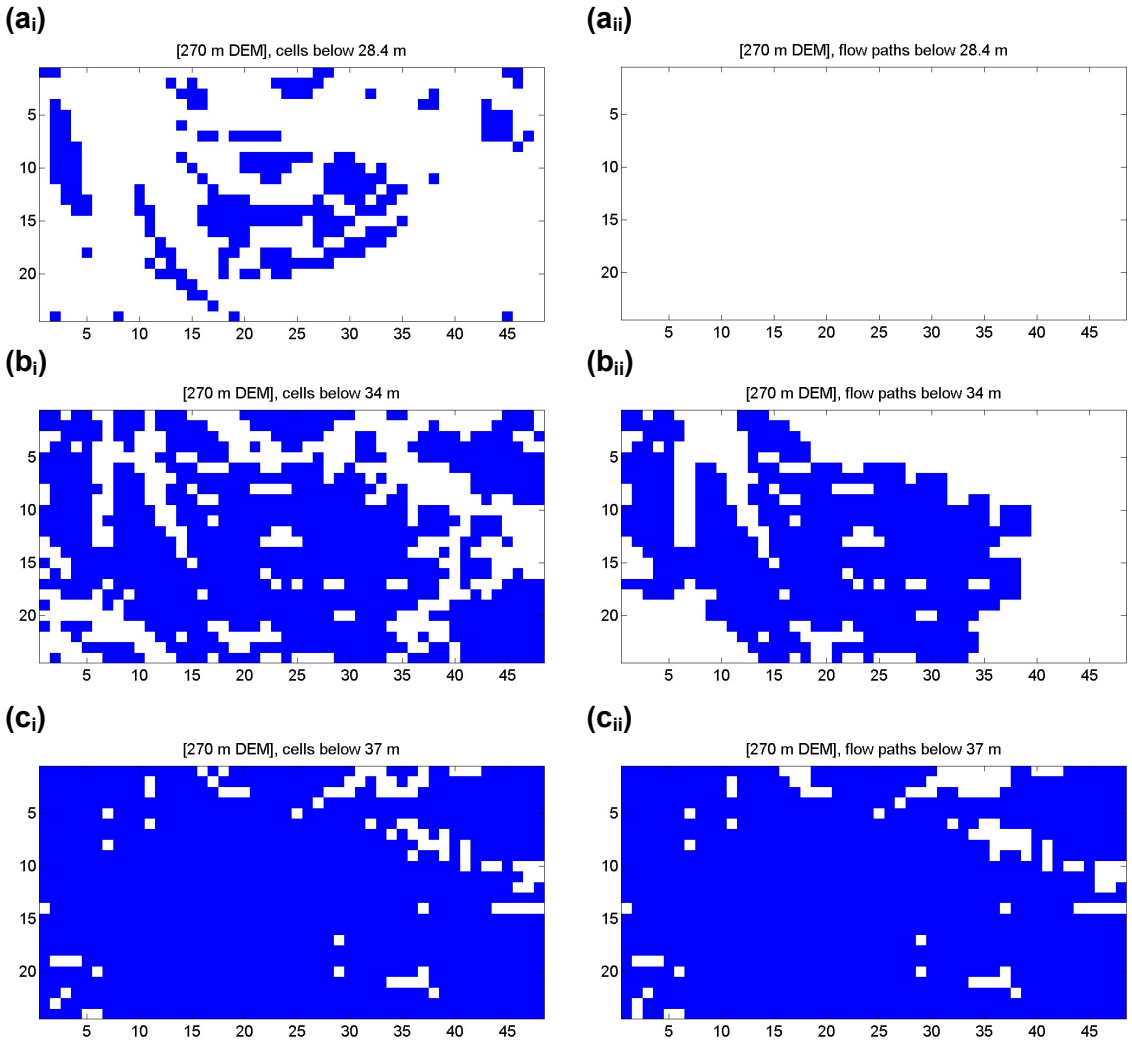

Figure 4-11 – 270 m DEM connectivity test results: (a) approximate maximum 1996 main channel water elevation [28.4 m]; (b) minimum water elevation for which there is a connection across the DEM [34.0 m]; and (c) approximate maximum 1996 JERS calibrated model water elevation [37.0 m]; with plots on the left ($_i$) showing cells below test elevation, and plots on the right ($_{ii}$) showing connected flow paths below test elevation. Axis numbers represent DEM cell count.

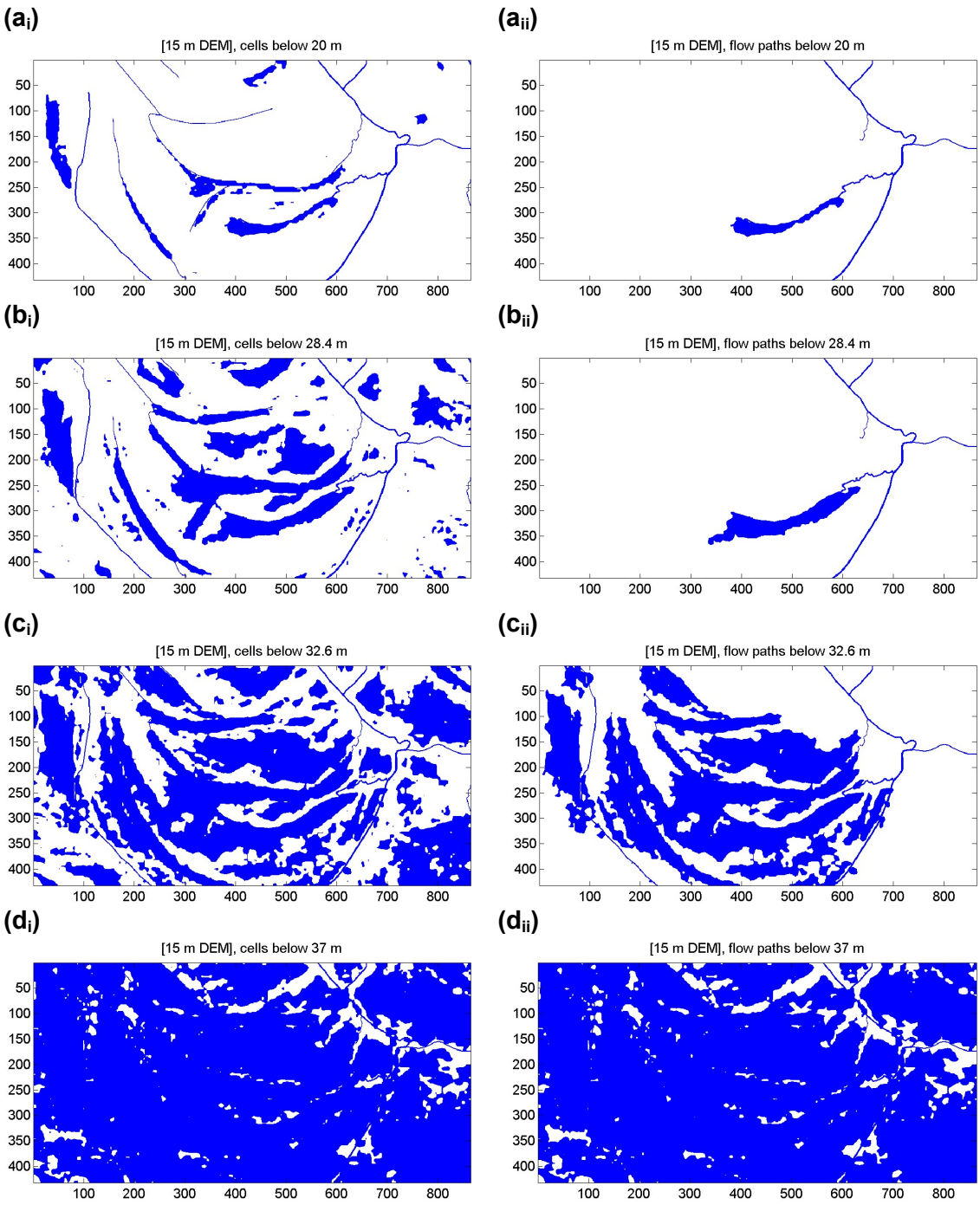

Figure 4-12 – 15 m DEM connectivity test results: (a) approximate minimum water elevation for which there is a connection across the DEM [20.0 m]; (b) maximum 1996 main channel water elevation [28.4 m]; (c) minimum water elevation for which there is a connection across the 90 m DEM [32.6 m]; and (d) approximate maximum 1996 JERS calibrated model water elevation [37.0 m]; with plots on the left ($_i$) showing cells below test elevation, and plots on the right ($_{ii}$) showing connected flow paths below test elevation. Axis numbers represent DEM cell count.

Figure 4-13 shows how the cumulative flow area and plan area characteristics of the test area vary with elevation. The cumulative flow area for each DEM tested is plotted against elevation in Figure 4-13(a), together with the key maximum water elevations from the adjacent main channel. The flow area is calculated by summing the minimum number of connecting cells and multiplying this by the cell width and the depth interval, as described in section 4.4.2. The cumulative flow area includes all flow area below a given the elevation. The extra flow area provided by the added floodplain channels in the 15 m DEM is clear between 20 and 32 m elevation, and continues to have an effect above this range. The reduction in connectivity due to mean resampling in the 270 m DEM is also evident when compared to the 90 m DEM curve. The cumulative surface area elevation curves derived from the 15 m, 90 m and 270 m DEMs are shown in Figure 4-13(b), together with the key maximum water elevations from the adjacent main channel. The percentage wet area (84.5%) from the May 1996 JERS image is also shown on the curve for reference. The stepped appearance of the 90 curve is likely to be due to the 1 m vertical precision of the SRTM data.

Subtracting the cumulative flow area derived from a 15 m DEM without the channels, from a 15 m DEM with the channels, yields the contribution of the channels to the total flow area across the DEM. The variation of the flow area contribution of the floodplain channels with flood elevation is shown in Figure 4-14.

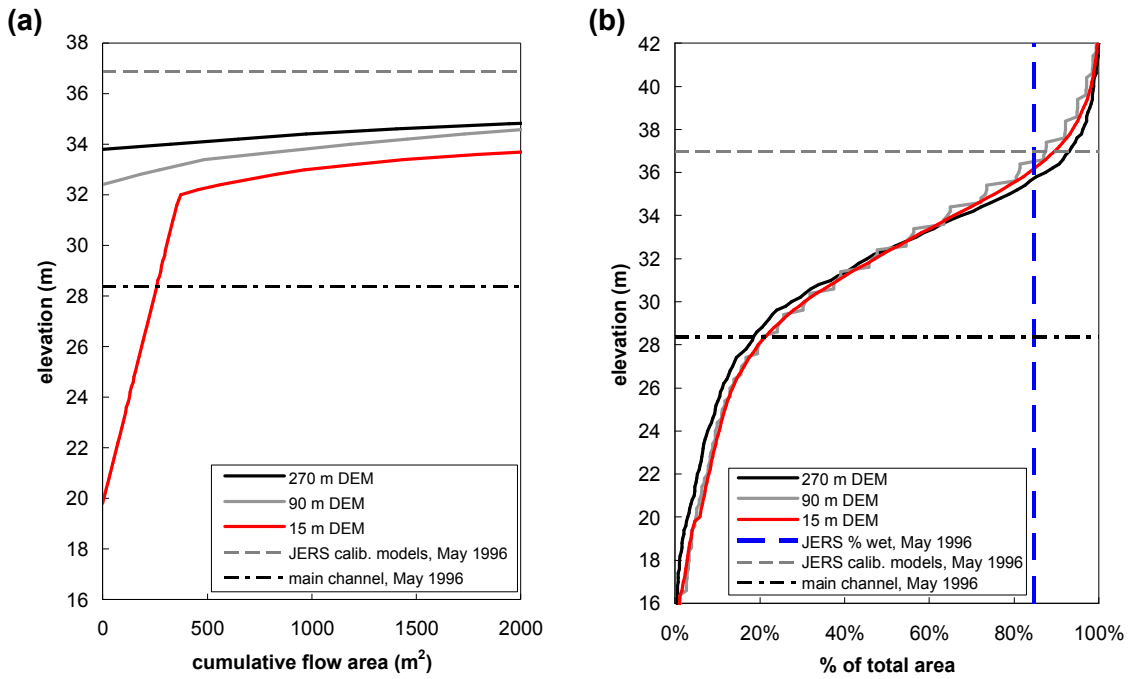

Figure 4-13 – (a) Cumulative minimum flow area, from top to bottom of test area, for 15 m, 90 m and 270 m DEMs; (b) Cumulative DEM surface area for 15 m, 90 m and 270 m DEMs. Key maximum water elevations are also shown.

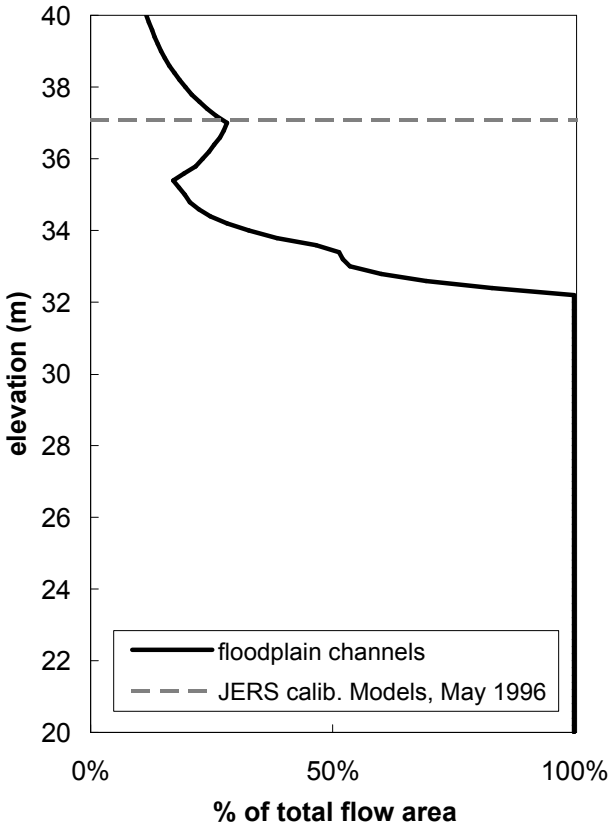

Figure 4-14 – Contribution of floodplain channels to total flow area.

4.4.4 DEM connectivity discussion

The 90 m vegetation-corrected SRTM DEM does not show connectivity across the test area until an elevation of 32.6 m. This elevation is 4.4 m higher than the peak water level in the main channel in 1996 of 28.4 m and 3.2 m higher than the maximum estimated 2009 highest level of 29.6 m. At the 1996 peak elevation, 21% of the area is below 28.4 m, but there is no connection across the area. When the domain does connect at 32.6 m, the resulting pattern is one of filled lakes with connections at low points between them, as would be expected for diffusive overbank flows, only at an unrealistically high elevation. Results for the 270 m DEM show no connection until the higher elevation of 34 m, a result of each cell elevation being a mean of 9 of the 90 m cells, smoothing out low points and high points in the DEM. Connection patterns for the 270 m DEM are similar to the 90 m DEM, only cruder with no detail of the connections between the lakes.

The 15 m DEM incorporating the floodplain channels shows connection across the domain at 20 m. This elevation is between the 1995 low water of 16.5 m and the 1996 high water of 28.4 m, an elevation that might be typical of rising flood waters. The connections are along the network of channels with a connection to the main lake in the centre of the area. Interestingly, several floodplain channel paths that visually connect on the left hand side of the area do not show as connections in the connected paths figure, Figure 4-12 (a_{ii}). Closer inspection reveals that this is due to the DEM cells of these channels only touching in the diagonal orientation and as the connectivity tool uses the same orthogonal flow assumption as LISFLOOD-FP, there would be no flow along these channels. In reality these channels would connect and at the 1996 high water elevation of 28.4 m, Figure 4-12 (b_i) shows a series of filled lakes interconnected by the floodplain channels. However, even though there is connectivity across the area, only 21% of the area would be flooded, compared to the 84.5 % expected from the JERS extent data for the same date, see Figure 4-13. There is no

vegetation correction to SRTM data in the lake areas and the fact that these are all flooded at a realistic high water elevation while the surrounding vegetated areas are not, implies that there may remain some vegetation artefacts in the corrected SRTM data.

Figure 4-13 also shows the relatively flat nature of the floodplain area, with 50% of the land area lying between 30 and 36 m. This implies that the hydraulic model will be sensitive to uncertainties in the DEM. These uncertainties include vegetation height estimates for the vegetation correction of the SRTM, the 50% canopy penetration factor assumed for the SRTM data (Wilson *et al.*, 2007) and also any mismatch of datum between the channel gauging stations and SRTM data.

The significance of the floodplain channel flow area compared to the total flow area across the DEM can be seen in Figure 4-14. The channels provide all the flow area up to the point where overbank diffusive flow occurs and continue to provide a flow area of 17 to 28% of the total, even at high water. This is likely to be an underestimate, as this connectivity test does not include the effects of hydraulic friction, which will be much less in the channels than on the heavily vegetated floodplain. In addition, the low water SRTM elevations used to represent the floodplain channels do not include the channel depths under any water surface. The kinks in the flow area curve also indicate that there are threshold effects as the water levels increases, with new connections across the floodplain suddenly providing increased flow area.

Connectivity itself is a fairly loose term which can mean different things in different research fields (Michaelides and Chappell, 2009). The connectivity assessed in this section encompasses hydraulic connectivity of the floodplain channels, DEM cell connectivity and the hydraulic model processes connectivity. Given that the results are dependent upon the DEM resolution and the representation of the channels within that DEM, a geostatistical approach as suggested by Michaelides and Chappell (2009) may allow a more consistent comparison of results across a range of scales and between different floodplain areas.

4.5 Floodplain channel connectivity in the hydraulic model

In Section 4.2 floodplain filling and draining problems were identified with the 1D/2D LISFLOOD-FP hydraulic model when it is calibrated to realistic main channel water levels. One of the most obvious omissions from the 2D SRTM data used for the model was that of the many floodplain channels. These floodplain channels were characterised in Section 4.3, and while they are each relatively small compared to the main channel, they are significant in terms of their numbers and are intrinsic to the floodplain hydraulic processes resulting in identifiable *floodplain hydrologic units*. In Section 4.4 it was demonstrated, through experimentation with a sample area of floodplain, that if these channels are represented in the DEM at a resolution similar to the channel widths, they play a significant role in the flow connectivity in the DEM and, therefore, on the floodplain. Hence, it is important that these channels are included in some form in the hydraulic model in order to correctly represent the floodplain hydrodynamics.

4.5.1 Model development

In Section 4.4, the floodplain channels identified in the Landsat ETM+ images were represented in a 15 m DEM, resampled from the 90 m DEM, by "burning in" the minimum SRTM elevation along the channel using a channel buffer equal to the width of the channel. Unfortunately it is not computationally feasible to run the LISFLOOD-FP model at a 15 m resolution for domains of this scale, so applying this method to the model requires modification. In order to further test the hypothesis that including these channel pathways is important to floodplain filling and draining, the same burning in process was applied to the 270 m model DEM, but using a minimum buffer width of 270 m. This obviously leads to an overly wide representation of the channels in the

DEM, but model results should show whether adding channels in this form reintroduces at least some of the missing connectivity.

In Section 4.4.3 it was noted that the lack of diagonal flow in the model also limits connectivity in the DEM, so in order to ensure a continuous connection in the 270 m DEM for all floodplain channels, a second model was built with floodplain channels "burnt in" using a 400 m buffer width. The length of the 270 m cell diagonal is 381.8 m, but tests showed that a slightly wider buffer of 400 m was required to ensure continuous orthogonal connection, allowing for any lateral mismatch between the SRTM dataset and Landsat ETM+ image mosaic. The need for the second model DEM is illustrated in Figure 4-15, where both the model DEMs are shown. The first DEM shows the result of using a 270 m buffer width to burn in the channels, and many of the channels that lie in a diagonal orientation are represented by a string of staggered cells. The model DEM created using the 400 m wide buffer shows these diagonal channels connected orthogonally with extra cells. Both the 270 m wide and 400 m wide floodplain channel buffer models were run using the same friction values as the main channel water level calibrated model in Section 4.2.

It was noted in Section 4.2.3 that using a fixed timestep could be another limiting factor in representing the dynamics on the floodplain. Unfortunately with such a large model domain it is not computationally feasible to run the model at the adaptive timestep of around 0.24 s (~12 months run time). In order to test the model results sensitivity to timestep, the 400 m wide channel buffer model was run at 40, 10 and 5 s as well as the original model timestep of 20 s.

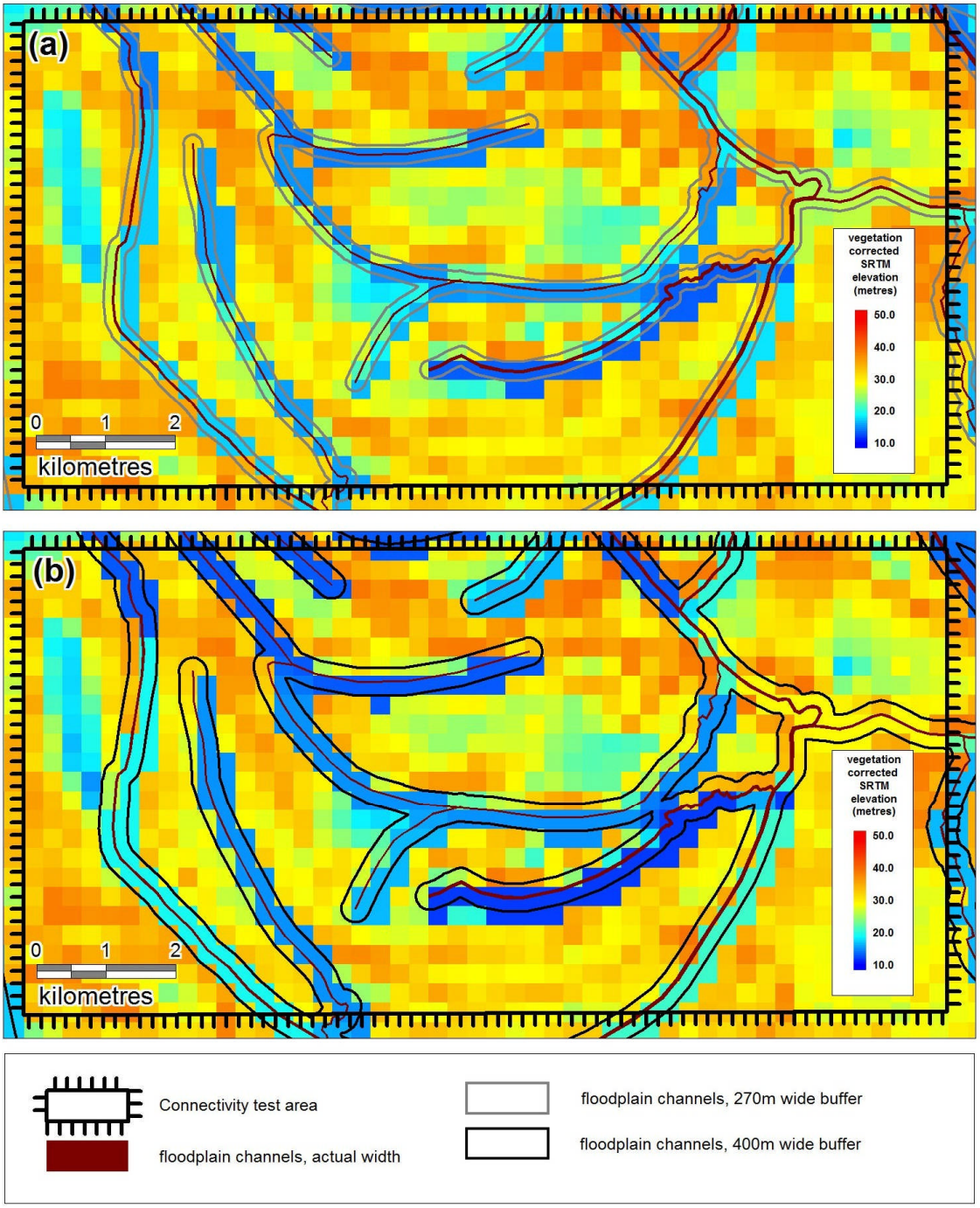

Figure 4-15 – (a) connectivity test area with 270 m wide floodplain channel buffers and resulting "burnt in" 270 m DEM; (b) connectivity test area with 400 m wide floodplain channel buffers and resulting "burnt in" 270 m DEM.

4.5.2 Model calibration and results

Figure 4-16 shows the flood extent comparison between the model results and JERS images for the three different floodplain models. These are for approximately the low water period (19-Oct-95) and approximately the high water period (26-May-96). All these models were calibrated to gauged channel water levels, as modelling results from Section 4.2 demonstrated that calibration to the JERS extents results in unrealistic friction values and overly high channel water levels. It should also be noted that the results shown in Figure 4-16(a) are the same as those in Figure 4-1(b). Figure 4-16(b) and (c) show the effect of including burnt in channels compared to the original DEM (a). Table 4-10 shows the associated fit statistic (*F*) results for the three model runs, also for low and high water. The *F* results for the Wilson *et al.* (2007) model are shown for comparison.

Figure 4-16 shows a binary comparison between the flooded cells in the model and the flooded cells derived from the JERS images (Figure 4-1(d)). Low water comparison is shown in the first image (i) and high water shown in the second image (ii). Three primary colours illustrate the results of the binary comparison: blue shows cells that are wet in the model and in the JERS image; red cells show where the model predicts the DEM is wet, but the JERS image shows it is dry (overprediction) and green shows where the JERS image is wet but the model predicts it is dry (underprediction). Grey shows areas excluded from the fit statistic (*F*) results.

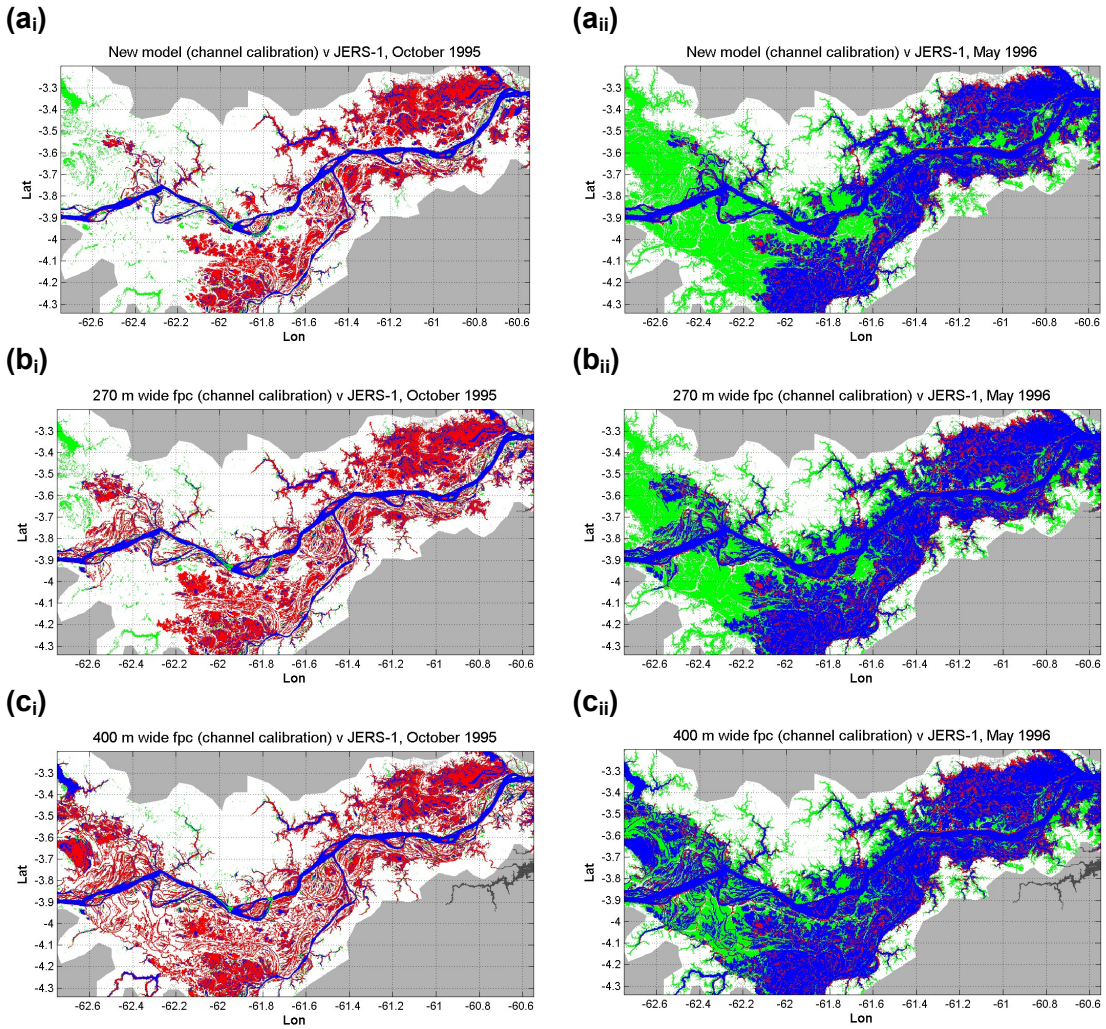

Figure 4-16 – 2D low ($_i$) and high ($_{ii}$) water model results; (a) Improved channel model calibrated to channel water levels; (b) model with floodplain channels "burnt in" at 270 m buffer width; and (c) model with floodplain channels "burnt in" at 400 m buffer width. Blue is flooded in both model and JERS, red is overprediction by the model, green is underprediction, white is non-flooded. Grey shows masked out non-floodplain areas.

Table 4-10 – 1D/2D Models, with and without floodplain channels, JERS *F* results

No.	Model	2D DEM	*F* Oct 95 (~low water)	*F* May 96 (~high water)
0	Wilson *et al.* (2007), JERS calibration	Original 270m DEM	22.73%	71.70%
1	1D/2D diffusive channel model from Section 4.2	Original 270m DEM	27.70%	46.90%
2	Addition of 270 m wide floodplain channels	Original DEM with floodplain channels "burnt in" with 270 m buffer	26.08%	53.72%
3	Addition of 400 m wide floodplain channels	Original DEM with floodplain channels "burnt in" with 400 m buffer	26.60%	61.12%

Table 4-11 shows the results of the timestep sensitivity runs with the 400 m wide floodplain channel model. As timestep is decreased, both low and high water model fit improves.

Table 4-11 – Timestep sensitivity results for 400 m channel buffer DEM model

Model timestep (s)	*F* Oct 95 (~low water)	*F* May 96 (~high water)
40	26.1%	59.6%
20	26.6%	61.1%
10	26.9%	62.0%
5	27.0%	63.8%

4.5.3 Model discussion

The model results show that including even a crude representation of the floodplain channels in the DEM provides improved DEM connectivity. This results in an improved high water JERS fit, with the model wetting more of the 2D domain to give a 14% increase in the *F* results. While still not as good a high water fit as the Wilson et al (2007) JERS calibrated model, this is achieved with more realistic main channel water levels. The models including the floodplain channels show more uniform wetting across the whole domain. The 270 m wide channel buffer DEM still shows areas that are not connected and these are areas where there are many channels diagonal to the DEM grid. These dry areas connect up in the 400 m wide channel buffer DEM model, confirming that it is the lack of diagonal flow in the model that is preventing the wetting of these areas at this coarse grid scale.

The inclusion of the floodplain channels means that more of the domain is wet during the low water period, which will lower the *F* result. The overly wide channel representation also exacerbates this over wetting at low water, because of the wet floodplain channel cells. However, improvements in the general drainage due to the added floodplain channels mean that many floodplain areas also have a reduction in wetted extent, resulting in a marginally lower *F* fit when compared to the diffusive channel calibrated model, and almost 4% better than the JERS calibrated Wilson *et al.* (2007) model. Low water *F* results for the original DEM and the “burnt in” 270m channel models may be artificially high as both models result in areas that never flood at high water and therefore do not need to drain for the low water extent.

Looking closely at the high water results from the 400 m wide channel buffer model (Model 3) in Figure 4-16 (c_{ii}), there are areas of the floodplain that are in green, showing they are wet in the JERS image but dry in the model. However, these green areas are crisscrossed by the flooded floodplain channels (in blue) indicating that flow through the channels is occurring but out of bank flow onto the floodplain is not. JERS

classification accuracy has been estimated at 30% (Martinez and Le Toan, 2007), but the discrepancy between the model and JERS data is significant enough to imply other problems with the model DEM. Lake areas, which have no vegetation correction, wet and dry better with the inclusion of floodplain channels, but surrounding vegetated areas remain dry, implying artefacts remain in the DEM from the vegetation correction of the SRTM. This implication was highlighted in Section 4.4.4, but these results demonstrate the same effect for a hydraulic model of the full study area. Wilson et al (2007) also noted similar problems with the model DEM when comparing satellite altimetry data with the predicted water elevations on the floodplain, and these problems were thought to be due to vertical error in the DEM data.

Finally, the timestep sensitivity runs indeed show that reducing the timestep improves both low and high water results for the model. The lower timestep allows more realistic hydrodynamics in the 2D floodplain of the model, resulting in both an increased high water flood extent and improved low water drainage. Although not computationally feasible at the moment, ideally the model should be run at the adaptive timestep (approximately 0.24 s) for the study of floodplain dynamics.

4.6 Conclusions

In this chapter, the first dedicated study of the spatial variation and characteristics of the Amazon floodplain channels for a representative 30,000 km^2 portion of the central Amazon mainstem was presented. Analysis of a Landsat ETM+ image mosaic showed a total of 1,762 channels in the study area, ranging in width from 900 m down to the minimum resolvable width of around 20 m, with a mean width of 47 m. The floodplain channels ranged from 160 m to 67 km long, with a mean of 5.3 km and total length of 9,293 km. Comparing channel width with their frequency reveals a power law relationship, showing patterns of structure that are self-similar or fractal-like over many orders of magnitude (Brown *et al.*, 2002; Rinaldo *et al.*, 2006). This relationship allows estimation of the number of floodplain channels below the Landsat ETM+ image resolution of 15 m, and reveals that these smaller channels account for an extra 2,400 channels, more than the sum of all the other channels. While the mean length of these smaller channels is shorter than the other channels, they still add another 6,719 km (+72%) to the total length of floodplain channels.

Despite the inherent complexity of the floodplain network, grouping the floodplain channels by their connection network shows that there are distinct and mostly separate networks of channels in the floodplain and that these networks can in turn be grouped by their characteristics. Delineation of the "catchment" areas represented by each network shows that these areas can be grouped into six types based on differing hydrological inputs as well as their network characteristics. These are here termed "*floodplain hydrologic units*" (FHU) as they represent distinct separate areas of floodplain that seem to function as single units from a hydrological perspective. It is likely that under high water level conditions that these units will connect through diffuse overland flow, but the hydrological inputs, hydraulic gradients and sediment availability in each area ensures relative isolation of surface flows for considerable portions of the flood cycle.

The six types of unit indentified can be grouped into three classes of FHU, each with two types of unit. The first class are those units found closest to the river and are completely dominated by river floodwater and sediment deposition and have very little in the way of local hydrology runoff input other than direct rainfall. The second class covers central areas of floodplain with low topography that are generally isolated to some extent from river flow by the first class of unit, but also receive little input from terrace runoff bordering the floodplain. The final class of unit encompasses areas with direct and indirect runoff inputs from the terrace hillslopes. This is the first time that a method of breaking down the complex heterogeneity of the Amazon floodplain into functional units has been demonstrated. Whilst it is not claimed that this method is definitive, it does show broad patterns that appear to be correct overall and further study should be able to confirm this and hopefully extend it, whilst providing more objective classification of the units. The fact that these floodplain areas have very different hydrological characteristics (e.g. drainage density and water sources) has important implications for many biogeochemical studies in the Amazon which rely on an understanding of these characteristics in order to quantify and estimate dependent processes.

SRTM topography data is currently some of the best available topography data for the Amazon floodplain and many studies of the floodplain use these data, including recent large-scale hydraulic models (Wilson *et al.*, 2007). Comparison of the floodplain channel networks derived from Landsat ETM+ data with the vegetation-corrected SRTM data of the floodplain shows that most of these floodplain channels are poorly represented in the 90 m SRTM DEM, with 95.7% of the channels being less than 90 m in width.

Experiments were conducted in order to explicitly include the channels in the SRTM data by “burning” them into a resampled 15 m DEM derived from the 90 m DEM. Connectivity analysis of the resulting DEMs demonstrate that inclusion of the channels significantly changes the hydraulic connectivity of the DEM, allowing connections at

much lower elevations than without the channels. The channels provide all the flow area in the DEM up to the point where overbank diffusive flow occurs and continue to provide a flow area of 17 to 28% of the total, including at high water. This is likely to be an underestimate, as the connectivity analysis did not include the effects of hydraulic friction, which will be much less in the channels than on the heavily vegetated floodplain. Additionally, the low water SRTM elevations used to represent the floodplain channels do not include the channel depths under any water surface present at the time of SRTM over flight, and this remains an unknown channel characteristic. Sudden changes in connectivity at different elevations also point to threshold effects within the floodplain. These experiments demonstrate that these floodplain channels could be playing a much more significant role in the floodplain hydrodynamics then previously acknowledged, and studies for which these dynamics are important will need to allow for this.

This missing floodplain channel connectivity in the SRTM data explains some of the floodplain filling and draining problems encountered with recent large scale hydraulic modelling of the Amazon channel and floodplain (Wilson *et al.*, 2007). These filling and drainage issues are even more evident when a diffusive main river channel is included, which ensures more realistic, but lower, water elevations in the main channel during the simulation, as demonstrated in Chapter 3. Experiments to include the floodplain channels in the 270 m model DEM by “burning in” all the channels reintroduces some of this missing connectivity and allows better filling and draining of the 2D floodplain. However, given the overly wide representation of the channels in the DEM and the fact that the 270 m model DEM loses further detail, and hence connectivity, when it is mean resampled from the 90 m SRTM data, further work is required to find a suitable method for incorporating these channels into the hydraulic model. The filling and emptying of floodplain lakes in the model at realistic water elevations, while surrounding vegetated areas remain dry, is in contrast to the JERS images which show the vegetated areas are also wet, and this indicates that there may

still be vegetation artefacts remaining from the vegetation correction procedure that require further investigation. In addition, the floodplain hydrologic units identified in this chapter would indicate that local hydrology plays an important role in certain areas of the floodplain but, as yet, local hydrology inputs have not been included in the hydraulic model.

The methods used in this chapter to quantify and characterise the floodplain channels and their networks, for which there is little published data, rely heavily on the use of remotely sensed data. Data resolution, overhanging vegetation and difficulties in sensing beneath the water surface have all been identified as introducing error to the results and limiting the conclusions that can be drawn from those results. In order to provide a more complete dataset from which to study the floodplain channels, a survey was undertaken to measure the characteristics of these floodplain channels in the field and this is described in the following chapter.

CHAPTER 5
Floodplain channel survey

5.1 Introduction

One of the incongruous things about carrying out hydraulics research in the Amazon is the availability of a relatively large amount of data for, what is in general, a relatively remote and inaccessible area. This is in part due to the scale of the rivers, which allow even fairly coarse spatial and temporal resolution remote sensing instruments to collect useful data. For example, the interferometric SAR data from the Japanese Earth Resource Satellite 1 (JERS-1) has a resolution of 100m (Rosenqvist *et al.*, 2000) and the Amazon main river in the study area has a mean width of around 4000 m.

A limitation of the remote sensing data that are available for the Amazon River is the difficulty that the instruments have in penetrating the water surface, resulting in a knowledge gap regarding bathymetry of the water bodies of the Amazon. In order to address this gap for the main river, a significant amount of original main channel bathymetric data was collected for reaches of the Amazon and Purus rivers by Wilson *et al.* (2007). These data were utilised in full for the research carried out for the main channel flood wave hydraulics, described in Chapter 3. Without the availability of such fundamental bathymetric data, it would have been impossible to characterise the channel geometry or the hydraulics of the flow in the channel with any certainty.

For the floodplain itself, very few bathymetric data are available, except for spot depths from dated navigation charts (Mertes *et al.*, 1996; Latrubesse and Franzinelli, 2002). Some location specific bathymetric data have been collected for lake studies (Panosso *et al.*, 1995; Bonnet *et al.*, 2005), but it is difficult to apply these general findings more broadly to the wider floodplain. Bonnet *et al.* (2008) combined field

measured water elevations with flood extents derived from JERS-1 images to derive a low to high water bathymetric DEM of the Curuaí floodplain near Óbidos. However, for permanently flooded lake areas and nine floodplain channels connecting the lakes to the main river, spot measurements of depth from the field were still required to estimate bathymetry.

The work detailed in Chapter 4 highlights the importance of the large number of floodplain channels to the river and floodplain hydrodynamics. Analysis of remote sensing images was used to provide key information regarding the spatial characteristics of these floodplain channels. The results of this analysis showed that 95.7% of the floodplain channels in the study area are narrower than the 90 m resolution of the SRTM topographic data and that many of these channels are permanently wet. To complement the work carried out in Chapter 4, a systematic study of the bathymetric properties of the Amazon floodplain channels was carried out. The overall aim of the field work described in this chapter was to survey the depth and width characteristics of the floodplain channels, sampling floodplain channels from all of the different floodplain hydrologic unit (FHU) types identified in the Landsat ETM+ image analysis. The objectives were to carry out longitudinal traverses of the channels with periodic cross-sections and undertake periodic channel width measurements. As well as providing basic geomorphological characteristics for the different types of floodplain channels, the survey also provided the opportunity to observe the high-water flood dynamics first hand.

5.2 Survey methodology

5.2.1 Survey timing

The timing of the bathymetry survey during the early high water period was important in order to ensure access to remote channels in the floodplain by ensuring sufficient draft of water above channel beds and submerged vegetation. High water sampling allowed the measurement of channels that may be dry during the low water period of the year and access to smaller, shallower channels. The disadvantage of a high water survey is that some low water features and bank locations may be obscured. Furthermore, the survey timing was chosen to coincide with the rising limb of the hydrograph to allow observation of the flooding dynamics in action during the filling phase of the inundation of the floodplain.

The survey was carried out for a total of 9 days between the 7th and 15th of April 2009. The high water period for the study area is between April and September, with the flood peak usually occurring around the end of June or the beginning of July. The year 2009 was an unusual year, with the peak water level in Manaus reaching 29.75m (local datum), breaking the previous 106 year record set in 1953 of 29.69m. This meant that at the time of the survey, water levels were already at the mean annual maximum level of 27.72m for Manaus. Figure 5-1 shows the water levels at Manaus during the field survey compared to the mean levels and for the years 1953 and 2009.

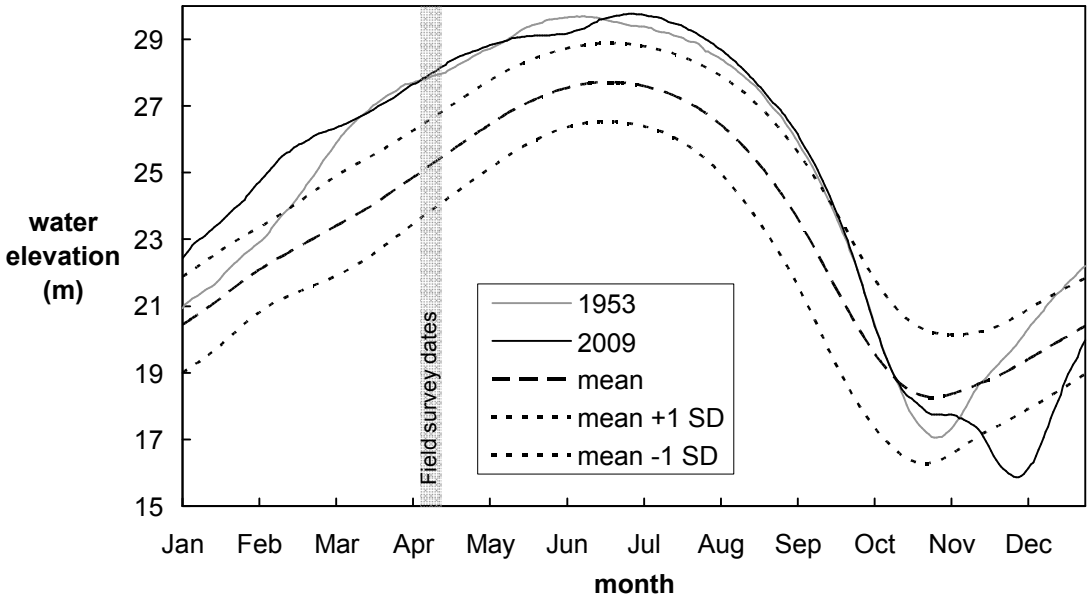

Figure 5-1 – Manaus mean water elevation curve, together with 2009 and 1953 data. Field survey period is highlighted.

5.2.2 Survey overview

A common method of carrying out research on the Amazon River is to use a large river boat as a base, which slowly cruises up the reach of interest. Small boats equipped for survey are then launched for the day to allow access to specific areas of interest. This was the method employed in the 2005 bathymetry survey and allows a number of research teams to share logistics and the significant costs of the large boat hire. Unfortunately due to local logistics issues, timing issues with other research teams and funding limitations, this was not possible for this survey.

Having identified a suitable and knowledgeable guide with a small boat available for hire, an alternative survey method was derived whereby small towns and villages along the reach would be used as night bases and the survey carried out from there during the day, avoiding the need for a costly base ship. This allowed access to a

significant portion of the study area and also introduced more flexibility to allow for bad weather or blocked channels.

Routes were planned using a combination of GIS with Landsat images and more detailed Google Earth images, where available, and uploaded to a navigation GPS unit and the sonar GPS unit. These routes were then navigated and surveyed during the day, allowing plenty of reserve range and time to return from the remote areas of the floodplain. This method allowed the channel survey to be carried out up to 140 km into the floodplain each day. The routes were not always straightforward to navigate with *capim* (floating macrophytes) sometimes blocking the channel. This would entail identifying alternative routes around the blockage using the laptop to check the Landsat and Google Earth images, manually pulling the boat through the flooded canopy if the blockage was for a short distance, or inquiring about alternative routes from locals, when available.

In all, 1400km of survey were carried out, 56% of which were specifically floodplain channels. Figure 5-2 shows the final routes taken as well as the towns used as bases at night.

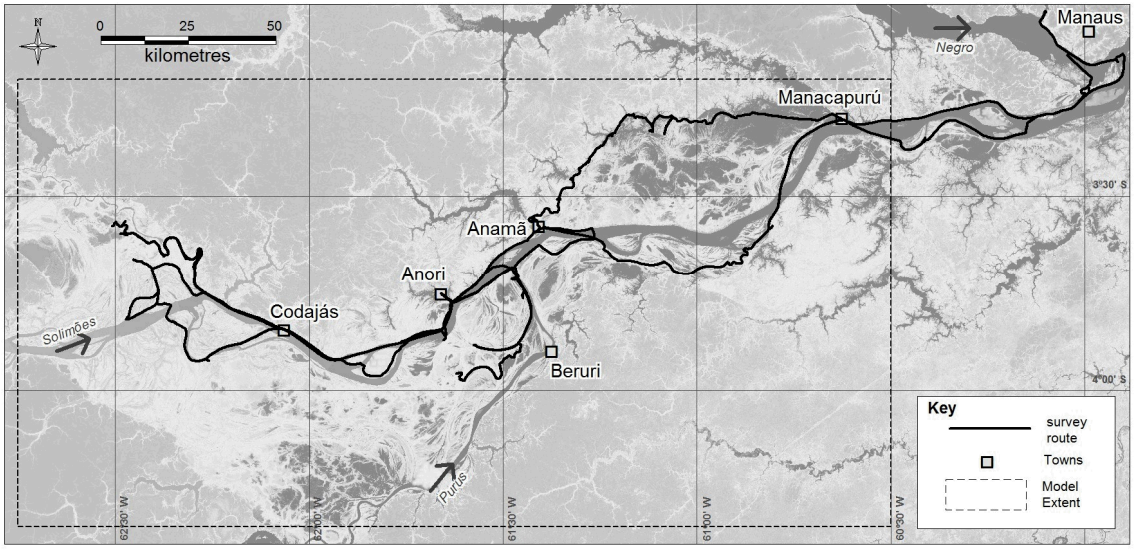

Figure 5-2 – Floodplain channel survey routes and town bases.

5.2.3 Equipment

The boat used for the survey work was a 6m long aluminium hulled boat with a Suzuki 50 hp 4-stroke engine, a draft of just under 1m and a range of around 220km. Figure 5-3 shows the boat and guide on the Amazon River, together with two example pictures of two of the floodplain channels surveyed. A standard Garmin hand-held GPS unit was used for navigation purposes.

Figure 5-3 – (a) 6m Aluminium hulled boat used for survey, with Clive Maquire as guide, (b) floodplain channel (fpcs7b), and (b) floodplain channel (fpcn1b)

In order to collect bathymetric data, a Garmin 450S combined sonar and GPS System was used. The dual frequency sensor (50 KHz & 200 KHz) was transom mounted and is shown in Figure 5-4, also showing the sensor offset of 0.25 m for water level. The unit has a depth range of 457 m (dual freq) and transmit power of 500 W

(RMS). The unit has an SD card slot and this was used to transfer the recorded data to a laptop on a daily basis. The unit has a 10,000 points active track memory and can be set to record at a minimum 1 s interval. A 2 s interval was normally used, which allowed the active track memory to record a whole day of survey. With an average boat speed of around 30 km/hr, this gave a mean sonar point spacing of around 16.5 m. A total of 93,083 depth measurements were recorded, together with GPS locations for each point.

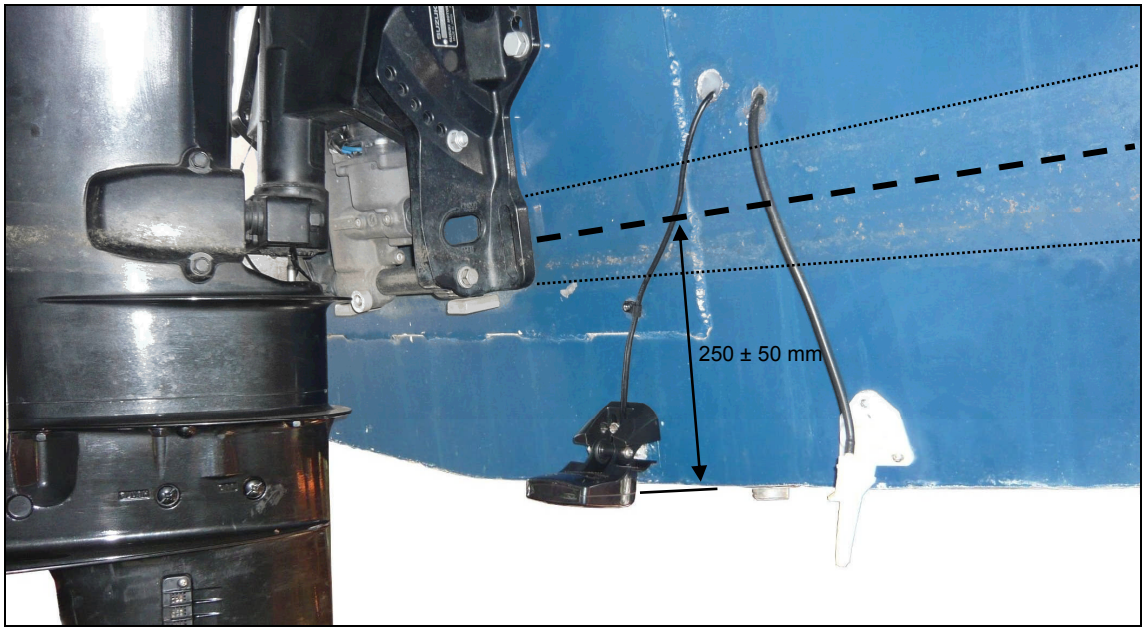

Figure 5-4 – Sonar sensor mounted on transom. Also note the offset for water level, 250mm above sensor.

A Longridge, Pin Point, laser distance rangefinder was used to measure the widths of the channels. This uses a six times optical magnification and has a range of up to 400 m with ranging error of ± 1 m to ± 0.1 % of the range.

5.2.4 Bathymetric data collection

Two forms of bathymetric survey were carried out on the floodplain channels. Longitudinal profiles of the channels were taken by traversing along the length of the channels. Where possible the boat was steered down the centre of the channels in order to measure the central channel depth, away from the banks. Perpendicular channel cross-sections were also surveyed periodically along the channel lengths. Start and end points of the cross-sections were as close to the overhanging bank vegetation as was safely possible.

5.2.5 Channel width measurements

Channel widths were measured at varying intervals during the longitudinal channel traverses. The laser range finder was aimed at both banks, one after the other and readings taken from the edge of the vegetation. A waypoint was recorded on the GPS each time this was done to locate the width measurement spatially.

5.2.6 General observations

General observations were made throughout the survey and these were also waypointed to record their spatial location. These included: (i) observations of water levels close to or at bank level; (ii) locations where the bank was overtopping; (iii) occasional readings of vegetation heights using the laser rangefinder vertically; (iv) drift rate when the boat was stopped in the channel; and (v) changes in water colour from black to white water and visa versa.

5.3 Data pre-processing

5.3.1 Data preparation

Two specific datasets were collected during the survey: the active track logs from the sonar/GPS unit, and the waypoints with their corresponding notes. The sonar/GPS unit recorded the following information for each point in the active track and the waypoint datasets: index, date, time, depth in metres, elevation in metres, water temperature in degrees Celsius, leg length in metres, leg time in seconds, speed in km/hour, leg heading, latitude and longitude. Both these datasets needed some pre-processing before they could be used for analysis. Below is a summary of the steps involved in the pre-processing;

1. Garmin Mapsource v6.15.6 software was used to process the waypoint and track data into Excel format.
2. For the waypoint dataset, notes were transcribed into the waypoint excel table, adding fields for channel width measurements, vegetation heights, bank elevation relative to water level and general notes.
3. For the active track dataset, points recorded while the boat was stationary (i.e. speed was zero) were identified and removed so the amount of data was not overestimated.
4. For the active track dataset, unique point IDs were added for the whole dataset to replace the point index which starts at the same number for each day's track data. The final number of unique sonar depth data points was 93,083.
5. Tables of both datasets were read into ArcMap GIS and used to create points from the latitude and longitude.
6. Dataset points were assigned spatially to the channel network groups (from Chapter 4) to allow sub-selection of data for later analysis by channel type.

5.3.2 Deriving water elevations

Some of the analysis methods used on the datasets required the water surface elevation and hence bed elevation, in addition to the depth. This was not recorded directly by the sonar and so required indirect derivation. While the GPS elevation of the boat was recorded, the vertical element of a GPS location is known to contain significant error. An estimate of this vertical error for the survey dataset was derived by comparing the GPS elevations to a planar water slope in the main channel calculated from the gauged water elevations, as described below. This estimate showed that the vertical error was in the order of ±15 m at best. This is well outside of the range required to resolve a water slope of around 3 cm/km (Chapter 3).

An alternative to a directly measured water surface elevation is to derive water elevations for the data from a planar water surface slope calculated from gauging station measurements. There are 5 main river gauging stations along the survey route that can be used: Manaus, Manacaparu, Anama, Codajas, Itapeua, shown in Figure 5-2. Unfortunately, the only data for most of these stations was available from the Hidroweb website (http://hidroweb.ana.gov.br/) which at the time of writing only contained data up to 2007 and so did not include the survey period. However, since it is an active shipping port, Manaus publishes daily data from their gauge on their website (http://www.snph.am.gov.br/), so this was available for the survey period and in addition, its record is the longest of any of the gauges in the Amazon, extending back to 1903. Where recorded gauged data are not available for a period of interest, it is common to use an analogue period, with similar hydrological characteristics, from the data that are available. The fact that the monomodal flood pulse of the Amazon is very regular and predictable (Schongart and Junk, 2007) means that this is relatively straightforward and should provide a reasonable approximation of the actual water elevations at the time of survey. It should be noted here that the implicit assumption is that the water surface in the floodplain is the same as that in the main channel, which

has been demonstrated as incorrect (Alsdorf *et al.*, 2007a). However, the high water timing of the survey means that water levels across the floodplain are at there most homogeneous, minimising the error introduced by this approximation. The variation in floodplain water elevations over an 88 day high water period measured by Alsdorf *et al.* (2007a) showed maximum differences across the floodplain of the order of ~60 cm. Whilst this is not an absolute water level difference, it does imply that water level differences across the floodplain during the 9 day survey period are likely to be less than a metre, and given the range of depths measured of between 8 to 20 m, this represents a reasonable error for a first order approach to the estimation of bed elevation.

Due to the availability of up-to-date daily stage data and its long record, the Manaus gauge was used to identify an analogue period for the analysis. In order to derive a water slope, ideally measurements from all five gauges were needed, meaning only the common record period of 1971 to 2007 could be used for this. Due to 2009 being an unusually high flood year, of this subset of years, only 16 years covered the same elevation range as that recorded during the survey at Manaus. Even with the regularity of the Amazon flood wave, there are differences in the timing and rate of rise of water between the years. In order to identify the best analogue 9 day period by similarity in slope as well as mean stage, a longer overlapping 27 day period was used for comparison. The timing differences were removed by adjusting the periods until the mean stage matched that of 2009. The slope match was then measured by calculating the RMSE of each year against 2009. The best match was with the year 1997 with an RMSE of 1.91 cm for the 27 day analysis period of the Manaus data. Figure 5-5 shows this process of identifying an analogue period for the survey. The survey period (7–15 April 2009) and chosen analogue period (3–11 May 1997) are shown, together with all three closest matching years (1997,1999 and 2002).

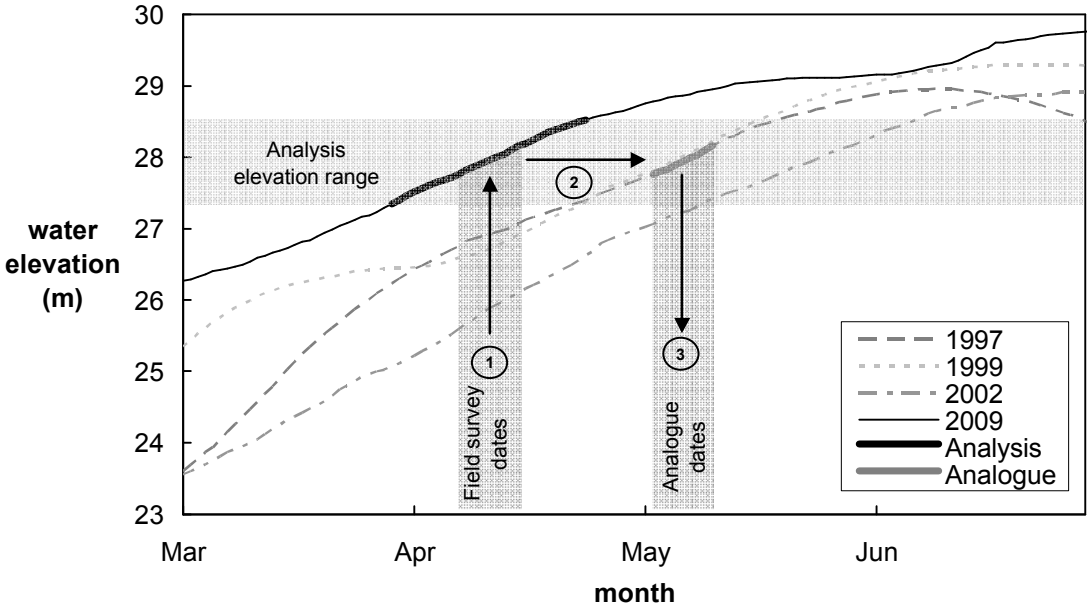

Figure 5-5 – Identification of analogue period for derivation of water surface elevations: (1) locate elevation range using survey dates; (2) use elevation range and slope to identify suitable analogue year; and (3) identify analogue year dates.

The stage readings for all 5 gauging stations of interest were then extracted for the analogue period and adjusted to water elevations using a common datum (Kosuth *et al.*, 2006). Table 5-1 shows the resulting water elevations for each gauging station for the survey period.

Table 5-1 – Water surface elevations in metres at gauging stations derived from analogue period

Survey date	Manaus	Analogue date	Manaus	Manacapuru	Anama	Codajas	Itapeua
07-Apr-09	20.25	**03-May-97**	20.25	22.50	24.61	27.05	29.68
08-Apr-09	20.31	**04-May-97**	20.29	22.56	24.65	27.10	29.71
09-Apr-09	20.35	**05-May-97**	20.32	22.60	24.69	27.13	29.75
10-Apr-09	20.40	**06-May-97**	20.38	22.65	24.73	27.16	29.80
11-Apr-09	20.45	**07-May-97**	20.43	22.69	24.79	27.20	29.84
12-Apr-09	20.49	**08-May-97**	20.48	22.75	24.83	27.24	29.88
13-Apr-09	20.53	**09-May-97**	20.52	22.79	24.88	27.29	29.91
14-Apr-09	20.59	**10-May-97**	20.59	22.85	24.93	27.35	29.95
15-Apr-09	20.65	**11-May-97**	20.65	22.91	24.96	27.40	30.03
channel distance (m)	18,016	-	18,016	91,850	190,611	282,639	397,556

In order to derive the water surface elevation for each sonar depth location, it was necessary to interpolate an elevation from the main channel water surface calculated above. This was carried out as follows:

1. The centreline of the main river was digitised from the start of the survey near Manaus to upstream at Itapeuá.
2. This digitised centreline was divided into equally spaced points using GIS.
3. A centreline distance (chainage) was calculated for each point, with the start of the survey in Manaus assigned as zero.
4. The centreline distance (chainage) was calculated for each gauging station.
5. A water elevation was assigned to each river centreline point for each survey day by linear interpolation using the gauging station elevations.

6. GIS proximity analysis was then used to identify for each sonar depth point which river centreline point was the closest.
7. The water elevation from the centreline point for the specific survey date was then assigned to the sonar depth point.
8. The bed elevation was then calculated for each point by subtracting the depth from the water elevation.

The use of ArcMap's proximity analysis to derive the water surface elevations for the sonar points required the use of discrete points along the centreline of the river. ArcMap limited the division of the single polyline representing the 270 km river centreline into equally spaced points with a 500 m spacing. Using this discrete spacing rather than a continuous interpolation introduces an approximate error of 1 cm on the derived water elevation for each point.

5.3.3 Long term water elevation statistics

In addition to using them to derive an approximation to the water surface during the field survey, gauging stations were also used to calculate the long term water elevation statistics which were used in later analyses. The long term water elevation statistics calculated were: minimum annual minimum, mean annual minimum, annual mean, mean annual maximum and the maximum annual maximum. These were calculated for a 32 year common period (1972-2007) for the gauging stations at Manaus, Manacapurú and Itapeuá. The years 1988, 1990 and 2003 were excluded due to missing data at either critical high or low periods at one or more stations. The stations at Anamã and Codajás were excluded from this analysis as they had insufficient record length to calculate reliable long-term statistics, as well as having a higher number of missing data periods than the other stations. Comparison of the 32 year period used with the 105 year record available at Manaus shows a maximum

difference of any of the statistics of only 5.1%, indicating the subset is reasonably representative of the 105 year record. Table 4-1 shows the long term water surface elevation statistics, as well as the percentage difference with the long term record for each statistic.

Table 5-2 – Long term water surface elevation statistics (period 1972-2007)

Statistic	% difference to long term record	Manaus (m)	Manacapurú (m)	Itapeuá (m)
minimum annual minimum	5.1%	6.83	8.90	18.92
mean annual minimum	3.0%	10.60	12.55	22.57
annual mean	1.7%	16.24	18.30	25.80
mean annual maximum	0.3%	20.61	22.64	29.89
maximum annual maximum	1.2%	22.10	23.98	31.35

The long term statistics were calculated for each sonar depth point by linear interpolation and proximity to the main river centreline using the method described in Section 5.3.2.

5.3.4 Bathymetric data noise error estimation

While the method of collecting bathymetric data using small sonar GPS units, more commonly used for fish finding, is not novel (Kvernevik *et al.*, 2002), published estimates of the error associated with the method are hard to find. For this survey, being based overnight in towns along the main river, both on the way upstream and on the way downstream, provided numerous tracks from different days which crossed each other. In addition, floodplain channel routes that resulted in a return traverse along the same channel, either planned or due to blockages, also provided crossing survey tracks. This presented an invaluable opportunity to estimate the noise error in the method by comparing coincident pairs of sonar depth points.

Matlab was used to identify all the unique coincident pairs of points that were located within 1 m (GPS resolution) of each other and with at least a 1 hr separation in sample time. This resulted in 117 unique pairs of points from the full dataset of 93,083 sonar depth points. Examples of multiple crossing tracks near Anori and the location of the 117 unique coincident pairs spread across the study area are shown in Figure 5-6.

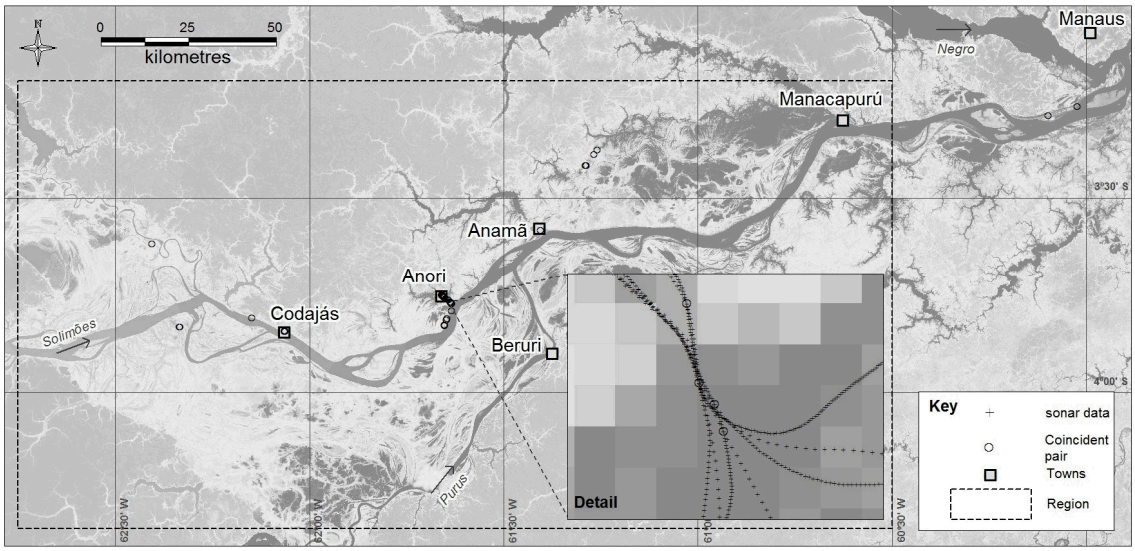

Figure 5-6 – Location of the 117 unique coincident sonar pairs with detail of multiple crossing tracks near Anori.

Statistical analysis of the absolute depth difference and absolute bed elevation difference for each pair was then carried out. The results are detailed in Table 5-3 and plotted in Figure 5-7. The overall RMSE in the depth is 0.46 m and in the bed elevation is 0.43 m. The marginally lower error in the bed elevation is likely due to the fact that many of the pairs of points were measured on different days and therefore will have a different water surface elevation. The method of deriving the water surface elevation described in Section 5.3.2 takes into account these daily changes, resulting in a lower error in the bed estimate and also giving some confidence in the derived water surface elevation. This noise error analysis provides a good estimate of the overall error in the survey methodology, as it includes the error associated with estimating the water surface elevation, different boat speeds, GPS positional accuracy as well as sonar

performance and calibration. The overall error in the survey undertaken by Wilson *et al.* (2007) was estimated at around 1 m (Chapter 3). The results of this noise error analysis indicate that the overall error for this survey is also likely to be around 1 m.

Table 5-3 – Sonar noise error statistics

Statistic	Depth (m)	Bed elevation (m)
Mean absolute difference	0.32	0.29
Max absolute difference	1.70	1.66
RMSE	0.46	0.43

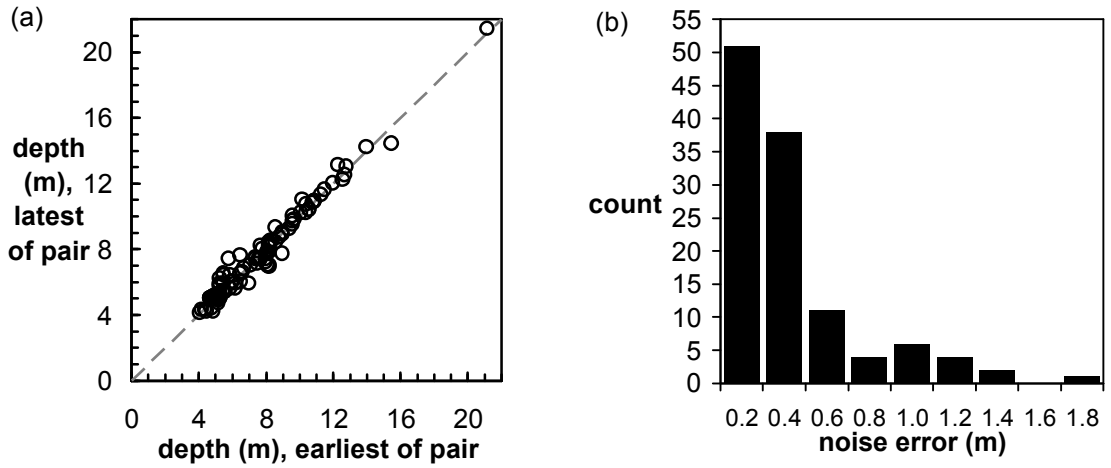

Figure 5-7 – Coincident point pair analysis, (a) plot of pair depths showing no systematic bias, (b) frequency plot of noise error showing the majority of errors lie below 0.4 m.

5.4 Analysis and results

5.4.1 Channel profile analysis

During the preprocessing, the sonar data were assigned a group according to location, allowing an overall assessment of data collected by category. The data were grouped into five main categories: main river, island channel, floodplain lake and floodplain channel, north and south sides. Of the total data collected 56.3% were specific to the floodplain or island channels, with a total of 36 channels identified for further analysis. Table 5-4 shows a summary of the information for each category, and Figure 5-8 shows the location of all the floodplain channels identified.

Table 5-4 – Sonar data category summary

No.	Data Category	Description	No. sonar points	No. Channels	% of Total
1	Main river	Solimões, Purus, Negro main river channels	40,682	-	43.7%
2	Island channel	channels through or around large islands in the main river channels	7,143	7	7.7%
3	floodplain lake	large floodplain lakes	12,600	3	13.5%
4	floodplain channel N	floodplain channels located on the north side of the main Solimões River	14,582	15	15.7%
5	floodplain channel S	floodplain channels located on the south side of the main Solimões River	18,076	11	19.4%
	Total		**93,083**	**36**	

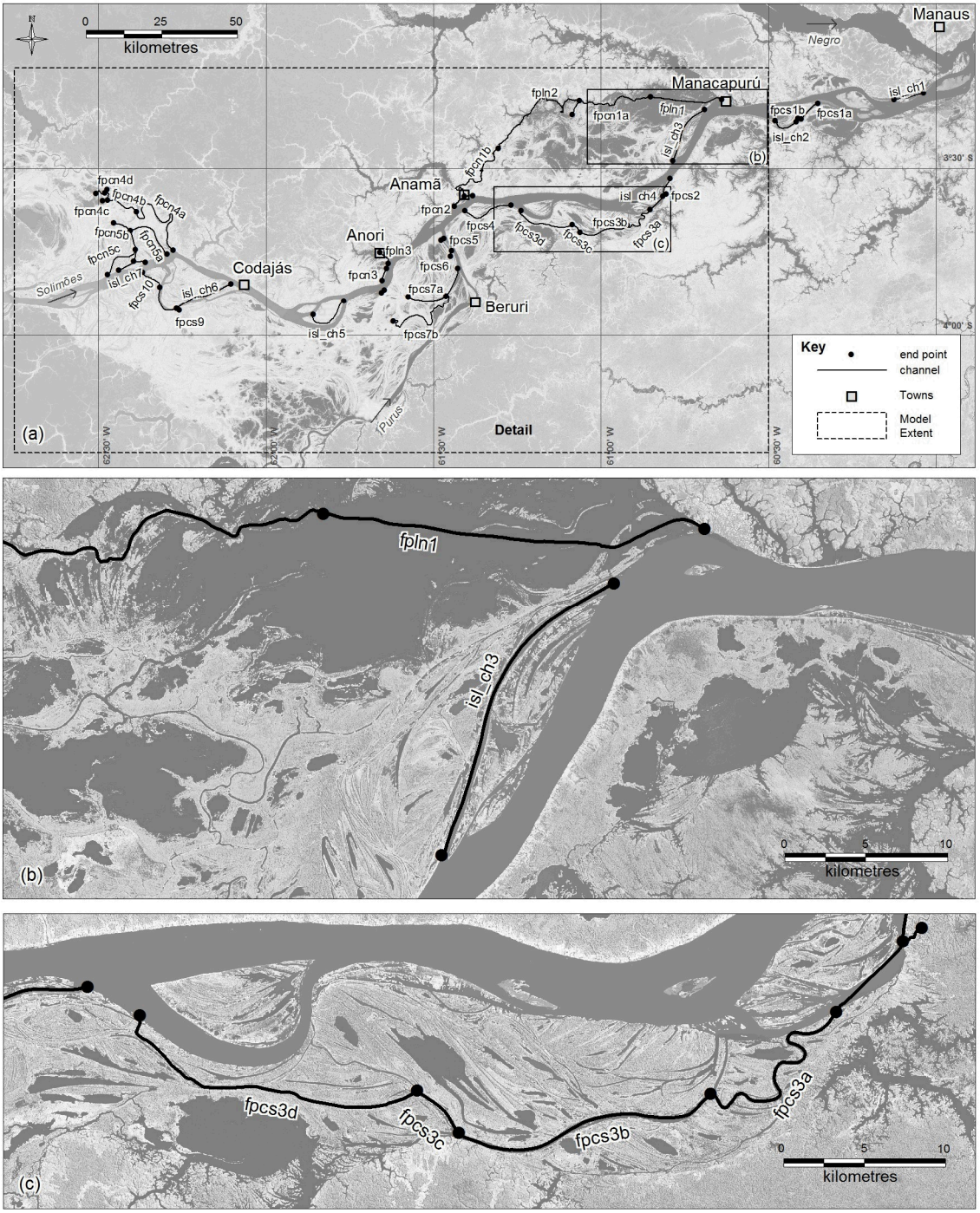

Figure 5-8 – (a) Location of floodplain channels analysed, (b) detail of lake channel and island channel types, (c) detail of a series of channels on the south bank of the main river. Longitudinal elevation profiles of these channels are shown in Figure 5-9.

Further processing of all 36 identified channels was carried out on a channel by channel basis. The longitudinal profile of the surveyed bed of each channel was plotted together with the water elevation of the survey at the time and the long term water elevation statistics. All traverses of the channel were plotted separately. Profile plots use a zero distance for the upstream end of the channel. Three examples of channel profiles from the different data categories are given in Figure 5-9.

Summary statistics for each of the channels were also calculated and these are presented in Table 5-5. Any channels with significant local hydrology inputs, as previously determined in Chapter 4, were noted in the “other characteristics” column. In addition, island channels that were large enough to carry a large amount of river flow and could therefore be considered part of the main channel hydraulically were noted as main river.

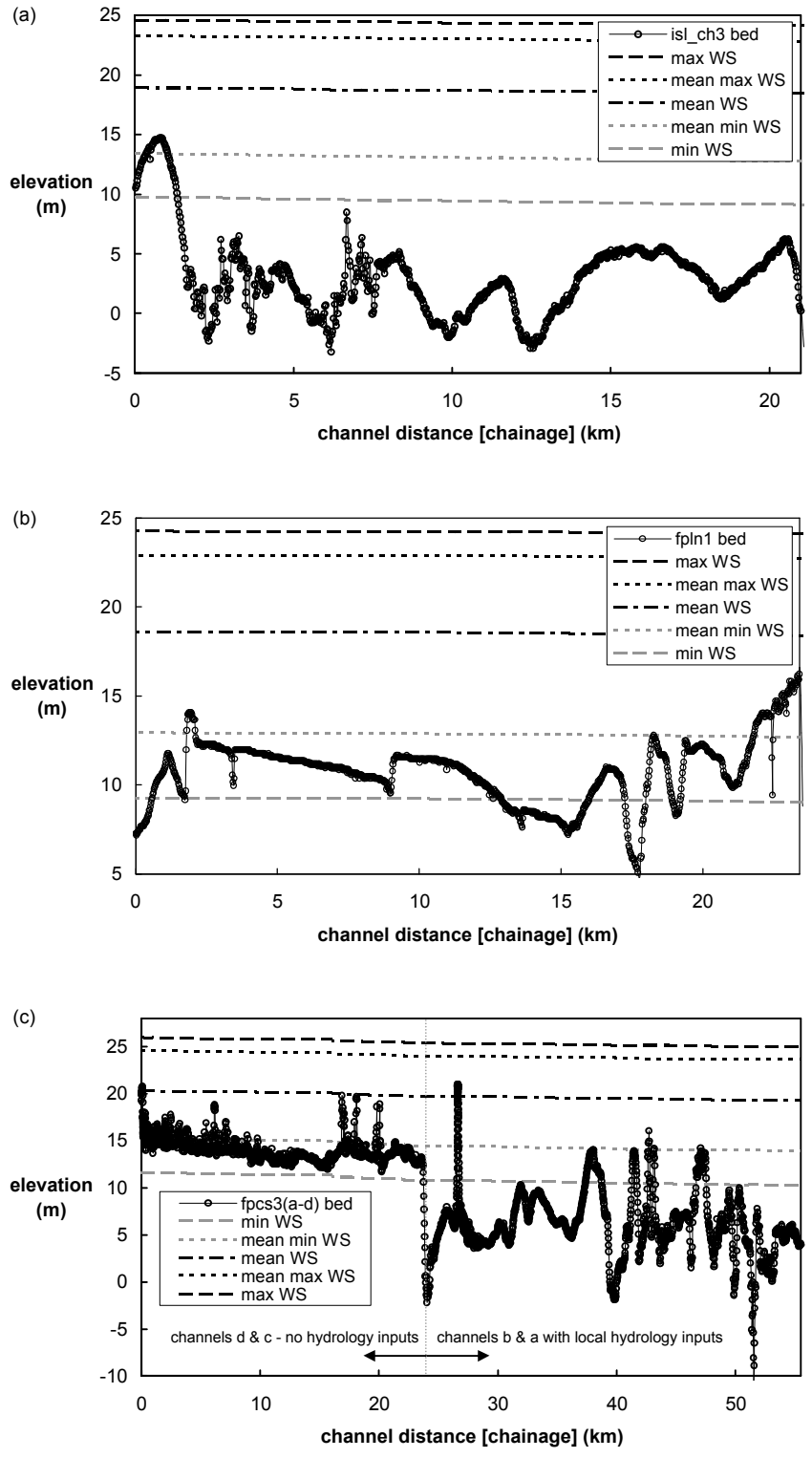

Figure 5-9 – (a) Island channel 3, longitudinal profile example, (b) Floodplain lake 1, longitudinal profile example, (c) Floodplain channels 3a,3b,3c,3d, longitudinal profile example. Channels 3a and 3b have extra catchment inputs, 3c and 3d have no local runoff input. Note, WS is water surface.

Table 5-5 – Channel summary

No.	ID	Data Cat.	Sonar points	Other characteristics	Width (m)	Traver-ses	Survey length (km)	Channel length (km)	% of Channel surveyed	Mean depth (m)	Mean bed elev (m)
1	isl_ch1	2	1092	-	118	2	20.5	10.3	100%	9.84	11.04
2	isl_ch2	2	1190	Main River	394	2	12.0	14.6	73%	13.70	8.70
3	isl_ch3	2	906	Main River	384	1	21.1	21.1	100%	20.17	3.08
4	isl_ch4	2	570	Main River	727	1	12.7	20.2	63%	18.72	4.98
5	isl_ch5	2	1443	-	219	1	16.7	16.7	100%	8.40	18.02
6	isl_ch6	2	1490	Main River	913	1	32.6	41.0	79%	20.33	7.35
7	isl_ch7	2	452	Main River	182	1	10.1	10.1	100%	15.77	12.36
8	fpln1	3	1232	Local Runoff	n/a	1	24.2	n/a	n/a	12.11	10.57
9	fpln2	3	5825	Local Runoff	n/a	1	73.4	n/a	n/a	6.86	17.37
10	fpln3	3	5543	Local Runoff	n/a	7	33.8	n/a	n/a	9.70	15.93
11	fpcs1a	4	799	Local Runoff	130	1	7.7	9.9	78%	14.86	7.29
12	fpcs1b	4	190	-	60	1	2.0	2.0	100%	8.19	14.11
13	fpcs2	4	569	-	60	2	3.2	6.1	26%	7.90	15.78
14	fpcs3a	4	660	Local Runoff	170	1	14.6	14.6	100%	18.06	5.80
15	fpcs3b	4	993	Local Runoff	220	1	16.7	16.7	100%	17.97	6.09
16	fpcs3c	4	181	-	150	1	3.6	3.6	100%	10.77	13.43
17	fpcs3d	4	1201	-	60	1	20.1	20.1	100%	10.01	14.52
18	fpcs4	4	946	-	200	1	17.7	17.7	100%	10.79	14.09
19	fpcs5	4	435	-	60	2	3.6	2.7	47%	10.83	14.28
20	fpcs6	4	566	-	50	2	4.6	6.2	37%	9.93	15.23
21	fpcs7a	4	2585	-	100	2	47.6	25.4	94%	12.76	12.83
22	fpcs7b	4	3456	-	120	2	66.9	33.4	100%	12.42	13.34
23	fpcs8	4	472	-	124	2	2.7	6.1	22%	10.59	15.20
24	fpcs9	4	497	-	40	2	2.2	5.5	20%	8.15	19.45
25	fpcs10	4	1032	-	105	1	8.5	8.5	100%	8.75	19.28
26	fpcn1a	5	2344	Local Runoff	155	2	38.8	33.0	100%	13.65	9.68
27	fpcn1b	5	2830	Local Runoff	110	1	35.5	35.5	100%	14.32	10.25
28	fpcn2	5	1704	-	269	1	5.7	7.9	71%	10.97	13.79
29	fpcn3	5	1530	-	95	3	13.9	4.6	100%	7.85	17.89
30	fpcn4a	5	2945	Local Runoff	381	2	75.9	102.0	38%	17.06	10.75
31	fpcn4b	5	2826	Local Runoff	135	2	39.3	57.2	34%	15.65	12.37
32	fpcn4c	5	301	-	120	2	5.2	2.6	100%	11.34	16.75
33	fpcn4d	5	132	-	70	2	2.5	5.2	24%	11.81	16.25
34	fpcn5a	5	2390	-	190	1	38.4	38.4	100%	11.44	16.63
35	fpcn5b	5	715	-	100	2	12.8	13.0	49%	10.43	17.66
36	fpcn5c	5	359	-	130	2	12.8	6.4	100%	8.20	19.89

Plotting the mean depth of the channels against their width, with symbol shape according to characteristics shows a distinctive pattern (Figure 5-10).

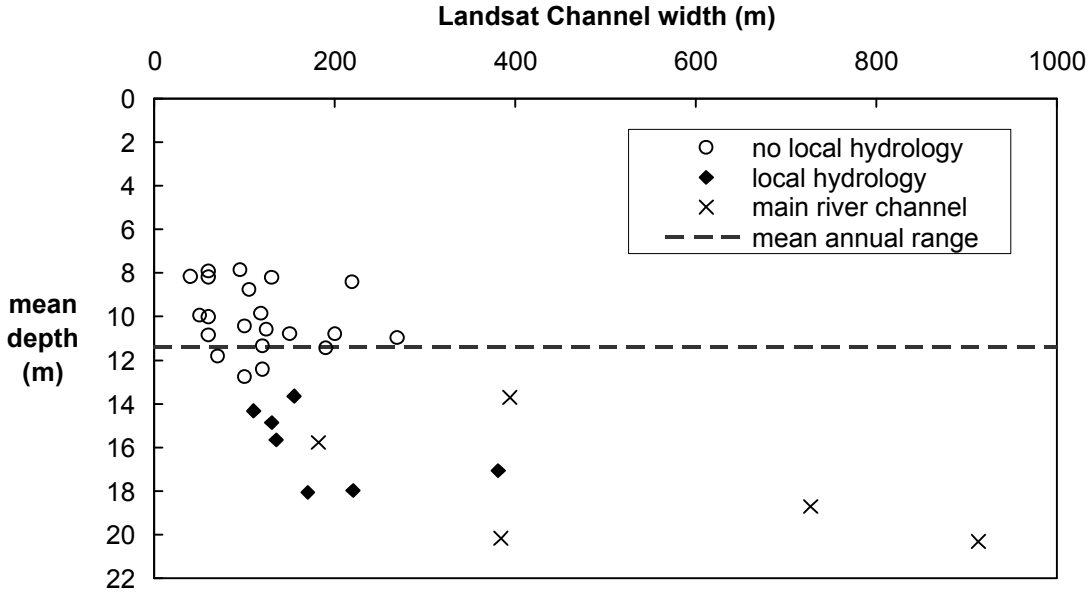

Figure 5-10 – Mean channel depth against channel width grouped by channel type.

All the floodplain channels with no runoff input are clustered around a mean depth of 10.4 m which is close to the mean annual range of the Amazon flood wave in the study area (11.4 m). These channels range from 50 m to 269 m wide. Channels with local runoff input have a significantly deeper mean depth (mean of 15.9 m) due to the flows being sustained by the local catchment even when the flood flow contribution from the main channel is small. Channels strongly connected in hydraulic terms to the main river tend to be much wider (mean width 520 m) and are deeper still with a mean depth of 17.7 m.

5.4.2 Channel cross-sections

Another useful tool in assessing the characteristics of river channels is that of perpendicular cross-sections. A total of 43 cross-sections were sampled from 16 of the channels during the survey. Figure 5-11 shows the locations of these sections and Table 5-6 provides summary information about the channels and cross-sections.

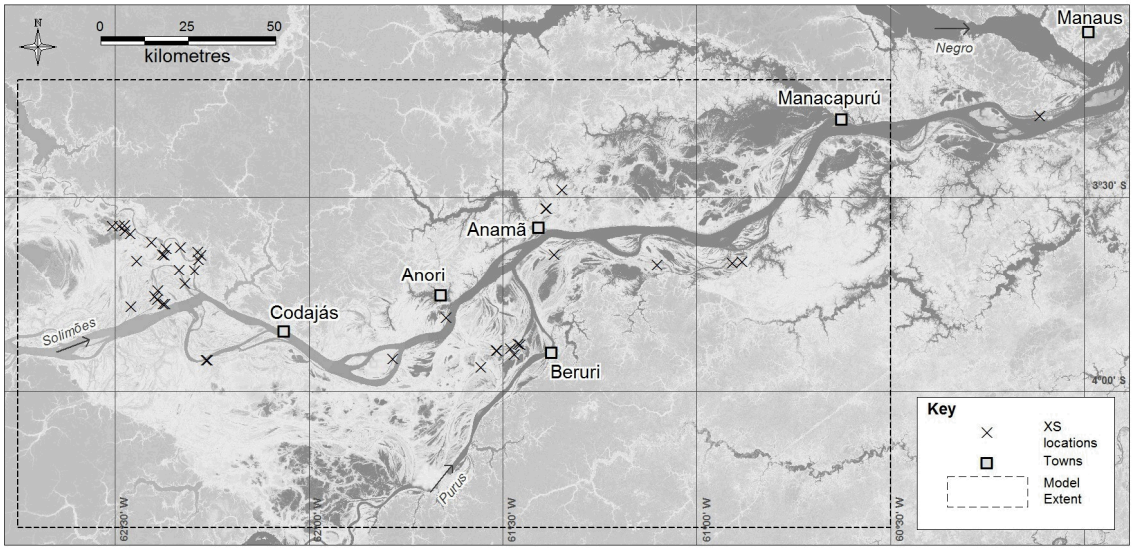

Figure 5-11 – Floodplain channel cross-section locations

The surveyed bed of each cross-section was plotted using the left bank as zero chainage (distance). The water elevation at the time of the survey and the long term water elevation statistics were also plotted. Where cross-sections were not taken perpendicular to the channel, the chainage was adjusted by the angle to provide a pseudo-perpendicular cross-section of equivalent flow area.

Table 5-6 – Channel cross-section summary

Number	Channel	Type	Other characteristics	number of XS	Channel width (m) (Landsat)	mean depth (m)
1	isl_ch1	Island channel	no	1	118	9.84
5	isl_ch5	Island channel	no	1	219	8.40
7	isl_ch7	Island channel	Main River	2	182	15.77
14	fpcs3a	floodplain channel S	Local Runoff	2	170	18.06
17	fpcs3d	floodplain channel S	no	1	60	10.01
18	fpcs4	floodplain channel S	no	1	200	10.79
21	fpcs7a	floodplain channel S	no	3	100	12.76
22	fpcs7b	floodplain channel S	no	4	120	12.42
24	fpcs9	floodplain channel S	no	2	40	8.15
27	fpcn1b	floodplain channel N	Local Runoff	3	110	14.32
29	fpcn3	floodplain channel N	no	1	95	7.85
30	fpcn4a	floodplain channel N	Local Runoff	8	381	17.06
31	fpcn4b	floodplain channel N	Local Runoff	7	135	15.65
34	fpcn5a	floodplain channel N	no	5	190	11.44
35	fpcn5b	floodplain channel N	no	1	100	10.43
36	fpcn5c	floodplain channel N	no	1	130	8.20

Figure 5-12 provides two example cross-sections from two different types of floodplain channel. One of the cross-sections is from a floodplain channel without any local runoff catchment (fpcn5a) and shows the typical features which are due to flood flow from the main channel, namely a relatively flat bottom (bed elevation variation of around 5m) at or around the minimum water levels experienced in the main river channel. The other cross-section is from a channel with significant local hydrology (either hydrological input or runoff) input (fpcn4a) and this is much more deeply incised with bed elevation variation of around 14 m, in this case.

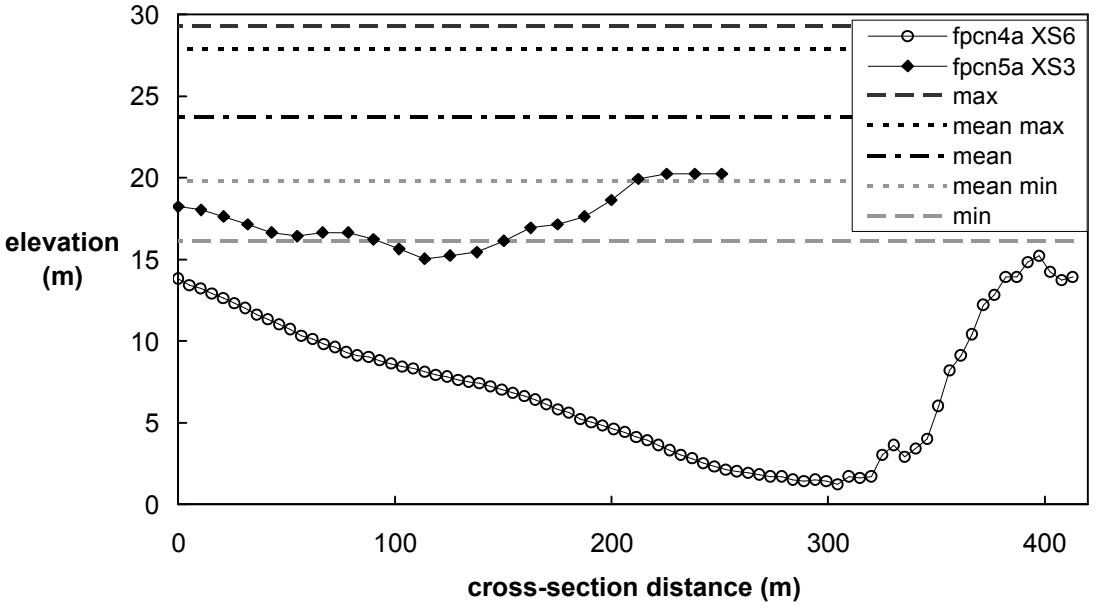

Figure 5-12 – Cross-section examples, fpcn5a is typical of a channel with local runoff input, and fpcn4a is typical of a channel with no local runoff input.

5.4.3 Landsat channel width assessment

The waypointed measurements of channel width provide the opportunity to carry out a ground truth assessment of the remote sensing width measurement method used on the Landsat images, as described in the previous chapter. Figure 5-13 shows the location of all the field width measurements carried out.

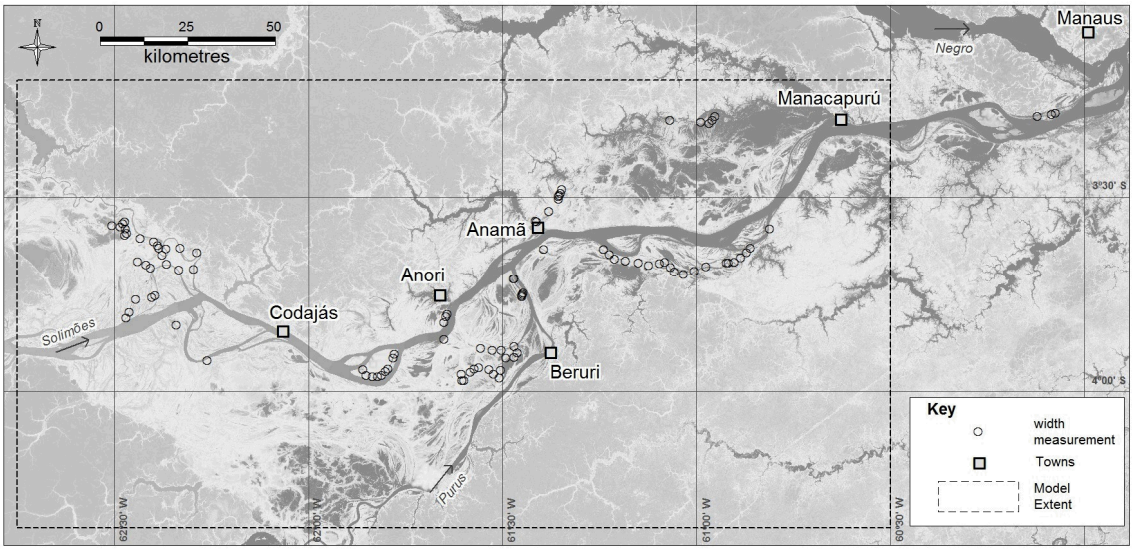

Figure 5-13 – Location of laser range finder width measurements

In total, there were 101 measurements made across 25 channels with a mean sample of four measurements per channel. These covered a range of channel widths from around 50 m to 450 m. It was difficult to get reliable readings with the laser range finder over 250 m, limiting the maximum channel width that could be measured to around 500 m. A summary of the field width measurements and associated Landsat width estimate by channel are shown in Table 5-7.

Table 5-7 – Channel width measurement summary

No.	Channel	count	mean laser width (m)	mean Landsat width (m)
1	isl_ch1	3	94	147
2	isl_ch5	9	225	206
3	fpln1	3	298	290
4	fpcs10	1	170	161
5	fpcs2	1	56	66
6	fpcs3a	5	240	227
7	fpcs3b	5	290	288
8	fpcs3c	2	165	150
9	fpcs3d	7	64	63
10	fpcs4	1	274	220
11	fpcs5	2	52	47
12	fpcs6	4	56	50
13	fpcs7a	4	97	106
14	fpcs7b	13	102	111
15	fpcs8	1	204	170
16	fpcs9	1	60	45
17	fpcn1a	2	202	180
18	fpcn1b	8	121	120
19	fpcn3	3	128	125
20	fpcn4a	6	449	432
21	fpcn4b	7	150	155
22	fpcn4c	1	170	160
23	fpcn4d	2	106	102
24	fpcn5a	7	258	210
25	fpcn5b	3	70	69

The difference in width between the two methods varies between -52 m to 54m with a mean of 8 m and RMSE of 21.4 m. Figure 5-14 graphically compares the widths measured by the two methods. The plot shows that as the channels get wider the laser range finder measurements are generally higher than the Landsat estimate. This could be due to a number of reasons: reduction in laser range finder accuracy with increased

distance, range finder measurements were carried out at high water and the Landsat images used were at low water when wider channels would have more bank exposed than smaller channels. For smaller channels, laser measurements were noticeably affected by overhanging vegetation, which could alter a measurement by as much as 5 m per bank, 10 m for a channel. Overhanging vegetation also affects the Landsat method.

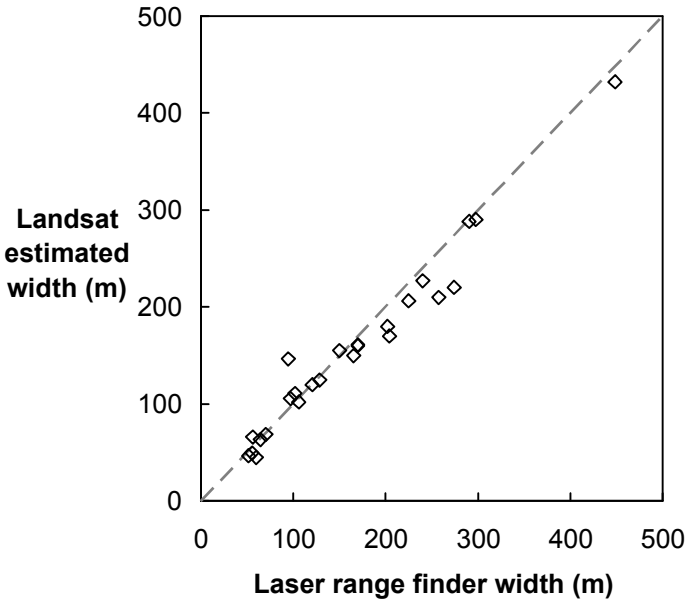

Figure 5-14 – Channel width plot comparing laser range finder measurements with Landsat estimates. Pearson's product-moment coefficient 0.979.

5.4.4 Bank elevation estimates

Field observations of water levels relative to bank levels allow an assessment of the vegetation-corrected SRTM data used in the original hydraulic modelling (Wilson *et al.*, 2007). The derived water elevations for the survey data together with the field notes of visual estimates of water levels relative to bank levels, allow bank elevations to be estimated for the waypointed locations. The 27 bank elevation waypoint locations are shown in Figure 5-15.

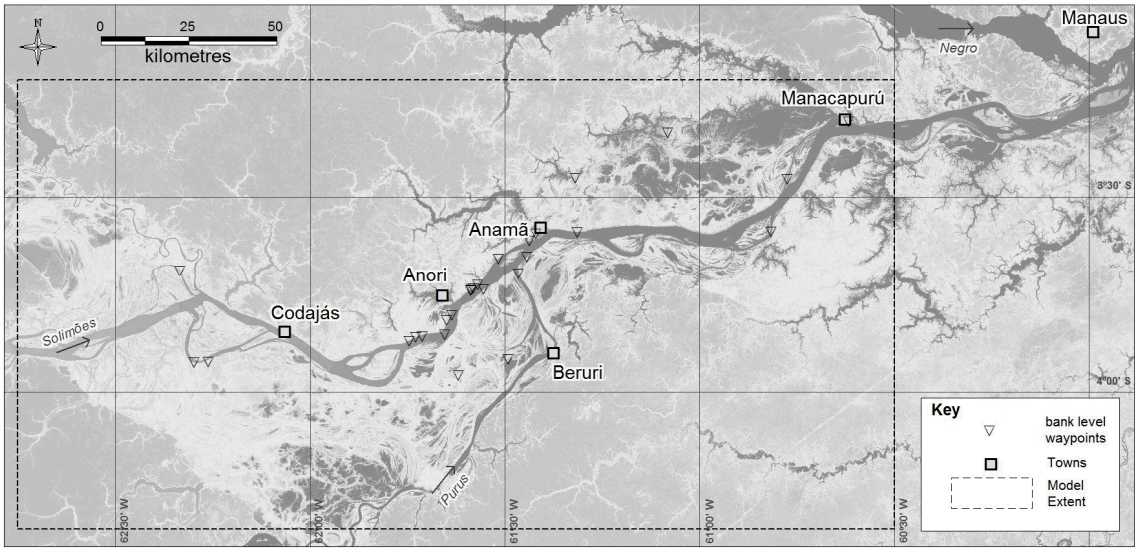

Figure 5-15 – Bank level waypoint locations

For each of the locations, the mean elevation of the nearest six bank pixels (90 m) from the vegetation-corrected SRTM was calculated and a note made of the predominant vegetation type within the six cells. This allowed the measurements to be grouped according to the vegetation classes used in the original SRTM vegetation correction (Hess *et al.*, 2003). These classes, together with the original measurements of vegetation height and vegetation correction applied in the Wilson *et al.* (2007) model are shown in Table 5-8.

The Wilson *et al.* (2007) vegetation heights in Table 5-8 were measured as follows: (i) digital photos of the flooded vegetation were taken from a boat some distance from the bank, (ii) the distance to the bank at the centre of the photo was measured by laser range finder, (iii) the standing depth of flood water at the vegetation was measured with a sonar, (iv) the photos were turned into silhouettes using matlab and the mean vegetation height for the photo was calculated using the laser range finder distance and optical properties of the camera lens, (v) any measured flood water depth below the vegetation is added to the calculated mean vegetation height above the water (Wilson and Horritt, personal communication, Jan, 2007).

Table 5-8 – Original mean vegetation heights measured and correction used for the Wilson *et al.* (2007) hydraulic model

Class	Description	measured mean vegetation height (m)	vegetation correction (m)
1	open water	-	-
2	very low grass	-	5.4
3	low grass	10.9	5.4
4	medium grass	5.5	5.4
5	high grass	13.3	5.4
6	low shrub	12.6	5.4
7	medium shrub	13.4	5.4
8	high shrub	7.2	5.4
9	very low forest	13	6.5
10	low forest	15.8	7.8
11	medium forest	16.1	7.8
12	high forest	-	7.8

The results of the analysis are shown in Table 5-9. The DEM elevation range as well as the mean for the six sample cells is shown. Predominant habitat class and survey bank elevation estimate are also shown.

Table 5-9 – Bank elevation estimates grouped by habitat class. Numbers 1-4 are grass, 5-7 shrub, and 8-27 forest.

No.	DEM min (m)	DEM mean (m)	DEM max (m)	Predominant habitat class	Estimated bank elevation (m)
1	18.6	20.3	23.6	4	24.88
2	13.0	17.0	20.0	4	25.29
3	17.6	20.3	22.6	5	24.21
4	16.6	20.4	22.6	5	22.43
5	30.6	33.7	37.6	7	25.00
6	30.6	33.1	34.6	7	27.51
7	27.6	30.9	36.6	8	25.57
8	21.5	23.6	25.6	9	22.45
9	25.2	28.2	29.5	9	24.25
10	26.5	28.5	30.5	9	24.90
11	23.5	30.3	34.6	9	25.55
12	27.5	31.5	36.2	9	25.45
13	24.5	26.9	29.5	9	24.58
14	22.5	24.8	27.5	9	21.83
15	27.5	29.7	31.6	9	27.11
16	18.2	20.0	23.6	10	18.94
17	25.5	27.7	29.2	10	24.33
18	23.2	26.6	29.5	10	24.82
19	27.2	28.6	31.2	10	25.28
20	14.2	21.8	26.5	10	20.67
21	25.2	27.6	29.5	10	24.85
22	21.2	23.3	27.5	10	21.75
23	23.2	25.6	28.6	10	24.89
24	25.2	27.2	30.5	10	25.19
25	27.2	27.4	28.5	10	24.67
26	25.2	27.7	31.5	11	25.59
27	24.2	27.8	33.6	11	24.93

The bank elevation estimates from the two methods are plotted in Figure 5-16, grouped by overall habitat class: grass, shrub and forest. It can be seen that there are systematic errors which are correlated with vegetation type. For the original vegetation height estimates: grasses are over estimated (mean error 4.7 m), forest underestimated (mean error 2.6 m) and shrubs underestimated (mean error 6.6 m). Whilst some of these differences may be due to secondary effects, such as a change in vegetation since the original survey or misclassification, it suggests that the original vegetation height estimates used in Wilson *et al.* (2007) may need further refinement.

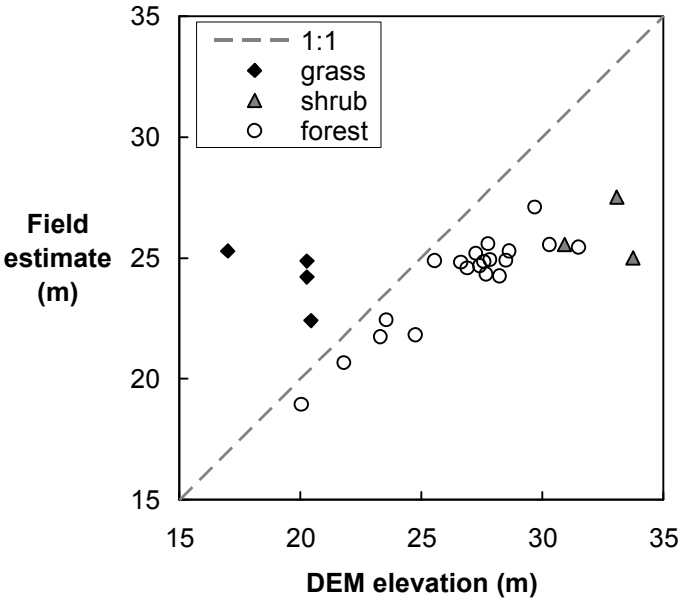

Figure 5-16 – Bank elevation comparison

Worbes *et al.* (1992) and Wittmann *et al.* (2004) studied natural forest succession in the *várzea* floodplain and this work included detailed measurements of vegetation heights. Table 5-10 shows how these might be applied to estimate the heights of the Hess vegetation classes (Hess *et al.*, 2003). The original vegetation correction used by Wilson *et al.* (2007) is shown together with a proposed correction based on the successional vegetation heights and the difference between the two corrections is shown in the final column.

Table 5-10 – Measured successional vegetation heights assigned to Hess vegetation classification with SRTM vegetation corrections

Class*	Description*	Successional stage**	Stand heights (m)**	Original vegetation correction (m)***	Proposed vegetation correction (m)	Vegetation correction difference (m)
1	open water	-	-	-	-	-
2	very low grass	early succession	3 – 10	5.4	0.5	4.9
3	low grass			5.4	1	4.4
4	medium grass			5.4	2	3.4
5	high grass			5.4	3	2.4
6	low shrub			5.4	4	1.4
7	medium shrub	early secondary	10 – 18	5.4	5	0.4
8	high shrub			5.4	7	-1.6
9	very low forest	secondary	14 – 20	6.5	9	-2.5
10	low forest	late secondary	20 – 30	7.8	12	-4.2
11	medium forest	late succession	30 – 35	7.8	16	-8.2
12	high forest	climax	35 – 40	7.8	18	-10.2

*** (Hess *et al.*, 2003), ** (Worbes *et al.*, 1992; Wittmann *et al.*, 2004), *** (Wilson *et al.* 2007)**

The difference between the two vegetation corrections in Table 5-10 shows a similar pattern to that identified from the field survey shown in Figure 5-16. This pattern shows that, in general, the height of grasses may be overestimated, and forest underestimated in the original Wilson *et al.* (2007) correction. Contrary to the field survey results (Figure 5-16), shrubs appear to be a reasonable estimate in the original SRTM vegetation correction, although the field survey only includes three samples so may not be representative. The data in Table 5-10 does show a much wider range of vegetation heights than previously assumed and it is likely that this is because both the original vegetation estimation measurements (Wilson *et al.*, 2007) and those for this field survey, were carried out from boats. Boat access will be biased towards areas of *low várzea*, composed of species adapted to deeper water conditions with number of tree species restricted due to the deeper water (Wittmann *et al.*, 2002). This bias towards *low várzea* will result in a general underestimation in forest heights. Both sets

of measurements from the boats were carried out at high water, meaning much of the grass classes would have been underwater, increasing uncertainty in the grass height estimates. Additionally, the original SRTM penetration factor of 50% is likely to vary by vegetation class as well, due to differences in density and structure (Farr *et al.*, 2007). Given that elevation analysis of the floodplain in Section 4.4 shows that 50% of the floodplain area lies within a 6 m elevation range, vegetation correction errors of up to 10 m are significant.

5.5 Discussion and conclusions

5.5.1 Summary

This chapter has detailed the field survey carried out to collect original bathymetric data as well as other key characteristics of the vegetation and floodplain channels within the study area. The survey was carried out for a total of 9 days between the 7th and 15th of April 2009, covering 1400 km of river and floodplain. In total, 93,083 sonar points were collected, 56% of which were specifically within floodplain channels. The collected data were subdivided into five main categories for further analysis; main river, island channel, floodplain lake and floodplain channel, north and south sides. Thirty six floodplain channels were identified and analysed individually. In addition, 43 cross-sections were sampled from 16 of these channels during the survey and 101 measurements of channel width were taken from 25 of the channels. Estimations of bank elevation relative to water surface were noted at 27 locations during the survey.

5.5.2 Channel characteristics

One of the main aims of the planned survey work was to identify key morphological characteristics of the floodplain channels in order to better understand their function as well to enable a better physical representation within the 2D element of the hydraulic model. Following on from the work in the previous chapter, which shows that the channels can be grouped by connectivity into different categories, data were collected from three main types of channel; those carrying only flow from the annual flood wave, channels that also carried local catchment runoff and island channels which were strongly connected with the main channel at all flow levels.

The mean depth of the channels only carrying main river flood water was strongly correlated with the flood wave's mean annual range of 11.4 m, resulting in floodplain channel bed elevations similar to the main channel low water elevations. These channels connect the main river to the floodplain throughout the year from low to high water and provide a direct connection which feeds flood water onto the floodplain as the water level rises, as well as providing drainage of the floodplain as main river water levels drop. Some of these channels can flow both from the river and to the river depending on hydraulic conditions. This strong hydraulic connection to the Amazon flood wave results in channels which are no deeper than main channel low water levels and which have characteristically shallow bed cross-sections compared to a typical river. Although flow measurements were not taken, it could be reasonably assumed that if the channel depths are limited by the hydraulics of the annual flood wave, then channel flow must be directly related to channel width. This fits with observations of the channel networks, where multiple small channels feed water from the main channel onto the floodplain, connecting up to become quite wide channels draining the floodplain back to the main river further downstream.

For those channels which not only carry main river flood water, but which also have a portion of flow provided by local hydrology inputs from small catchments alongside the main river, the mean depth (15.9 m) can be substantially deeper than the channels carrying only river flood water. Although these channels with local hydrology inputs also carry significant main river flood flow during the flooding phase of the river, they also carry flow from their own catchments throughout the year. It is hypothesised here that this additional flow provides the hydraulic conditions necessary to incise deeper channels into the floodplain. Cross-sections of these channels with additional hydrology inputs typically show more variation across the bed of the channel compared with the main river floodwater only channels.

Most of the main river island channels showed a strong hydraulic connection with the main channel, and although none of them had any sizeable additional

catchment area, mean depths were typically much greater than floodplain channels with additional hydrology. This close connection means the island channels are exposed to the more dynamic regime of main channel flows with greater scouring and deposition resulting in more varied bed profiles as well as deeper mean depths (17.7m).

This work represents the first dedicated field survey of the morphological characteristics of the Amazonian floodplain channels and provides new insights into how the hydraulic conditions may be controlling the characteristics of these channels. These findings have important implications in terms of quantification of the hydraulic connectivity on the floodplain (Chapter 4), which in turn has implications for the understanding of the floodplain hydrodynamics, which is explored in the following chapter. These floodplain channel findings are also important for wider environmental studies of the floodplain. Environmental gradients, such as water depths and nutrient availability, which are brought about by the flood wave, are vitally important for most of the ecology that is adapted to life in the floodplain (Petry *et al.*, 2003). In Chapter 3 it was determined that the floodplain channels are an important component in shaping these environmental gradients, so an understanding of the characteristics of these channels and the source of the water in the channels will aid in a wider understanding of environmental gradients within the floodplain.

5.5.3 Ground truthing

Due to the access difficulties and the scale of the study area, for the purposes of studying the hydraulics, there is a necessary emphasis on the use of remote sensing data sets. While such data sets provide large amounts of useful data, it is important to ground truth these against field observations in order to understand the limitations of their application as well as to provide additional point source data for study. The opportunity was taken during this field survey to do this for the width estimation method

based on Landsat data used in the previous chapter and the vegetation removal methodology applied to SRTM topography data used for the 2D floodplain element of the hydraulic model.

Manual measurement of channel widths and comparison of these with those estimated from Landsat imagery provide an RMSE of 21.4 m. This is close to the pansharpened resolution of 15m of Landsat images used and also well within the ability of the hydraulic model to represent the channels using a 270 m cell size for the floodplain. Carrying out manual measurements of width also highlighted the uncertainties introduced by overhanging vegetation as well as the effects on width of different water levels.

Being present in the field during the flooding phase of the flood wave provided an opportunity to ground truth the vegetation-corrected SRTM DEM with estimated bank elevations from observations. Vegetation heights were estimated from field measurements made in 2005 (Wilson *et al.*, 2007) and these were used with a vegetation classification (Hess *et al.*, 2003) and a 50% canopy penetration factor to provide a vegetation correction to the SRTM DEM. There is significant room for error in this process: given different datums, uncertainties in canopy penetration factors and vegetation height measurement errors. Estimating the bank elevations from the water elevations in the field and grouping these by bank vegetation type provides an alternative method of deriving bare earth elevations for spot locations throughout the study area. The results show that the differences between the elevations from the two methods are strongly correlated with vegetation type. Whilst not enough data were collected across all the vegetation types to provide a definitive alternative to the original vegetation correction method, it certainly indicates errors that would be worth investigating via a sensitivity analysis using the model. Published measurements of vegetation heights from the Amazon floodplain also show that the original vegetation heights from the Wilson *et al.* (2007) survey are underestimated, and it is likely that the

vegetation correction would be more reliable using published figures of vegetation heights (Worbes *et al.*, 1992; Wittmann *et al.*, 2004).

5.5.4 General observations

As well as measuring basic characteristics of the floodplain channels, another important part of the field survey was observing flood mechanisms first hand. The basic mechanisms of diffusive overbank flow and floodplain channel connections to the main channel have been noted before (Mertes *et al.*, 1995, Mertes *et al.*, 1996). From observations, the flow carried by the floodplain channels is significant and occurs throughout most of the flood wave cycle. The diffusive overbank flow only starts to occur when the river levels are relatively high and above main river bank levels. At the start of the rising limb of the flood wave, the *floodplain hydrologic units* (FHU) identified in the previous chapter will generally stay isolated from each other because the channel networks are unconnected. When water levels are high enough to overtop the high points between the FHUs they connect through diffusive flow. The Solimões River carries a high sediment load and this is deposited as velocities drop away from the main channel (Mertes, 1994). The survey of the floodplain channels shows this sedimentation process leaves noticeable ridges of sediments at the mouths of the channels where they convey water onto the floodplain and also builds up on the banks where diffusive flow occurs. When the water levels are very high, breaches in the sediment levees can also remove these sediments and there was also evidence of this with very strong scouring flow at points onto the floodplain. Where overbank flow initially begins to break through the sediment ridge on the bank and flow down to the relatively low areas behind, the current is sufficient to generate turbulent flow (see Figure 5-17a). These points may also be the genesis of a new floodplain channel connection to the main river.

Figure 5-17 – (a) bank overtopping with turbulent flow, (b) floodplain channel blocked with *capim* (macrophytes)

The sediment rich flood water from the main river has a distinct brown colour compared with black water sourced from local runoff. While travelling through the floodplain, this meant that the progression of the flooding from the main river was clear. At the stage of flooding that was occurring during the survey, many of the channels showed brown water in the half of the channel connected to the main river upstream and black water in the half of the channel connected to the main channel downstream. There were a number of locations where black water was being flushed into the brown water channel from the side, indicating that there was also overbank flow coming across the floodplain from other directions. The implication is that during the low water phase of the flood cycle, the water in the floodplain is generally sourced from local rainfall and runoff in addition to previous cycle floodwater that has had sufficient residency time for sediment to deposit. This water then gets flushed out during the flooding phase and replaced with sediment rich Solimões water. The exception seems to be the large channels with significant local catchments that run along the side of the main river floodplain and these maintain a significant proportion of black water during most of the flood cycle. Even these may get overwhelmed as water levels in the main channel become very high. For example, channel fpcn4a is around 380 m wide and carries a significant quantity of local runoff, however, locals related that at the flood

peak, brown Solimões water often backs up this channel and fills the large low basin lakes in the middle of the floodplain just north of the main channel.

Melack and Forsberg (2001) demonstrate that the growth of macrophytes (floating vegetation) is strongly correlated with the availability of nutrients in the water (i.e. sediments). This was particularly noticeable while travelling through the floodplain channels, with channels regularly blocked by macrophytes, locally called *"capim"* (see Figure 5-17b). These blockages only ever occurred in the brown water reaches of the channels that were connected to the main river at their upstream end. While there was some evidence of the vegetation along the banks in black water areas, this was sparse and never blocked the channel. The supposition is that as the brown water passes down the floodplain, these macrophytes begin to grow rapidly from bank locations and eventually block the channel. Flow still continues underneath these blockages, but they are significant enough that they must affect the hydraulics, perhaps forcing more water onto the floodplain from these channels due to increased flow resistance and the resulting higher water levels.

It has been demonstrated that even with a limited time and budget, it is possible to collect meaningful first hand data regarding hydraulic characteristics of the floodplain channels. The use of what are now quite advanced and relatively low cost fish finder sonars has been shown to be a valid tool for this purpose with acceptable noise error under 0.5 m. Further data collection over a larger number of channels and perhaps at different times during the flood cycle would add useful information to that gained. However, sufficient data has been collected such that novel and useful conclusions have been possible. This understanding can now be used, together with the rest of the research carried out, to bring together a synthesis of current knowledge regarding the Amazon river and floodplain dynamics.

CHAPTER 6
Floodplain hydrodynamics

6.1 Introduction

The research presented thus far in Chapters 3, 4 and 5 has concentrated on exploring specific hydraulic and spatial aspects of the Amazon River and floodplain. These chapters adopted a reductionist approach and used a variety of tools and methods in order to quantify key characteristics of the complex floodplain hydrodynamic processes. In this chapter the findings from all the previous chapters, together with findings from other published work, are combined to present a synthesis of knowledge regarding the workings of the floodplain hydrodynamics in the central Amazon. This synthesis approach allows an understanding of how the different, separately measured and observed aspects of the processes, may interact and affect each other, and therefore contributes to advances in the current conceptual understanding of the floodplain hydrodynamics in the wider research community.

Before drawing on the work already presented in previous chapters, it is important to understand the current state of knowledge regarding the Amazon floodplain hydrodynamics as reported in the scientific literature. While some of this research was covered in the context presented in Chapter 2, here the focus will be on more specific aspects of previous research that help build a rational framework, or conceptual model, of the floodplain hydrodynamic processes.

After looking at the research context, the relative importance of the various sources of water in the floodplain and the timings of the input of these different sources is investigated. This investigation used flows derived from a large scale hydrological model of the entire Amazon basin (Beighley *et al.*, 2009) and applied them to the study

area using the detailed spatial understanding of the floodplain gained in Chapter 4. The resulting flows, volumes and timings provide an important understanding of the relative importance of these differing sources within the study area floodplain.

The chapter then continues with a study of the drivers and modifiers of flow between the main channel and floodplain, as well as flow on the floodplain. Flow is driven by a difference in water elevations, known as the hydraulic head. The gauged water elevations in the main river (Chapter 3) were compared with bank and floodplain channel bed elevations measured in the field (Chapter 5) in order to understand when the channelised flows and diffusive overbank flows are active during the flood cycle. Although hydraulic head is the primary driver of flow between locations, the topography modifies the direction, timing and magnitude of that flow due to the effect of barriers, friction and preferential flow paths. A schematic plan and cross-section of the floodplain, derived from the floodplain hydrologic units identified in Chapter 4, is used to explain how the floodplain topography has a controlling effect on the movement of water across the floodplain from the different sources.

Finally, the chapter concludes by presenting a hypothesis of how the floodplain hydrodynamics changes through the flood cycle using schematics of five overlapping stages of floodplain filling and draining based on the sources, timings, drivers and modifiers already identified. This hypothesis is then tested against patterns of temporal water level changes on the floodplain observed in satellite data (Alsdorf *et al.*, 2007a).

6.2 Current rational framework

In Chapter 2, it was found that there is little detailed information regarding Amazonian floodplain hydrodynamics which has been published, and no specific framework, that is applicable across the central mainstem floodplain, has as yet been proposed. Even though an existing framework is not explicitly detailed in the literature, there are many elements of a potential framework that exist already and indeed, many researchers studying different aspects of the floodplain will have a conceptual model of the processes active there, hopefully informed by current research. The complexity of Amazonian floodplain processes and the resulting topography requires examination of a wide variety of research studies in order to build a rational framework that encompasses the many aspects of those processes.

The complexity of flow dynamics on floodplains in general has been studied in some detail and there are already general frameworks for the active processes and inundation sequences observed, such as that described by Lewin and Hughes (1980). These studies show that there are many relevant processes that may be active in the Amazon floodplain, such as: groundwater rise, bank breaching, bank spilling, tributary flooding, channelised flows, diffusive flows, infiltration, evaporation and overbank returns. The combined effect of these processes during a flooding event produces a distinct hysteresis in the flood extent, elevation and duration behaviour which varies from one event to another and from one floodplain to another. This hysteresis behaviour for flood volumes and water elevations has been observed on the Amazon floodplain (Meade *et al.*, 1991; Birkett *et al.*, 2002; Frappart *et al.*, 2005). It is clear from the work in Chapter 3 that the Amazon is not a typical river, hydraulically, due to its monomodal flood wave, scale and very shallow hydraulic slope, and therefore general findings must be applied with particular care to the Amazon floodplain.

While many Amazon studies report field observations of general floodplain processes, there are relatively few that attempt quantification or assessment of their

relative importance to the floodplain dynamics. Hydrological modelling studies of the entire basin have shown that the volume of water stored in the floodplain has a significant effect on the flood wave as it passes down the mainstem, attenuating the flow and altering the effect of timings of inflows, thus contributing towards the formation of the monomodal flood wave (Vorosmarty *et al.*, 1989). In addition, these models show strong links between climatic variability and discharge in cycles of ~3-4 years and ~28 years (Coe *et al.*, 2002). Junk *et al.* (1989) introduced the flood pulse concept which states that rivers and their floodplains are integrated components of a single dynamic system, linked by strong interactions between hydrological and ecological processes. This has been shown to be an important way of understanding the Amazon floodplain system and has led to many advances in understanding how the ecology of the floodplain responds to hydrological gradients (Junk and Piedade, 1993; Melack and Forsberg, 2001; Wittmann *et al.*, 2004). However, the application of the flood pulse concept in the Amazon has focused mainly on the ecology side of the floodplain system, leaving many details of the hydrological side yet to be investigated.

Most of the advances in the current understanding of the floodplain processes active within the Amazon floodplain come from geomorphology studies. These studies have provided an important understanding of the long term geological context of the floodplain, detailing how forces such as plate tectonics and sea level changes have shaped the existing floodplain (Forsberg *et al.*, 2000; Latrubesse and Franzinelli, 2002; Rossetti and Valeriano, 2007). However, only a few studies have looked in detail at processes that are active in decadal timescales, which is of most interest in the context of this thesis (Mertes *et al.*, 1993; Mertes, 1994; Mertes *et al.*, 1995; Mertes *et al.*, 1996; Mertes, 1997; Dunne *et al.*, 1998). Mertes *et al.* (1996) drew on the geological history and used mapping of wetland features from radar images and radar altimetry to present a basic framework from which to understand the channel-floodplain geomorphology of the river and floodplain. This important study divided the central floodplain into three reaches, each with a distinct geomorphology linked to river slope,

sediment transport and geological controls. The upper reach is characterised by the erosion of sand in the main channel and deposition of sediment in the floodplain, producing intricate scroll-bar topography. In contrast, the downstream reach is characterised by channels restricted by stabilising levee building and floodplain construction dominated by overbank flow depositions that gradually buries scroll topography. The central reach, which is the location of the study area of this thesis, shows a mixture of the upstream and downstream reach characteristics.

Through studying surface suspended sediment distribution in Landsat TM images, these geomorphological studies also show the importance of local rainfall and runoff to the flooding dynamics (Mertes *et al.*, 1993; Peixoto *et al.*, 2009). Mertes (1997) goes on to define the area of mixing between the river and local water as the perirheic zone and demonstrates that for the Amazon, only part of the floodplain is flooded by the river, with significant areas being dominated by local water, thus emphasising the heterogeneity of the floodplain dynamics. Mertes *et al.* (1995) proposed a three stage inundation of the Amazon floodplain. Initially, the floodplain begins to fill, at a river stage approximately 3 m above low water, as a result of a rising water table and water flowing through levee breaks associated with the deepest floodplain drainage channels. As the stage increases from 4 to 7 m above low water, the numerous levee breaks associated with shallower floodplain channels are inundated, but the floodplain water is still comprised largely of local tributary, rain, or ground water. Finally, river water begins to enter the floodplain rapidly overbank once the stage exceeds approximately 10 m above the low water level.

Although geomorphological studies provide important information on the macro controls on the floodplain dynamics, ultimately their main focus is on the sedimentology rather than the hydraulics and leaves many details of floodplain hydrodynamics yet to be explored. Localised field studies provide more detailed quantification of some of the processes at work in the floodplain (Engle and Melack, 1993; Lesack and Melack, 1995; Lesack, 1995; Cullmann *et al.*, 2006). Many of these studies are focused

specifically on floodplain lakes, meaning that the wider role and relative importance of the floodplain channels is not as well studied.

The complex of interconnected lakes at Curuaí near Óbidos has been studied for many years under the HyBAm (Hydrology and Geochemistry of the Amazonian Basin) research programme, using a combination of direct measurement, water balance modelling and remote sensing techniques to investigate and quantify the floodplain processes at work (Bonnet *et al.*, 2005; Bourgoin *et al.*, 2007; Bonnet *et al.*, 2008) and their effects on the geochemistry (Moreira-Turcq *et al.*, 2004; Barroux *et al.*, 2006; Maia *et al.*, 2009). This programme has added an important subset of knowledge regarding river-floodplain interactions and corroborated many of the findings and hypotheses of earlier work in the Amazon. Specifically, these studies found a net contribution of water from the floodplain to the river, and that the flood water from the Amazon River dominated (77%) the inputs to the lakes year round. Rainfall, runoff and seepage accounted for 9%, 10% and 4% respectively to the annual inputs. Hydrologic residency of water in the lake was around three months. The importance and relative stability of floodplain channels connecting the river to the lakes and between the lakes is also demonstrated by these studies and they provide some of the few published measurements of floodplain channel characteristics. Although the Curuaí lakes represent a 4,000 km^2 area of the floodplain, this area is still relatively small compared to the whole central Amazon floodplain estimated at 300,000 km^2 (Hess *et al.*, 2003) and is only representative of the most downstream of the three broad floodplain types described by Mertes *et al.* (1996).

There is a demonstrable need for a framework of the floodplain hydrodynamics that links the broad scale processes revealed by the geomorphology studies with the site specific detail measured by the field studies. This would also provide an important tool in interpreting the complex spatial and temporal patterns observed on the floodplain as recently mapped by remote sensing instruments (Alsdorf *et al.*, 2007a).

6.3 Flow sources

Due to differing nutrient content, the source of floodplain water has been identified by many studies as an important biological aspect of floodplain inundation (Junk and Piedade, 1993; Putz, 1997; Melack and Forsberg, 2001; Phlips *et al.*, 2008). Water sources and timing also affects the location of the perirheic zone and sediment movement, and so are an essential component of floodplain dynamics (Mertes *et al.*, 1993, Mertes, 1997). In Chapter 4, the floodplain was divided into *floodplain hydrologic units* (FHUs) by connectivity. This differing connectivity for different areas of the floodplain means that it is important to consider these units when assessing flow sources on the floodplain. Table 6-1 summarises the three classes and six types of FHUs identified in Chapter 4.

Table 6-1 – Floodplain hydrologic unit class and type descriptions

Class	FHU types	Description
1	1a - island 1b - bypass	Located directly adjacent to the main river and dominated by river flow leaving and re-entering the main river via floodplain channels and overbank flow. Significant sediment deposits resulting in scroll-bar topography.
2	2a - connect 2b - basin	Central area of floodplain that is isolated from the main river flow and the terrace runoff catchments for much of the year by sediment deposits. At high water these units receive diffusive flows from the main river banks and over the FHU unit sediment boundaries. The main channel draining water from the unit to the river may experience flow reversal due a change in the hydraulic gradient when main river levels rise rapidly. Receives little river sediment.
3	3a - indirect 3b - direct	All local terrace slopes/minor catchments that line the boundary of the floodplain. Split into those that flow directly into the main river and those that flow into the floodplain and then into the main river via a long collector channel. Floodplain area of the indirect type consists of a narrow band of floodplain along the foot of the terrace marking the floodplain edge. Dominated by one long, deep and sinuous collector / drainage channel that connects to the main river upstream and downstream. The collector channel is dominated by local runoff for most of the year until high main stem water levels occur, when a flood wave from the main river passes down the channel, over spilling the banks of the collector channel, leaving sediment deposits that confine the flows to the strip of floodplain along the foot of the river terrace.

Other than widely spaced gauging stations on the main stem and a few major tributaries, the majority of the many tributaries of the Amazon are ungauged (Alsdorf *et*

al., 2007b). This lack of gauges means that currently the only way to assess the relative importance of the local water sources compared to the main channel flows in the thesis study area is to use hydrological modelling to estimate these local sources. Recent advances in the detail and process representation of these hydrological models for the Amazon basin mean that it is now possible to look at the various floodplain inputs in broad terms for the study area. Flow data, catchment extents and river networks from the Beighley *et al.* (2009) hydrological Amazon model were provided by researchers at the San Diego State University for the purpose of better understanding the hydrological inputs for the floodplain in the thesis study area.

Catchments and stream networks from the Beighley *et al.* (2009) hydrological model were compared with the floodplain channel networks and floodplain hydrologic units derived in this thesis for the floodplain area. This comparison of floodplain representation showed that, despite using the same SRTM data to represent the floodplain, there were significant channel location and boundary differences that meant it was difficult to use the hydrological model output directly as point source inputs to the hydraulic model. The difficulties with floodplain representation in the hydrological model is perhaps not surprising when considering that: (i) the methods to derive the model catchments are biased towards steep sloping runoff catchments and not shallow sloped floodplain catchments; (ii) the model covers over 6 million km^2 compared to the 30,000 km^2 study area used in this thesis; and (iii) the current limited state of knowledge regarding the Amazon floodplain hydrodynamics.

In addition to the main Solimões channel and Purus tributary inputs, two other tributary inputs to the thesis study area were indentified and extracted from the hydrological model data. Runoff inputs for the floodplain areas and local terrace runoff catchments located within the thesis study area were calculated using the net rainfall minus evapotranspiration (net P-ET) from the hydrological model, and FHU areas from Chapter 4. The hydrological model output provided covered a period of 1/1/2000 to 29/06/2008, but the first couple of months of 2000 include a model start up phase so

was discounted. This leaves six complete calendar years of data for analysis, 2001 to 2007. Figure 6-1 shows the four main flow inputs into the study area and highlights the local terrace runoff area and floodplain area.

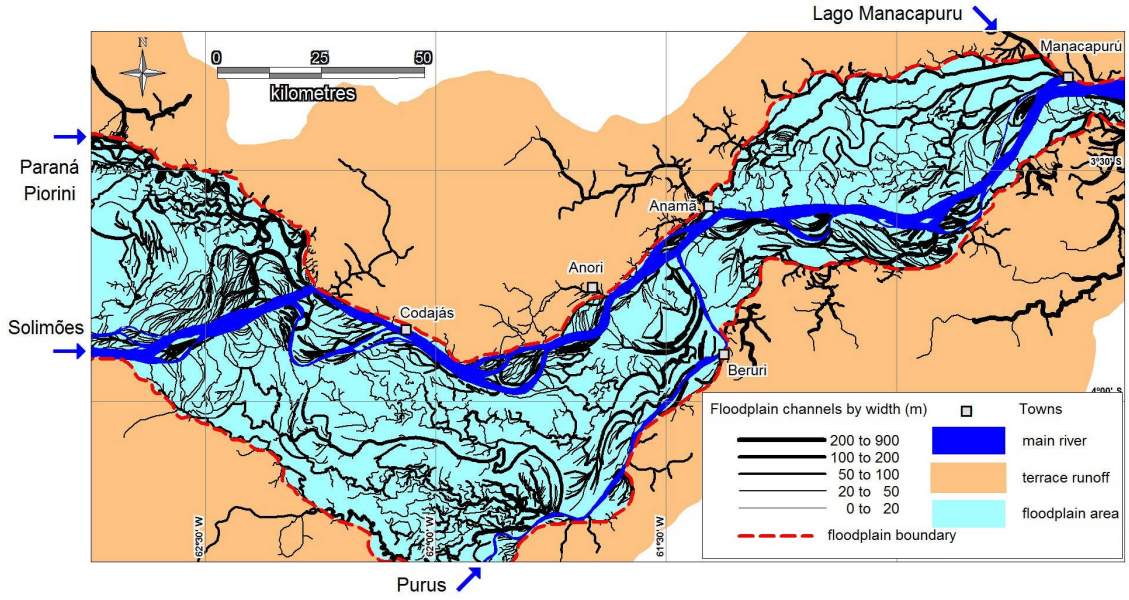

Figure 6-1 – Main flow inputs for study area

Table 6-2 shows the contributing area and flows for the runoff inputs to the study area, broken down into main river and floodplain inputs. Values are the mean of output from the hydrological model for the period 2001-2007.

Comparing the mean flows shows that the local sources are only 1.6% of the size of the main river flows, but this increases to 3% at high flows. Initially this might lead one to assume local sources are not significant, but much of the flow in the main river will remain in the main channel, so it would be better to compare local sources to the out of bank river flows. Estimates have been made in a number of studies of the flux between the main channel and floodplain which give some indication of what might be expected. Richey *et al.* (1989b) estimate local runoff for this study reach at 5000 m^3/s using catchment areas and rainfall-runoff calculations which is not too dissimilar from the peak of 4,320 m^3/s in Table 6-2. Richey *et al.* (1989b) conclude from their calculations that some 30% of the main river flow is derived from flow passing through the floodplain either from local runoff or river flood water fluxes through the floodplain. Water balance modelling of the Curuaí lakes also yields an estimate of this flux at 35%

(Bonnet *et al.* 2005, Bourgoin *et al.* 2007). Dunne *et al.* 1998 use the same method as Richey *et al.* to break down this general estimate for the three main stem reaches and calculate an out of bank flow of approximately 200 m^3/s/km (54,000 m^3/s, 44% of main channel flow) for the thesis study reach. This suggests that large quantities of river water are flowing through the floodplain in addition to the local sources. Another factor to consider is that much of the local runoff input from the small tributaries and terrace catchments is fed into the main collector channels that run along the foot of the terrace at the edge of the floodplain. This means that the ratio of river water to local runoff will be different for these *indirect* FHUs compared to those that are strongly linked to the main river such as the *island* and *bypass* FHUs.

Table 6-2 – Areas and flows for study area hydrology inputs, mean values for 2001-07 (See Figure 6-1 for locations and areas)

Input	Hydrological Model Unit ID	Type	area (km^2)	min daily flow (m^3/s)	mean daily flow (m^3/s)	max daily flow (m^3/s)
Solimões (top of reach)	9339	main river inflow	1,787,127	57,140	86,707	122,489
Purus (top of reach)	9211	main river inflow	379,648	2,830	10,635	21,633
direct rainfall on main river	-	net (P-ET)	1,100	3	30	97
		total main river	**2,167,875**	**59,973**	**97,372**	**144,219**
Paraná Piorini	9325	west tributary inflow	17,756	87	575	1,311
Lago Manacapuru	9123	north tributary inflow	11,420	42	337	807
floodplain area	-	net (P-ET)	10,390	26	283	913
local terrace catchments	-	net (P-ET)	14,660	37	399	1,289
		total floodplain	**54,226**	**192**	**1,593**	**4,320**
		% of total main river	**2.5%**	**0.3%**	**1.6%**	**3.0%**

Another factor that affects the relative importance of local sources when compared to water derived from the main river is the total volume of water that is stored on the floodplain. Problems with the vegetation correction of the SRTM data identified in Chapter 4 and 5 make it difficult at this stage to calculate accurate storage volumes

on the study area floodplain. However, an initial estimate can be made using a range of reported flood depths that will allow a first order comparison of volumes. Table 6-3 shows a summary of calculations used to derive estimated flood volumes for the thesis study area using information from two different studies. Bonnet *et al.* (2008) used bathymetry derived from SAR data and field measurements in order to model the storage on the Curuaí lakes floodplain. The range of water volumes for the 1997-2003 period modelled are shown in Table 6-3. Assuming this volume of water is spread over the whole floodplain area, this provides a floodplain, high water, maximum depth range of between 2.6 and 3.6 m. From these results, it can be seen that the water volume on the floodplain will vary considerably year to year.

For the connectivity test area in Chapter 4, the JERS May 1996 image (near high water) shows approximately 84.5% of the area is wet. Using the elevation-area curve derived from the SRTM data for the same connectivity test area (Figure 4-13(b)), this wet area equates to a flood water volume of 0.4 km^3. Assuming this flood water volume is spread over the whole connectivity test area, gives a mean depth of 5.2 m. Thus an estimate of the mean maximum floodplain water depth for the whole floodplain of the current thesis study area can reasonably assumed to be between 2.5 and 5 m at high water. Over a floodplain area of 10,390 km^2, in the thesis study area, this equates to a flood volume of between 26 and 52 km^3. Mean floodplain depths across the whole floodplain are used for comparison, rather than just wet floodplain area, to provide a first order volume range estimate that is independent of a particular event.

Table 6-4 shows the minimum, mean and maximum monthly water volumes, as well as annual total volumes for the runoff inputs to the study area (from the Beighley *et al.* (2009) data), broken down into main river and floodplain inputs. Values are the mean of the output from the hydrological model for the period 2001-2007. Monthly values are chosen to allow a similar order comparison of input water volumes with floodplain storage volumes.

Table 6-3 – Floodplain water volume calculation summary

Data Source	Curuaí lakes, (Bonnet *et al.*, 2008)	Curuaí lakes, (Bonnet *et al.*, 2008)	connectivity test area, Chapter 4	thesis study area, whole floodplain, Calculation	thesis study area, whole floodplain, Calculation,
Water level condition	High water range (1997-2003), low end	High water range (1997-2003), high end	Near high water 1996	Calculation range, low end	Calculation range, high end
Floodplain area (km^2)	2,430	2,430	84	10,390	10,390
% of area wet	69.2%	83.4%	84.5%	-	-
Water volume (km^3)	6.3	9.3	0.4	**26.0**	**52.0**
mean water depth across whole floodplain (m)	**2.6**	**3.8**	**5.2**	2.5	5.0

Table 6-4 – Water volumes for study area runoff inputs, mean values for 2001-07

Input	**Hydrological Model unit ID**	**Type**	**minimum monthly vol (km^3)**	**mean monthly volume (km^3)**	**maximum monthly volume (km^3)**	**total annual volume (km^3)**
Solimões	9339	main river inflow	175.99	227.87	307.06	2,734.39
Purus	9211	main river inflow	9.98	27.95	52.92	335.38
main river area	-	net (P-ET)	0.02	0.08	0.17	0.94
		total main river	185.99	255.89	360.16	3,070.72
Paraná Piorini	9325	west tributary inflow	0.37	1.51	2.96	18.15
Lago Manacapuru input	9123	north tributary inflow	0.22	0.88	1.83	10.62
floodplain	-	net (P-ET)	0.17	0.74	1.63	8.91
local terrace catchments	-	net (P-ET)	0.24	1.05	2.30	12.57
		total floodplain	1.00	4.19	8.72	50.25
		% of main river	0.5%	1.6%	2.4%	1.6%

Comparing the volumes in Table 6-4 with the estimated floodplain water volumes of 26 and 52 km^3 from Table 6-3, it can be seen that local runoff is not as minor as the comparison with main river flows might suggest. Mean monthly local input volumes of 4.2 km^3 with a maximum of 8.7 km^3 indicate that the local source could fill significant volumes of the floodplain in a few months especially if this preceded the arrival of the main river floodwater. In addition, the uneven distribution of these inputs over the FHUs, means that local sources will be very important to the overall floodplain hydrodynamics, as first demonstrated by Mertes *et al.* (1993, 1997).

Figure 6-2 shows a schematic of the floodplain inputs and flows between the different floodplain units. This schematic shows that local inputs are proportionally more important for some floodplain unit classes, and, how sediment deposits form the boundaries between the units, limiting connectivity between these areas to times of high water diffuse over-boundary flows.

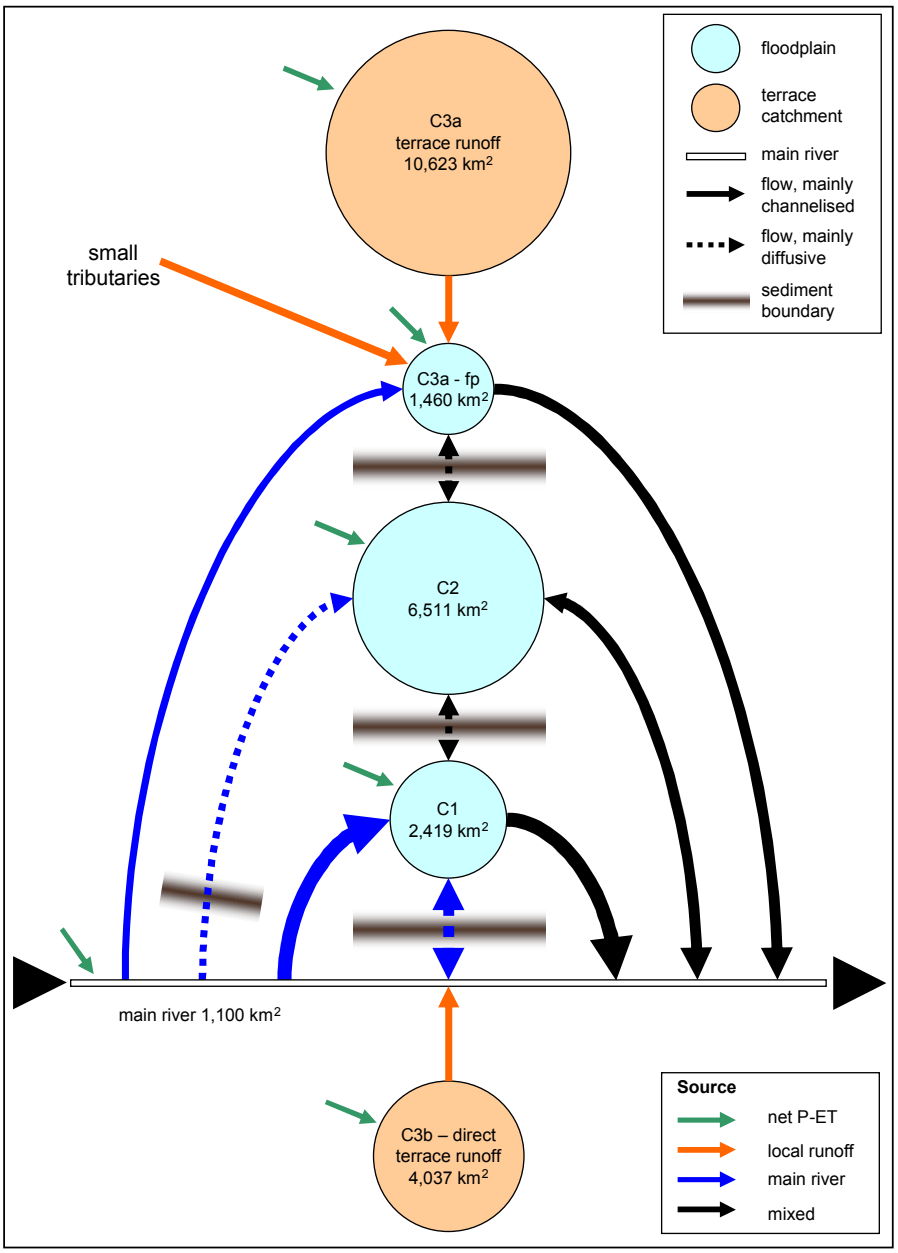

Figure 6-2 – Schematic of floodplain inputs and flows based on floodplain hydrologic unit classes. The three different classes of floodplain units are shown as circles with the area proportional to the area of different classes in the study area. The indirect FHU types are divided into a runoff catchment portion and floodplain portion for clarity. Arrow sizes are only indicative of relative flow sizes.

6.4 Flow timings

In Section 6.3, local runoff inputs were found to be important to the hydrodynamics on the floodplain and that if they precede the overbank flow input from the main river, they have sufficient volume to fill significant portions of the floodplain. In order to better understand the significance of the timings of these flows on the hydrodynamics of the floodplain, timing analysis was carried out on the same Beighley at al. (2009) hydrological model output data that was used for the flow analysis in Section 6.3.

Figure 6-3 shows the hydrographs of main flow inputs to the study area for the model run period of 2001-2008. The results of the timing analysis can be seen in Figure 6-4.

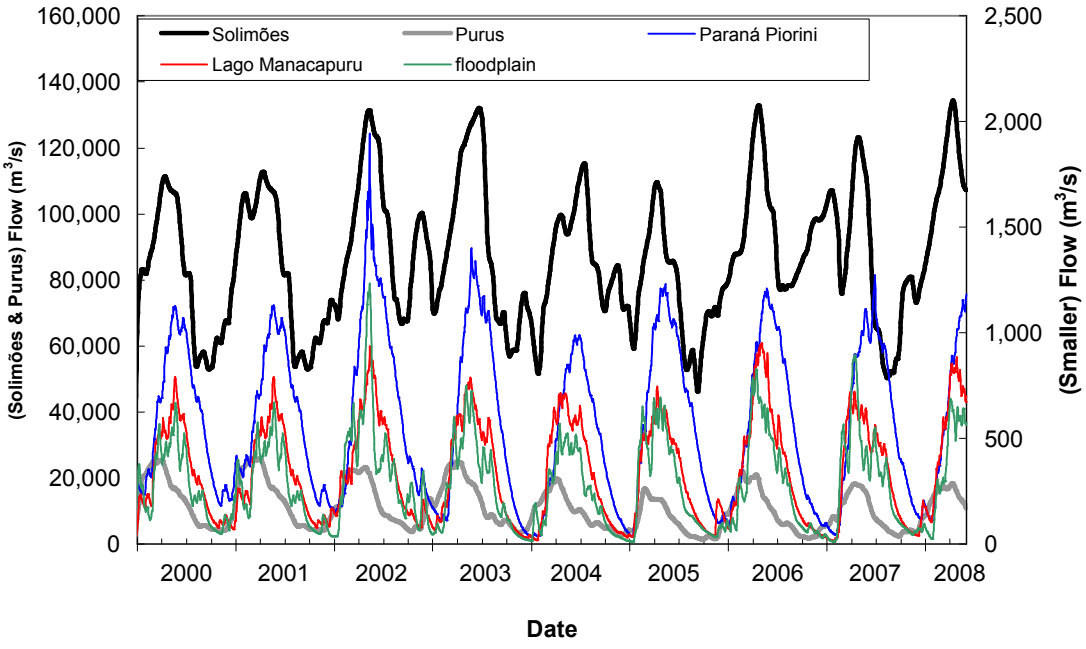

Figure 6-3 – Hydrographs for main flow inputs in study area. Note, the left y axis is for the larger Solimões and Purus flows and the right y axis is for all other, smaller, flows. For clarity, the runoff from terrace catchments is not shown as it is derived from the same net P-ET data as the floodplain input, and so add no additional timing information.

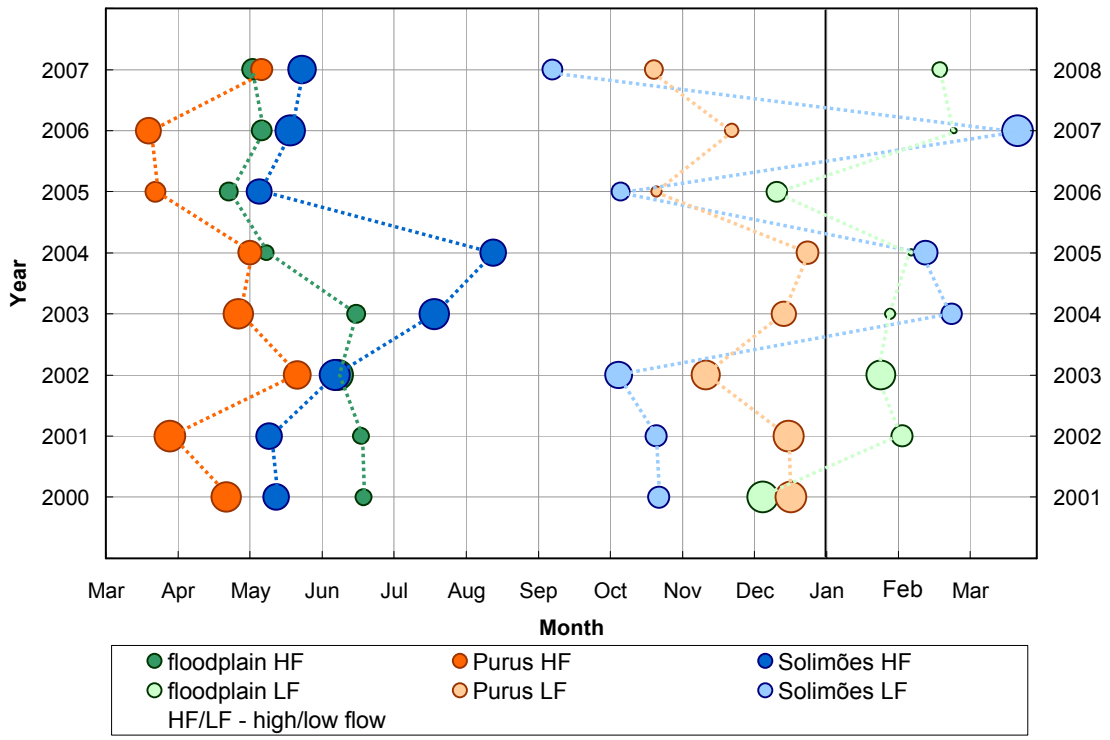

Figure 6-4 – Flow input maxima and minima timing (2000-2008). Circles indicate the times for which the maxima and minima annual inflows occur for each input source for the years 2000-2008. Circle size is relative to the size of the other values in each high or low point dataset, not between datasets.

From Figure 6-4 it can be seen that the peak of the Purus inflow always precedes that of the Solimões by between 0.5 and 3 months, with a mean of 1.5 months. The peak input for the local runoff, represented here by the floodplain inflow, generally precedes the Solimões peak and almost always comes after that of the Purus. The minimum inflows show an even wider variation in times and this will result in different patterns of floodplain drainage from year to year. There is also more variation in the actual low flow value from year to year, represented by circle size, than the high flow values, although this might be partly due to fact that the low flows are more sensitive to model parameters (Beighley *et al.*, 2009). There is a considerable variation in timing between the maxima and minima for the Solimões inflow, from 3.5 months in 2007-08 to over 10 months in 2006-07. The floodplain inflows also show a

varied gap of 6 to 10 months. The gap between the maxima and minima for the Purus inflows are less varied at between 5 and 7 months.

Even for this short dataset of eight complete flood wave cycles, there is considerable variation in the timings of the peak inflows, meaning that from year to year the pattern of flooding and drainage from the various sources will be different. Birkett *et al.* (2002) found similar inter-annual variability in peak timings using TOPEX/POSEIDON water-level measurements over a 7.5 year period (1993-2000). It should be emphasised here that these data show the maxima and minima timing for the inflows and not the water levels, which will be different due to storage on the floodplain. For example, if the next flood wave is beginning before the last wave has finished draining then the floodplain may already be partially filled from the previous year's flood water leading to higher starting water levels than a year which drains fully.

6.5 Flow drivers and pathways

The primary driver of flow on the floodplain is the water elevation difference between different locations (hydraulic head). Timings of flow inputs and also floodplain storage volumes, as discussed in Section 6.4, affect the hydraulic head and therefore flow magnitude and direction. Topographic features such as sediment deposits provide barriers to flow and floodplain channels provide preferential flow pathways, resulting in two main types of flow on the Amazon floodplain: channelised flows and diffusive overbank flows (Mertes *et al.*, 1996). By comparing the water elevation of the flood wave in the main channel to the elevations of the floodplain topographic features measured in the field, it is possible to identify when each type of flow is active in the flood cycle and it is also possible to gauge their relative importance. Using the field measurements described in Chapter 5, this is now possible for the thesis study area.

Figure 6-5 shows the mean water elevation of the Amazon flood wave at the Manaus gauging station, taken from the full record (1903 to 2009) with range indicated by ±2 standard deviations. Also plotted on the figure are the mean main river bank elevation and range which shows at what water elevations diffusive overbank flows occur. The mean and range for the floodplain channel bed elevations, for channels without any extra terrace runoff input, shows that when these channels are connected to the main river and channelised flow occurs. In Chapter 5, it was shown that the floodplain channels with significant terrace runoff input have deeper channels than floodplain channels that drain only direct rainfall and river water inputs. The mean elevation of the channels with the extra runoff input is also shown for reference and is around 3 m lower than the lowest recorded water levels in the main river. It should be noted here that the bank and channel bed elevations are measured over the whole study reach, but the water elevations shown are from the downstream end of the study area and so may vary along the reach by up to 1 m due to water surface slope.

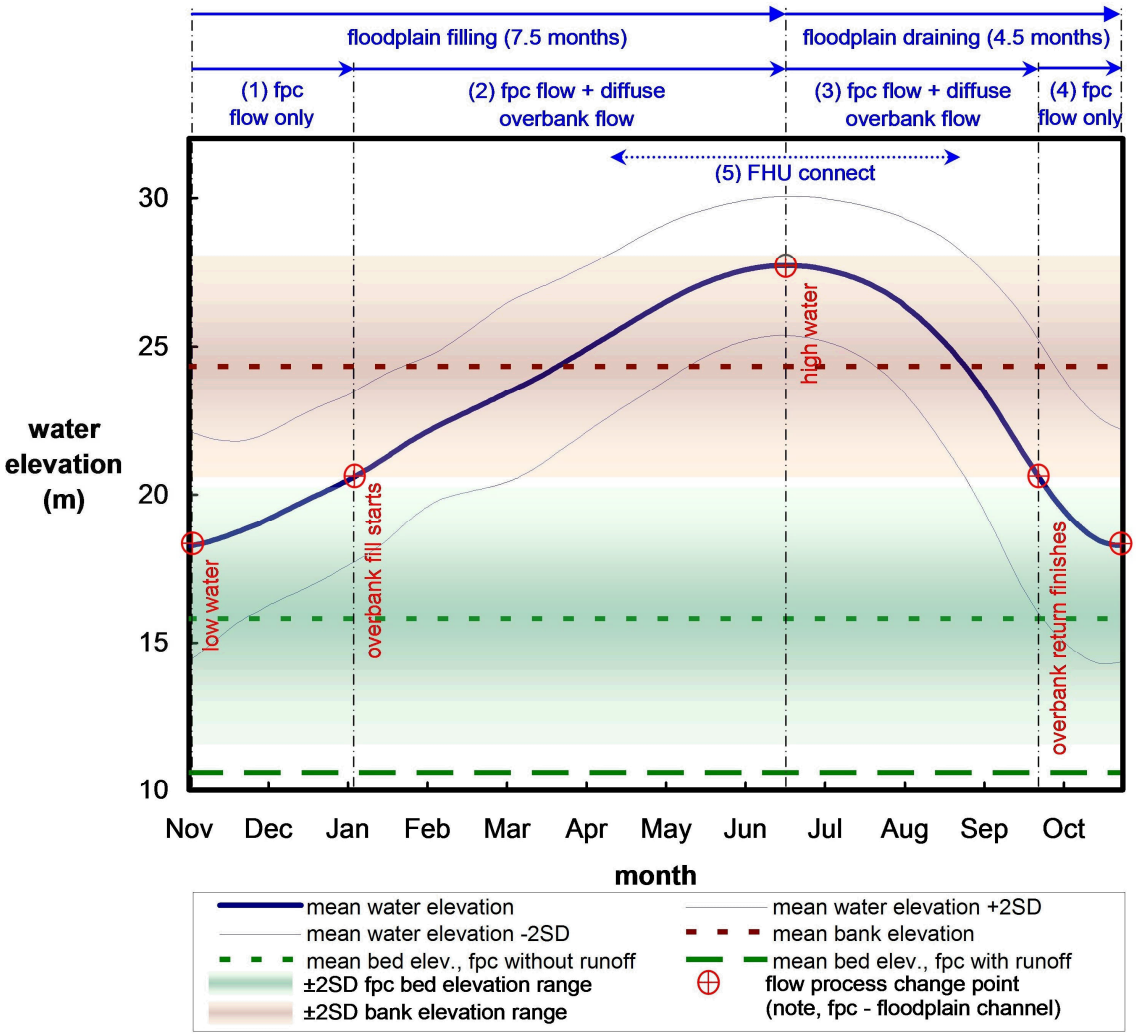

Figure 6-5 – Flood wave elevation relative to floodplain topographic features for the study area, showing floodplain filling and draining phases. Manaus mean elevation hydrograph (1903-2009) with ±2SD. Measured mean bank elevation with ±2SD and floodplain channel (fpc) bed elevation with ±2SD.

The key change points in the flow processes are marked on Figure 6-5 and these allow the division of the floodplain inundation and draining cycle into five phases characterised by the processes that are active during those phases. First the cycle can be divided into floodplain filling and draining phases by the peak water level which is about mid June. In general, it can be seen that the floodplain filling phase is around twice the length of the draining phase. Both the filling and draining phases can each be broken down into two further phases, one at lower water elevations where only

channelised flow occurs, and another longer phase where both channelised and overbank diffusive flow occurs. Given the separation of the floodplain channel networks by sediment boundaries (Chapter 4), a fifth phase which occurs at around the peak stages of the flood wave is proposed. This fifth phase occurs where sediment barriers between the floodplain hydrologic units are overtopped by diffusive flow. The onset of this phase is less clearly defined as it depends on a number of factors in addition to the higher water levels. Time of travel across the floodplain and the time required to fill floodplain storage as well as the fact that most FHUs will also be draining back to the river will all affect the timing of this fifth phase. Further analysis of the topographic characteristics of the FHUs may provide more detail about this phase for each FHU.

Mertes *et al.* (1995) also identified progressive floodplain inundation phases for the Amazon floodplain: deep floodplain channel filling, shallow floodplain channel filling and diffusive overbank flow. Here, more detailed quantification of when those phases occur is provided and in addition, it is demonstrated through field measurement of channel depths that the channelised flow occurs at much lower water levels than has previously been assumed. Finally, an overlapping fifth phase based on FHU diffusive flow connection has been identified.

It is important to note that Figure 6-5 represents a generalisation of the processes that occur on the floodplain and their timings. The timings and spatial patterns of these processes will vary from year to year and be modified by many factors including; backwater effects, sediment movement, annual/interannual cyclic variability and seepage. These processes are also likely to be spatially dynamic, occurring at different times in different parts of the floodplain.

6.6 Flow dynamics

In Sections 6.3 to 6.5, different elements of the floodplain hydrodynamic processes were considered, including sources, timings, drivers and pathways. In this section, all these elements are drawn together to outline how these floodplain dynamics apply to the floodplain hydrologic units identified in Chapter 4, summarised in Table 6-1. Rather than including the full complexity of the Amazon floodplain as shown in Figure 4-6, a simplified schematic of the river and floodplain and their flow dynamics is presented in Figure 6-6. This includes a single representation of all the separate FHUs from Chapter 4, together with floodplain channel networks. In addition, a cross-section through the schematic floodplain is provided to illustrate the relative elevations of the different FHUs and channel beds. This cross-section is derived from the vegetation-corrected SRTM data, field measured channel bed elevations and gauged water elevations at Manaus.

The study reach represents only one of the several types of floodplain reach in the Amazon with different genesis, form and thus hydrodynamic functioning (Section 1.3). This means the framework will probably need to be extended to cover other types of floodplain, but the same methods and tools used in this thesis will be applicable.

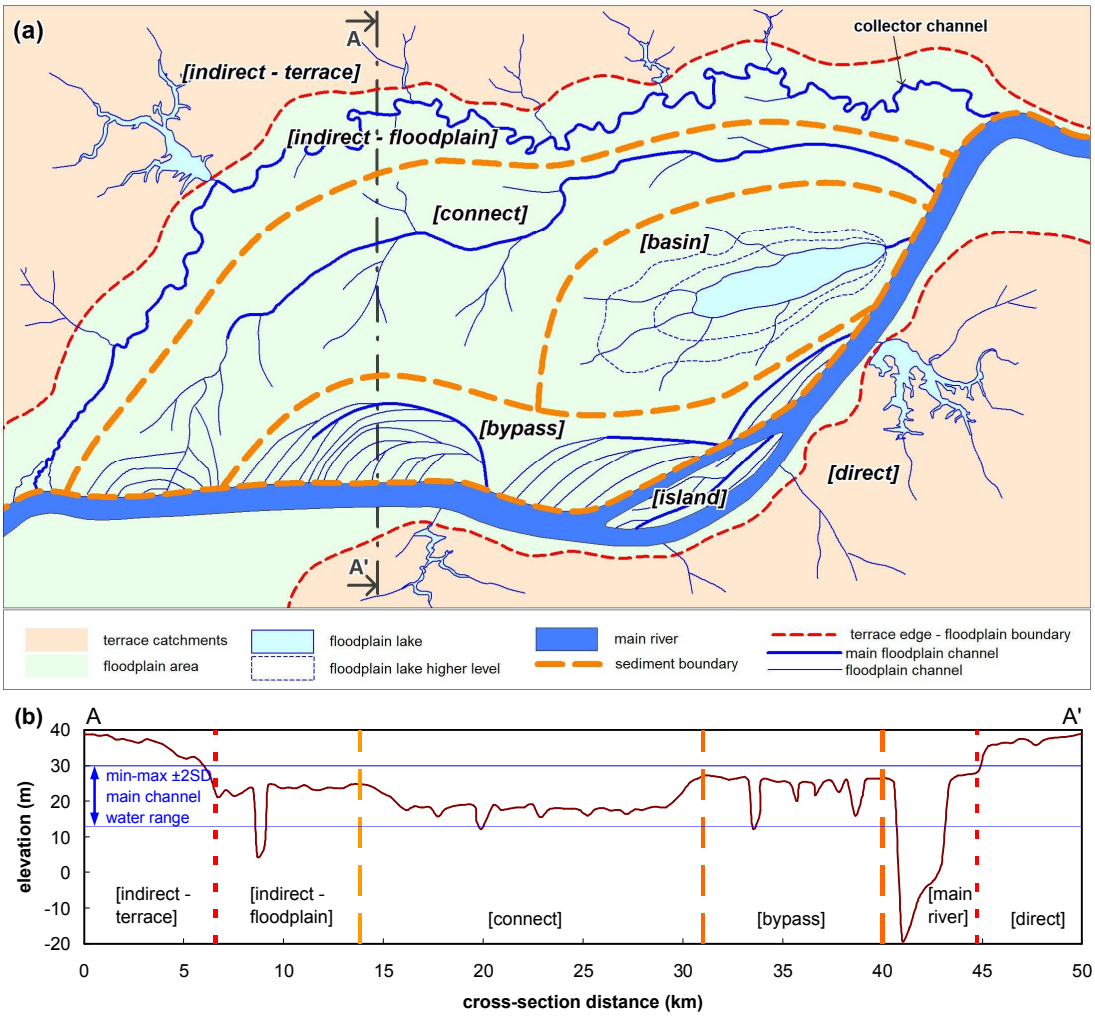

Figure 6-6 – (a) schematic of floodplain hydrologic units and floodplain channel networks, (b) floodplain cross-section A-A'

The five flood phases identified in Section 6.5 are illustrated using this schematic of the floodplain in Figure 6-7. A brief description of each phase is also provided.

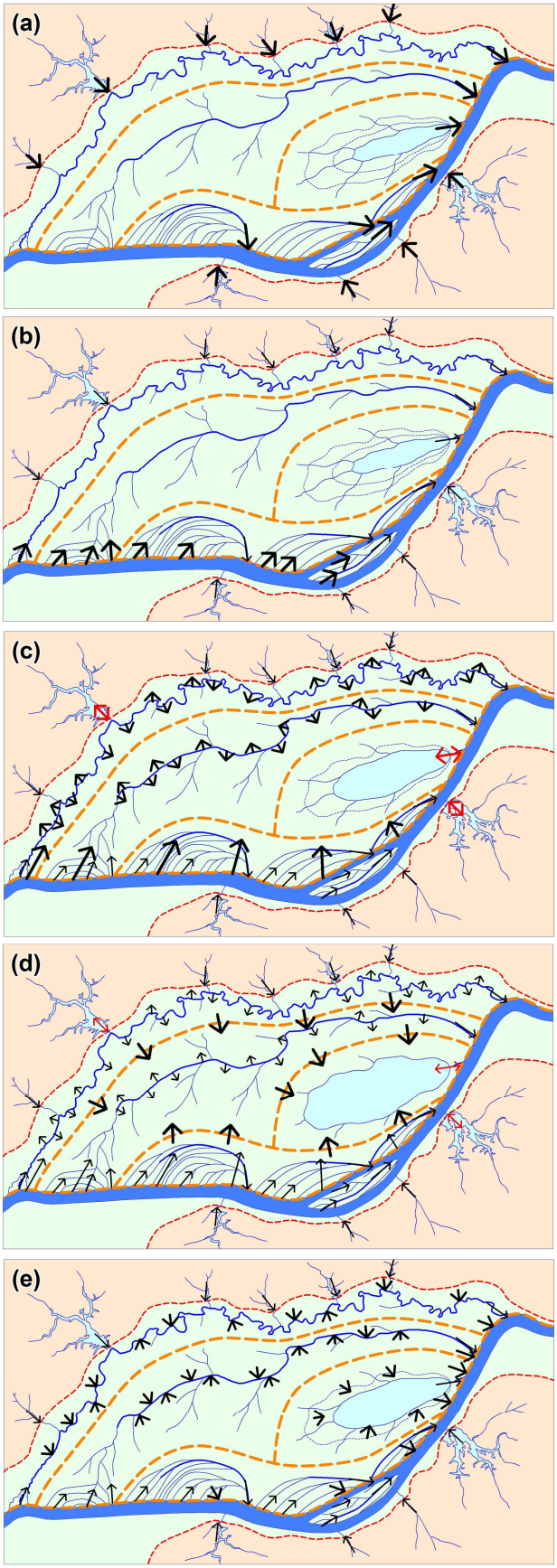

Low water, fpc only draining

Main river levels are low, and floodplain channels are still draining previous cycle's floodwater from the floodplain, as well as any additional direct rainfall input or runoff input from terrace catchments.

Filling fpc flow only

Main river levels begin to rise, allowing connection with the upstream ends of the floodplain channels (fpc). Flow into the floodplain interior starts through the bigger, deeper channels and the smaller channels progressively connect up as levels continue to rise. Meanwhile the floodplain may well continue to drain at the downstream end due to increasing rainfall on floodplain and terrace runoff input.

Filling fpc and overbank flow

Main river and main fpc levels are now higher than bank levels and diffusive overbank flow onto the floodplain begins. Sediment is deposited close to the banks by the overbank flows. Sediment is carried far into the floodplain by the deep main fpcs. Floodplain continues to drain at downstream end, but in places river levels may be high enough to reverse flow onto floodplain, especially into the low basin areas.

High water, FHU connect

Main river levels are now around their highest level in the cycle and fpc and diffuse overbank flow continues. Water levels on the floodplain are now high enough to overtop the majority of sediment barriers separating different areas of the floodplain (FHUs). This allows the FHUs to connect reducing the heterogeneity of water levels across the floodplain.

Draining, fpc and overbank draining

Main river levels are dropping and water levels on the floodplain have dropped below FHU sediment barriers. Flood water on the floodplain drains into main floodplain channels via overbank flows and smaller channels.

Figure 6-7 – schematic illustration of flood process phases. Arrow indicates flow direction. Arrow size is not indicative of flow size, but phase currently being illustrated.

6.7 Observed hydrodynamics and framework testing

The rational framework or conceptual model of the floodplain hydrodynamics outlined in Section 6.6 is more detailed than was previously available, and it is necessary to test the framework to see if it can be used to explain observed behaviour in the floodplain. The most interesting and perhaps the most challenging example of Amazon floodplain hydrodynamic observations to explain is that by Alsdorf *et al.* (2007a). Alsdorf *et al.* (2007a) used repeat-pass JERS SAR data to construct multi-temporal interferograms, essentially showing water level change over a 44 day period ($\delta h/\delta t$) at a 200 m spatial resolution. This was done for the mid-rising and high water stages of the Amazon flood wave during late 1995 to mid 1996. A figure from the paper is reproduced in Figure 6-8 to illustrate results for an area located in the centre of the thesis study area (location in Figure 6-9). Alsdorf *et al.* (2007a) interpret the observed patterns of changes to water elevation across the floodplain as follows: (i) timing and source of flooding is important to the pattern; (ii) the scroll bar topography and floodplain channels present a strong control during rising water; and (iii) at high water, patterns are simpler, implying less micro-topographic control at higher water levels. Despite these findings, there is still a need to explain in detail how the topographic features control the flood dynamics and what scale of feature is important in determining these dynamics.

Vegetation-corrected SRTM elevation data for the area of interest are shown in Figure 6-9, together with the floodplain channels and floodplain hydrologic units (FHU) derived in Chapter 4.

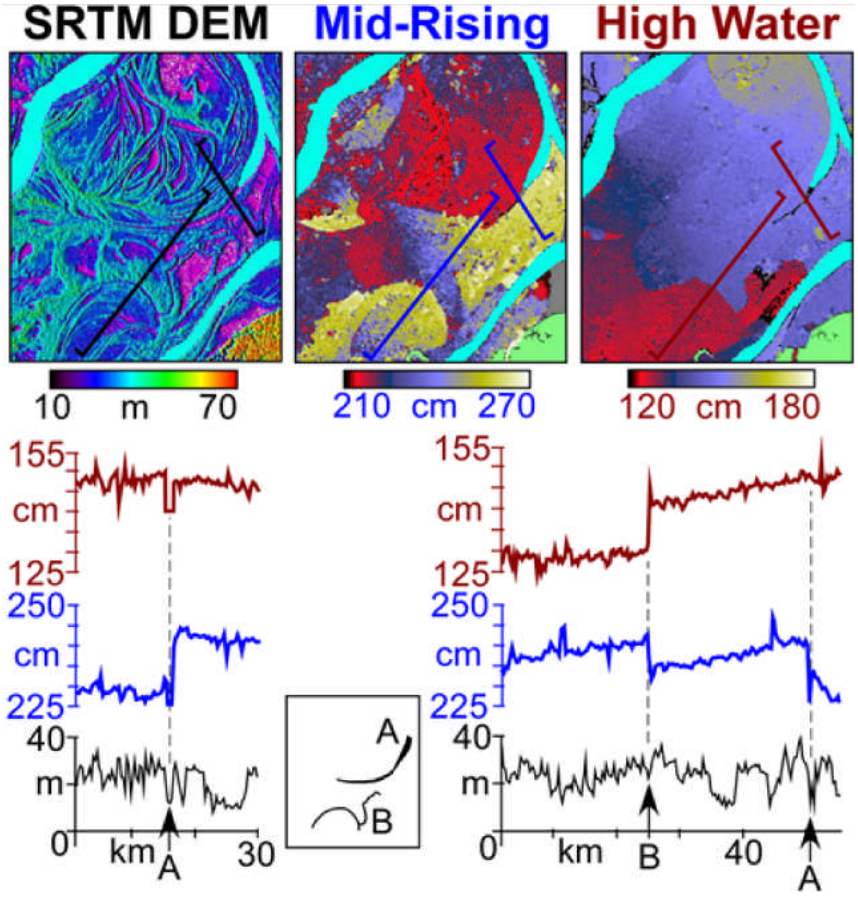

Figure 6-8 – Detail of interferometric SAR measurements and topography (Alsdorf *et al.*, 2007). The Shuttle Radar Topography Mission digital elevation model (SRTM DEM) delineates the complex Amazon floodplain geomorphology (see Figure 6-9 for location). Sinuous channels are numerous. Blue and red lines locate profiles of δh/δt at mid-rising and high water times, respectively, whereas black lines indicate floodplain topographic transects. Tic marks on plan view lines indicate view direction of profiles. Arrows A and B on plots note locations of two floodplain channels that coincide with sharp changes in δh/δt. Schematic in lower middle marks plan location of channels A and B.

From Chapter 4, channels A and B in Figure 6-8 are important floodplain drainage channels and are central to the drainage network for their FHU (SP). This is contrary to the assumption in Alsdorf *et al.* (2007a) that they are not especially prominent. Channels A and B were surveyed for their full length during field work described in Chapter 5, channels fpcs7a and fpcs7b respectively, and their minimum bed elevation is tied closely to the minimum flow elevations in the main river channels, 12 to 13 m elevation at this location. Channel A (fpcs7a) has a mean width of 100 m, widening rapidly as it reaches its outlet into the Purus to around 1 km across. Channel B (fpcs7b) has a mean width of 120 m.

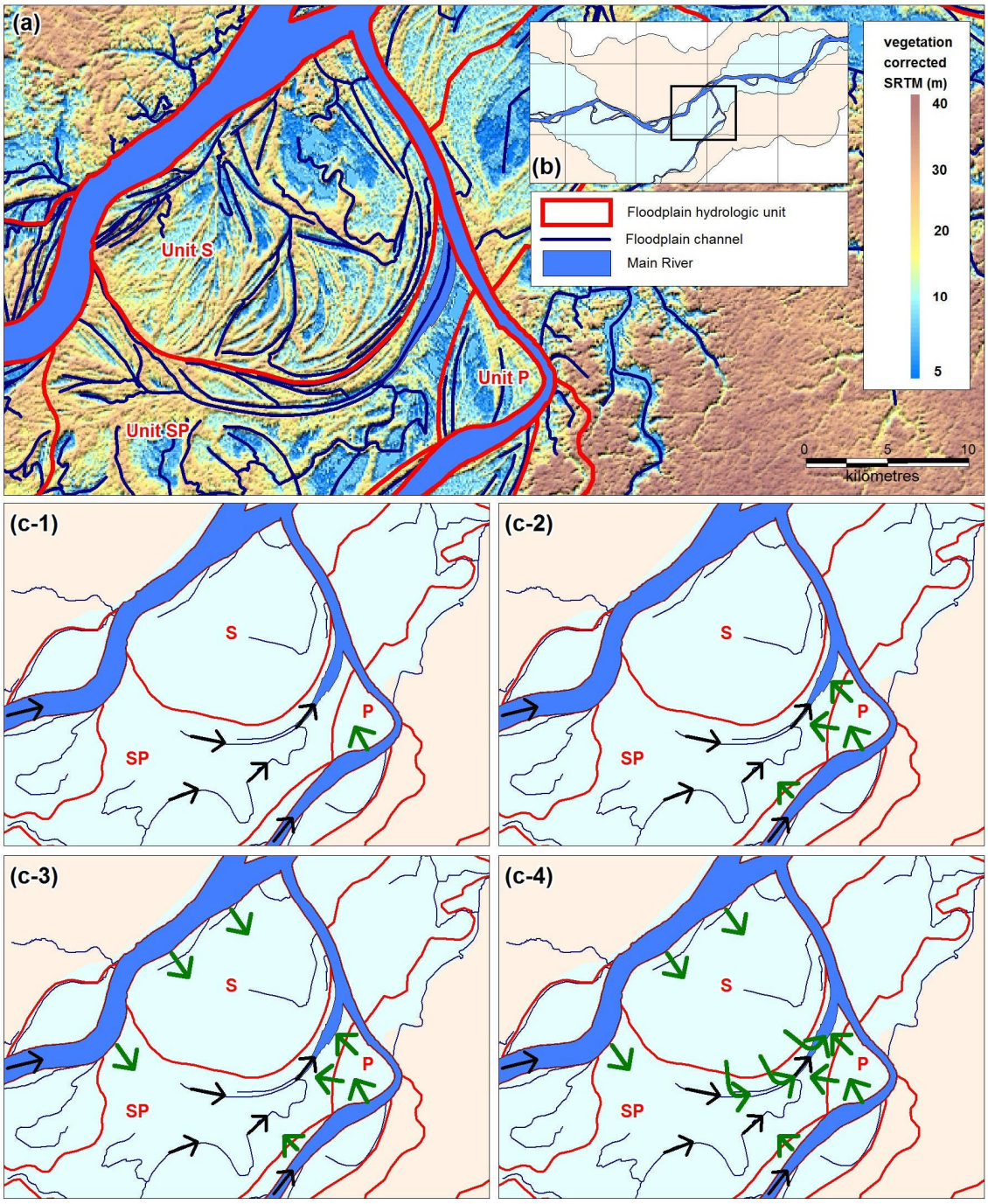

Figure 6-9 – (a) vegetation-corrected SRTM elevation, floodplain channels and floodplain hydrologic units, (b) location, (c-1) to (c-4) sequence of flooding. The three FHUs in the centre of the floodplain are labelled P, SP and S, with P being a bypass unit for the Purus and SP and S connect units between the Solimões and Purus. There is no local terrace runoff input into these units, so water sources will only come from direct rainfall or floodwater from the Solimões and Purus Rivers.

The Solimões River carries a heavy sediment load from the Andes and while the Purus is a white water river, its waters are considered to be relatively diluted and therefore distinctive to that of the Solimões and thus probably having chemical characteristics close to those of a lowland river (Boucheza *et al.*, 2010). This difference in sediment load will result in different sediment deposition from floodwaters onto the floodplain and this can be seen in the lower ground elevations in unit P and the Purus end of SP compared to unit S in Figure 6-9. North of channel A, the mean ground elevation is 18.1 m and south of the channel it is 15.7 m. This difference in ground elevation in itself may account for some of the sharp change in $\delta h/\delta t$ across channel A. If the levels across the area are more homogeneous at high water, then clearly water elevations will have to rise more in the area south of channel A due to lower starting levels in order to reach the same final level. The low sediment load in the Purus also results in lower bank levels which are overtopped earlier than the larger and higher levees created by the Solimões.

In Section 6.4, analysis of water source timings showed that the Purus peak precedes that of the Solimões by a mean of 1.5 months and the local rainfall input precedes slightly, or coincides with, the Solimões peak. From this, a sequence of the flooding events for the area of interest can be determined, illustrated in Figure 6-9 (c-1 to c-4) and described as follows, with typical timings from Section 6.4 and 6.5:

(1) The floodplain is draining what remains of the previous year's flood water and local rainfall inputs when the Purus begins to rise, overtopping its low banks into unit P, and begins to fill the low areas south of channel A. This would typically occur between November and December.

(2) As flooding continues to fill the low areas of the floodplain, floodplain water levels begin to rise in P sufficient to overtop the unit's low boundaries into unit SP. Main floodplain channels A and B continue to drain the floodplain and intercept flows from the Purus floodwater. Rainfall input to the floodplain is also

now reaching its peak providing additional water volume in the floodplain. This would typically occur between December and January.

(3) The Solimões now reaches levels where floodplain channel flows and diffuse overbank flows begin to fill the northern part of this area of the floodplain in units S and SP, depositing significant amounts of sediment in these areas. This would typically occur between January and March.

(4) Water levels in the northern parts of units S and SP are now high enough to overtop the sediment boundaries of these units. However, rising levels in the Solimões also increase the water levels in the Purus in this area due to backwater effects along the main Purus channel (Chapter 3), meaning that Purus levels now keep pace with those in the Solimões. This means that channels A and B now intercept floodwaters from both rivers on opposite banks, resulting in the Solimões flood water being confined to the north and Purus water to the south. This would typically occur between April and July.

The fact that the floodplain channels are preferential, low resistance, flow routes with existing hydraulic gradients means that they can function as interceptors of diffusive flow. This suggests that, until levels are high enough to swamp the floodplain channel's flow capacity, the channel will provide a strong control on changes to floodplain water levels from low to mid-rising waters, as evidenced by sharp boundaries in the mid-rising δh/δt across floodplain channels A and B in Figure 6-8. In addition to this intercept function, the differing bank heights will result in preferential flooding to one side of the channel when channel water levels are high enough. Thus the combination of: (1) a difference in flood timing between the Purus and Solimões; (2) continued drainage of the floodplain by floodplain channels while it is flooding; and (3) a difference in topographic levels in different floodplain units, results in the heterogeneity observed in the mid-rising δh/δt plot (12th February to 11th April 1993) in

Figure 6-8. Note that the dates for this δh/δt plot coincide closely with the flooding sequence stages 2 and 3 described above.

For the high water stage: (1) floodwater overtopping FHU boundaries; (2) flood inputs exceeding the floodplain channel drainage network capacity; and (3) equalising of Purus and Solimões main channel water levels due to backwater effects, result in more homogeneous flood levels across the floodplain, as shown in the high water δh/δt plot (15th April to 12th July 1996) in Figure 6-8. Note that the dates for the high water δh/δt plot coincide closely with flooding sequence stage 4 described above.

With the sediment rich waters of the Solimões confined by tectonic influence on channel location to the north part of this floodplain, sedimentation will be higher there, with correspondingly higher ground elevations than to the south as shown in the SRTM data. Unusual years such as 2002 (Section 6.4) where the Purus water levels rose late and the Solimões early, resulting in almost coincident timings, would result in a very different pattern to the norm for the area, with the Solimões waters reaching much further south into the floodplain, also carrying sediment further south. This difference in sedimentation may help explain why the Purus appears to have been pushed to the furthest southern edge of the floodplain before finally turning 90º to join the Solimões. If the sediment load differences between the floodwaters from the Purus and the Solimões are observable on Landsat images, then examination of images from the appropriate flood period may allow further testing of the sequence and processes proposed above.

In summary, the abrupt changes in δh/δt observed by Alsdorf *et al.* (2007a) are a result of a combination of topographic and hydraulic controls on the flood progression on the floodplain, and these controls can be explained by the proposed framework for the hydrodynamics of the floodplain. If the difficulties in representing the floodplain channel networks within the LISFLOOD-FP hydraulic model, used in Chapter 4, can be overcome, then in the future, it should be possible to model the floodplain

hydrodynamics sufficiently well enough to reproduce the ∂h/∂t patterns observed by Alsdorf *et al.* (2007a).

6.8 Conclusions

There is currently no detailed published framework or conceptual model of the Amazon floodplain hydrodynamics. Amazon research work is commonly undertaken within a macro level understanding of the spatial patterns (Mertes *et al.*, 1996) and flooding stages (Mertes *et al.*, 1995) within the floodplain, derived from sedimentology / geomorphology studies. More recent long term field work based studies are beginning to provide detailed quantification of many aspects of the floodplain hydrodynamic processes (Bonnet *et al.*, 2005; Bourgoin *et al.*, 2007; Bonnet *et al.*, 2008), but are by their nature somewhat site-specific and non-generic.

In this chapter, the existing macro level framework has been developed into a more detailed framework of the floodplain hydrodynamics using knowledge gleaned from a variety of published studies and in particular from the unique findings from the research presented in this thesis. This hydrodynamics framework synthesises existing knowledge with the understanding of the flood wave hydraulics gained from Chapter 3, the floodplain connectivity findings from Chapter 4 and the field survey measurements described in Chapter 5 into a coherent evidence-based model of the hydrologic components and processes of the floodplain that can be applied more generally across the Amazon floodplain.

The differing importance of the various water sources for different parts of the floodplain is shown by comparing flow inputs derived from a hydrological model of the Amazon (Beighley *et al.*, 2009) with floodplain volumes and the floodplain hydrologic units derived in Chapter 4. While local runoff inputs are found to be small by comparison (1.6% to 3%) with main stem flow, they often precede the flow input from the river and are of sufficient volume to fill significant portions of the floodplain, particularly for those floodplain hydrologic units that border the terrace at the edge of the floodplain.

Analysis of input timings shows that the Purus peak inflow always precedes that of the Solimões by between 0.5 and 3 months, with a mean of 1.5 months. The peak input for the local runoff generally precedes the Solimões peak and almost always comes after that of the Purus. Timing of inflow minima shows a wider variation than the inflow maxima and this will result in different patterns of floodplain drainage from year to year. There is a considerable variation in timing between the maxima and minima for the Solimões inflow, from 3.5 months in 2007-08 to over 10 months in 2006-07. The direct rainfall and hillslope runoff inputs to the floodplain show a varied timing gap between maxima and minima of 6 to 10 months. The gap between the maxima and minima for the Purus inflows is less varied at between 5 and 7 months. This year-to-year variation in inflow timings may result in spatial and temporal variations of the pattern of floodplain flooding and draining.

The primary driver of flow on the floodplain is the water elevation difference between different locations, also known as the hydraulic head. Timings of flow inputs, as well as floodplain storage volumes, affect the hydraulic head and therefore, flow magnitude and direction. Topographic features such as sediment deposits provide barriers to flow and floodplain channels provide preferential flow pathways, resulting in two main types of flow on the Amazon floodplain: channelised flows and diffusive overbank flows (Mertes *et al.*, 1996). By comparing the water elevation of the flood wave in the main channel to the elevations of the floodplain topographic features measured in the field, research presented here has identified when channelised and diffusive flows are active in the flood cycle and allowed an assessment of the relative importance of the flow type to the floodplain hydrodynamics. This allows the floodplain inundation and draining cycle to be divided into five phases, in terms of which processes are active during those phases. Primarily, the cycle can be divided into floodplain filling and draining phases by the peak water level, which is about mid June for this reach. In general, the floodplain filling phase is around twice the length of the draining phase. Both the filling and draining phases can each be broken down into two

further phases, one at lower water elevations where only channelised flow occurs, and another longer phase where channelised and overbank diffusive flow occurs. Given the separation of the floodplain channel networks by sediment boundaries identified in Chapter 4, a fifth overlapping phase was proposed which occurs around the peak stages of the flood wave. This fifth phase occurs where sediment barriers between the floodplain hydrologic units are overtopped by diffusive flow. The onset of this stage is less clearly defined as it depends on a number of factors in addition to the higher water levels. Time of travel across the floodplain and the time required to fill floodplain storage as well as the fact that most FHUs will also be draining back to the river will all affect the timing and duration of this fifth phase. Sediment transport in this phase is very low, so the intricate topography of the floodplain is not rapidly buried.

The complex spatial and temporal patterns of water level variation observed across the floodplain by Alsdorf *et al.* (2007a) provide our most complete view to-date of the complexity of the Amazon floodplain processes. The proposed Amazon hydrodynamic floodplain framework has been qualitatively validated against the Alsdorf *et al.* (2007a) data and used to explain the sharp variations in $\delta h/\delta t$ observed at specific locations on the floodplain. This application of the framework shows that in addition to providing general drainage for the floodplain, the floodplain channels also function as diffusive overbank flow interceptors, changing sediment distributions across the floodplain.

It will be important to modify and refine the framework with further research, but in its current form, it has already been shown to be of benefit when interpreting the complex spatial patterns on the Amazon floodplain and should therefore be useful to many areas of research currently being carried out in the Amazon floodplain. This Amazon framework uses many of the processes identified in more general frameworks of floodplain processes, such as that of Lewin and Hughes (1980), but goes on to demonstrate the relative importance of these processes for the Amazon floodplain. Furthermore this Amazon framework explains how and when these processes are

active within the hydrogeomorphic divisions (FHUs) of the floodplain identified in Chapter 4. The complexity of floodplain flow processes has been demonstrated for small rivers (Nicholas and Mitchell, 2003). The research presented here not only confirms that this complexity is also true for the larger scale Amazon floodplain, but also provides a general framework with which to understand and explain the complexity observed.

CHAPTER 7
Conclusions and recommendations

7.1 Summary

The overriding aim of the research presented in this thesis was to investigate the detailed hydrodynamic behaviour of the Amazon River and its floodplain, in order to better understand its components and processes and, therefore, provide a coherent, evidence based, conceptual framework to inform a broad range of future Amazon wetland research. To achieve this aim a synthesis of field work, gauging station data analysis, remote sensing data analysis and numerical modelling were used, together with a collation of specific hydraulic details gleaned from previous floodplain studies.

Individual elements of this research were presented in Chapters 3, 4 and 5. Chapter 3 covered investigations into the primary driver of the flood cycle, specifically the characterisation of the Amazon flood wave hydraulics and experiments into the importance of the main channel geometry for the hydraulics. Chapter 4 detailed a spatial analysis of the multitude of floodplain channels and their importance to the hydraulic connectivity across the floodplain. Chapter 5 presented the methodology and findings of original field work measuring the bathymetric properties of a large number and length of floodplain channels. Finally, Chapter 6 draws these elements of research into a conceptual framework of the hydrodynamic processes active in the floodplain.

7.2 Specific conclusions

7.2.1 Flood wave hydraulics

While some characteristics of the Amazon flood wave, such as the importance of backwater on water levels, have been highlighted in previous work, the work presented in Chapter 3 and published Trigg *et al.* (2009), is the first detailed and methodical assessment of the hydraulic characteristics of the Amazon flood wave.

These investigations showed that the Amazon flood wave is subcritical and diffusive in character. For the Solimões reach studied during the period of 1996/97, flood wave amplitude was 11.6 m, mean bathymetric bed slope was 5.0 cm/km, and mean gauged water surface slope was 2.8 cm/km. The flow in the main channel is deep and relatively slow moving, resulting in very low Froude numbers of the order of 0.05. Due to very shallow hydraulic gradients, backwater conditions control significant reach lengths in the central Amazon and these backwater conditions are present for low as well as high water states. The accurate prediction of water elevations using hydraulic models requires that these backwater effects are represented.

In order to provide a more appropriate diffusive representation of the Amazon flood wave and allow full use of large quantities of original bathymetric data collected for a previous kinematic channel Amazon hydraulic model (Wilson *et al.*, 2007), a 1D diffusive channel solver was implemented in the 1D/2D hydraulic model LISFLOOD-FP. Compared to the Wilson *et al.* (2007) model, the channel water levels in the new diffusive channel model showed a better match to observed data. Calibrated RMSE for the water elevations at the four gauging stations internal to the model are all less than 1m for low and high water results. Validation using water elevation altimetry data at one location on each river gives RMSEs under 1.5 m, and comparing the model to gauged slopes, gives a maximum RMSE of 0.62 cm/km. The addition of a diffusive solver to

LISFLOOD-FP is also enabling research work on other river systems (Durand *et al.*, in press).

The large quantity of original and up-to-date bathymetric information for the central Amazon River channel, collected for previous modelling by Wilson *et al.* (2007), were utilised in full to assess the importance of channel geometry on hydraulic behaviour of the flood wave. These data show the complexity of the river bed structure and provides an unprecedented first order data set for hydraulic analysis. For the Solimões reach, the channel width varies from 1,620 m to 5,624 m with a mean of 3,711 m and the minimum bed elevation varies from -26.45 m to 8.03 m with a mean of -8.44 m. At high water, channel depths range from 20 m to 52 m. For the Purus reach, the channel width varies from 600 m to 1,678 m with a mean of 1,114 m and the minimum bed elevation varies from -9.78 m to 9.48 m with a mean of 2.08 m. At high water, Purus channel depths range from 16 m to 35 m.

Experimentation with the physical process representation of the channel flow as well as bathymetric information content of the channel shows that, when compared to the amplitude of the Amazon flood wave, water levels are relatively insensitive to the bathymetric information content of the channel model. The error on predicted water elevation introduced by using a wide rectangular channel is in the order of 0.10 to 0.15 m and, by ignoring the acceleration and advection terms we introduce a further error in water elevation of the order of 0.02 to 0.03 m. The application of appropriate boundary conditions has also been demonstrated as essential in order to incorporate the backwater effects present along these reaches. These backwater effects are so important that even when reducing the complex bathymetry (which under free flow conditions would be hydraulically significant) to a linear bed slope with a single mean cross section in the model, we only introduce an error of the order of 0.5 m in the water elevation results. This insensitivity to channel geometry is likely due to the very low Froude numbers. Low Froude numbers show that inertia forces, which are sensitive to channel geometry, are low compared to gravitation forces, which are only sensitive to

the mean depth of flow. This implies that these results should translate to other large slow flowing deep rivers with low Froude numbers.

Despite excluding the floodplain from the models, comparison of results to the observed data shows a reasonably good fit. It is suggested therefore that the floodplain volume is relatively small compared to the volumes of the passing flows in the main channel and thus have relatively little effect on the geometry of the flood wave itself.

7.2.2 Floodplain connectivity

The analysis of floodplain channels and floodplain connectivity presented in this thesis represent the first dedicated study of the spatial variation and characteristics of the Amazon floodplain channels for a representative 30,000 km^2 portion of the central Amazon mainstem and demonstrate that these floodplain channels carry a significant portion of floodplain flow and are important to hydraulic connectivity of the floodplain.

The spatial analysis of Landsat TM images shows a total of 1,762 channels in the study area, ranging in width from 900 m down to the minimum resolvable width of around 20 m, with a mean width of 47 m. The floodplain channels ranged from 160 m to 67 km long, with a mean of 5.3 km and total length of 9,293 km. Comparing channel width with their frequency reveals a power law relationship, showing patterns of structure that are self-similar or fractal-like over many orders of magnitude (Brown *et al.*, 2002). This relationship allows estimation of the number of floodplain channels below the Landsat TM image resolution of 15 m, and reveals that these smaller channels account for an extra 2,400 channels (total length 6,719 km), more than the sum of all the other channels.

Despite the inherent complexity of the floodplain network, grouping the floodplain channels by their connection network shows that there are distinct and mostly separate networks of channels in the floodplain and that these networks can in

turn be grouped by their characteristics. Delineation of the "catchment" areas represented by each network shows that these areas can be grouped into six types based on differing hydrological inputs as well as their network characteristics. These are here termed "*floodplain hydrologic units*" (FHU) as they represent distinct separate areas of floodplain that appear to function as single units from a hydrological perspective. It is likely that under high water level conditions these units will connect through diffuse overland flow but the hydrological inputs, hydraulic gradients and sediment availability in each area ensures relative isolation of surface flows for considerable portions of the flood cycle.

The six types of unit indentified can be grouped into three classes of FHU, each with two types of unit. The first class are those units found closest to the river and are completely dominated by river floodwater and sediment deposition and have very little in the way of local hydrology runoff input other than direct rainfall. The second class covers central areas of floodplain with low topography that are generally isolated to some extent from river flow by the first class of unit, but also receive little input from terrace runoff bordering the floodplain. The final class of unit encompasses direct and indirect runoff inputs from the terrace hillslopes. This is the first time that a method of breaking down the complex heterogeneity of the Amazon floodplain into functional units has been proposed.

Hydraulic connectivity analysis of vegetation-corrected SRTM, with and without explicitly included floodplain channels, for a sample area of the floodplain shows that inclusion of the channels significantly changes the hydraulic connectivity of the DEM, allowing connections at much lower elevations with them than without them. The channels provide all the flow area in the DEM up to the point where overbank diffusive flow occurs and continue to provide a flow area of 17 to 28% of the total, even at high water. This is likely to be an underestimate, as the connectivity analysis did not include the effects of hydraulic friction or the depths of the channels below the water surface.

Sudden changes in connectivity at different elevations also point to threshold effects within the floodplain.

This missing floodplain channel connectivity in the SRTM data explains some of the floodplain filling and draining problems encountered with recent large scale hydraulic modelling of the Amazon channel and floodplain (Wilson *et al.*, 2007). These filling and drainage issues are even more evident when including a diffusive main river channel which is demonstrated in Chapter 3 as necessary in providing realistic main channel water elevations. Experiments to explicitly include the floodplain channels in the 270 m model DEM by "burning in" all the channels reintroduced some of this missing connectivity and allowed improved filling and draining of the 2D floodplain.

7.2.3 Floodplain channel survey

The field work undertaken for this research represents the first dedicated field survey of a representative sample of the Amazon floodplain channels, and the results provide information regarding the key morphological characteristics of the floodplain channels. As well as providing ground truthing for remote sensing analysis of channel width, bank elevations and vegetation corrections, the data provides important information below the water surface which is not generally available through satellite remote sensing. Data were collected from three main types of channel: (i) those carrying only flow from the annual flood wave; (ii) channels that also carried local catchment runoff; and (iii) island channels which were strongly connected with the main channel at all flow levels. The use of what are now quite advanced and relatively low cost fish finder sonars has been shown to be a valid tool for the purpose of collecting bathymetric data in the Amazon with a repeatability error of under 0.5 m.

The mean depth of the channels only carrying river flood water was strongly correlated with the flood wave's mean annual range of 11.4 m. These channels connect the main river to the floodplain throughout the year from low to high water and

provide a direct connection which feeds flood water onto the floodplain as the water level rises as well as providing drainage of the floodplain as main river water levels drop. This strong hydraulic connection to the Amazon flood wave results in channels which are no deeper than main channel low water levels and which have characteristically shallow bed cross-sections compared to a typical river.

For channels which not only carried river flood water but also have an element of local runoff provided by small catchments alongside the main river, the mean depth (15.9 m) is substantially deeper than for the floodplain channels only carrying river flood water. Although these channels also carry significant flood flow during the flooding phase of the river, they also carry flow from their own catchments throughout the year. This additional flow provides the hydraulic conditions necessary to incise deeper channels into the floodplain. Cross-sections of these channels typically show more variation across the bed of the channel.

Most of the main river island channels showed a strong hydraulic connection with the main channel and although none of them had any significant additional catchment area, mean depths were typically much greater than floodplain channels with additional runoff. This close connection means they are exposed to the dynamic regime of main channel flows with greater scouring and deposition resulting in more varied bed profiles as well as deeper mean depths (17.7 m).

Field survey measurement of channel widths and comparison of these with those estimated from Landsat ETM+ imagery resulted in an RMSE of 21.4 m. This is close to the pansharpened spatial resolution of 15 m for the Landsat images used. Carrying out field measurements of channel width also highlighted the uncertainties introduced by overhanging vegetation as well as the effect of different water levels on width.

Estimating the bank elevations from the water elevations in the field and grouping these by bank vegetation type provides an alternative method of deriving bare earth elevations, for spot locations, to that used by Wilson et al (2007). The results

show that the differences between the elevations from the two methods are strongly correlated with vegetation type. Whilst not enough data were collected across all the vegetation types to provide a definitive alternative to the original vegetation correction method, it certainly indicates substantial errors that would be worth investigating via a sensitivity analysis using the hydraulic model.

The floodplain channel survey also provided an important opportunity to observe flood mechanisms first hand across large areas of floodplain. Both floodplain flow mechanisms, diffusive overbank flow and channel flow, were observed and this confirmed that the flow carried by the floodplain channels is considerable, with evidence of strong currents in the channels and sediment laden river water being carried hundreds of kilometres into the floodplain. Flood water breaches through the sediment levees along the banks of the main channel as well as floodplain channels were also observed at numerous locations, allowing flow down to the relatively low areas behind, with velocities sufficient to generate turbulent flow.

The sediment rich flood water from the main river has a distinct brown colour compared with black water sourced from local runoff. While travelling through the floodplain, this meant that the progression of the flooding from the main river was clear. During the survey, many of the channels showed brown water in the upstream reach of the channel and black water in the downstream half. There were a number of locations where black water was being flushed into the brown water channel from the banks, indicating that there was also overbank flow coming across the floodplain from other directions.

There also appeared to be a correlation between distribution of macrophytes (floating vegetation) and the progress of the sediment rich Solimões flood water, particularly noticeable while travelling through the floodplain channels. Passage through the upstream reaches of floodplain channels filled with Solimões river water were commonly blocked by vigorously growing macrophytes, locally called *“capim”* While there was some evidence of the vegetation along the banks in black water areas,

this was sparse and never blocked the channel. The supposition is that as the brown water passes down the floodplain, these macrophytes begin to grow rapidly from bank locations and eventually block the channel. Flow still continues underneath these blockages, but they are significant enough that they must affect the hydraulics, perhaps forcing more water onto the floodplain from these channels due to increased flow resistance and resulting in higher water levels.

These findings from this dedicated survey provide new insights into how hydraulic conditions may be controlling the characteristics of these floodplain channels. These findings have important implications in terms of quantification of the hydraulic connectivity on the floodplain (Chapter 4), which in turn has implications for the understanding of the floodplain hydrodynamics (Chapter 6). These floodplain channel findings are also important for wider environmental studies of the floodplain. Environmental gradients, such as water depths and nutrient availability, which are brought about by the flood wave, are vitally important for most of the ecology that is adapted to life in the floodplain (Petry *et al.*, 2003). In Chapter 3, it was determined that the floodplain channels are an important component in shaping these environmental gradients, so an understanding of the characteristics of these channels and the source of the water in the channels will aid in a wider understanding of environmental gradients within the floodplain.

7.2.4 Floodplain hydrodynamics

The conceptual framework proposed in this thesis provides the first detailed, coherent, evidence based model of the hydrologic components and hydrodynamic processes on the floodplain that can be applied generally across the whole Amazon floodplain. The framework builds on an existing coarse macro level understanding of the floodplain hydrodynamics gleaned from a variety of published studies, but adds

significant new data and understanding from a synthesis of the results of the research carried out for this thesis.

The differing importance of the various water sources for different parts of the floodplain was shown by comparing flow inputs derived from a hydrological model of the Amazon with floodplain volumes and the floodplain hydrologic units derived in Chapter 4. While local hydrology inputs are found to be small by comparison (1.6% to 3%) with main stem flow, they often precede the flow input from the river and are of sufficient volume to fill sizeable portions of the floodplain, particularly for those floodplain hydrologic units that border the terrace at the edge of the floodplain.

Analysis of input timings shows that the Purus peak inflow always precedes that of the Solimões by between 0.5 and 3 months, with a mean of 1.5 months. The peak input for the local hydrology generally precedes the Solimões peak and almost always comes after that of the Purus. Timing of inflow minima shows a wider variation than the inflow maxima and this will result in different patterns of floodplain drainage from year to year. There is a considerable variation in timing between the maxima and minima for the Solimões inflow, from 3.5 months in 2007-08 to over 10 months in 2006-07. The direct rainfall and hillslope runoff inputs to the floodplain show a varied timing gap between maxima and minima of 6 to 10 months. The gap between the maxima and minima for the Purus inflows is less varied at between 5 and 7 months. This year-to-year variation in inflow timings may result in spatial and temporal variations of the pattern of floodplain flooding and draining.

Comparing the water elevation of the flood wave in the main channel to the elevations of the floodplain topographic features measured in the field, the flood cycle can be divided into five inundation and drainage phases according to which flow mechanisms are active, floodplain channel flow, diffuse overbank flows and diffuse inter-floodplain hydrologic unit flow. Primarily, the cycle can be divided into floodplain filling and draining phases by the peak water level, which occurs around mid June. In general, the floodplain filling phase is around twice the length of the draining phase.

Both the filling and draining phases can each be broken down into two further phases, one at lower water elevations where only channelised flow occurs, and another longer phase where channelised and overbank diffusive flow occurs. Due to the separation of the floodplain channel networks by sediment boundaries identified in Chapter 4, a fifth overlapping phase is proposed which occurs around the peak stages of the flood wave. This fifth phase occurs where sediment barriers between the floodplain hydrologic units are overtopped by diffuse flow. The onset of this stage is less clearly defined as it depends on a number of factors, in addition to the higher water levels. Time of travel across the floodplain and the time required to fill floodplain storage as well as the fact that most floodplain hydrologic units will also be draining back to the river will all affect the timing of this fifth phase.

The complex spatial and temporal patterns of water level variation observed across the floodplain by Alsdorf *et al.* (2007) provide our most complete view to-date of the complexity of the Amazon floodplain processes. The proposed Amazon hydrodynamic floodplain framework has been qualitatively validated against the Alsdorf *et al.* (2007) data and used to explain the sharp variations in $\delta h/\delta t$ observed at specific locations on the floodplain. This application of the framework shows that in addition to providing general drainage for the floodplain, the floodplain channels also function as diffusive overbank flow interceptors, changing sediment distributions across the floodplain.

7.3 Limitations of the current research

7.3.1 Data resolution and scale

In recent years, the availability of increasingly detailed remote sensing datasets that cover the Amazon floodplain areas has improved greatly, and, importantly for this thesis, these datasets can be used in hydrological and hydraulic analyses. This has made what is generally a vast and difficult to access study area, relatively data rich. Most notable of these datasets is the SRTM data which provides elevation data with a spatial resolution of 90 m across the entire Amazon Basin in one consistent dataset, and is now used for many studies of the Amazon floodplain. However, comparison of the floodplain channel networks derived from Landsat ETM+ data with the vegetation-corrected SRTM data of the floodplain shows that most of these floodplain channels are poorly represented in the 90 m SRTM DEM, with 95.7% of the channels being less than 90 m in width. Given that these channels have been shown in this thesis to have an important role in the floodplain hydrodynamics, this lack of channel representation has important implications for any research using SRTM data to study or represent the floodplain. This is particularly true of the 2D hydraulic modelling of the floodplain carried out for this thesis.

Even the Landsat TM, pansharpened mosaic's theoretical spatial resolution of 15 m, used for the digitisation of the floodplain channels, does not allow full identification of the smallest floodplain channels below 20 m. Extrapolation of the floodplain characteristics in Chapter 4 implies that these smaller channels will be more numerous than all the other channels added together. Thus these data resolution limits prevent a complete assessment of the floodplain channels.

The choice of the study area for the research presented in this thesis was focused on covering a large enough portion of the Amazon floodplain to be representative of the whole while remaining manageable. As described in Chapter 2,

the location of the study area means that it should include most of the features and processes expected from the entire floodplain. However the study area is still a subset of the whole and given the new findings from this research regarding the floodplain hydrologic units, there may be further types of units driven by different processes or combinations of processes in other areas of the Amazon floodplain. This also applies to the floodplain channels and their derived and measured characteristics, where a wider application of the techniques used here may show other patterns and behaviour that will provide a more complete framework of the Amazon floodplain hydrodynamics.

7.3.2 Vegetation and elevation datums

Difficulties with overhanging vegetation were encountered while measuring floodplain channel characteristics, both with the remote sensing data analyses and direct field measurement. These difficulties add to the uncertainty in the width measurements with a more pronounced effect on the smaller channels. In addition, partial canopy penetration by the SRTM instrument leads to difficulties in correcting the DEM to allow for vegetation. Comparison of LISFLOOD-FP 1D/2D hydraulic model results, based on the corrected SRTM DEM, with gauged data and expected JERS flood extents in Chapter 4 show that there are still considerable uncertainties associated with the vegetation correction. Issues with the vegetation correction were further highlighted with the bank level comparisons carried out in the field survey. The vegetation correction uncertainties hamper a more detailed assessment of the characteristics of the floodplain hydrologic units as well as the 2D element of the floodplain hydraulic modelling.

One of the difficulties of using a wide variety of elevation datasets is in ensuring a common datum applies to all the datasets. This is exacerbated in the Amazon due to its scale meaning that the Earth's geoid cannot be neglected. While the gauging station datums have been tied to a common reference network (Kosuth *et al.*, 2006) which, in

theory, is compatible with the SRTM and altimetry datums, this has not been tested here and thus remains an area of uncertainty.

7.3.3 Hydraulic model limitations

The work in Chapter 3 demonstrates that it is sufficient to use 1D diffusive hydraulic modelling and basic bathymetric data to simulate the key characteristics of the Amazon flood wave within the main channel. However the results of the modelling provide no direct information regarding the complex dynamics between the channel and floodplain. Indeed, the analysis of interferometric SAR data by Alsdorf *et al.*, (2007a) clearly demonstrates that the floodplain water levels cannot be assumed to be the same as channel water levels, highlighting the need for the addition of a detailed 2D floodplain element to the model in order to simulate these floodplain dynamics.

Attempts to include a detailed 2D element to the hydraulic model by Wilson *et al.* (2007), and in Chapter 4 of this thesis, show significant problems with representing the floodplain hydrodynamics given limitations of the current DEM data and computational limits preventing a fully dynamic model run by constraining the timestep. These problems prevent a realistic filling and draining of the floodplain and limit the usefulness of the model results. Given the potential application of the model results in a host of biogeochemical research studies, these issues will need to be addressed.

The floodplain hydrodynamics framework presented in this thesis also highlights the importance of the local runoff and rainfall input to the flooding sequence of the floodplain. Currently these local hydrology inputs are absent from the hydraulic model. Significant variation from year to year in source timings and flows mean that the current two year flood cycle (1995-1997) time period modelled is insufficient to draw more general longer term conclusions.

7.4 Directions for future research

Based on the work presented here, future research should focus on:

1. **Further floodplain channel networks and hydrologic units characterisation**

   The study of the floodplain channels presented in this thesis highlights their importance to the floodplain hydrodynamics. The characterisation methods used in this thesis could be extended to cover a wider expanse of the whole Amazon floodplain, perhaps using automated methods for identifying the floodplain channel widths from remote sensing data. In addition, it will be important to extend the field work already carried out to a wider range of floodplain channel types and over a wider range of flow conditions.

2. **Extension of the floodplain hydrodynamics framework**

   While the framework outlined in this thesis provides an important advance on the current knowledge regarding the Amazon floodplain hydrodynamics, it represents the beginnings of what could be a more comprehensive conceptual understanding. Some of the concepts are tentative and will need to be tested in more detail and more thoroughly with other datasets and methods. Expansion of the study area may also provide additional important understanding, as well as the enhancements which may be gained from the input of other scientists with their own data, experience and understanding. The potential for using the framework to build process based hydraulic models of the floodplain could also be explored.

3. **Hydraulic model improvements**

   The potential of using hydraulic modelling as a tool to study the hydrodynamics of the floodplain, as well as to provide water level, extent and duration results for input to other studies is so important that it should be an area of concerted

research effort. It is important that the model represents the floodplain channels well enough to simulate the dynamics, and this should be a main focus as well as improvements to the vegetation correction of the SRTM DEM using published vegetation heights (Worbes *et al.*, 1992, Wittmann *et al.*, 2004). The potential of using the new ASTER 30 m DEM should also be explored (Hayakawa *et al.*, 2008). Improvements to the model code speed will allow an adaptive timestep to be used that will result in a better simulation of the hydrodynamics as well as allow the simulation of a larger spatial and temporal model domain. Additional remotely sensed water level data for the floodplain should be identified to validate the simulations of the model, as this validation will be an important part of ensuring the model simulates these complex hydrodynamics correctly.

7.5 Research contribution to the scientific community

The research presented in this thesis represents several advances in the understanding of the Amazon River and floodplain hydrodynamics and has involved substantial original work across a broad range of disciplines, including field measurement, numerical modelling of hydraulics and connectivity, GIS and remote sensing analysis and characterisation techniques. The findings and conclusions have important implications for a wide range of scientific studies, some examples of which are outlined below.

1. Amazon flood wave hydraulics

It has been demonstrated that for any modelling or analysis involving the hydraulics of the Amazon flood wave it is important to use the appropriate methods to allow for the diffusive properties of the flood wave and allow representation of the backwater effects. The relative insensitivity of main channel water levels to the geometry of the main channel means that for studies of the central Amazon channel such as virtual missions for the proposed SWOT satellite mission, even relatively crude assumptions regarding the bathymetry will be valid as long as the mean cross sectional area can be reasonably well approximated. Remote measurement of water elevations and hence a derived slope and discharge will also implicitly take into account backwater effects through the water surface slope. These conclusions may well be applicable to other large rivers, where similar hydraulic conditions prevail, specifically the shallow sloped lower reaches.

2. Floodplain hydrologic units

It has been demonstrated that the floodplain can be divided into functional hydrologic units of differing types, essentially a subset of the more general hydrogeomorphic land units. Each type of unit can receive water from different

source at different times and therefore end up with very different characteristics. The importance of water source to many biogeochemical processes has been highlighted already, so the identification of these functional units, as well as the methodology used will provide many other studies with the tools to dissect the complex floodplain into units with known water source contributions.

3. Floodplain channels

The measurement and characterisation of the floodplain channels, as well as the numerical connectivity experiments carried out, demonstrate that these floodplain channels could be playing a much more significant role in the Amazon floodplain hydrodynamics then previously acknowledged, and any studies of the Amazon floodplain for which these dynamics are important will need to allow for the role of floodplain channels.

4. Floodplain hydrodynamics framework

The floodplain hydrodynamics framework proposed represents an extension to the macro level of understanding already available in the scientific literature. The extended framework has the potential to allow a better representation of the floodplain processes in hydrological models of the Amazon as well as in Global Climate Models that include a routing component. At the other end of the scientific study scale, the framework also has the potential to enable a more systematic approach to detailed field studies, allowing researchers to better understand the hydrodynamic context of their particular study site/s. Thus, the framework provides an important link between the macro level and detailed level study scale.

References

Achard, F, Eva, HD, Stibig, HJ, Mayaux, P, Gallego, J, Richards, T & Malingreau, JP (2002), 'Determination of deforestation rates of the world's humid tropical forests', *Science*, vol. 297, no. 5583, pp. 999-1002.

Alsdorf, D, Bates, P, Melack, J, Wilson, M & Dunne, T (2007a), 'Spatial and temporal complexity of the Amazon flood measured from space', *Geophysical Research Letters*, vol. 34, no. 8, p. 5.

Alsdorf, D, Birkett, C, Dunne, T, Melack, J & Hess, L (2001a), 'Water level changes in a large Amazon lake measured with spaceborne radar interferometry and altimetry', *Geophysical Research Letters*, vol. 28, no. 14, pp. 2671-4.

Alsdorf, D, Dunne, T, Melack, J, Smith, L & Hess, L (2005), 'Diffusion modeling of recessional flow on central Amazonian floodplains', *Geophysical Research Letters*, vol. 32, no. 21, p. 4.

Alsdorf, DE (2003), 'Water storage of the central Amazon floodplain measured with GIS and remote sensing imagery', *Annals of the Association of American Geographers*, vol. 93, no. 1, pp. 55-66.

Alsdorf, DE, Melack, JM, Dunne, T, Mertes, LAK, Hess, LL & Smith, LC (2000), 'Interferometric radar measurements of water level changes on the Amazon flood plain', *Nature*, vol. 404, no. 6774, pp. 174-7.

Alsdorf, DE, Rodriguez, E & Lettenmaier, DP (2007b), 'Measuring surface water from space', *Reviews of Geophysics*, vol. 45, no. 2.

Alsdorf, DE, Smith, LC & Melack, JM (2001b), 'Amazon floodplain water level changes measured with interferometric SIR-C radar', *Ieee Transactions on Geoscience and Remote Sensing*, vol. 39, no. 2, pp. 423-31.

Araujo-Lima, C & Oliveira, EC (1998), 'Transport of larval fish in the Amazon', paper presented to Annual Symposium of the Fisheries-Society-of-the-British-Isles on Tropical Fish Biology, Southampton, England, Jul 13-16.

Barroux, G, Sonke, JE, Boaventura, G, Viers, J, Godderis, Y, Bonnet, MP, Sondag, F, Gardoll, S, Lagane, C & Seyler, P (2006), 'Seasonal dissolved rare earth element dynamics of the Amazon River main stem, its tributaries, and the Curuai floodplain', *Geochemistry Geophysics Geosystems*, vol. 7.

Bartlett, KB, Crill, PM, Sebacher, DI, Harriss, RC, Wilson, JO & Melack, JM (1988), 'Methane flux from the central Amazonian floodplain', *Journal of Geophysical Research-Atmospheres*, vol. 93, no. D2, pp. 1571-82.

Bates, PD & De Roo, APJ (2000), 'A simple raster-based model for flood inundation simulation', *Journal of Hydrology*, vol. 236, no. 1-2, pp. 54-77.

Bates, PD, Horritt, MS, Smith, CN & Mason, D (1997), 'Integrating remote sensing observations of flood hydrology and hydraulic modelling', *Hydrological Processes*, vol. 11, no. 14, pp. 1777-95.

Bates, PD, Lane, SN & Ferguson, RI (2005), *Computational Fluid Dynamics: Applications in Environmental Hydraulics.*, Wiley, Chichester.

Beighley, RE, Eggert, KG, Dunne, T, He, Y, Gummadi, V & Verdin, KL (2009), 'Simulating hydrologic and hydraulic processes throughout the Amazon River Basin', *Hydrological Processes*, vol. 23, no. 8, pp. 1221-35.

Birkett, CM (1995), 'The contribution of TOPEX/POSEIDON to the global monitoring of climatically sensitive lakes', *Journal of Geophysical Research-Oceans*, vol. 100, no. C12, pp. 25179-204.

Birkett, CM (1998), 'Contribution of the TOPEX NASA radar altimeter to the global monitoring of large rivers and wetlands', *Water Resources Research*, vol. 34, no. 5, pp. 1223-39.

Birkett, CM, Mertes, LAK, Dunne, T, Costa, MH & Jasinski, MJ (2002), 'Surface water dynamics in the Amazon Basin: Application of satellite radar altimetry', *Journal of Geophysical Research-Atmospheres*, vol. 107, no. D20, p. 21.

Bonnet, MP, Barroux, G, Martinez, JM, Seyler, F, Moreira-Turcq, P, Cochonneau, G, Melack, JM, Boaventura, G, Maurice-Bourgoin, L, Leon, JG, Roux, E, Calmant, S, Kosuth, P, Guyot, JL & Seyler, P (2008), 'Floodplain hydrology in an Amazon floodplain lake (Lago Grande de Curuai)', *Journal of Hydrology*, vol. 349, pp. 18-30.

Bonnet, MP, Barroux, G, Seyler, P, Pecly, G, Moreira-Turcq, P, Lagane, C, Cochonneau, G, Viers, J, Seyler, F & Guyot, JL (2005), 'Seasonal-links between the Amazon-corridor and its-flood plain: The case of the varzea of Curuai', paper presented to International Symposium on Dynamics and Biogeochemistry of River Corridors and Wetlands held at the 7th Scientific Assembly of the International-Association-of-Hydrological-Sciences, Foz do Iguaco, BRAZIL, Apr 03-09.

Boucheza, J, Lajeunesseb, E, Gaillardeta, J, France-Lanordc, C, Dutra-Maiad, P & Mauriced, L (2010), 'Turbulent mixing in the Amazon River: The isotopic memory of confluences', *Earth and Planetary Science Letters*, vol. 290, no. 1-2, pp. 37-43.

Bourgoin, LM, Bonnet, MP, Martinez, JM, Kosuth, P, Cochonneau, G, Moreira-Turcq, P, Guyot, JL, Vauchel, P, Filizola, N & Seyler, P (2007), 'Temporal dynamics of water and sediment exchanges between the Curuai floodplain and the Amazon River, Brazil', *Journal of Hydrology*, vol. 335, no. 1-2, pp. 140-56.

Brown, JH, Gupta, VK, Li, BL, Milne, BT, Restrepo, C & West, GB (2002), 'The fractal nature of nature: power laws, ecological complexity and biodiversity', *Philosophical Transactions of the Royal Society B-Biological Sciences*, vol. 357, no. 1421, pp. 619-26.

Campos, ID, Mercier, F, Maheu, C, Cochonneau, G, Kosuth, P, Blitzkow, D & Cazenave, A (2001), 'Temporal variations of river basin waters from Topex/Poseidon satellite altimetry. Application to the Amazon basin', *Comptes Rendus De L Academie Des Sciences Serie Ii Fascicule a-Sciences De La Terre Et Des Planetes*, vol. 333, no. 10, pp. 633-43.

Castello, L (2008), 'Lateral migration of Arapaima gigas in floodplains of the Amazon', *Ecology of Freshwater Fish*, vol. 17, no. 1, pp. 38-46.

Chapelon, N, Douville, H, Kosuth, P & Oki, T (2002), 'Off-line simulation of the Amazon water balance: a sensitivity study with implications for GSWP', *Climate Dynamics*, vol. 19, no. 2, pp. 141-54.

Chow, VT (1959), *Open Channel Hydraulics*, McGraw-Hill, New York.

Coe, MT, Costa, MH, Botta, A & Birkett, C (2002), 'Long-term simulations of discharge and floods in the Amazon Basin', *Journal of Geophysical Research-Atmospheres*, vol. 107, no. D20, p. 17.

Coe, MT, Costa, MH & Howard, EA (2008), 'Simulating the surface waters of the Amazon River basin: impacts of new river geomorphic and flow parameterizations', *Hydrological Processes*, vol. 22, no. 14, pp. 2542-53.

Coe, MT, Costa, MH & Soares-Filhoc, BS (2009), 'The influence of historical and potential future deforestation on the stream flow of the Amazon River - Land surface processes and atmospheric feedbacks', *Journal of Hydrology*, vol. 369, no. 1-2, pp. 165-74.

Cole, CA, Brooks, RP, Shaffer, PW & Kentula, ME (2002), 'Comparison of hydrology of wetlands in Pennsylvania and Oregon (USA) as an indicator of transferability of hydrogeomorphic (HGM) functional models between regions', *Environmental Management*, vol. 30, no. 2, pp. 265-78.

Costa, MH & Foley, JA (1997), 'Water balance of the Amazon Basin: Dependence on vegetation cover and canopy conductance', *Journal of Geophysical Research-Atmospheres*, vol. 102, no. D20, pp. 23973-89.

Costa, MH, Oliveira, CHC, Andrade, RG, Bustamante, TR, Silva, FA & Coe, MT (2002), 'A macroscale hydrological data set of river flow routing parameters for the Amazon Basin', *Journal of Geophysical Research-Atmospheres*, vol. 107, no. D20, p. 9.

Costa, MPF (2004), 'Use of SAR satellites for mapping zonation of vegetation communities in the Amazon floodplain', *International Journal of Remote Sensing*, vol. 25, no. 10, pp. 1817-35.

Costa, MPF, Niemann, O, Novo, E & Ahern, F (2002), 'Biophysical properties and mapping of aquatic vegetation during the hydrological cycle of the Amazon floodplain using JERS-1 and Radarsat', *International Journal of Remote Sensing*, vol. 23, no. 7, pp. 1401-26.

Cox, PM, Betts, RA, Collins, M, Harris, PP, Huntingford, C & Jones, CD (2004), 'Amazonian forest dieback under climate-carbon cycle projections for the 21st century', *Theoretical and Applied Climatology*, vol. 78, no. 1-3, pp. 137-56.

Cox, PM, Betts, RA, Jones, CD, Spall, SA & Totterdell, IJ (2000), 'Acceleration of global warming due to carbon-cycle feedbacks in a coupled climate model', *Nature*, vol. 408, no. 6809, pp. 184-7.

Cullmann, J, Junk, WJ, Weber, G & Schmitz, GH (2006), 'The impact of seepage influx on cation content of a Central Amazonian floodplain lake', *Journal of Hydrology*, vol. 328, no. 1-2, pp. 297-305.

Da Silva, EF, de Melo, CE & Venere, PC (2007), 'Factors influencing the fish community in two environments in the lower Rio das Mortes, Bananal floodplain, Mato Grosso, Brazil', *Revista Brasileira De Zoologia*, vol. 24, no. 2, pp. 482-92.

Da Silva, JMC, Rylands, AB & Da Fonseca, GAB (2005), 'The fate of the Amazonian areas of endemism', *Conservation Biology*, vol. 19, no. 3, pp. 689-94.

Dillabaugh, CR, Niemann, KO & Richardson, DE (2002), 'Semi-automated extraction of rivers from digital imagery', *Geoinformatica*, vol. 6, no. 3, pp. 263-84.

Dunne, T & Mertes, LAK (2007), 'Rivers', in TT Veblen, KR Young & AR Orme (eds), *The physical geography of South America*, Oxford University Press, New York, pp. 79-90.

Dunne, T, Mertes, LAK, Meade, RH, Richey, JE & Forsberg, BR (1998), 'Exchanges of sediment between the flood plain and channel of the Amazon River in Brazil', *Geological Society of America Bulletin*, vol. 110, no. 4, pp. 450-67.

Durand, M, Andreadis, K, Alsdorf, D, Lettenmaier, D, Moller, D & Wilson, M (2008), 'Estimation of bathymetric depth and slope from data assimilation of swath altimetry into a hydrodynamic model', *Geophysical Research Letters*, vol. 35, no. 15.

Durand, M, Rodríguez, E, Alsdorf, DE & Trigg, M (in press), 'Estimating river depth from remote sensing swath interferometry measurements of river height, slope, and width', *Ieee Journal of Selected Topics in Applied Earth Observations and Remote Sensing*.

Engle, D & Melack, JM (2000), 'Methane emissions from an Amazon floodplain lake: Enhanced release during episodic mixing and during falling water', *Biogeochemistry*, vol. 51, no. 1, pp. 71-90.

Engle, DL & Melack, JM (1993), 'Consequences of riverine floodling for seston and the periphyton of floating meadows in an Amazon floodplain lake', *Limnology and Oceanography*, vol. 38, no. 7, pp. 1500-20.

Falloon, PD & Betts, RA (2006), 'The impact of climate change on global river flow in HadGEM1 simulations', *Atmospheric Science Letters*, vol. 7, no. 3, pp. 62-8.

Farr, TG, Rosen, PA, Caro, E, Crippen, R, Duren, R, Hensley, S, Kobrick, M, Paller, M, Rodriguez, E, Roth, L, Seal, D, Shaffer, S, Shimada, J, Umland, J, Werner, M, Oskin, M, Burbank, D & Alsdorf, D (2007), 'The shuttle radar topography mission', *Reviews of Geophysics*, vol. 45, no. 2, p. 33.

Figueiredo, J, Hoorn, C, van der Ven, P & Soares, E (2009), 'Late Miocene onset of the Amazon River and the Amazon deep-sea fan: Evidence from the Foz do Amazonas Basin', *Geology*, vol. 37, no. 7, pp. 619-22.

Foley, JA, Botta, A, Coe, MT & Costa, MH (2002), 'El Nino-Southern Oscillation and the climate, ecosystems and rivers of Amazonia', *Global Biogeochemical Cycles*, vol. 16, no. 4, p. 27.

Forsberg, BR, Hashimoto, Y, Rosenqvist, A & de Miranda, FP (2000), 'Tectonic fault control of wetland distributions in the Central Amazon revealed by JERS-1 radar imagery', paper presented to 1st Symposium on South American Paleohydrology, Curitiba, Brazil, 1997.

Frappart, F, Seyler, F, Martinez, JM, Leon, JG & Cazenave, A (2005), 'Floodplain water storage in the Negro River basin estimated from microwave remote sensing of inundation area and water levels', *Remote Sensing of Environment*, vol. 99, no. 4, pp. 387-99.

Getirana, ACV, Bonnet, MP, Calmant, S, Roux, E, Rotunno, OC & Mansur, WJ (2009), 'Hydrological monitoring of poorly gauged basins based on rainfall-runoff modeling and spatial altimetry', *Journal of Hydrology*, vol. 379, no. 3-4, pp. 205-19.

Grace, J & Malhi, Y (2002), 'Global change - Carbon dioxide goes with the flow', *Nature*, vol. 416, no. 6881, pp. 594-5.

Gran, K & Paola, C (2001), 'Riparian vegetation controls on braided stream dynamics', *Water Resources Research*, vol. 37, no. 12, pp. 3275-83.

Gregory, KJ & Walling, DE (1968), 'The variation of drainage density within a catchment', *Bull Int Ass Sci Hydrol*, vol. 13, no. 2, pp. 61-8.

Hamilton, SK & Lewis, WM (1990), 'Physical characteristics of the fringing floodplain of the Orinoco River, Venezuela', *Interciencia*, vol. 15, no. 6, pp. 491-500.

Hamilton, SK, Sippel, SJ & Melack, JM (2002), 'Comparison of inundation patterns among major South American floodplains', *Journal of Geophysical Research-Atmospheres*, vol. 107, no. D20, p. 14.

Hayakawa, YS, Oguchi, T & Lin, Z (2008), 'Comparison of new and existing global digital elevation models: ASTER G-DEM and SRTM-3', *Geophysical Research Letters*, vol. 35, no. 17, p. 5.

Henderson, F, M (1966), *Open Channel Flow*, Macmillan Series in Civil Engineering, Macmillan Company, New York.

Hervouet, JM & Van Haren, L (1996), 'Recent advances in numerical methods for fluid flows.', in MG Anderson, DE Walling & PD Bates (eds), *Floodplain Processes*, Wiley, Chichester, pp. 183-214.

Hess, LL, Melack, JM, Filoso, S & Wang, Y (1995), 'Delineation of inundated area and vegetation along the Amazon floodplain with the SIR-C synthetic-aperture radar', *Ieee Transactions on Geoscience and Remote Sensing*, vol. 33, no. 4, pp. 896-904.

Hess, LL, Melack, JM, Novo, E, Barbosa, CCF & Gastil, M (2003), 'Dual-season mapping of wetland inundation and vegetation for the central Amazon basin', *Remote Sensing of Environment*, vol. 87, no. 4, pp. 404-28.

Hess, LL, Melack, JM & Simonett, DS (1990), 'Radar detection of flooding beneath the forest canopy - A review', *International Journal of Remote Sensing*, vol. 11, no. 7, pp. 1313-25.

Horritt, MS & Bates, PD (2002), 'Evaluation of 1D and 2D numerical models for predicting river flood inundation', *Journal of Hydrology*, vol. 268, no. 1-4, pp. 87-99.

Horton, BK & DeCelles, PG (1997), 'The modern foreland basin system adjacent to the Central Andes', *Geology*, vol. 25, no. 10, pp. 895-8.

Houghton, RA, Hall, F & Goetz, SJ (2009), 'Importance of biomass in the global carbon cycle', *Journal of Geophysical Research-Biogeosciences*, vol. 114, p. 13.

Hunter, NM, Horritt, MS, Bates, PD, Wilson, MD & Werner, MGF (2005), 'An adaptive time step solution for raster-based storage cell modelling of floodplain inundation', *Advances in Water Resources*, vol. 28, no. 9, pp. 975-91.

Irion, G, Muller, J, deMello, JN & Junk, WJ (1995), 'Quaternary geology of the Amazonian lowland', *Geo-Marine Letters*, vol. 15, no. 3-4, pp. 172-8.

Johnsson, MJ & Meade, RH (1990), 'Chemical-weathering of fluvial sediments during alluvial storage; the Macuapanim island point-bar, Solimões River, Brazil', *Journal of Sedimentary Petrology*, vol. 60, no. 6, pp. 827-42.

Junk, WJ, Bayley, PB & Sparks, RE (1989), 'The flood pulse concept in river floodplain systems', *Can. Spec. Publ. Fish. Aquat. Sci.*, vol. 106, pp. 110-27.

Junk, WJ & Piedade, MTF (1993), 'Biomass and primary-production of herbaceous plant-communities in the Amazon floodplain', *Hydrobiologia*, vol. 263, no. 3, pp. 155-62.

Kiel, B, Alsdorf, D & LeFavour, G (2006), 'Capability of SRTM C- and X-band DEM data to measure water elevations in Ohio and the Amazon', *Photogrammetric Engineering and Remote Sensing*, vol. 72, no. 3, pp. 313-20.

Koblinsky, CJ, Clarke, RT, Brenner, AC & Frey, H (1993), 'Measurement of river level variations with satellite altimetry', *Water Resources Research*, vol. 29, no. 6, pp. 1839-48.

Kosuth, P, Blitzkow, D & Cochonneau, G (2006), 'Establishment of an Altimetric Reference Network over the Amazon Basin using Satellite Radar Altimetry (Topex Poseidon)', paper presented to 15 Years of Progress in Radar Altimetry Symposium, Venice, Italy, 13-18 March 2006.

Kvernevik, TI, Zambri Mohd Akhir, M & Studholme, J (2002), 'A low-cost procedure for automatic seafloor mapping, with particular reference to coral reef conservation in developing nations', *Hydrobiologia*, vol. 474, no. 1-3, pp. 67-79.

Latrubesse, EM (2008), 'Patterns of anabranching channels: The ultimate end-member adjustment of mega rivers', *Geomorphology*, vol. 101, no. 1-2, pp. 130-45.

Latrubesse, EM & Franzinelli, E (2002), 'The Holocene alluvial plain of the middle Amazon River, Brazil', paper presented to Shanghai Conference of the International-Association-of-Geomorphologists-Working-Group on Large Riveres, Shanghai, Peoples R China, 1999.

LeFavour, G & Alsdorf, D (2005), 'Water slope and discharge in the Amazon River estimated using the shuttle radar topography mission digital elevation model', *Geophysical Research Letters*, vol. 32, no. 17, p. 5.

Leon, JG, Calmant, S, Seyler, F, Bonnet, MP, Cauhope, M, Frappart, F, Filizola, N & Fraizy, P (2006), 'Rating curves and estimation of average water depth at the upper Negro River based on satellite altimeter data and modeled discharges', *Journal of Hydrology*, vol. 328, no. 3-4, pp. 481-96.

Lesack, LFW (1995), 'Seepage exchange in an Amazon floodplain lake', *Limnology and Oceanography*, vol. 40, no. 3, pp. 598-609.

Lesack, LFW & Melack, JM (1995), 'Flooding hydrology and mixture dynamics of lake water derived from multiple sources in an Amazon floodplain lake', *Water Resources Research*, vol. 31, no. 2, pp. 329-45.

Lewin, J & Hughes, D (1980), 'Welsh floodplain studies: II. Application of a qualitative inundation model', *Journal of Hydrology*, vol. 46, no. 1-2, pp. 35-49.

Lewinsohn, TM & Prado, PI (2005), 'How many species are there in Brazil?', *Conservation Biology*, vol. 19, no. 3, pp. 619-24.

Li, WH, Fu, R & Dickinson, RE (2006), 'Rainfall and its seasonality over the Amazon in the 21st century as assessed by the coupled models for the IPCC AR4', *Journal of Geophysical Research-Atmospheres*, vol. 111, no. D2, p. 14.

MacDonald, I, Baines, MJ, Nichols, NK & Samuels, PG (1997), 'Analytic benchmark solutions for open-channel flows', *Journal of Hydraulic Engineering-Asce*, vol. 123, no. 11, pp. 1041-5.

Maia, PD, Maurice, L, Tessier, E, Amouroux, D, Cossa, D, Perez, M, Moreira-Turcq, P & Rheault, I (2009), 'Mercury distribution and exchanges between the Amazon River and connected floodplain lakes', *Science of the Total Environment*, vol. 407, no. 23, pp. 6073-84.

Makarieva, AM & Gorshkov, VG (2007), 'Biotic pump of atmospheric moisture as driver of the hydrological cycle on land', *Hydrology and Earth System Sciences*, vol. 11, no. 2, pp. 1013-33.

Malhi, Y & Grace, J (2000), 'Tropical forests and atmospheric carbon dioxide', *Trends in Ecology & Evolution*, vol. 15, no. 8, pp. 332-7.

Malhi, Y, Roberts, JT, Betts, RA, Killeen, TJ, Li, WH & Nobre, CA (2008), 'Climate change, deforestation, and the fate of the Amazon', *Science*, vol. 319, no. 5860, pp. 169-72.

Martinez, JM & Le Toan, T (2007), 'Mapping of flood dynamics and spatial distribution of vegetation in the Amazon floodplain using multitemporal SAR data', *Remote Sensing of Environment*, vol. 108, no. 3, pp. 209-23.

Meade, RH, Rayol, JM, Daconceicao, SC & Natividade, JRG (1991), 'Backwater effects in the Amazon river basin of Brazil', *Environmental Geology and Water Sciences*, vol. 18, no. 2, pp. 105-14.

Melack, JM & Forsberg, BR (2001), 'Biogeochemistry of Amazon floodplain lakes and associated wetlands.', in ME McClain, RL Victoria & JE Richey (eds), *The biogeochemistry of the Amazon basin and its role in a changing world.*, Oxford Univ. Press., Oxford, pp. 235-76.

Melack, JM, Hess, LL, Gastil, M, Forsberg, BR, Hamilton, SK, Lima, IBT & Novo, E (2004), 'Regionalization of methane emissions in the Amazon Basin with microwave remote sensing', *Global Change Biology*, vol. 10, no. 5, pp. 530-44.

Mertes, LAK (1994), 'Rates of floodplain sedimentation on the central Amazon river', *Geology*, vol. 22, no. 2, pp. 171-4.

Mertes, LAK (1997), 'Documentation and significance of the perirheic zone on inundated floodplains', *Water Resources Research*, vol. 33, no. 7, pp. 1749-62.

Mertes, LAK (2001), 'Remote sensing of riverine landscapes', paper presented to 1st International Symposium on Riverine Landscapes, Ascona, Switzerland, Mar 25-30.

Mertes, LAK, Daniel, DL, Melack, JM, Nelson, B, Martinelli, LA & Forsberg, BR (1995), 'Spatial patterns of hydrology, geomorphology, and vegetation on the floodplain of the Amazon River in Brazil from a remote-sensing perspective', *Geomorphology*, vol. 13, no. 1-4, pp. 215-32.

Mertes, LAK, Dunne, T & Martinelli, LA (1996), 'Channel-floodplain geomorphology along the Solimoes-Amazon River, Brazil', *Geological Society of America Bulletin*, vol. 108, no. 9, pp. 1089-107.

Mertes, LAK, Smith, MO & Adams, JB (1993), 'Estimating suspended sediment concentrations in surface waters of the Amazon River wetlands from Lansat images', *Remote Sensing of Environment*, vol. 43, no. 3, pp. 281-301.

Michaelides, K & Chappell, A (2009), 'Connectivity as a concept for characterising hydrological behaviour', *Hydrological Processes*, vol. 23, no. 3, pp. 517-22.

Moreira-Turcq, P, Jouanneau, JM, Turcq, B, Seyler, P, Weber, O & Guyot, JL (2004), 'Carbon sedimentation at Lago Grande de Curuai, a floodplain lake in the low Amazon region: insights into sedimentation rates', paper presented to 31st International Geological Congress, Rio De Janeiro, Brazil, Aug 16-18.

Morris, CS & Gill, SK (1994a), 'Evaluation of the TOPEX/POSEIDON altimeter system over the Great Lakes', *Journal of Geophysical Research-Oceans*, vol. 99, no. C12, pp. 24527-39.

Morris, CS & Gill, SK (1994b), 'Variation of Great Lakes water levels derived from Geosat altimetry', *Water Resources Research*, vol. 30, no. 4, pp. 1009-17.

Mouchot, MC, Alfoldi, T, Delisle, D & McCullough, G (1991), 'Monitoring the water bodies of the Mackenzie Delta by remote-sensing methods', *Arctic*, vol. 44, pp. 21-8.

Moussa, R & Bocquillon, C (1996), 'Criteria for the choice of flood-routing methods in natural channels', *Journal of Hydrology*, vol. 186, no. 1-4, pp. 1-30.

Nardi, F, Vivoni, ER & Grimaldi, S (2006), 'Investigating a floodplain scaling relation using a hydrogeomorphic delineation method', *Water Resources Research*, vol. 42, no. 9, p. 15.

Neal, J, Fewtrell, T & Trigg, M (2009), 'Parallelisation of storage cell flood models using OpenMP', *Environmental Modelling & Software*, vol. 24, no. 7, pp. 872-7.

Nicholas, AP & Mitchell, CA (2003), 'Numerical simulation of overbank processes in topographically complex floodplain environments', *Hydrological Processes*, vol. 17, no. 4, pp. 727-46.

Nobre, CA, Sellers, PJ & Shukla, J (1991), 'Amazonian deforestation and regional climate change', *Journal of Climate*, vol. 4, no. 10, pp. 957-88.

Nunn, JA & Aires, JR (1988), 'Gravity-anomalies and flexure of the lithosphere at the Middle Amazon Basin, Brazil', *Journal of Geophysical Research-Solid Earth and Planets*, vol. 93, no. B1, pp. 415-28.

Panosso, RD, Muehe, D & Esteves, FD (1995), 'Morphological characteristics of an Amazon floodplain lake (Lake Batata, Para State, Brazil)', *Amazoniana-Limnologia Et Oecologia Regionalis Systemae Fluminis Amazonas*, vol. 13, no. 3-4, pp. 245-58.

Pavelsky, TM & Smith, LC (2008), 'RivWidth: A software tool for the calculation of river widths from remotely sensed imagery', *Ieee Geoscience and Remote Sensing Letters*, vol. 5, no. 1, pp. 70-3.

Peixoto, JMA, Nelson, BW & Wittmann, F (2009), 'Spatial and temporal dynamics of river channel migration and vegetation in central Amazonian white-water floodplains by remote-sensing techniques', *Remote Sensing of Environment*, vol. 113, no. 10, pp. 2258-66.

Petry, P, Bayley, PB & Markle, DF (2003), 'Relationships between fish assemblages, macrophytes and environmental gradients in the Amazon River floodplain', *Journal of Fish Biology*, vol. 63, no. 3, pp. 547-79.

Phlips, EJ, Havens, KE & Lopes, MRM (2008), 'Seasonal dynamics of phytoplankton in two Amazon flood plain lakes of varying hydrologic connectivity to the main river channel', *Fundamental and Applied Limnology*, vol. 172, no. 2, pp. 99-109.

Poulter, B & Halpin, PN (2008), 'Raster modelling of coastal flooding from sea-level rise', *International Journal of Geographical Information Science*, vol. 22, no. 2, pp. 167-82.

Puhakka, M, Kalliola, R, Rajasilta, M & Salo, J (1992), 'River types, site evolution and successional vegetation patterns in Peruvian Amazonia', *Journal of Biogeography*, vol. 19, no. 6, pp. 651-65.

Putz, R (1997), 'Periphyton communities in Amazonian black- and whitewater habitats: Community structure, biomass and productivity', *Aquatic Sciences*, vol. 59, no. 1, pp. 74-93.

Quay, PD, Wilbur, DO, Richey, JE, Hedges, JI, Devol, AH & Victoria, R (1992), 'Carbon cycling in the Amazon River - implications from the C-13 compositions of particles and solutes', *Limnology and Oceanography*, vol. 37, no. 4, pp. 857-71.

Rasanen, ME, Salo, JS & Jungner, H (1991), 'Holocene floodplain lake sediments in the Amazon: ^{14}C dating and palaeoecological use', *Quaternary Science Reviews*, vol. 10, no. 4, pp. 363-72.

Reis, AH (2006), 'Constructal view of scaling laws of river basins', *Geomorphology*, vol. 78, no. 3-4, pp. 201-6.

Richey, JE, Melack, JM, Aufdenkampe, AK, Ballester, VM & Hess, LL (2002), 'Outgassing from Amazonian rivers and wetlands as a large tropical source of atmospheric CO2', *Nature*, vol. 416, no. 6881, pp. 617-20.

Richey, JE, Mertes, LAK, Dunne, T, Victoria, RL, Forsberg, BR, Tancredi ACNS & Oliveira, E (1989b), 'Sources and Routing of the Amazon River Flood Wave', *Global Biogeochem. Cycles*, vol. 3, no. 3, pp. 191-204.

Richey, JE, Nobre, C & Deser, C (1989a), 'Amazon River discharge and climate variability - 1903 to 1985', *Science*, vol. 246, no. 4926, pp. 101-3.

Rinaldo, A, Banavar, JR & Maritan, A (2006), 'Trees, networks, and hydrology', *Water Resources Research*, vol. 42, no. 6, p. 19.

Rodriguez, E, Morris, CS & Belz, JE (2006), 'A global assessment of the SRTM performance', *Photogrammetric Engineering and Remote Sensing*, vol. 72, no. 3, pp. 249-60.

Rodriguez-Iturbe, I & Rinaldo, A (1997), *Fractal river basins*, Cambridge University Press, New York.

Rosenqvist, A, Forsberg, BR, Pimentel, T, Rauste, YA & Richey, JE (2002), 'The use of spaceborne radar data to model inundation patterns and trace gas emissions in the central Amazon floodplain', *International Journal of Remote Sensing*, vol. 23, no. 7, pp. 1303-28.

Rosenqvist, A, Shimada, M, Chapman, B, Freeman, A, De Grandi, G, Saatchi, S & Rauste, Y (2000), 'The Global Rain Forest Mapping project - a review', *International Journal of Remote Sensing*, vol. 21, no. 6-7, pp. 1375-87.

Rossetti, DF & Valeriano, MM (2007), 'Evolution of the lowest amazon basin modeled from the integration of geological and SRTM topographic data', *Catena*, vol. 70, no. 2, pp. 253-65.

Roux, E, Cauhope, M, Bonnet, MP, Calmant, S, Vauchel, P & Seyler, F (2008), 'Daily water stage estimated from satellite altimetric data for large river basin monitoring', *Hydrological Sciences Journal-Journal Des Sciences Hydrologiques*, vol. 53, no. 1, pp. 81-99.

Schongart, J & Junk, WJ (2007), 'Forecasting the flood-pulse in Central Amazonia by ENSO-indices', *Journal of Hydrology*, vol. 335, no. 1-2, pp. 124-32.

Sippel, SJ, Hamilton, SK & Melack, JM (1992), 'Inundation area and morphometry of lakes on the Amazon River floodplain, Brazil', *Archiv Fur Hydrobiologie*, vol. 123, no. 4, pp. 385-400.

Sippel, SJ, Hamilton, SK, Melack, JM & Choudhury, BJ (1994), 'Determination of inundation area in the Amazon River floodplain using the SMMR 37 GHz polarization difference', *Remote Sensing of Environment*, vol. 48, no. 1, pp. 70-6.

Sippel, SJ, Hamilton, SK, Melack, JM & Novo, EMM (1998), 'Passive microwave observations of inundation area and the area/stage relation in the Amazon River floodplain', *International Journal of Remote Sensing*, vol. 19, no. 16, pp. 3055-74.

Slater, JA, Garvey, G, Johnston, C, Haase, J, Heady, B, Kroenung, G & Little, J (2006), 'The SRTM data "finishing" process and products', *Photogrammetric Engineering and Remote Sensing*, vol. 72, no. 3, pp. 237-47.

Solomon, S, Qin, D, Manning, M, Chen, Z, Marquis, M & Averyt, KB (2007), *IPCC, 2007: Climate Change 2007: The Physical Science Basis. Contribution of Working Group I to the Fourth Assessment*, IPCC.

Steffen, W, Andreae, MO, Bolin, B, Cox, PM, Crutzen, PJ, Cubasch, U, Held, H, Nakicenovic, N, Scholes, RJ, Talaue-McManus, L & Turner, BL (2004), 'Abrupt changes: The Achilles' heels of the Earth System', *Environment*, vol. 46, no. 3, pp. 8-20.

Steffen, W, Sanderson, A, Tyson, PD, Jager, J, Matson, PA, Moore, B, Oldfield, F, Richardson, K, Schellnhuber, HJ, Turner, BL & Wasson, RJ (2005), 'Global Change and the Earth System: A Planet Under Pressure', in *Global Change and the Earth System: A Planet Under Pressure*.

Tejerina-Garro, FL, Fortin, R & Rodriguez, MA (1998), 'Fish community structure in relation to environmental variation in floodplain lakes of the Araguaia River, Amazon Basin', *Environmental Biology of Fishes*, vol. 51, no. 4, pp. 399-410.

Tockner, K, Malard, F & Ward, JV (2000), 'An extension of the flood pulse concept', *Hydrological Processes*, vol. 14, no. 16-17, pp. 2861-83.

Toivonen, T, Maeki, S & Kalliola, R (2007), 'The riverscape of Western Amazonia - a quantitative approach to the fluvial biogeography of the region', paper presented to Annual Meeting of the Association-for-Tropical-Biology-and-Conservation, Uberlandia, BRAZIL, 2005.

Tricart, JLF (1977), 'Types of alluvial plains and river beds in Amazonia', *Annales De Geographie*, vol. 86, no. 473, pp. 1-54.

Trigg, MA, Wilson, MD, Bates, PD, Horritt, MS, Alsdorf, DE, Forsberg, BR & Vega, MC (2009), 'Amazon flood wave hydraulics', *Journal of Hydrology*, vol. 374, no. 1-2, pp. 92-105.

Vieira, JHD (1983), 'Conditions governing the use of approximations for the Saint-Venant equations for shallow surface-water flow', *Journal of Hydrology*, vol. 60, no. 1-4, pp. 43-58.

Villar, JCE, Guyot, JL, Ronchail, J, Cochonneau, G, Filizola, N, Fraizy, P, Labat, D, de Oliveira, E, Ordonez, JJ & Vauchel, P (2009), 'Contrasting regional discharge evolutions in the Amazon basin (1974-2004)', *Journal of Hydrology*, vol. 375, no. 3-4, pp. 297-311.

Vital, H & Stattegger, K (2000a), 'Lowermost Amazon River: evidence of late Quaternary sea-level fluctuations in a complex hydrodynamic system', paper presented to 1st Symposium on South American Paleohydrology, Curitiba, Brazil, 1997.

Vital, H & Stattegger, K (2000b), 'Sediment dynamics in the lowermost Amazon', *Journal of Coastal Research*, vol. 16, no. 2, pp. 316-28.

Vorosmarty, CJ, Moore, B, III, Grace, AL, Gildea, MP, Melillo, JM, Peterson, BJ & Rastetter, ED (1989), 'Continental-scale models of water balance and fluvial transport: An application to South America', *Global Biogeochemical Cycles*, vol. 3, no. 3, pp. 241-65.

Williams, MR, Fisher, TR & Melack, JM (1997), 'Chemical composition and deposition of rain in the central Amazon, Brazil', *Atmospheric Environment*, vol. 31, no. 2, pp. 207-17.

Wilson, M, Bates, P, Alsdorf, D, Forsberg, B, Horritt, M, Melack, J, Frappart, F & Famiglietti, J (2007), 'Modeling large-scale inundation of Amazonian seasonally flooded wetlands', *Geophysical Research Letters*, vol. 34, no. 15.

Wittmann, F, Anhuf, D & Junk, WJ (2002), 'Tree species distribution and community structure of central Amazonian varzea forests by remote-sensing techniques', *Journal of Tropical Ecology*, vol. 18, pp. 805-20.

Wittmann, F, Junk, WJ & Piedade, MTF (2004), 'The varzea forests in Amazonia: flooding and the highly dynamic geomorphology interact with natural forest succession', *Forest Ecology and Management*, vol. 196, no. 2-3, pp. 199-212.

Wittmann, F & Parolin, P (2005), 'Aboveground roots in Amazonian floodplain trees', *Biotropica*, vol. 37, no. 4, pp. 609-19.

Wittmann, F, Schongart, J, Montero, JC, Motzer, T, Junk, WJ, Piedade, MTF, Queiroz, HL & Worbes, M (2006a), 'Tree species composition and diversity gradients in white-water forests across the Amazon Basin', *Journal of Biogeography*, vol. 33, no. 8, pp. 1334-47.

Wittmann, F, Schongart, J, Parolin, P, Worbes, M, Piedade, MTF & Junk, WJ (2006b), 'Wood specific gravity of trees in Amazonian white-water forests in relation to flooding', *Iawa Journal*, vol. 27, no. 3, pp. 255-68.

Worbes, M, Klinge, H, Revilla, JD & Martius, C (1992), 'On the dynamics, floristic subdivision and geographical distribution of várzea forests in Central Amazonia', *Journal of Vegetation Science*, vol. 3, no. 4, pp. 553-64.

Zakharova, EA, Kouraev, AV, Cazenave, A & Seyler, F (2006), 'Amazon River discharge estimated from TOPEX/Poseidon altimetry', *Comptes Rendus Geoscience*, vol. 338, no. 3, pp. 188-96.